RAC-1333
~~(SSD-1027)~~
~~17 June 1963~~

N64-17699

# SYNCHRONOUS METEOROLOGICAL SATELLITE (SMS) STUDY

## Volume 5

## Communications, Power Supply, and Thermal Control

RAC-1333

Prepared for

NATIONAL AERONAUTICS AND SPACE ADMINISTRATION
Goddard Space Flight Center
Greenbelt, Maryland

under
Contract No. NAS5-3189

[redacted]

REPUBLIC AVIATION CORPORATION
Farmingdale, L.I., N.Y.

## FOREWORD

This final report on Contract NAS 5-3189 is presented by Republic Aviation Corporation to the Goddard Space Flight Center of the National Aeronautics and Space Administration and consists of the seven volumes listed below. The period of the contract work was February through May, 1963.

The sub-titles of the seven volumes of this report are:

1 Summary and Conclusions

2 Configurations and Systems

3 Meteorological Sensors

4 Attitude and Station Control

5 Communications, Power Supply, and Thermal Control

6 System Synthesis and Evaluation

7 Classified Supplement on Sensors and Control

Except for Volume 7, all of these are unclassified. Volume 7 contains only that information on specific subsystems which had to be separated from the other material because of its present security classification. Some of these items may later be cleared for use in unclassified systems.

Volumes 3, 4, and 5 present detailed surveys and analyses of subsystems and related technical problems as indicated by their titles.

In Volume 2, several combinations of subsystems are reviewed as complete spacecraft systems, including required structure and integration. These combinations were selected primarily as examples of systems feasible within different mass limits, and are associated with the boosters to be available.

Volume 6 outlines methods and procedures for synthesizing and evaluating system combinations which are in addition to those presented in Volume 2.

Volume 1 presents an overall summary and the principal conclusions of the study.

TABLE OF CONTENTS


| Section | Title | Page |
|---|---|---|
| 1 | COMMUNICATIONS | 1-1 |
| A. | General Parametric Relationships | 1-1 |
| 1. | General Transmission Equations | 1-1 |
| 2. | Factors Affecting Choice of Frequencies | 1-2 |
| a. | Free Space Attenuation | 1-2 |
| b. | Signal Absorption | 1-5 |
| c. | Refraction and Faraday Rotation | 1-6 |
| 3. | Total Effective Noise Temperature Considerations | 1-7 |
| a. | Antenna Temperature | 1-8 |
| b. | Line Losses | 1-11 |
| c. | Receiver Noise Temperature | 1-12 |
| d. | Front End Devices | 1-13 |
| e. | Total Effective Noise Temperature Contribution | 1-15 |
| 4. | Modulation Considerations | 1-18 |
| a. | Amplitude Modulation | 1-19 |
| b. | Single Sideband | 1-19 |
| c. | Frequency Modulation | 1-20 |
| d. | FM Demodulator with Negative Feedback | 1-22 |
| e. | Phase-Lock Loop Detection | 1-24 |
| f. | Receiver Bandwidth | 1-25 |
| g. | Comparison of Transmission Systems | 1-27 |
| h. | Comparison of FM and PCM Systems | 1-28 |
| 5. | Antenna Considerations | 1-32 |
| a. | Spacecraft Antennas | 1-38 |
| b. | Spin Stabilized Antennas | 1-38 |
| c. | Multi-Frequency Operation | 1-39 |
| B. | Systems Description | 1-40 |
| 1. | Sensor Data Link | 1-40 |
| a. | Frequency Considerations | 1-40 |
| b. | Power Amplifier Considerations | 1-41 |
| c. | Antenna Considerations | 1-49 |

TABLE OF CONTENTS (Continued)


| Section | Title | Page |
|---|---|---|
| | d. Modulation Methods | 1-51 |
| | e. Modulation Method Comparison | 1-53 |
| 2. | Telemetry Link | 1-57 |
| | a. Telemetry Modulation Methods | 1-57 |
| | b. Comparison of Telemetry Techniques | 1-58 |
| | c. Error Probabilities and RMS Error in PCM-FM | 1-59 |
| | d. Minimum IF Bandwidth vs Bit Rate in PCM Telemetry | 1-61 |
| | e. The Telemetry Radio Frequency Link | 1-61 |
| 3. | Command Receiver | 1-70 |
| | a. System Requirements and Calculations | 1-71 |
| | b. Power Budget | 1-72 |
| | c. Conclusions | 1-72 |
| 4. | SMS Transponder Relay System | 1-74 |
| | a. Characteristics of Relayed Information | 1-74 |
| | b. Transmission Time | 1-77 |
| | c. Signal to Noise Ratio | 1-78 |
| | d. S-Band Transponder | 1-78 |
| | e. VHF Transponder | 1-80 |
| 5. | Satellite Beacon and Tracking | 1-86 |
| | a. SMS Launch and Orbit Injection Path | 1-86 |
| | b. Goddard Range and Range Rate System | 1-88 |
| | c. Minitrack Tracking Stations | 1-94 |
| | d. CDA Station Tracking | 1-95 |
| | e. Transportable Angular Tracking Stations | 1-96 |
| | f. Ionospheric Refraction Effects | 1-98 |
| | g. Optical Tracking Methods | 1-99 |
| 6. | Command Data Acquisition Station | 1-100 |
| | a. Antenna Considerations | 1-100 |
| | b. Sensor Data Receiver | 1-102 |
| | c. Command Transmitter | 1-104 |
| | d. Telemetry Receiver | 1-105 |
| | e. Relay Transmitter | 1-106 |

TABLE OF CONTENTS (Continued)


| Section | | Page |
|---|---|---|
| | 7. Multiple Data Acquisition Station | 1-106 |
| | a. Raw Data Acquisition | 1-107 |
| | b. Processed Meteorological Information | 1-108 |
| | c. Nimbus Automatic Picture Transmission Ground Stations | 1-109 |
| | C. References | 1-115 |
| 2 | DATA HANDLING | 2-1 |
| | A. Sensor Data System | 2-1 |
| | 1. Overall Description | 2-1 |
| | 2. Error Correcting Codes | 2-2 |
| | 3. Coordinate Delta-Encoding | 2-2 |
| | 4. Photo-Interpreter Data | 2-8 |
| | 5. Heat Budget Sensor Data | 2-8 |
| | 6. Summary | 2-9 |
| | B. Command Data System | 2-9 |
| | 1. Overall Description | 2-9 |
| | 2. Tone Digital System | 2-9 |
| | 3. Control Commands | 2-11 |
| | 4. PCM Command System | 2-12 |
| | 5. Programming | 2-14 |
| | 6. Summary | 2-16 |
| | C. Telemetry System | 2-18 |
| 3 | POWER SYSTEM STUDY | 3-1 |
| | A. Introduction | 3-1 |
| | B. Description of Power Systems | 3-1 |
| | 1. Solar Power | 3-1 |
| | a. Solar Thermoelectric Power System | 3-1 |
| | b. Solar Thermionic Power System | 3-4 |
| | c. Solar Cells (Photovoltaic) | 3-6 |
| | d. Photoemissive Cathode Power System | 3-12 |
| | e. Photochemical Power System | 3-13 |
| | f. Solar Regenerative Fuel Cell | 3-15 |
| | g. Solar Turboelectric Power System | 3-15 |
| | h. Thermal Storage System | 3-17 |

TABLE OF CONTENTS (Continued)


| Section | Title | Page |
|---|---|---|
| | 2. Nuclear Power | 3-17 |
| | a. General | 3-17 |
| | b. Nuclear Thermoelectric Power System | 3-18 |
| | c. Nuclear Thermionic Power System | 3-19 |
| | d. Nuclear Turboelectric Power System | 3-22 |
| | e. Summary of SNAP Systems | 3-23 |
| | 3. Chemical Power | 3-27 |
| | a. Primary Batteries | 3-30 |
| | b. Secondary Batteries | 3-31 |
| | c. Fuel Cells (Degenerative Type) | 3-35 |
| | d. Chemical Turbines | 3-39 |
| | 4. Microwave Transmitted Power | 3-41 |
| | 5. Summary of Power Sources and Energy Storage Systems | 3-43 |
| | C. Space Radiation Effects on Solar Cells at Synchronous Orbit | 3-46 |
| | 1. Cosmic Rays | 3-47 |
| | 2. Solar Flares | 3-47 |
| | 3. Van Allen Belt (Natural and Artificial) | 3-47 |
| | 4. Radiation Sensitivity of Silicon Solar Cells | 3-48 |
| | 5. Expected Cell Degradation | 3-50 |
| | D. Power System Design Considerations | 3-51 |
| | E. Power and Energy Requirements of the SMS Power System | 3-55 |
| | F. Power System Design Illustration | 3-56 |
| | G. Bibliography | 3-63 |
| 4 | THERMAL CONTROL | 4-1 |
| | A. Summary and Introduction | 4-1 |
| | 1. Summary | 4-1 |
| | 2. Introduction | 4-2 |
| | B. Factors Influencing Thermal Design | 4-3 |
| | 1. Introduction | 4-3 |
| | 2. Thermal Environment | 4-4 |
| | a. Remote Energy Sources | 4-4 |

TABLE OF CONTENTS (Continued)


| Section | Title | Page |
|---|---|---|
| | b. Contact Energy Sources | 4-12 |
| | c. Internal Energy Sources | 4-13 |
| | 3. Surface Characteristics | 4-13 |
| | a. Thermal Properties | 4-13 |
| | b. Physical Properties | 4-14 |
| | c. Environmental Effects on Surface Characteristics | 4-14 |
| | 4. Component Temperature Limits | 4-21 |
| C. | Passive Temperature Control | 4-22 |
| | 1. Introduction | 4-22 |
| | 2. Thermal Analysis | 4-24 |
| | a. Heterothermal Satellite | 4-24 |
| | b. SMS Thermal Design Approach | 4-27 |
| | c. Isothermal Condition | 4-30 |
| | 3. Thermal Control Schemes | 4-32 |
| | a. Thermal Control by Surface Properties | 4-35 |
| | b. Shadow-Box Thermal Control | 4-38 |
| | c. Thermal Control by Heat Storage Materials | 4-40 |
| | d. Thermal Control by Heating Elements | 4-42 |
| D. | Semiactive Temperature Control | 4-44 |
| | 1. Introduction | 4-44 |
| | 2. Mechanically Variable Radiative Surface Properties | 4-44 |
| | a. Movable Shutters | 4-44 |
| | b. Rotatable Vanes | 4-46 |
| | 3. Mechanically Variable Thermal Resistance | 4-47 |
| | a. Variable Conductance Devices (Thermal Switch) | 4-47 |
| | b. Variable Contact Area Devices | 4-48 |
| | 4. Forced Convection Loop (Cold-Plate System | 4-49 |
| | a. System Operation | 4-49 |
| | b. Possible SMS Design | 4-50 |

TABLE OF CONTENTS (Continued)


| Section | Title | Page |
|---|---|---|
| E. | Active Temperature Control | 4-52 |
| | 1. Introduction | 4-52 |
| | 2. Vapor Cycle Refrigeration | 4-52 |
| | a. Description | 4-52 |
| | b. Analysis | 4-53 |
| | 3. Gas Cycle Refrigeration | 4-57 |
| | a. Description | 4-57 |
| | b. Analysis | 4-57 |
| | 4. Absorption Cycle Refrigeration | 4-63 |
| | a. Description | 4-63 |
| | b. Refrigerants | 4-64 |
| | c. Disadvantages | 4-64 |
| | 5. Themoelectric (Peltier) Cooling | 4-64 |
| | a. Description | 4-64 |
| | b. Analysis | 4-65 |
| | c. Design | 4-68 |
| | d. System Disadvantages | 4-69 |
| | e. Advantages | 4-70 |
| F. | Infrared Cooling | 4-71 |
| | 1. Introduction | 4-71 |
| | 2. Direct-Contact Coolers | 4-71 |
| | 3. Joule-Thompson Cryostats | 4-72 |
| | 4. Expansion Engines | 4-73 |
| | 5. Thermoelectric Coolers | 4-75 |
| G. | Solar Cells | 4-77 |
| | 1. Introduction | 4-77 |
| | 2. Analysis | 4-77 |
| | 3. Results | 4-78 |
| H. | List of Symbols | 4-82 |
| I. | References | 4-85 |

## LIST OF ILLUSTRATIONS


| Figure | Title | Page |
|---|---|---|
| | SECTION 1 | |
| 1-1 | Satellite Communications Nomograph, Assumed Antenna Efficiency 55% | 1-3 |
| 1-2 | Free Space Attenuation | 1-4 |
| 1-3 | Attenuation and Slant Range Correction Curve | 1-4 |
| 1-4 | Atmospheric Losses | 1-5 |
| 1-5 | Additional Atmospheric Losses vs Elevation Angle | 1-6 |
| 1-6 | Atmospheric Refraction Errors | 1-7 |
| 1-7 | Equivalent Antenna Temperature vs Frequency | 1-9 |
| 1-8 | Sun Temperature Curve | 1-10 |
| 1-9 | Sun Outage Time | 1-11 |
| 1-10 | Total Effective Input Temperature vs Line Loss | 1-12 |
| 1-11 | Receiver Noise Temperature vs Noise Factor | 1-13 |
| 1-12 | Receiver Front End Noise Temperature | 1-14 |
| 1-13 | Receiver Noise Power vs Bandwidth | 1-16 |
| 1-14 | Overall Receiver Temperature vs Antenna Temperature | 1-17 |
| 1-15 | Relative Sensitivity Improvement | 1-18 |
| 1-16 | Typical FM Threshold Curves | 1-20 |
| 1-17 | FM S/N Improvement Ratio | 1-21 |
| 1-18 | FMFB Receiver Block Diagram | 1-22 |
| 1-19 | Design Parameters for Optimum Feedback FM Systems | 1-23 |
| 1-20 | Phase-Locked Loop Detector Block Diagram | 1-24 |
| 1-21 | Degradation Caused by Combining Two Signals | 1-26 |
| 1-22 | Comparison of FM vs Binary PCM (Above Threshold) | 1-29 |
| 1-23 | Receiver IF Bandwidth vs Modulation System | 1-30 |
| 1-24 | Output S/N vs RF Power Output | 1-31 |
| 1-25 | Error Probability | 1-32 |

LIST OF ILLUSTRATIONS (Continued)


| Figure | Title | Page |
|---|---|---|
| | SECTION 1 (Continued) | |
| 1-26 | Parabolic Antenna Gain vs Frequency and Size | 1-34 |
| 1-27 | Antenna Gain vs Beamwidth | 1-34 |
| 1-28 | Frequency vs Wavelength | 1-35 |
| 1-29 | Antenna Beamwidth vs Aperture Width for Rectangular Apertures | 1-36 |
| 1-30 | Antenna Beamwidth vs Aperture Width for Circular or Elliptical Apertures | 1-36 |
| 1-31 | Impedance Match Characteristic | 1-37 |
| 1-32 | Paraboloidal Gain Loss Due to Random Errors | 1-38 |
| 1-33 | QKS 997A Amplitron Voltage - Current Characteristics | 1-44 |
| 1-34 | VTM Injection Frequency Locking | 1-47 |
| 1-35 | Typical Solid-State Power Output Section, Block Diagram | 1-48 |
| 1-36 | Typical Electronically Stabilized Sensor Data Link Antenna Configuration for Spin Stabilized Satellite | 1-50 |
| 1-37 | Linear Element Array for Sensor Data-Link, Antenna for Spin-Stabilized Satellite | 1-50 |
| 1-38 | FM Modulation Methods | 1-51 |
| 1-39 | PCM Bi-Phase Modulator | 1-52 |
| 1-40 | Optimized System Comparison Chart for 2% Error | 1-59 |
| 1-41 | PAM-FM and PCM-FM Performance for Various Accuracies | 1-60 |
| 1-42 | Minimum IF Bandwidth vs Bit Rate for PCM Telemetry | 1-61 |
| 1-43 | Telemetry Power vs Bandwidth for Various Effective Temperatures | 1-64 |
| 1-44 | Telemetry Power vs Bandwidth for Various C/N | 1-64 |
| 1-45 | Telemetry Power vs Bandwidth for Various Ground Antenna Diameters | 1-66 |
| 1-46 | Telemetry Transmitter Weight vs Power Output | 1-68 |
| 1-47 | Comparison of Threshold Level and Signal to Noise of Phase-Locked Loop and Ordinary Discriminators | 1-70 |
| 1-48 | Relay Baseband Frequency vs Transmission Time for Facsimile Pictures | 1-77 |

LIST OF ILLUSTRATIONS (Continued)


| Figure | Title | Page |
|---|---|---|
| | SECTION 1 (Continued) | |
| 1-48A | Types of Relay Repeaters | 1-79 |
| 1-49 | S-Band Transponder Relay | 1-81 |
| 1-50 | VHF Transponder Relay | 1-84 |
| 1-51 | SMS Transfer Ellipse Characteristics | 1-87 |
| 1-52 | SMS Coverage Map | 1-88 |
| 1-53 | Goddard Range and Range Rate System | 1-89 |
| 1-54 | VHF Range and Range Rate System | 1-91 |
| 1-55 | S-Band Range and Range Rate System | 1-92 |
| 1-56 | SMS Tracking Azimuth and Elevation Data During the Transfer Ellipse (as seen from Rosman, N.C.) | 1-94 |
| 1-57 | SMS Tracking Range Rate and Slant Range During the Transfer Ellipse (as seen from Rosman, N.C.) | 1-95 |
| 1-58 | Tracking Accuracy vs Antenna Diameter | 1-96 |
| 1-59 | Refraction Error vs Frequency | 1-98 |
| 1-60 | CDA Communications, Block Diagram | 1-101 |
| 1-61 | Approximate Cost of Parabolic Antenna with Equatorial Mount | 1-102 |
| 1-62 | Automatic Picture Transmission Ground Station, Block Diagram | 1-111 |
| 1-63 | Satellite Transmitter Power vs Distance (Using Nimbus APT Ground Station, Frequency = 136 MC) | 1-112 |
| | SECTION 2 | |
| 2-1 | Sensor Data Handling System | 2-2 |
| 2-2 | Correction Capability vs Frequency | 2-5 |
| 2-3 | Coordinate Delta System | 2-6 |
| 2-4 | Coordinate Word Size | 2-7 |
| 2-5 | PCM Command System | 2-10 |
| 2-6 | Pulse Configuration | 2-12 |
| 2-7 | Clock Generator | 2-13 |

LIST OF ILLUSTRATIONS (Continued)


| Figure | Title | Page |
|---|---|---|
| | SECTION 2 (Continued) | |
| 2-8 | Pulse Generator | 2-13 |
| 2-9 | Code Correlator | 2-14 |
| 2-10 | Ground Station Control of Proportional Commands | 2-15 |
| 2-11 | Telemetry Data Handling | 2-18 |
| 2-12 | Analog-to-Digital Converter | 2-19 |
| 2-13 | Analog-to-Digital Converter, Sawtooth Type | 2-26 |
| 2-14 | Two-Wire System Based on Local Serializing | 2-28 |
| | SECTION 3 | |
| 3-1 | Solar Thermoelectric Configuration | 3-2 |
| 3-2 | Solar Power Source Weight vs Power Output | 3-5 |
| 3-3 | Solar Thermionic Converter | 3-5 |
| 3-4 | Solar Cell Diagram (Photovoltaic Effect) | 3-8 |
| 3-5 | Effect of Temperature on Current-Voltage Characteristic of Solar Irradiated Cell (1 x 2 cm) | 3-10 |
| 3-6 | Typical Variation of Voltage-Current at Optimum Power with Temperature | 3-10 |
| 3-7 | Cross Section of Paddle Segment | 3-11 |
| 3-8 | Photochemical Cell | 3-13 |
| 3-9 | Solar Regeneration Fuel Cell | 3-16 |
| 3-10 | Solar Turboelectric System | 3-16 |
| 3-11 | Nuclear Thermoelectric System | 3-20 |
| 3-12 | High Power Nuclear Thermoelectric System | 3-20 |
| 3-13 | SNAP-10 System | 3-21 |
| 3-14 | Nuclear Thermionic System | 3-21 |
| 3-15 | Nuclear Thermionic System (Elements Inside Core) | 3-22 |
| 3-16 | Nuclear Turboelectric System | 3-24 |
| 3-17 | Nuclear Power Source Weight vs Power Output | 3-24 |
| 3-18 | Primary Battery | 3-30 |

LIST OF ILLUSTRATIONS (Continued)


| Figure | Title | Page |
|---|---|---|
| | SECTION 3 (Continued) | |
| 3-19 | Cycle Life of Sealed Nickel Cadmium Cells | 3-33 |
| 3-20 | Energy vs Unit Weight for Various Batteries | 3-33 |
| 3-21 | Energy vs Unit Volume for Various Batteries | 3-36 |
| 3-22 | Capacity vs Temperature for Various Batteries | 3-36 |
| 3-23 | Hydrogen-Oxygen, Liquid Electrolyte Fuel Cell | 3-38 |
| 3-24 | Application of Space Power Systems | 3-43 |
| 3-25 | Proton Radiation Effects on Solar Cells | 3-48 |
| 3-26 | Electron Radiation Effects on Solar Cells | 3-49 |
| 3-27 | Comparison of Electron Energy Radiation Effects on p-n and n-p Solar Cells | 3-49 |
| 3-28 | Range-Energy Curves for Electrons and Protons in Quartz | 3-51 |
| 3-29 | Power System Configuration | 3-53 |
| | SECTION 4 | |
| 4-1 | Umbra and Penumbra Patterns for a Synchronous Equatorial Satellite | 4-2 |
| 4-2 | Effect of the Earth's Yearly Motion | 4-5 |
| 4-3 | Variation of Solar Heat Input with Calendar Time Spin-Stabilized Configuration | 4-7 |
| 4-4 | Variation of Solar Heat Input with Time of Day and Seasons | 4-7 |
| 4-5 | Parameter for Earth Thermal Emission Incident to a Spherical Satellite as a Function of Altitude | 4-9 |
| 4-6 | Parameter for Earth Thermal Emission Incident to a Flat Plate as a Function of Altitude and Plate Attitude Angle | 4-9 |
| 4-7 | Parameter for Earth-Reflected Radiation Incident to a Spherical Satellite as a Function of Altitude and Sun Elevation Angle | 4-11 |
| 4-8 | Ultraviolet Degradation of Thermal Control Paints in Vacuum | 4-20 |
| 4-9 | Approximate Component Temperature Limits | 4-22 |

LIST OF ILLUSTRATIONS (Continued)


| Figure | Title | Page |
|---|---|---|
| | SECTION 4 (Continued) | |
| 4-10 | Failure Rates vs Ambient Temperature for Various Electronic Components | 4-23 |
| 4-11 | Surface Temperature Distribution on a Three-Axis Stabilized Satellite | 4-26 |
| 4-12 | Effect of Thermo-Structural Parameters on Satellite Isothermality | 4-27 |
| 4-13 | Effect of Equipment Position and Orbital Period on Temperature Amplitude Ratio | 4-29 |
| 4-14 | Temperature Distribution on a Spin-Stabilized Cylindrical Satellite | 4-31 |
| 4-15 | Effect of RPM & Power Density on a Spin-Stabilized, Solar-Cell-Covered Satellite | 4-31 |
| 4-16 | Effect of Surface Characteristics and Internal Power Density on Spacecraft Surface Temperature, 0.0 watts/ft$^2$, Spin-Stabilized Configuration | 4-33 |
| 4-17 | Effect of Surface Characteristics and Internal Power Density on Spacecraft Surface Temperature, 0.5 watts/ft$^2$, Spin-Stabilized Configuration | 4-33 |
| 4-18 | Effect of Surface Characteristics and Internal Power Density on Spacecraft Surface Temperature, 1.0 watts/ft$^2$, Spin-Stabilized Configuration | 4-33 |
| 4-19 | Effect of Surface Characteristics and Internal Power Density on Spacecraft Surface Temperature, 2.0 watts/ft$^2$, Spin-Stabilized Configuration | 4-33 |
| 4-20 | Effect of Surface Characteristics and Internal Power Density on Spacecraft Surface Temperature, 5.0 watts/ft$^2$, Spin-Stabilized Configuration | 4-34 |
| 4-21 | Effect of Surface Characteristics and Internal Power Density on Spacecraft Surface Temperature, 10.0 watts/ft$^2$, Spin-Stabilized Configuration | 4-34 |
| 4-22 | Temperature Response Characteristics During Equinoctial Passage, Cylindrical Satellite | 4-34 |
| 4-23 | Temperature Response Characteristics During Equinoctial Passage, Minimum Performance Configuration | |
| 4-24 | Temperature Response Characteristics During Equinoctial Passage, Medium Performance Configuration | 4-35 |

LIST OF ILLUSTRATIONS (Continued)


| Figure | Title | Page |
|---|---|---|
| | SECTION 4 (Continued) | |
| 4-25 | Temperature Response Characteristics During Equinoctial Passage, High Performance Configuration | 4-35 |
| 4-26 | Effect of Surface Characteristics and Internal Power Density on Spacecraft Surface Temperature, 0 watts/ft$^2$, Non-Spinning Satellite | 4-36 |
| 4-27 | Effect of Surface Characteristics and Internal Power Density on Spacecraft Surface Temperature, 0.5 watts/ft$^2$, Non-Spinning Satellite | 4-36 |
| 4-28 | Effect of Surface Characteristics and Internal Power Density on Spacecraft Surface Temperature, 1.0 watts/ft$^2$, Non-Spinning Satellite | 4-36 |
| 4-29 | Effect of Surface Characteristics and Internal Power Density on Spacecraft Surface Temperature, 2.0 watts/ft$^2$, Non-Spinning Satellite | 4-36 |
| 4-30 | Effect of Surface Characteristics and Internal Power Density on Spacecraft Surface Temperature, 5.0 watts/ft$^2$, Non-Spinning Satellite | 4-37 |
| 4-31 | Effect of Surface Characteristics and Internal Power Density on Spacecraft Surface Temperature, 10.0 watts/ft$^2$, Non-Spinning Satellite | 4-37 |
| 4-32 | Performance of Thermal-Storage Temperature Control Systems | 4-43 |
| 4-33 | Closed-Loop, Movable Shutter System | 4-45 |
| 4-34 | Closed-Loop Rotatable-Vane System | 4-46 |
| 4-35 | Thermal Contact Conductance For Aluminum and Magnesium Joints in Vacuum | 4-47 |
| 4-36 | Thermal Switch for Control of Conductivity | 4-47 |
| 4-37 | Device for Contact-Area Variation | 4-48 |
| 4-38 | Cold Plate System Schematic | 4-49 |
| 4-39 | Typical Cold Plate Schematic | 4-49 |
| 4-40 | Vapor Cycle Refrigeration Schematic | 4-53 |
| 4-41 | Vapor Cycle Performance, Freon-11 | 4-55 |
| 4-42 | Vapor Cycle Performance, Freon-21 | 4-56 |
| 4-43 | Vapor Cycle Performance, Water | 4-56 |
| 4-44 | Vapor Cycle, Refrigeration Compression Ratio | 4-56 |

LIST OF ILLUSTRATIONS (Continued)


| Figure | Title | Page |
|---|---|---|
| | SECTION 4 (Continued) | |
| 4-45 | Gas Cycle Refrigeration Schematic | 4-58 |
| 4-46 | Gas Cycle Performance, Air and Hydrogen | 4-59 |
| 4-47 | Gas Cycle Performance, Compressor Work | 4-62 |
| 4-48 | Absorption Cycle Refrigeration Schematic | 4-63 |
| 4-49 | Thermoelectric (Peltier) Cooling System Schematic | 4-65 |
| 4-50 | Dependence of Maximum Coefficient of Performance on the Temperature Difference and Z | 4-68 |
| 4-51 | Basic Direct-Contact Cooling System Schematic | 4-72 |
| 4-52 | Joule-Thompson Cooler Schematic | 4-72 |
| 4-53 | Gifford-McHamon Expansion Engine Schematic | 4-74 |
| 4-54 | Performance of Expansion Engine, Infrared Cooler (Cryogenerator) | 4-74 |
| 4-55 | Power Requirements vs Attainable Temperature for Expansion Engine IR Cooler (Cryogenerator) | 4-74 |
| 4-56 | Performance of a Single-Stage Thermoelectric Infrared Cooler (Ohio Semiconductors, TU-6 Unit) | 4-75 |
| 4-57 | Infrared Cooling System, Required Radiator Areas | 4-75 |
| 4-58 | Temperature Degradation of a Typical Solar Cell | 4-77 |
| 4-59 | Effect of Solar Cell Mounting Geometry on Cell Temperature | 4-79 |
| 4-60 | Solar Cell Temperature Histories for the Various Configurations | 4-79 |
| 4-61 | Solar Cell Temperature Distribution on a Gravity Gradient Cylindrical Satellite | 4-80 |
| 4-62 | Solar Cell Temperature History During the Equinoctial Occultations | 4-80 |

## SECTION I - COMMUNICATIONS

### A. GENERAL PARAMETRIC RELATIONSHIPS

The communications aspect of the SMS study is concerned with the general relationships of all the basic parameters related to the electronic system design. The net results of this study will be to enable one to trade-off conflicting parameters such as receiver IF bandwidth, output signal to noise ratio, transmitter power, and operating frequency in order to attain a satisfactory reliable transmission system.

#### 1. General Transmission Equations

The receiver input carrier to noise ratio, C/N, for any receiver can be readily calculated from the beacon or one-way range equation. The received signal power is given by the following equation

$$P_R = P_T - [36.6 + 20 \log D + 20 \log f] + G_T + G_R - L_o \qquad (1\text{-}1)$$

The receiver noise power can be determined from

$$P_n = -144 + 10 \log B + 10 \log \frac{T_e}{290°K} \qquad (1\text{-}2)$$

where
- $P_R$ = received signal power, DBW
- $P_T$ = transmitted power, DBW
- $P_n$ = received noise power, DBW
- $B$ = receiver IF bandwidth, MC
- $D$ = one-way transmission distance, statute miles
- $f$ = operating frequency, MC
- $T_e$ = total effective noise temperature, °K
- $G_T$ = transmitter antenna gain, DB
- $G_r$ = receiver antenna gain, DB
- $L_o$ = Overall losses; line, duplexer, fading etc., DB

The effective radiated power necessary to produce a desired C/N ratio, at the receiver end, can be derived from following equations. In terms of transmitted power, $P_T$ in DBW the equation is

$$P_T = 10 \log B + 20 \log f + 20 \log D + L_o + C/N + NF_o - G_T - G_R - 167 \qquad (1\text{-}3)$$

or

$$P_T = \alpha + C/N + L_o - G_T - G_R + P_n \qquad (1\text{-}4)$$

where
- $C/N$ = Desired carrier to noise ratio
- $NF_o$ = Overall receiver noise figure $= \dfrac{(T_a + T_r) + 290°K}{290°K}$ (1-5)

$T_a$ = Effective noise temperature of antenna and transmission line at receiver input terminals (with a noiseless receiver)

$\alpha$ = Free space attenuation, DB

$T_r$ = Effective receiver noise temperature = 290 (NF-1)°K

A nomograph (Ref. 1-1) relating all the pertinent factors necessary to establish the C/N ratio versus transmitter power is given in Figure 1-1.

## 2. Factors Affecting Choice of Frequencies

The choice of frequencies for the SMS Earth-space communication links (sensor data, telemetry, command, beacon, and relay) is a trade-off between many factors, both technical and economic. The latter is included not only because of the cost of equipment, but because it may be economically imperative to use existing ground stations (for telemetry and command functions) which have been established for the Mercury, the Apollo, and other scientific satellite programs.

The technical factors which affect the transmission of a radio signal in the Earth-space communication link are:

(1) Free space attenuation

(2) Signal absorption in atmosphere

(3) Refraction

(4) Faraday effect

These effects will be described fully in the following sections.

### a. Free Space Attenuation

The total attenuation of the transmitted signal is determined mainly by the free space attenuation between the receiving and transmitting antennas, neglecting losses through the atmosphere. The atmospheric losses, in comparison, are minimal providing the elevation angle above the ground is greater than 5°. The free space attenuation follows the inverse square law and can be readily described.

$$\alpha = 36.59 + 20 \log F + 20 \log D \qquad (1\text{-}6)$$

where f = frequency, MC
D = distance statute miles

The variation in free space attenuation versus frequency, for a range of 22,240 miles (distance from satellite location in zenith to nadir, here considered a point directly below the satellite on the Earth), is shown in Figure 1-2.

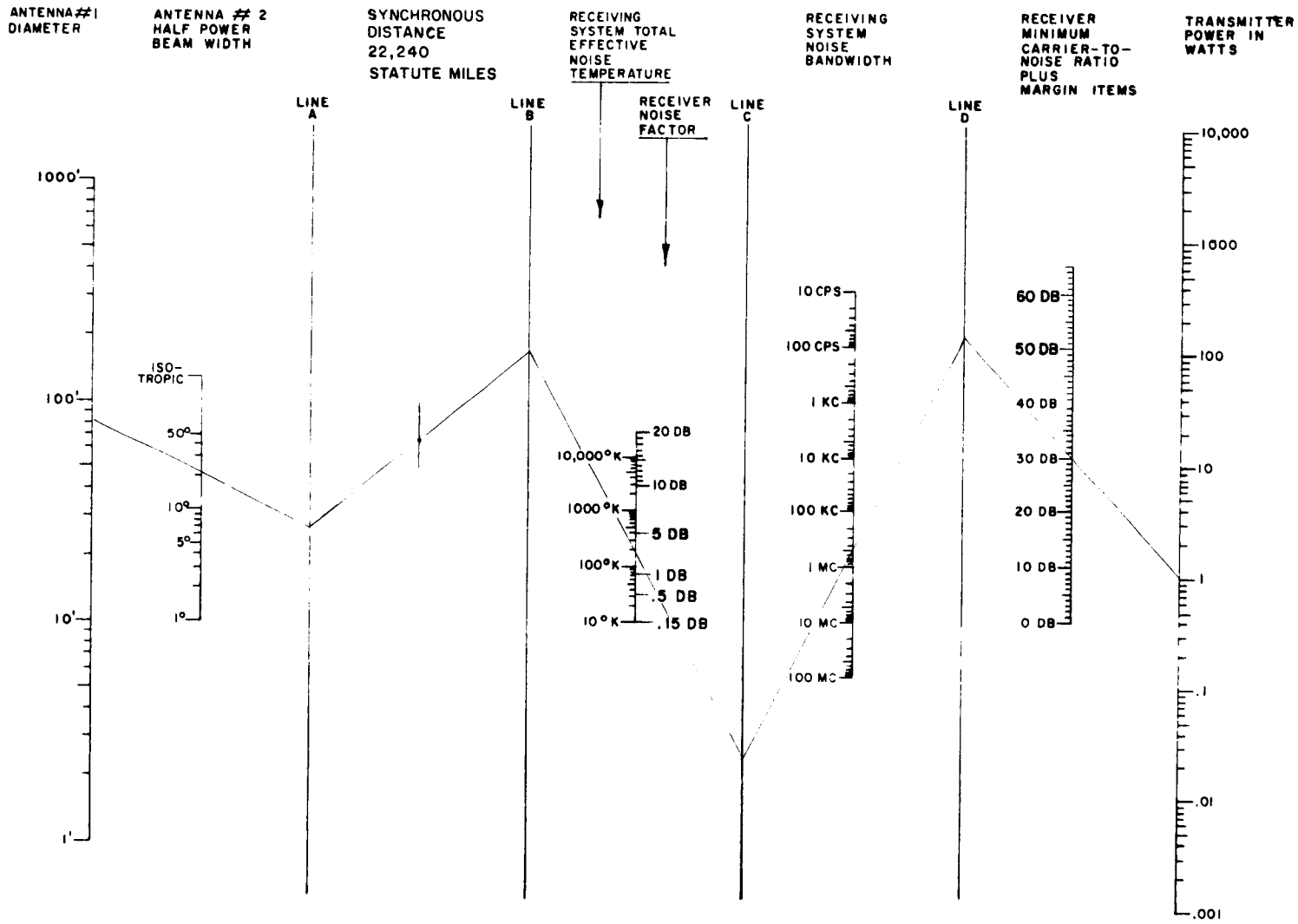


Figure 1-1. Satellite Communications Nomograph Assumed Antenna Efficiency 55%

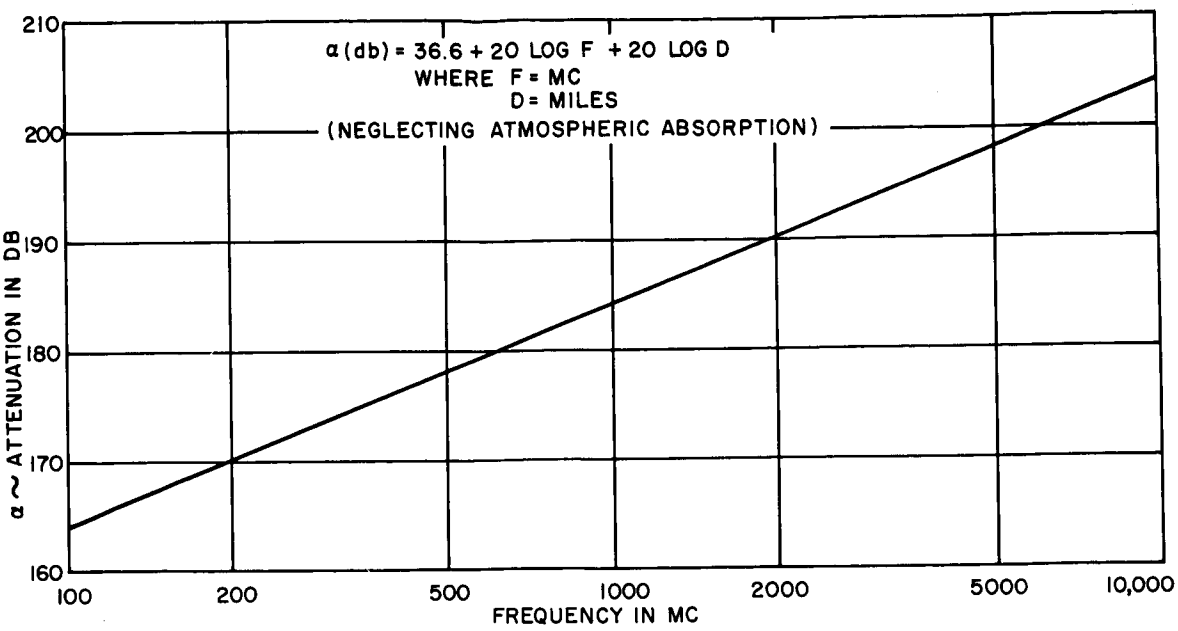


Figure 1-2. Free Space Attenuation

For simplicity, it is assumed that the SMS satellite is in a truly stabilized equatorial orbit over longitude 90°W and 0° latitude on the Earth. The slant range and additional path length free space attenuation are given in Figure 1-3 as a function of subtended angle (between the observation point and the SMS as seen from the center of the Earth) and also nautical miles from the nadir.

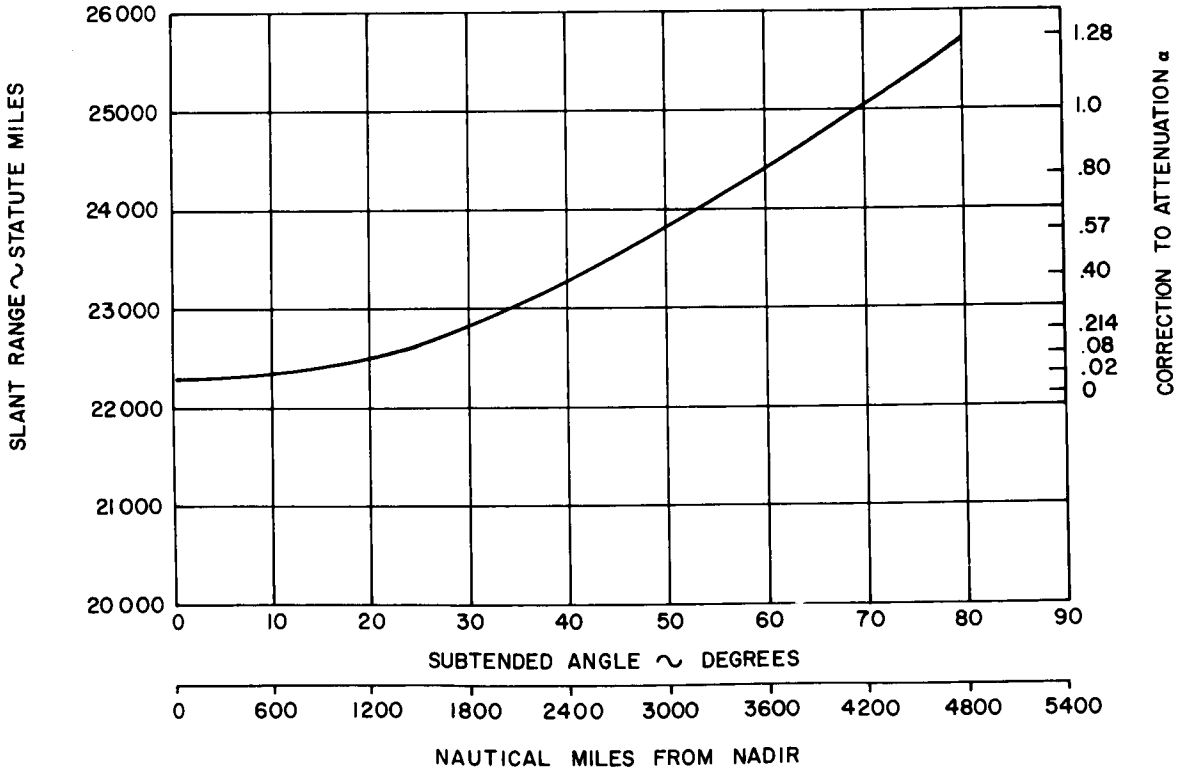


Figure 1-3. Attenuation and Slant Range Correction Curve

b. Signal Absorption

There are additional propagation losses in the troposphere and ionosphere (sometimes called atmospheric losses) which must be accounted for and added to the free space losses in order to account for the total signal attenuation. For frequencies less than 10 KMC the two major contributors to the so-called atmospheric losses are precipitation absorption and water vapor absorption.

The signal attenuation per kilometer of path length (Ref. 1-2) due to rain and fog is small for frequencies less than 5 KMC. This effect increases with frequency and is caused by partial absorption of radio waves by the water droplets in the air. Its value is normally less than 0.25 DB/km at 5 KMC for elevation angles greater than 10°.

The normal absorption losses through a humid atmosphere typical of Washington, D.C., in summer have been calculated (Ref. 1-3) and are presented in Figure 1-4

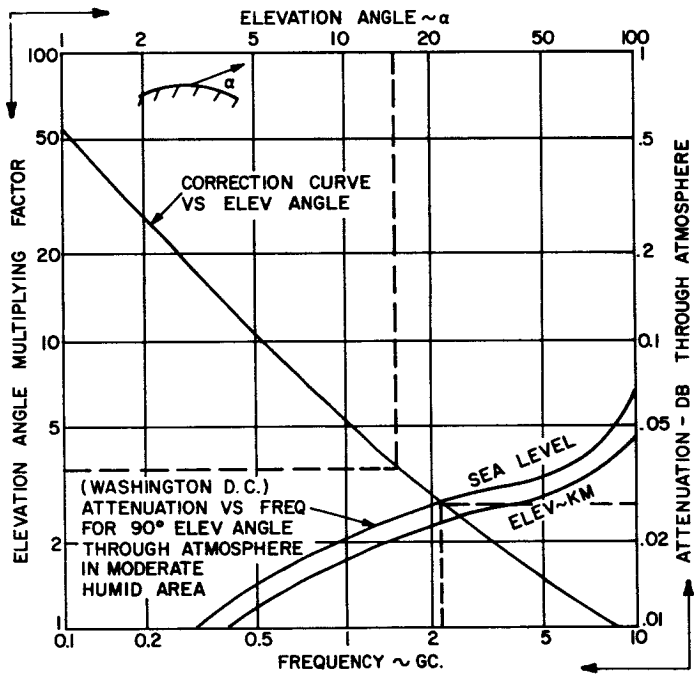


Figure 1-4. Atmospheric Losses

These calculations are for an elevation angle of 90°. A correction curve (Ref. 1-4) for other angles is also included. This correction curve is independent of frequency and increases with diminishing angular value. A correction curve showing the additional free space loss plus the atmospheric loss contribution for station locations other than the nadir is shown in Figure 1-5.

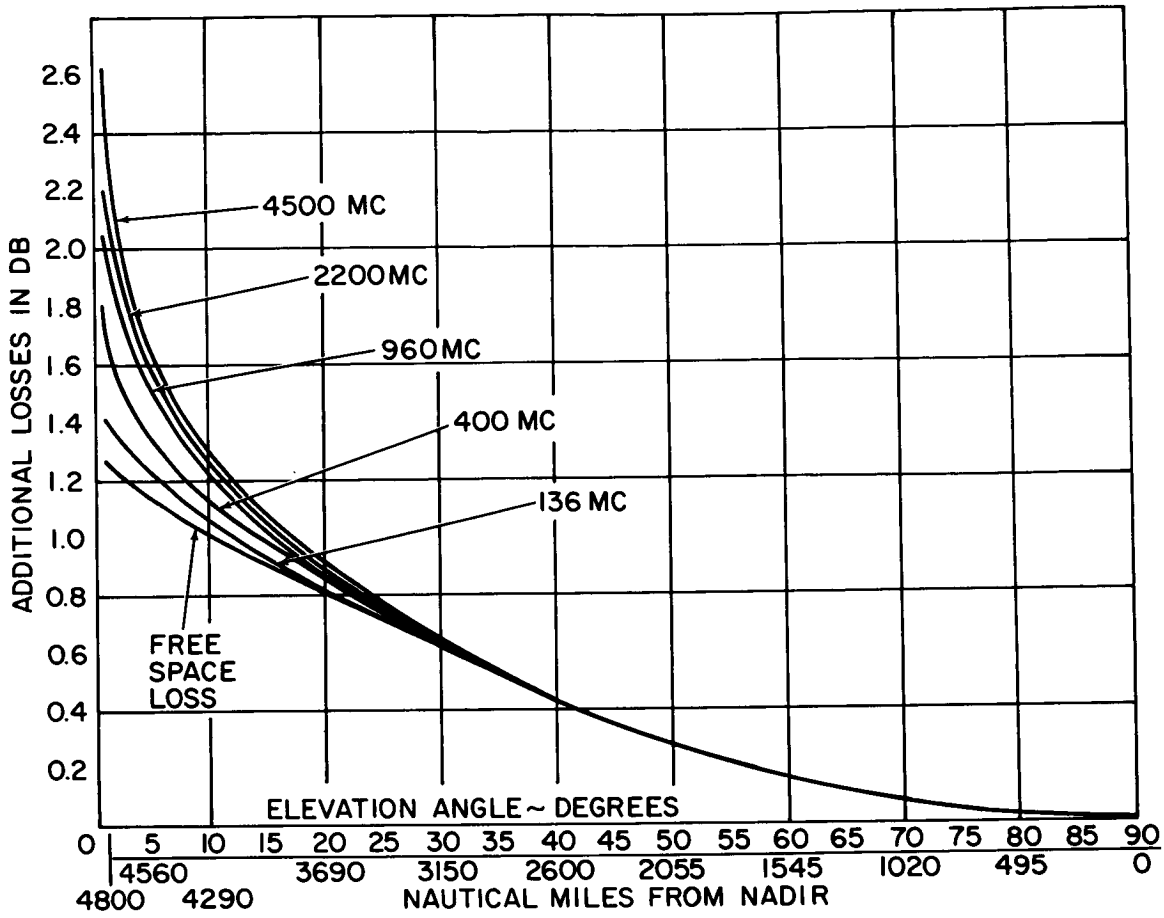


Figure 1-5. Additional Atmospheric Losses vs Elevation Angle

c. Refraction and Faraday Rotation

Refraction or bending of the electromagnetic waves through the troposphere results from the slowing down of the wave velocity in these regions resulting in an apparent angular displacement or bearing error. This error becomes negligible at elevation angles greater than 10°. See Figure 1-6. It is dependent in part upon the air temperature, total pressure, water vapor pressure and the electron density (Refs. 1-5 and 1-6). The greatest variation is found in tropical regions. The atmospheric diffraction error is considered to be frequency independent.

The ionospheric refraction error is frequency dependent but is negligible at frequencies above 1 KMC. At 100 MC the approximate ionosphere refraction error will be less than 0.1° for elevation angles greater than 10°.

This effect will be considered in more detail in the part of this section dealing with tracking and the NASA Range and Range Rate system.

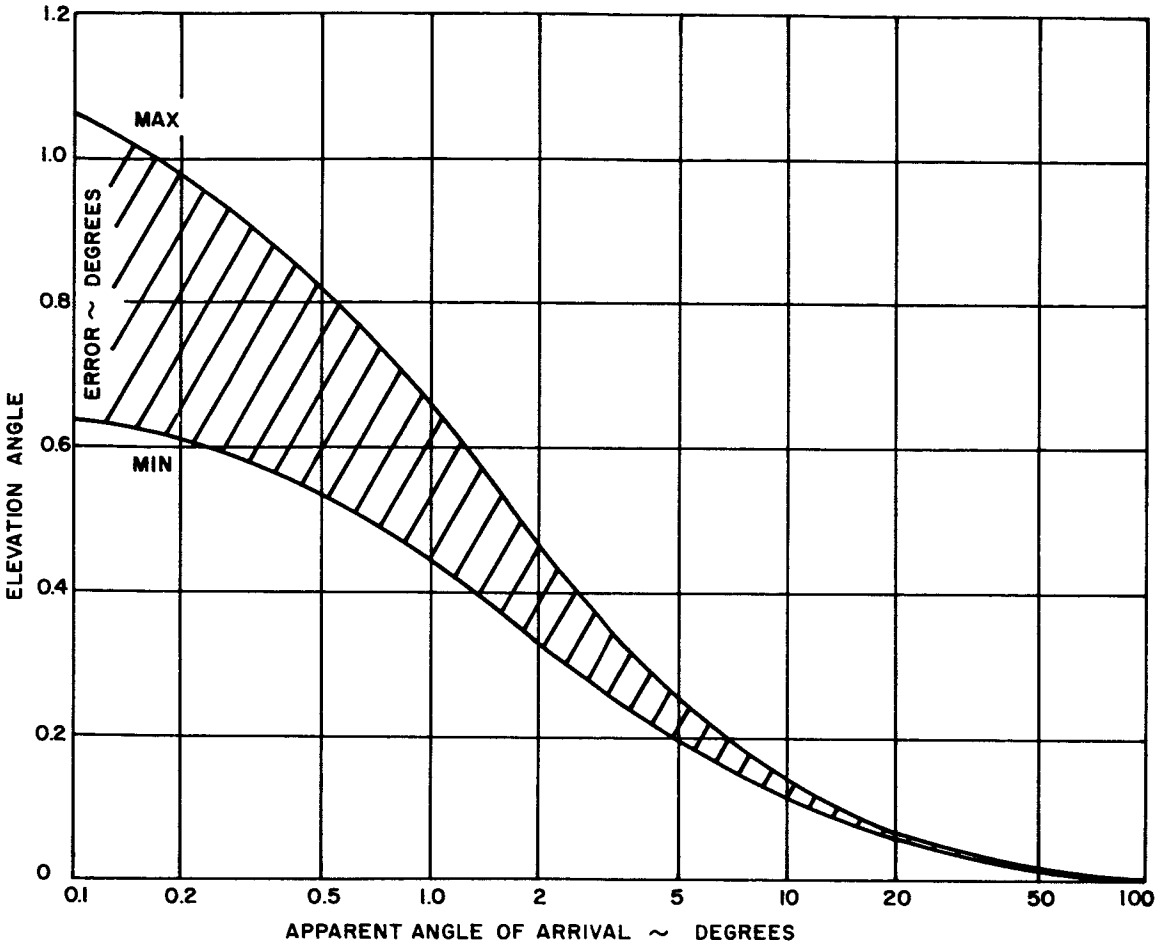


Figure 1-6. Atmospheric Refraction Errors

Faraday rotation of the radiated, plane polarized, wave is caused by interaction with the Earth's magnetic field and the free electrons in the ionosphere. The amount of wave rotation is dependent on the frequency, elevation angle and direction of the Earth's magnetic field. Under average conditions, it is negligible above 5 GC. This effect can be eliminated for all practical purposes by utilizing a circularly polarized antenna feed at the receiving end (at the expense of a 3 DB loss in signal strength) compared to that for a linearly polarized antenna assuming no Faraday effect and optimum antenna polarization alignment. Faraday rotation manifests itself as a drop-off in received signal strength as the incoming signal plane of polarization becomes perpendicular to the plane of the receiving antenna.

3. Total Effective Noise Temperature Considerations

The receiver noise power (Eq 1-2), previously described, indicates the necessity of minimizing the total effective noise temperature. Minimizing the receiver noise figure and the antenna noise contribution is required since the receiver carrier to noise ratio is inversely proportional to the total effective noise temperature which is the sum of the antenna and receiver noise temperature. The antenna noise temperature, $T_a$, and receiver noise temperature, $T_r$, contributions will be discussed briefly in the following paragraphs.

a. Antenna Temperature

The antenna effective noise temperature $T_a$, (Ref. 1-7) can be derived by assuming the antenna to be a physical resistance equal in value to its radiation resistance at a temperature T. The noise power temperature is then defined as the value necessary to produce a resistor noise power equal to the antenna noise power.

The idealized antenna (neglecting side lobes) has a noise temperature

$$T_a = \frac{\theta_n^2 T_n G}{4\Pi} \tag{1-7}$$

where $\theta_n^2$ = solid angle subtended by noise temperature source

$T_n$ = noise source temperature °K

$G$ = antenna gain averaged over solid angle

An actual physical antenna, with side lobes, has an equivalent antenna temperature

$$T_a = \sum \overline{T}_a \overline{G} \frac{\Delta\theta_i}{2\Pi} \tag{1-8}$$

where $\overline{G} \frac{\Delta\theta_i}{2\Pi}$ = averaged gain figure in direction $\Delta\theta_i$

$\overline{T}_a$ = average gain in direction interval $\Delta\theta_i$

The total noise pickup by the main and side lobes can then be summed up. Satellite-borne antennas have a noise temperature based on the contribution by galactic emission and Earth only, whereas the ground station based antennas have 3 contributions, galactic, atmospheric and Earth (black body), via the side and back lobes. This latter affect can be greatly attenuated by utilizing a wire screen ground plane to shield the antenna from the black body thermal radiation from the Earth. By this artifice, the back and side lobe contributions may be reduced to approximately 10 to 20% of the Earth temperature, i.e., 290°K.

The galactic noise contribution (Refs.1-8, 1-9, 1-10, and 1-11) to the total effective antenna noise temperature is the summation of many sources, namely; star, Moon, Earth and Sun. Solar and extra terrestrial radiation decreases with frequency above 100 MC. Above 1 KMC the received extra terrestrial noise temperature is below 20°K even in the galactic center. The galactic interference band is not uniformly distributed across the heavens but lies in a band approximately 15° wide. The major stellar noise sources in descending order are Cassiopeia, Cygnus A, Taurus A, and Centaurus A. The planets Venus and Jupiter can be

regarded as noise sources with intensity decreasing with frequency. The noise temperature from Cassiopeia will be much less since its subtended angle on Earth will be much smaller than the Sun and will occuply only a fraction of the area subtended by the antenna beam. In addition, its intensity decreases much faster with frequency than that of the Sun.

Both the Moon and Earth can be regarded for the main part as ideal black bodies with an equivalent black - body radiating temperature of approximately 290°K. The equivalent antenna temperature vs frequency as a function of elevation angle is plotted in Figure 1-7.

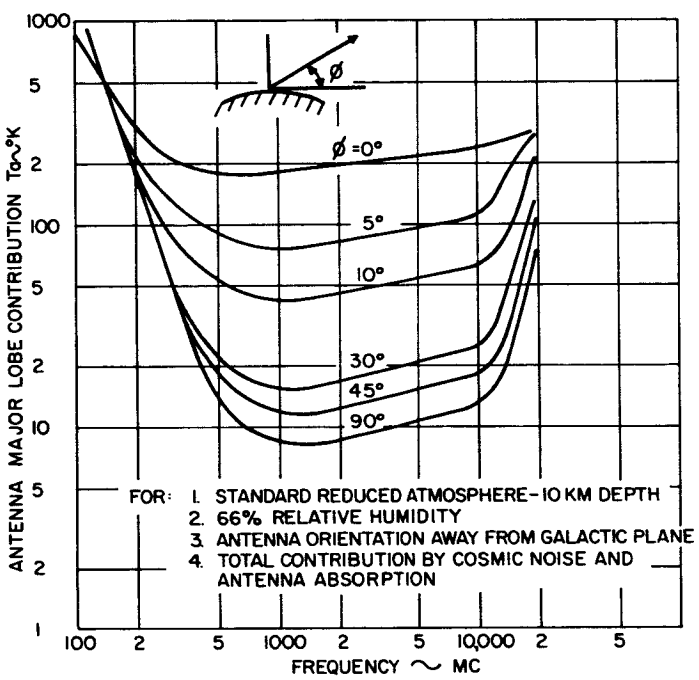


Figure 1-7. Equivalent Antenna Temperature vs Frequency

The Sun or solar noise is frequency dependent and varies with the amount of Sun spot activity. The apparent antenna noise temperature decreases from about 1,000,000°K at 30 MC to about 10,000°K at 30 KMC and is dependent upon the ratio of Sun width to antenna beam width.

The noise temperature contribution caused by pointing the antenna main beam directly at the Sun (for the case where the antenna main beamwidth is equal to or less than the angle subtended by the Sun is given by

$$T_s = \frac{675 \times 290°K}{f} \qquad (1\text{-}9)$$

When the antenna main beam bandwidth is smaller than the solid angle, $\theta$ subtended by the Sun, the resultant antenna temperature becomes

$$T_a = \frac{\theta_s^2 \, T_s \, G}{4\pi} \tag{1-10}$$

where $f$ = frequency in KMC
$T_s$ = Sun temperature
$G$ = antenna gain

provided the antenna is pointing directly at the noise source. The Sun temperature and angle correction curves are shown in Figure 1-8.

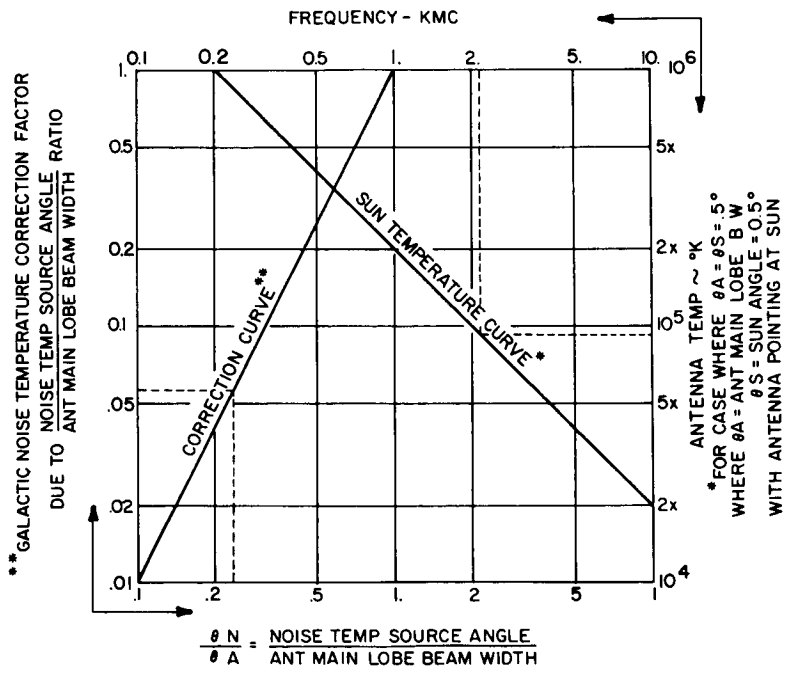


Figure 1-8. Sun Temperature Curve

The example shown in Figure 1-8 indicates that for an operating frequency of 2200 MC and a beam width of 2°, the antenna noise temperature would be

$$T_a = 9\text{x}10^4 \text{°K x Correction Factor}$$
$$= 9 \times 10^4 \text{°K} \times 0.06 = 0.54 \times 10^4 \text{°K}$$

The apparent diameter of the Sun, as seen from the Earth, appears to subtend 9 milliradians of arc (an angle of about 1/2°). The actual mean value is 31' 59". Inspection of Figure 1-8 indicates that the Sun noise temperature is in the order of $10^5$ °K at 2000 MC for an antenna greater than 60'. Assuming that the antenna side lobe levels are down approximately 30 DB from the main lobe, the side lobe Sun noise temperature (for the case of side lobes pointing at the Sun) would be $10^5$°K less 30 DB or 100°K.

It will be necessary to consider the excessive noise temperatures seen at the antenna terminals where the Sun is behind the satellite and in the main and secondary beam pattern of the ground parabolic antenna. Excessive noise temperatures will degrade the C/N ratio to such an extent that the received weather data will be unusable. For the example, above, such an appreciable increase in noise contributed by the Sun can completely disrupt communications. A curve has been prepared (Figure 1-9) showing the approximate outage time to be expected at 2200MC for antennas of various main beamwidths.

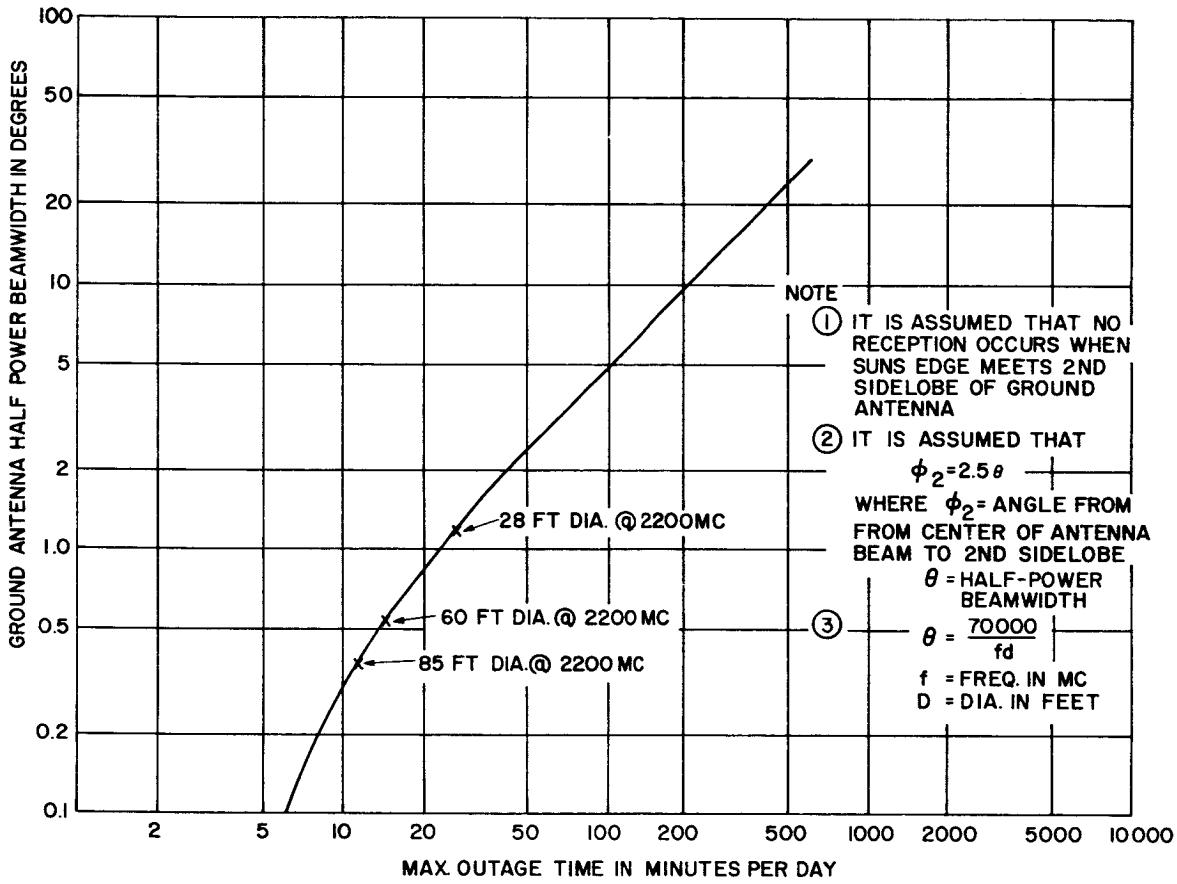


Figure 1-9. Sun Outage Time

b. Line Losses

Line losses in the microwave structure, transmission line, duplexers etc., between the antenna and the receiver front end can add materially to the total effective noise temperature when the normal antenna temperature is less than 290°K. The noise temperature at the transmission line output is

$$T_{out} = \frac{\ell - 1}{\ell} T_o + \left(\frac{1}{\ell}\right) T_a \qquad (1\text{-}11)$$

where $\ell$ = attenuation ratio (input to output)

$T_o$ = ambient temperature (290°K)

$T_a$ = external antenna temperature

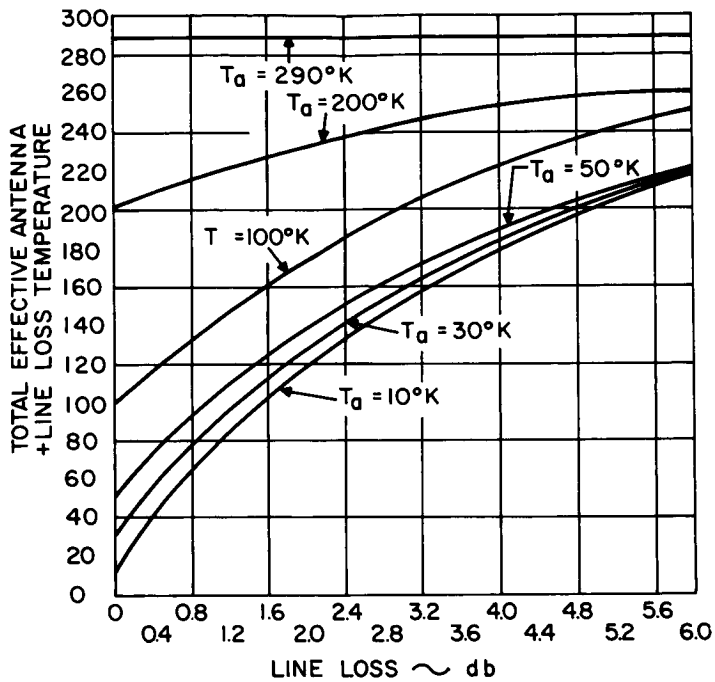


Figure 1-10. Total Effective Input Temperature vs Line Loss

This is shown very effectively in Figure 1-10. It should be remembered that the total effective antenna noise temperature adds an additional attenuation loss and consequent degraded C/N ratio in addition to that contributed by the line losses. It is especially important in low noise front ends such as the maser, parametric, and tunnel diode types, that these addidtional noise temperature contributions be held to a minimum in order to not degrade the already low effective antenna noise temperature.

c. Receiver Noise Temperature

The relationship between receiver noise temperature, $T_r$, and noise figure, NF, is given in Figure 1-11. The term noise figure denotes a noise source bandwidth product KTB equal to $4 \times 10^{-15}$ watts per MC bandwidth with a source temperature of 290°K. The noise temperature obtained by the substitution method employing a noise diode source is equal to the increase in input (source) temperature to the receiver input terminals required to double the receiver output noise level over that obtained when originally connected to a noise free source.

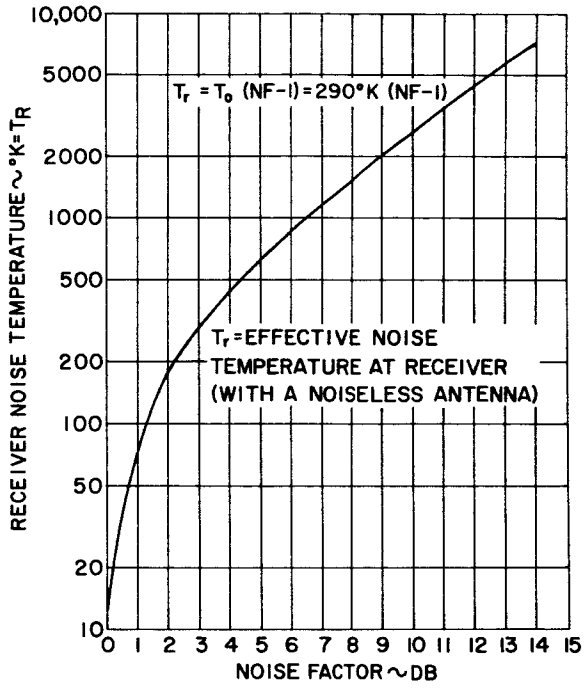


Figure 1-11. Receiver Noise Temperature vs Noise Factor

It is desirable that a receiver noise figure be employed which will not degrade the effective antenna noise temperature more than 50 percent.

The relationship of antenna temperature vs frequency due to atmospheric absorption and galactic noise was shown in Figure 1-5. It is seen that the antenna noise temperature is approximately 400 to 700°K in the range of 130 to 150 MC, the frequency range of the ground telemetry and satellite command receivers and about 8 to 50°K for the 1700 to 2200 MC band for elevation angles from 10° to 90°.

d. Front End Devices

The receiver noise figure limitation will be imposed by the type of front end employed. The lowest noise figures are furnished by the following devices:

(1) maser (helium cooled)

(2) maser (nitrogen cooled)

(3) parametric amplifier

(4) tunnel diode amplifier

(5) transistor amplifier.

A comparison of the noise temperature vs frequency for the above front end devices is shown in Figure 1-12

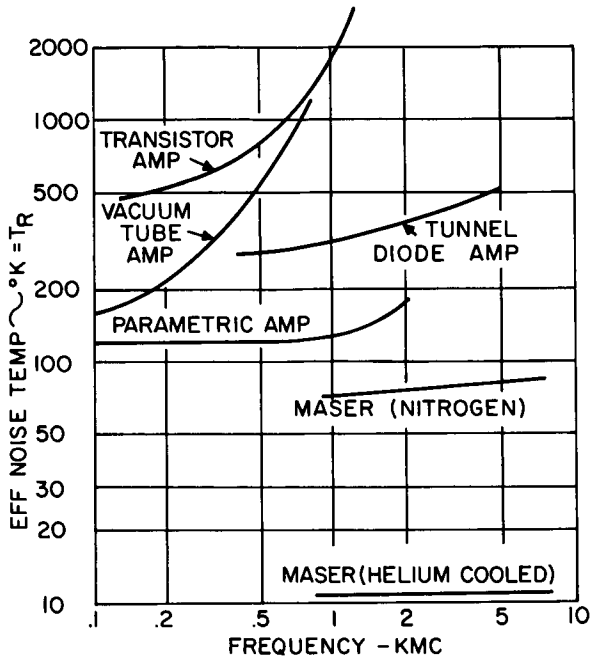


Figure 1-12. Receiver Front End Noise Temperature

The term parametric amplifier is used loosely and actually is a classification given to a group of devices (mainly semiconductor) used for amplifying and frequency converting by means of a non-linear element, normally capacitive. Its outstanding feature is a low noise figure obtained because of the stage amplification through the noiseless reactance. Resistive noise contributions can be minimized by operating at low ambient temperatures. The effective noise temperature for the various types of front ends is shown in Figure 1-12. It is not advisable to utilize a parametric type amplifier in the spacecraft in spite of its low effective noise temperature because of the requirement for an oscillator to serve as the pump. The weight of the oscillator plus its power requirements would impose a severe penalty. It is far more advantageous to use the tunnel diode pre-amplifier even though its effective noise temperature is slightly higher. The net decrease in the overall C/N ratio in the spacecraft receiver would be minimal.

Tunnel diode amplifiers use the negative resistance effect of the semi-conductor elements obtained when the tunnel diodes are DC biased in the forward direction at low voltage. The negative resistance is due to quantum mechanical tunneling on the majority carriers through the potential barriers in the heavily doped p-n junction. The diode will act as an amplifier up to its cut-off frequency.

These devices have gains in the order of 15 to 20 DB, bandwidths of 5 to 10% and noise fugures varying from 3 to 5 DB over the frequency range from 400 to 5000 MC. Hybrid circulators are interposed between the antenna and the tunnel diode amplifier as well as between the tunnel diode preamplifier and the receiver proper in order to assure unconditionally stable amplification.

Transistors can be operated as amplifiers up to nearly 2 KMC when operated conventionally, i.e., up to the frequency at which the gain drops to unity. It is possible to operate certain transistors, such as the 2N700 and 2N709, as parametric frequency converters (Ref. 1-12) and obtain gain as well as a moderate noise figure (approximately 5 DB) at frequencies in excess of 2 KMC. By this means, the effects of undesirable input phase shift and the base spreading resistance are avoided. The upper limit of performance is determined only by the transit time of minority carriers across the effective base width. As a result of the self oscillation mode of operation the noise figure and conversion gain, both attain optimum values. However, considerable work remains to be done in this field before reliable, consistent results are obtained.

The maser is a type of ultra low-noise microwave amplifier, whose operation is based upon electron spin energies within a ruby crystal heavily doped with paramagnetic ions. When a DC magnetic field is applied to the crystal, the resultant polarization produces an electron movement, at a frequency proportional to the characteristic angular velocity. Upon introducing an external RF input signal to create a circularly polarized synchronized RF magnetic field, the spin will absorb energy. Only certain spin energies can occur. In order to shift the spin from a lower to a higher energy state, the excitation must be a frequency equal to the difference in energy states, divided by Planck's constant. The microwave power so generated has a very low noise figure if the paramagnetic crystal is cooled to a very low temperature.

The entire maser installation, including refrigeration or coolant, must be mounted very close to the focal point of the antenna system in order to reduce line losses as previously discussed.

Since the ultra low-noise maser amplifier is large, bulky and expensive, it is suitable only for the ground CDA station.

e. Total Effective Noise Temperature Contributions

The total noise power, $P_n$, of a receiving system is composed of two separate sources; the antenna noise power generated at the receiver input terminals, and the receiver internally generated noise, which can be referred to the input terminals by its noise figure.

Total receiver noise power, $P_n$, can be computed from the relation: $P_n = KT_e B$ where K is Boltzmann's constant. Figure 1-13 illustrates the above relationship between receiver noise power, total effective noise temperature, and IF bandwidth.

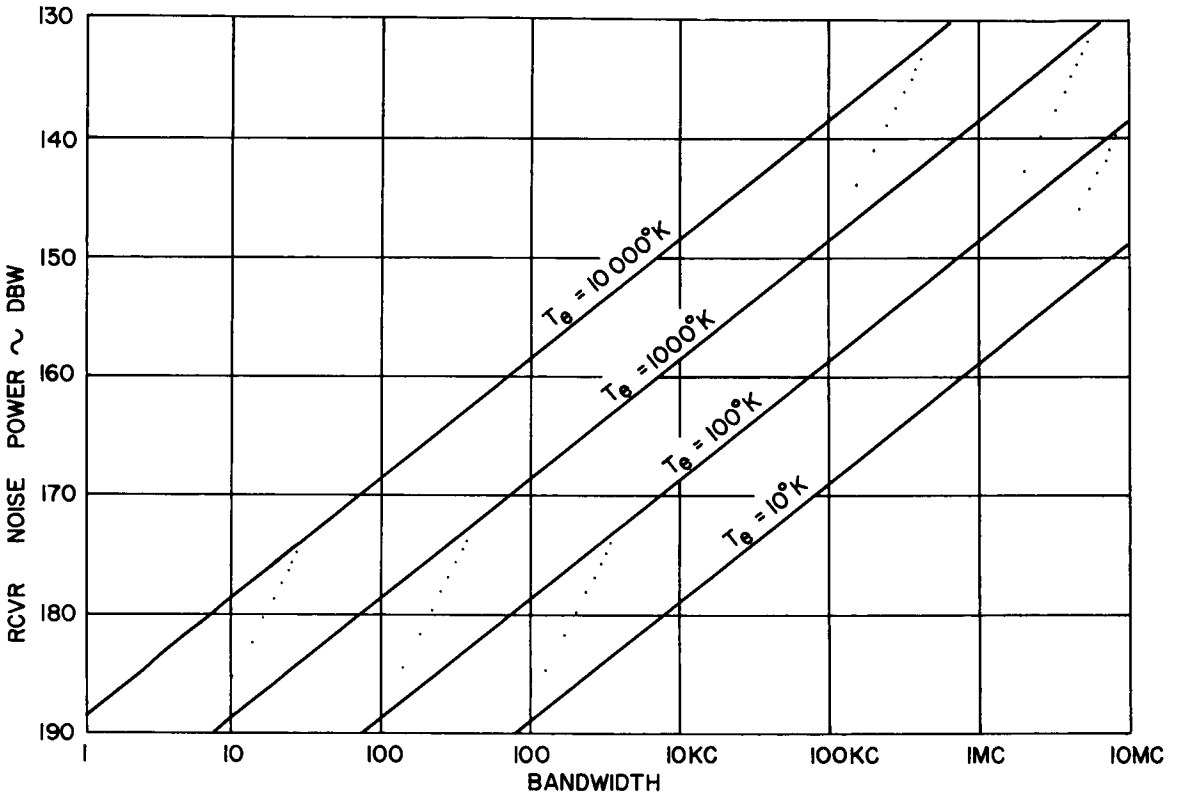


Figure 1-13. Receiver Noise vs Bandwidth

Figure 1-14 shows the effect on the total effective noise temperature of changing the receiver noise figure from 0 to 20 DB over a range of antenna input noise temperatures from 10 to 10,000°K. It is apparent from this curve that merely decreasing the receiver noise figure does not result in a system improvement until the antenna effective noise temperature becomes low.

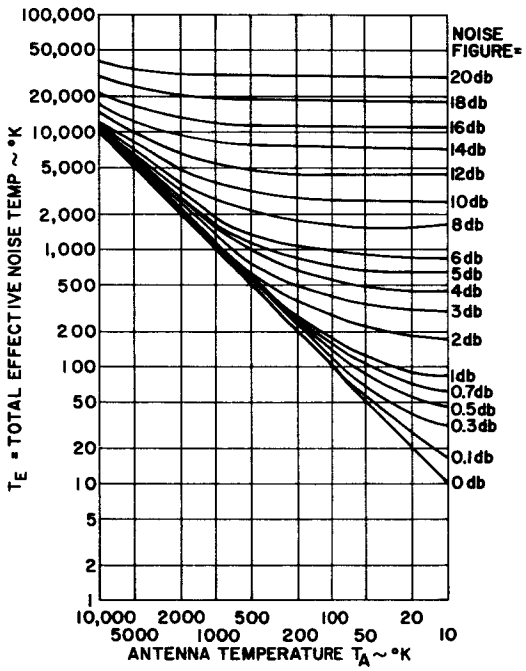


Figure 1-14. Overall Receiver Temperature vs Antenna Temperature

Figure 1-15 shows in a graphic manner the overall C/N ratio improvement in DB for a given antenna noise temperature, gained by decreasing the receiver noise figure to a lower value (Ref. 1-13). The actual improvement is the difference between the DB readings on the "Relative DB Improvement" scale.

These curves for relative sensitivity improvement (RSI) can be derived from

$$RSI = 1 + \frac{T_r}{T_a}$$

However, $T_r = 290\ (NF-1)\ °K$

$$RSI = 1 + \frac{290(NF-1)}{T_a}$$

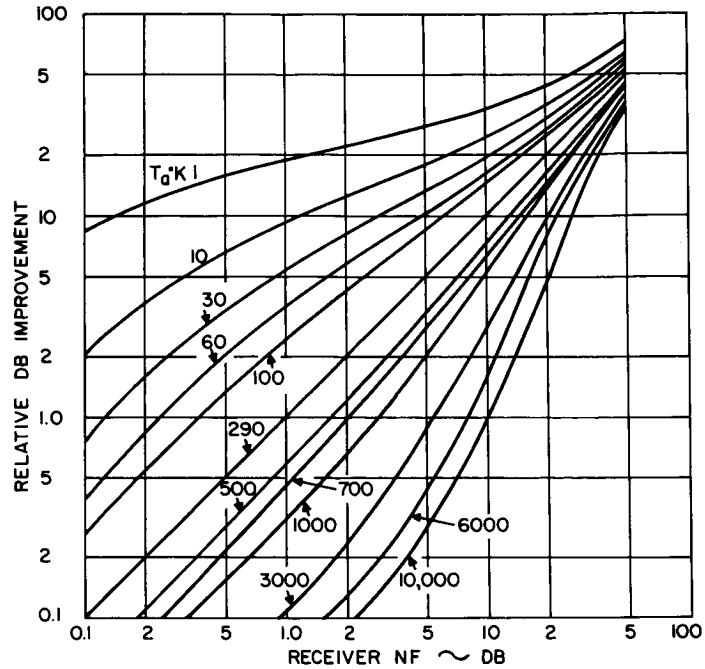


Figure 1-15. Relative Sensitivity Improvement

It is seen from the example given in the graph that the RSI is greater than the decrease in receiver noise figure. It will be found from examination of the graph that this will occur when the effective antenna noise temperature, $T_a$, is less than 290°K. However, when $T_a$ is greater than 290°K it will be found that the RSI is less than the decrease in receiver noise figure. This effect becomes more pronounced as $T_a$ differs widely from the median value of 290°K.

4. Modulation Considerations

Various carrier modulation techniques suitable for the transmission of the wide-band sensor data, the telemetry digital data, and the digital command data are as follows:

(1) amplitude modulation, AM

(2) single sideband, suppressed carrier amplitude modulation, SSB

(3) frequency modulation, FM

(4) frequency modulation with receiver negative feedback, FBFM

(5) pulse code modulation, amplitude modulated carrier, PCM-AM

(6) pulse code modulation, biphase modulated carrier, PCM-Biphase

There are two methods of information transmission; analog and digital. AM, SSB and FM are basically analog or continuous information transmission types whereas PCM-FM, PCM-AM and PCM-Biphase utilize quantized digital encoding of the original sensor data analog information.

Unquantized pulse modulation methods such as PAM (pulse amplitude modulation) and PPM (pulse position modulation) are all analog data transmission methods which have found widespread application.

a. Amplitude Modulation

An amplitude modulation, AM, transmission consists of a carrier and two symmetrical sidebands. At 100% modulation, the average carrier power is twice the sideband power. The carrier contains no information; the two sidebands contain identical data. The carrier bandwidth is twice the highest modulation frequency plus any carrier frequency variations.

Severe frequency-selective fading resulting in excessive intermodulation and harmonic distortion can result if the propagation path introduces frequency-variable time delays. Such delays would be caused by the ionosphere at certain frequencies if the antenna elevation angle of the ground receiving station were low and the various ionosphere levels were grazed by the transmitted signal. If the information contained in both sidebands can be correlated in the detection process, a 3 DB improvement will result as compared to the use of a conventional AM receiver with an envelope detector. This can be done by using synchronous detection techniques utilizing two channels. One channel is a normal or zero phase, phase channel and the other is a quadrature, or 90 degree phase channel. A common local oscillator, tuned to the incoming carrier, is provided to produce a zero frequency carrier. The phase of the local oscillator is adjusted so that the contributions of the two sidebands reinforce each other.

b. Single Sideband

In single sideband transmission, only one of the two sidebands of the suppressed (pilot) carrier is used. For detecting single sideband transmissions a local carrier that is identical in frequency and phase to the original suppressed carrier must be inserted at the receiver. This type of transmission is not subject to selective frequency fading since there is no carrier present. The only effects of propagation differential time delay is the destruction of the original phase relationships among the various sideband components. This is not serious in voice communications; however, waveform dependent information (such as video data) can be seriously degraded. SSB has a 9 DB carrier to noise advantage over AM for the same power output since the carrier and one sideband are absent.

The AM threshold is also called the tangential sensitivity point and refers to the sensitivity at the level when a digital pulse can just be detected above the peak amplitude of the background noise. At this point the RMS (effective) signal power is just equal to the RMS noise power. The peak value of the noise power is approximately 13 DB higher, however, contrasted to the 3 DB difference between the peak and RMS value of the signal power.

c. Frequency Modulation

A frequency modulation transmission consists of a carrier plus symmetrical sidebands composed of components spaced at modulation frequency intervals. The number and relative amplitudes of these sidebands are determined by the modulation frequencies and the modulation index m which is the ratio of the maximum carrier frequency shift or deviation $\delta F$ to the highest modulating frequency $f_m$. FM systems provide an advantage over AM systems in that higher signal to noise, S/N, ratios can be obtained by employing higher values of modulation index. When the signal level is increased about 10 DB so that the RF peak signal is equal to the peak noise the FM improvement threshold is attained (Figure 1-16). As the signal is increased the noise is reduced and suppressed, not masked as in AM or SSB. When the signal level is below the threshold value, the performance of a simple FM system degrades rapidly and becomes worse than a simple AM system.

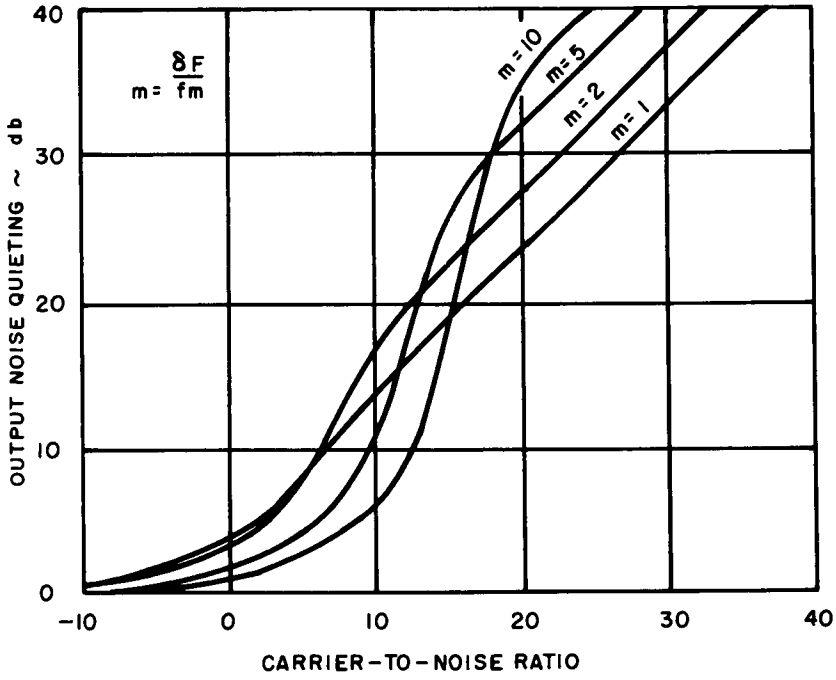


Figure 1-16. Typical FM Threshold Curves

When the FM receiver is operated above the threshold value, the S/N relationship at the limiter output (discriminator input) is in excess of the input carrier to noise relationship by the factor

$$S/N = 3m^2 (C/N) \tag{1-14}$$

This curve is plotted in Figure 1-17. Thus by increasing the modulation index, an improvement in output S/N can be obtained. However, this is at the expense of

increased bandwidth, which indicates that the transmitter power has to increase in order to maintain the original C/N ratio, if the FM S/N improvement is to be realized.

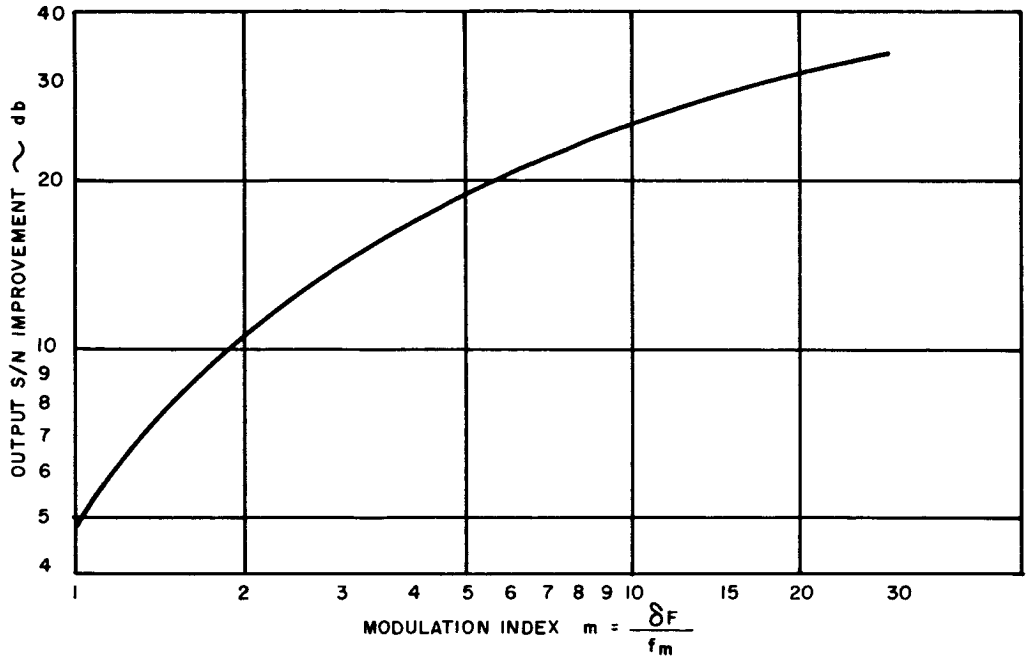


Figure 1-17. FM S/N Improvement Ratio

As previously stated the receiver IF bandwidth, B, is related to the modulation index, m, by

$$B = 2f_m (1 + m) \tag{1-15}$$

This value of bandwidth will be sufficient to recover 99% of the signal energy in the signal spectrum.

FM has a noise power reduction advantage over AM of

$$R = 3m^2 \tag{1-16}$$

for 100% AM modulation and equal average output power.

On the basis of the same peak transmitter power SSB has a noise advantage over AM of about 8 to 1 (approximately 9 DB). When peak power is used as the comparison basis, FM has an additional noise advantage of about 4 to 1 or approximately 15 DB total over AM. The noise advantage of FM as compared to SSB is

$$R = \frac{3f_m^2}{2} \tag{1-17}$$

d. FM Demodulator with Negative Feedback

The FM receiver output S/N ratio can be increased considerably by employing a modulation technique that trades bandwidth for S/N ratio. Such a trade-off can be obtained by utilizing FMFB (FM Demodulator with Negative Feedback) and thus enhance the signal (Refs. 1-14 and 1-15). A simplified block diagram of this circuit is shown in Figure 1-18.

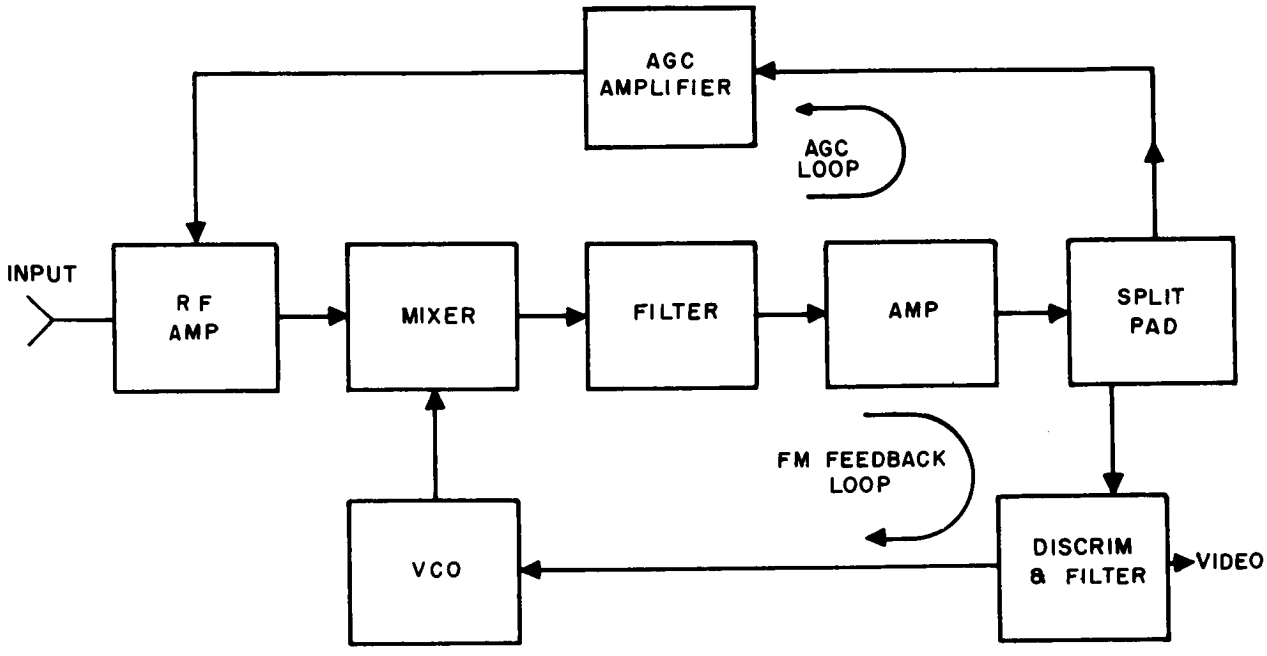


Figure 1-18. FMFB Receiver Block Diagram

FMFB serves as an AFC loop to resonate a VCO at the exact frequency being received at any instant, despite the video signal varying over a wide frequency band. The result is a reduction of the deviation ratio or modulation index of the IF signal relative to the index of the RF input signal. This effect is negative feedback and results in a reduction of the IF index or deviation ratio to D/F where F is the feed back factor. Since the IF index is smaller than the corresponding RF value, the IF noise bandwidth can be reduced considerably and an improved threshold can be obtained compared to the conventional FM threshold. The minimum noise bandwidth of the IF filter must exceed $2f_m$. The purpose of the AGC loop is to maintain the FM feedback (loop gain) proportional to the carrier level at the discriminator input. The FMFB S/N output is the same as conventional FM above the threshold, i.e.,

$$S/N = 3m^2$$

The optimum value of feedback for any value of S/N ratio above threshold and transmitted modulation index can be obtained from Figure 1-19.

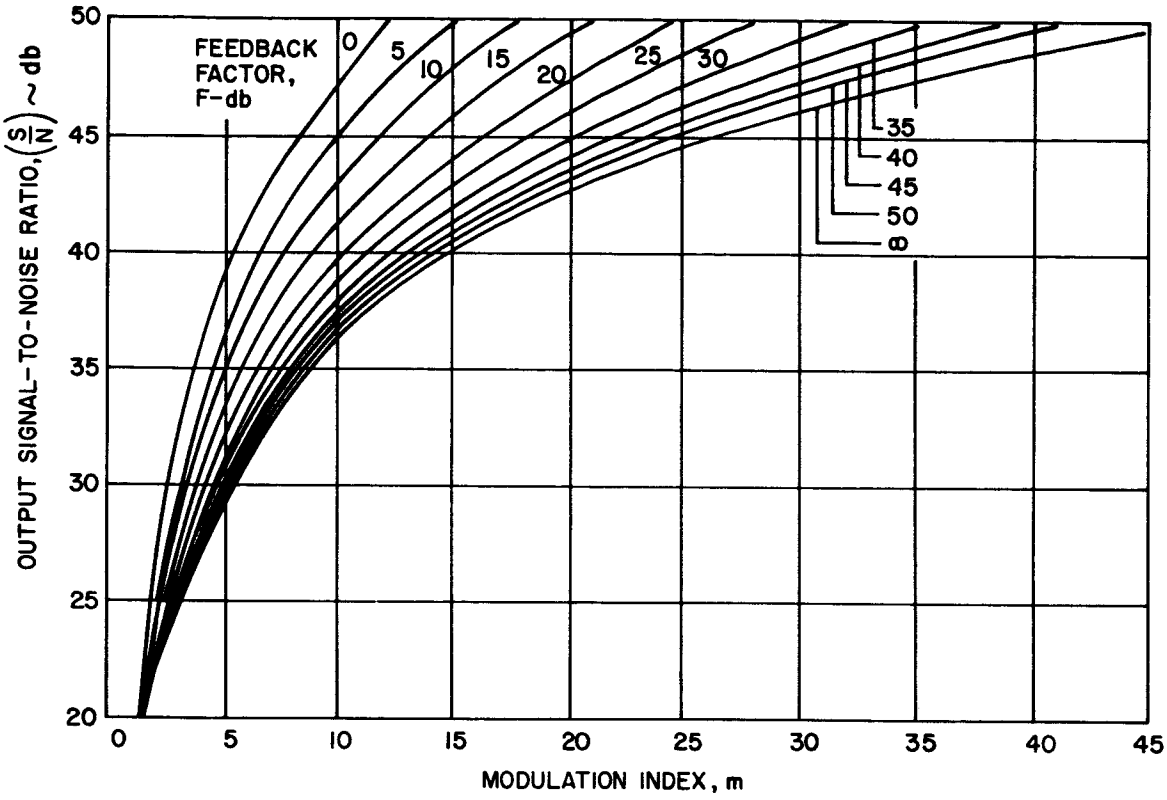


Figure 1-19. Design Parameters for Optimum Feedback FM Systems

The transmitted modulation index and therefore the IF amplifier bandwidth, B, is reduced by the amount of negative feedback introduced

$$B = 2\left(1 + \frac{m_{rf}}{F}\right) f_m$$

where $m_{rf}$ = transmitted modulation index

Stability criteria in this feedback system limits the amount of feedback to less than 50 DB. The system can be optimized (Ref. 1-16) for any application by choosing the modulation index which produces the minimum desirable S/N ratio at the quieting or improvement threshold. This is accomplished by employing the proper amount of negative feedback which in turn will determine the carrier power vs bandwidth trade-off. Nonoptimum modulation indexes, especially lower values, can increase the power requirements by 10 or more.

Upon applying negative feedback to an already existent FM receiver (suitably modified), it will become necessary to increase the transmitter modulation index in order to maintain the original desired S/N ratio.

The use of feedback will result in the following characteristics

(1) lower net receiver IF modulation index $\frac{m_{rf}}{F}$

(2) narrower IF bandwidth

(3) lowering of the improvement threshold

(4) increased threshold output S/N ratio

e. Phase-Lock Loop Detection

An advanced technique in communications system design for detecting small signals in noise is to use a phase-locked loop detector with either FM or AM receivers. A typical phase-lock loop detector is shown in Figure 1-20. It should be noted that it is very similar to FMFB previously described. Phase-lock correctly applied to a circuit can result in a significant decrease in the signal power required. This is accomplished by the reduction of receiver bandwidth of the phase-lock loop. This produces a reduction of the noise introduced into the receiver and thus increases the C/N ratio.

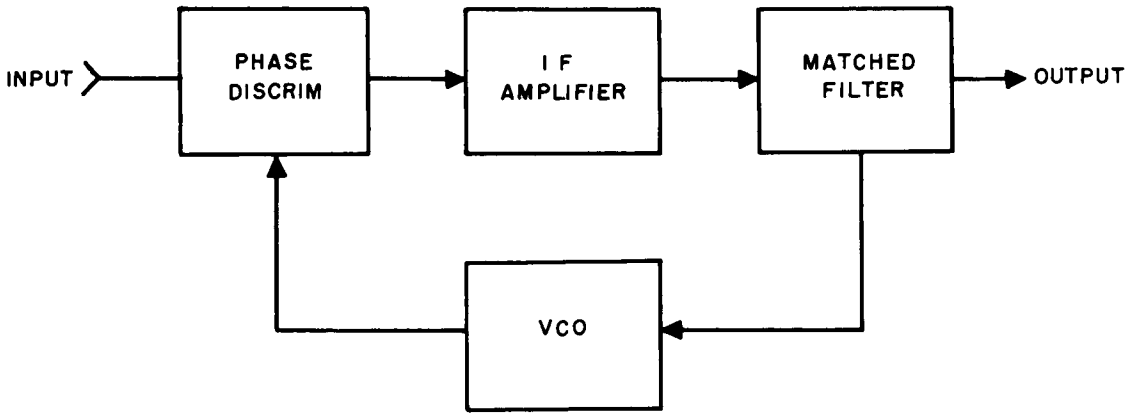


Figure 1-20. Phase-Locked Loop Detector Block Diagram

It is also possible to obtain reception with low C/N ratio by employing coherent detection techniques. This is possible when the receiver is optimally designed to receive a digital signal of known waveform. Basically, this is done in the receiver by cross correlation of the incoming signal and noise with an internally generated replica of the transmitted waveform and comparing the result with a fixed threshold. The correlation output will indicate the presence of a signal. The process of cross correlation is performed by either one of the two following methods:

(1) Passing the received signal through a linear (Weiner type) filter with an impulse response that is the inverse of the transmitted waveform (matched-filter method).

(2) Multiplication of the received signal with the replica of the transmitted waveform and integration of the product multiplier-integrator method.

The phase-lock loop and cross correlation detection methods are ideally suited for the reception of narrow bandwidth signals such as telemetry data from the spacecraft.

The FMFB detector and phase-locked detectors are of the synchronous or homodyne detector type. It is mandatory that this type of detector be utilized for PM detection, but it is optional for FM detection. This type of detector affords about a 4 DB S/N advantage compared to a non-synchronous detector.

f. Receiver Bandwidth

The normalized receiver bandwidth vs base or highest modulating frequency relationship for transmission system suitable for sensor data transmission are shown in Table 1-1.

TABLE 1-1
BANDWIDTH COMPARISONS

| Modulation Type | Receiver IF Bandwidths |
|---|---|
| AM | 2 |
| SSB | 1 |
| FM | $2f_m$ (1+m) contains 99% of RF energy |
| FM | $2.8f_m$ (1+m) contains 99.9% of RF energy |
| PCM Bandwidth | Practically 2 ($f_m$ x n); theoretically ($f_m$ x n) |
| PCM-AM | Practically 4 ($f_m$ x n); theoretically 2($f_m$ x n) |
| (FSK) PCM-FM; 99% | 2($f_m$ x n) (1+m) |
| PCM-Biphase | 2n $f_m$; theoretically |
| PCM-Biphase | 4n $f_m$; practically |

where $f_m$ = highest modulating frequency

n = number of bits to encode each sample

m = modulation index = $\frac{\text{carrier swing}}{f_m} = \frac{\delta f}{f_m}$

It is assumed in the PCM transmission system that, 1) the percentage of modulation is unity, 2) that $f_o \tau = 0.5$, where $f_o$ is the cut-off frequency of the ideal low pass filter preceding the decoder and $\tau$ is the percentage time occupied by the binary code pulse, and 3) that a sinusoidal modulating waveform is assumed.

It will be noted the carrier or receiver bandwidths for SSB and AM are 1 and 2 times respectively the information bandwidth depending whether the upper and lower sidebands are transmitted. The receiver bandwidths for 99% retrieval of FM transmission and the PCM-Biphase modes are the same whereas the PCM-FM mode is extremely inefficient and extremely wasteful in bandwidth for large sampling rates.

It may be necessary to make the IF bandwidth (if a superheterodyne circuit is employed) larger than theoretically required by the modulation technique employed, in order to allow for local oscillator drift.

The final overall S/N ratio is defined by 1) the C/N ratio obtained as a result of the one way transmission equations and selected system parameters, 2) the modulation technique employed, i.e., FM, SSB which may produce an output S/N ratio greater than the input C/N ratio depending upon the system employed, and 3) the S/N ratio of the original signal input to the transmitter.

The effect of cascading these three logarithmetic S/N quantities is shown in Figure 1-21. It will be noted that a degradation of 1 DB in the overall received signal requires that the effective communication channel S/N be 6 DB greater than the input S/N ratio.

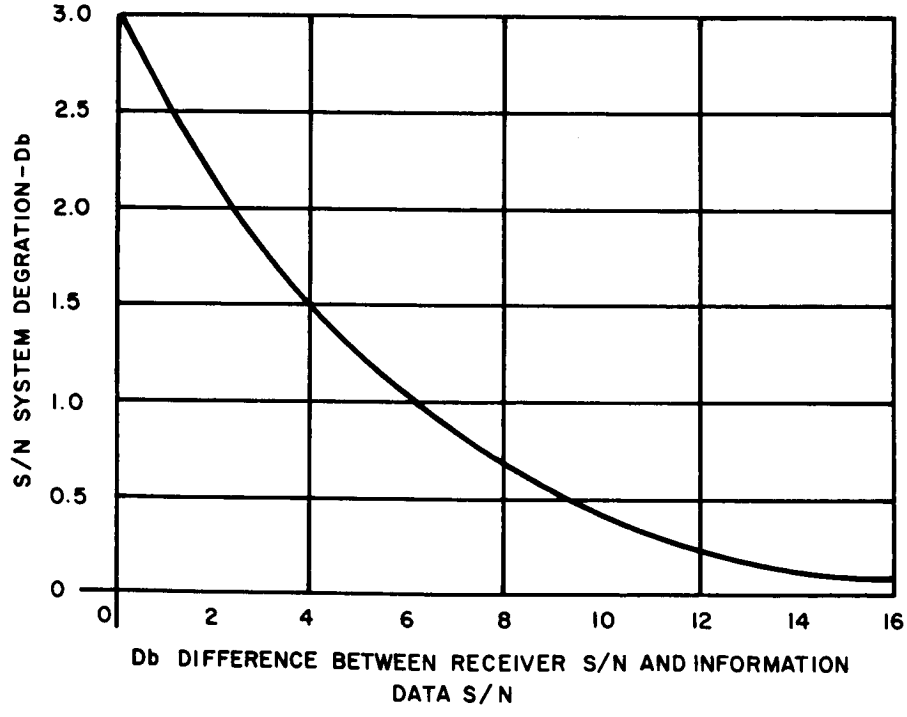


Figure 1-21. Degradation Caused by Combining Two Signals

g. Comparison of Transmission Systems

Table 1-2 (Ref. 1-17) lists improvement ratios of various pulse systems (compared to a fully modulated, conventional AM system with the same carrier power and the same RMS noise per unit bandwidth in the carrier channel) as well as the improvement threshold values, relative to noise. These systems are normally used in telemetry transmission.

TABLE 1-2
MODULATION SYSTEMS COMPARISONS

| SYSTEM | IMPROVEMENT RATIO | RMS CARRIER THRESHOLD |
|---|---|---|
| AM | 1 | — — — — |
| FM | $\sqrt{3}D$ | $\frac{4K_1(B\,\delta\,f)^{\frac{1}{2}}}{\sqrt{2}}$ |
| PAM-AM | 1 | — — — — |
| PAM-FM | $\frac{\pi r^{\frac{1}{2}} D}{\alpha}$ | $\frac{4K_1(B\,\delta\,f)^{\frac{1}{2}}}{\sqrt{2}}$ |
| PDM-AM | $\sqrt{\frac{2f_m}{\alpha x N}}$ | — — — — |
| PDM-FM | $\sqrt{6}\,\delta\,F/\alpha\,\sqrt{fm\,N}$ | $2\left(2f_m\right)^{\frac{1}{2}} K_2$ |
| PDM-AM | $\frac{5f_m}{4\alpha N}$ | $4\,K_2\,N^{\frac{1}{2}}$ |
| PCM-AM | — — — — | $2\,K_2\,(2MN)^{\frac{1}{2}}$ |
| PCM-FM | — — — — | $2(2f_m)^{\frac{1}{2}}\,K_2$ |

Legend

| | | |
|---|---|---|
| D | = | deviation ratio $= \frac{\delta f}{f_m}$ |
| B | = | bandwidth |
| $\delta F$ | = | peak frequency deviation |
| $f_m$ | = | highest video frequency |
| m | = | number of pulses per sample |
| $\frac{1}{\alpha}$ | = | fraction of time pulse is on (duty cycles) |

| | | |
|---|---|---|
| F | = | sampling rate |
| $K_1$ | = | RMS fluctuation noise per unit root IF bandwidth |
| $K_2$ | = | RMS fluctuation noise per unit root at AM demodulator output |
| r | = | Ratio of highest video frequency to sampling rate |

h. Comparison of FM and PCM Systems

PCM method of modulation has many advantages over the other digital methods but at the expense of a wider transmitted bandwidth. In this system the amplitude range of the analog signal is divided into a discrete number of steps (quantized) and a code combination is assigned to each step. If a binary code is used, the number of amplitude values which may be distinguished is $2^n$ where n is the number of digits required for each sample. A four digit code can represent 16 amplitude levels and a 5 digit code permits 32 levels. Each additional digit provides a 6 DB noise advantage but also requires an increase in bandwidth in proportion to the number of digits.

The output S/N ratios are determined when the signal level is greater than 1 DB above the threshold.

Above the threshold, the receiver IF bandwidth will increase linearly with the number of quantized levels. Therefore, the output S/N ratio for a binary PCM system will increase linearly with the bandwidth increase whereas in an FM system the S/N ratio in DB will increase as the logarithm of bandwidth.

Inspection of Figure 1-22 reveals a cross-over point (Ref. 1-18) between the two systems as the relative bandwidth is increased to a normalized value of 5. Unless an output S/N ratio of much over 40 DB is desired, no significant gain is achieved through the use of PCM over the more conventional and readily implemented FM system.

Theoretically, PCM-Biphase modulation is one of the most attractive approaches to high data transmission rates available. In this technique the binary coded data, in a nonreturn to zero form (NRZ), is used to attenuate the carrier phase, i.e., shift the transmitter carrier phase through 180 degrees each time the binary cycle code changes from 0 to 1 or vice versa. PM has the advantage of being, 1) insensitive to level variations, and 2) able to transmit low or zero modulating frequency. It is able, theoretically, of utilizing the least bandwidth for a given transmission bit rate. Practically, phase modulation transmission methods have very great difficulty in approaching the theoretical superiority over other modulation methods such as PCM-FM, FSK, etc. Any variation in phase shift such as atmospheric effects will affect the accuracy of results. Another major problem is phase ambiguity caused by external disturbance, man made or electrical storms. Any signal interruption will result in the decoder being unable to determine whether the first data pulse after the interruption is the reference phase or whether it is a mark or space (1 or 0). If the decoder makes the wrong decision all other data transmitted after the interruption would be completely misinterpreted resulting in a completely garbled message unless a reference timing pulse and/or pilot

tone is transmitted. Such techniques reduce the system efficiency. Most of the theoretical 2 DB advantage over FM and 7 DB over AM for the ideal pulse modulation system is lost in preventing phase ambiguity. It is possible to achieve the maximum theoretical advantage, at this time, by the use of complex circuitry and high signal power levels.

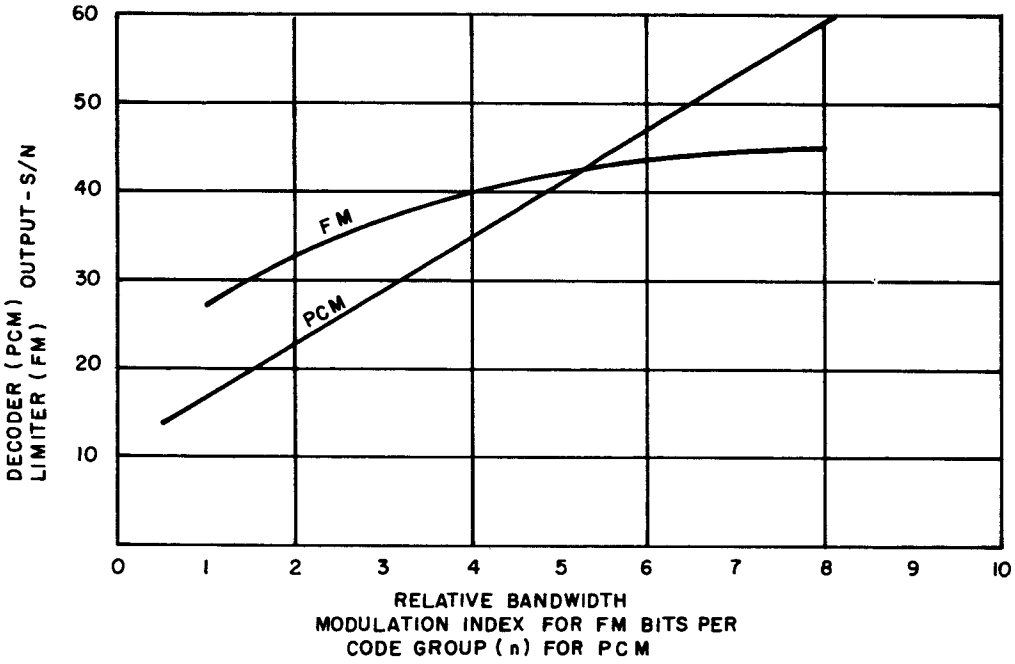


Figure 1-22. Comparison of FM vs Binary PCM (Above Threshold)

The apparent power advantage of phase modulated PCM is based on the more efficient utilization of power at the detector. PCM-Biphase possesses a 4 DB improvement over FSK and is a potential property of any waveform polarity reversal technique over one using independent signals (Ref. 1-19). A binary amplitude modulated PCM system is at best no different than a phase reversal method, except for the presence of a carrier that takes half the available power without carrying any information. The real advantage of coherent phase detection comes from the modulation output generated by the cross correlation of the signal and the coherent reference.

It is necessary that phase-lock or synchronization be maintained between the receiver and transmitter in a PCM-Biphase system to permit optimum pulse decoding. It is normally necessary that the phase reference signal be transmitted by means of another carrier signal or else the reference signal can be recreated by use of correlation techniques from the signal itself and so achieve coherent detection. This added complexity and penalty should be weighed when considering any PCM-PM system.

A comparison of the receiver IF bandwidths for various modulation systems vs information bandwidth expressed in the proper terms for each type system is shown in Figure 1-23. It will be noted that a practical realizable PCM-Biphase system requires more IF bandwidth than a comparable FM analog system.

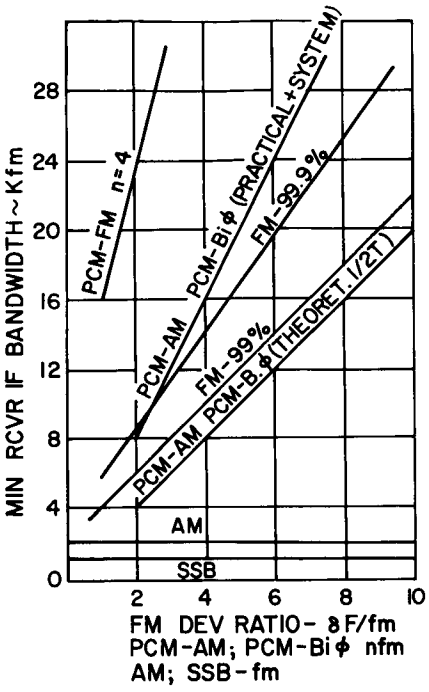


Figure 1-23. Receiver IF Bandwidth vs Modulation System

The S/N ratio at the output of the PCM decoder or decision circuit will increase as the square of the number of bits n, per code group, and is determined primarily by the quantization noise. The quantization noise results from the fact that the samples are represented by a discrete number of steps. Once quantized, the original instantaneous sampled values can never be restored or recreated exactly. The amount of error (noise) introduced by this process can be reduced to any desired value by increasing the number of quantum steps, thereby reducing the amplitude between each step. For a binary PCM system

$$S/N\ DB = 10 \log 12 + 20\, n \log 2$$

$$S/N\ DB = 10.8 + 6n$$

where $S/N = \dfrac{\text{peak signal}}{\text{RMS noise}}$

The above formula can be represented in tabular form:

| n | Min S/N (DB) |
|---|---|
| 2 | 22.8 |
| 3 | 28.8 |
| 4 | 34.8 |
| 5 | 40.8 |
| 6 | 46.8 |
| 7 | 52.8 |

It will be noted from Figure 1-24 that PCM-Biphase does not assume any advantage ever the particular FMFB system shown until its output S/N is over 53 DB. In general, a PCM-PM system utilizing an ideal phase coherent detection system requires about 3 to 5 DB less power than an equal quality conventional FM system but requires about 5 DB more power than a feedback FM system using 35 to 40 DB of feedback. However, the PCM system will require about 40 to 50% of the spectral bandwidth of the FMFB system.

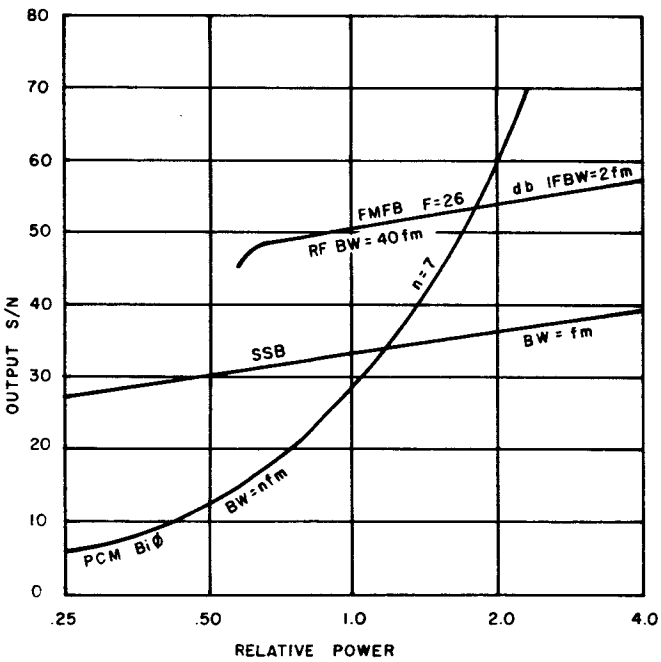


Figure 1-24. Output S/N vs RF Power Output

The error rate analysis of binary digit transmission is based upon the contribution of false pulse noise or the error caused by the receiver misinterpreting whether a fixed amplitude pulse was or was not transmitted during the sample interval. The number of errors resulting from the decoding process are related to the magnitude of the peak current level to the RMS noise level ratio at the decorder input. Figure 1-25 is a plot of error rates of PCM-AM, PCM-FM, PCM-Biphase and FSK vs C/N.

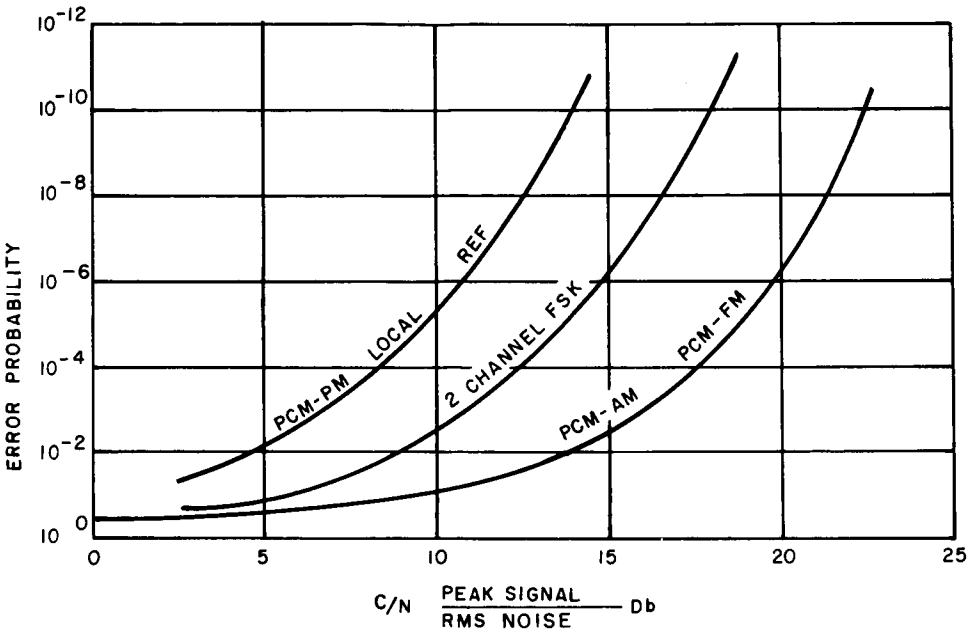


Figure 1-25. Error Probability

A comparative tabulation (Refs. 1-20 and 1-21) taken from this graph shows S/N ratios required for a $10^{-4}$ error probability are as follows.

| Modulation Technique | S/N |
|---|---|
| PCM-AM | 17 DB |
| PCM-FM (Discriminator detector) | 17 DB |
| FSK (2 channel) | 12 DB |
| PCM-Pm (Biphase-local refl.) | 8 DB |

The above curves are based on the assumption that the receiver noise is uniformly spread over the receiver bandwidth and that its amplitude characteristic is gaussian in distribution.

5. Antenna Considerations

Antennas are basic transition devices of any electronic system which depends on free space as the propagation media The antenna is the connecting element between the propagation media and the transmitter or receiver. The properties of an antenna which are of most interest are the radiation pattern, polarization, gain, and impedance. For a linear passive antenna, these properties are identical for both transmitting and receiving functions by virtue of the reciprocity theorem.

The specific application will dictate the properties of an antenna, such as radiation pattern, gain, polarization and impedance, although many types of basic antennas may be utilized to fulfill these needs. Probably the most significant property peculiar to space communication is the effect of the Earth's magnetic field which causes the ionosphere to be a magneto-ionic medium and rotate the plane of polarization of any electromagnetic radiation passing through it. This effect, called Faraday rotation, amounts to about 750 degrees in passing through the Earth's atmosphere at 120 MC, and will decrease with the square of the frequency to about 7.5 degrees at 1200 MC. Since the electron density of the ionosphere is not uniform, the magnitude of the rotation will be different for different parts of the sky and will also vary with time for any given part of the sky. This variation amounts to about 20% of the rotation and has a time period of about one minute to insure adequate signal reception and to avoid serious signal fades. The transmitting and/or receiving antenna must be omnipolarized. The transmission signal should be either linear or omnipolarized (such as by circular polarization) and the receiving antennas should be omnipolarized to ensure no loss. Where transmission and receiving antennas are both omnipolarized with the polarization changing as a function of time (as in circular polarization), the sense of rotation of the electric field vector for transmission and reception must be compatible.

Gain of an antenna basically relates the directivity of antenna to a reference antenna, most commonly an isotropic radiation (hypothetical point source antenna) or a half-wave dipole. The gain is defined as the ratio of the maximum radiation intensity in a given direction to the maximum radiation intensity produced in the same direction from the reference antenna with the same power input. Gains herein will always be referred to as isotropic and will be referred to as the absolute gain ($G_{abs}$) of the antenna.

The absolute gain is related to the effective area of the antenna as is tabulated in Table 1-3.

TABLE 1-3
ANTENNA CHARACTERISTICS

| Antenna | Gain | Effective Area |
|---|---|---|
| Isotropic | 1 | $\lambda^2/4\pi$ |
| Infinitesimal Dipole | 1.5 | $1.5\lambda^2/4\pi$ |
| Half-Wave Dipole | 1.64 | $1.65\lambda^2/4\pi$ |
| Optimum Horn | $10\ A/\lambda^2$ | 0.81 A |
| Parabola or Lens | $(6.3 \text{ to } 7.5)A/\lambda^2$ | (0.5 to 0.6)A |
| Broadside Array | $4\pi A/\lambda^2$ (man) | A (max) |

The variation in parabolic antenna gain vs frequency and size is shown in Figure 1-26.

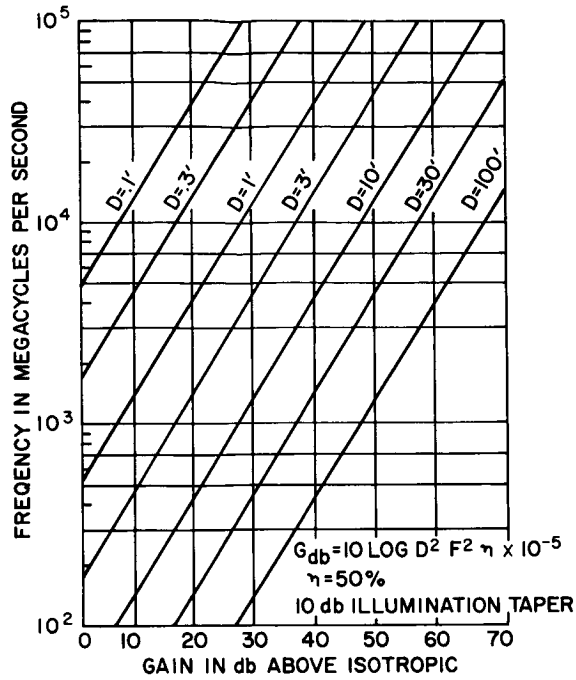


Figure 1-26. Parabolic Antenna Gain vs Frequency and Size

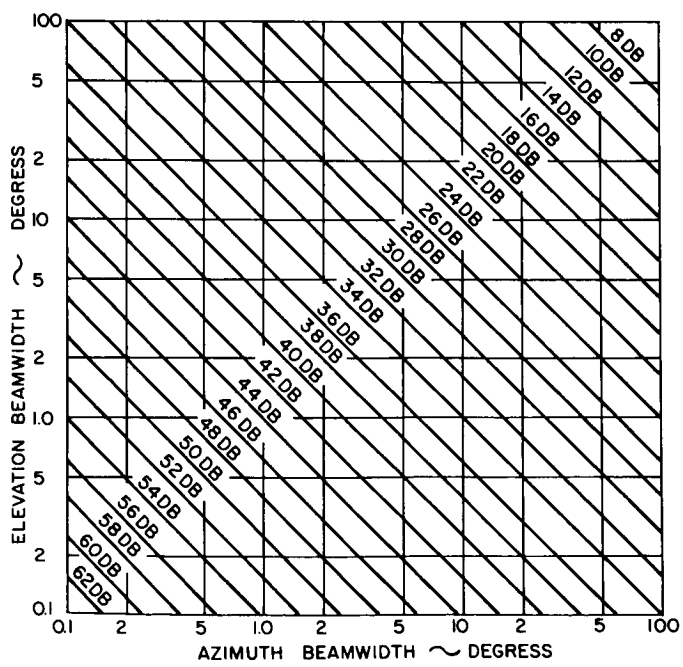


Figure 1-27. Antenna Gain vs Beamwidth

The associated beamwidth in the E and H plane is related to the linear dimensions in the E and H planes, absolute gain relationship as a function of E and H plane bandwidths are plotted in Figure 1-27 for rapid reference. Figure 1-28 can be used for rapid frequency to wavelength conversion.

The radiation pattern required is dictated by the area coverage on the angular beamwidth required. Typical aperture vs beamwidth relationship for various aperture illumination for rectangular and circular (or elliptical) apertures are plotted in Figures 1-29 and 1-30 respectively. The aperture illumination used will determine the radiation pattern characteristics, such as beamwidths, side lobe level, angular positions of the side lobes, etc. The specific application will determine the characteristics desired.

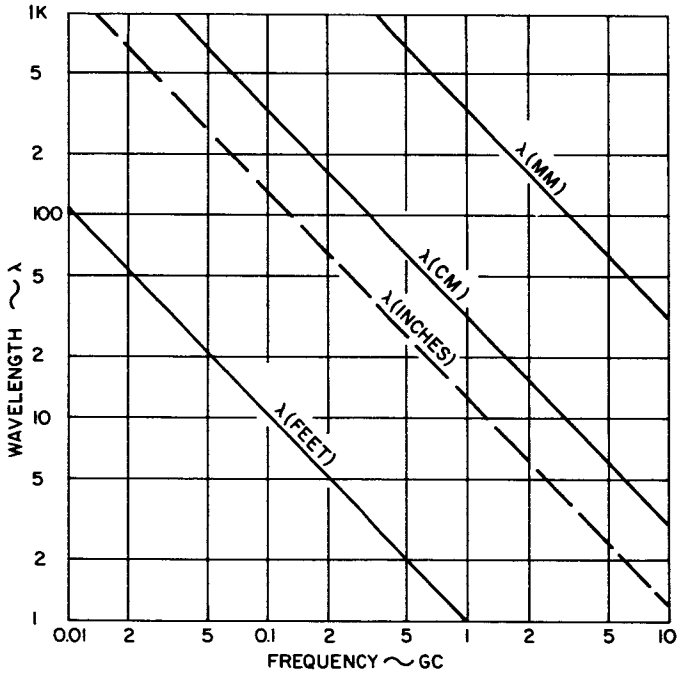


Figure 1-28. Frequency vs Wavelength

The input impedance parameter of an antenna is particularly significant in transmission since a badly mismatched antenna to a transmitter can seriously degrade its power output and power stability as well as the frequency output and frequency stability. Impedance mismatch vs loss is power delivered to the load is shown in Figure -131.

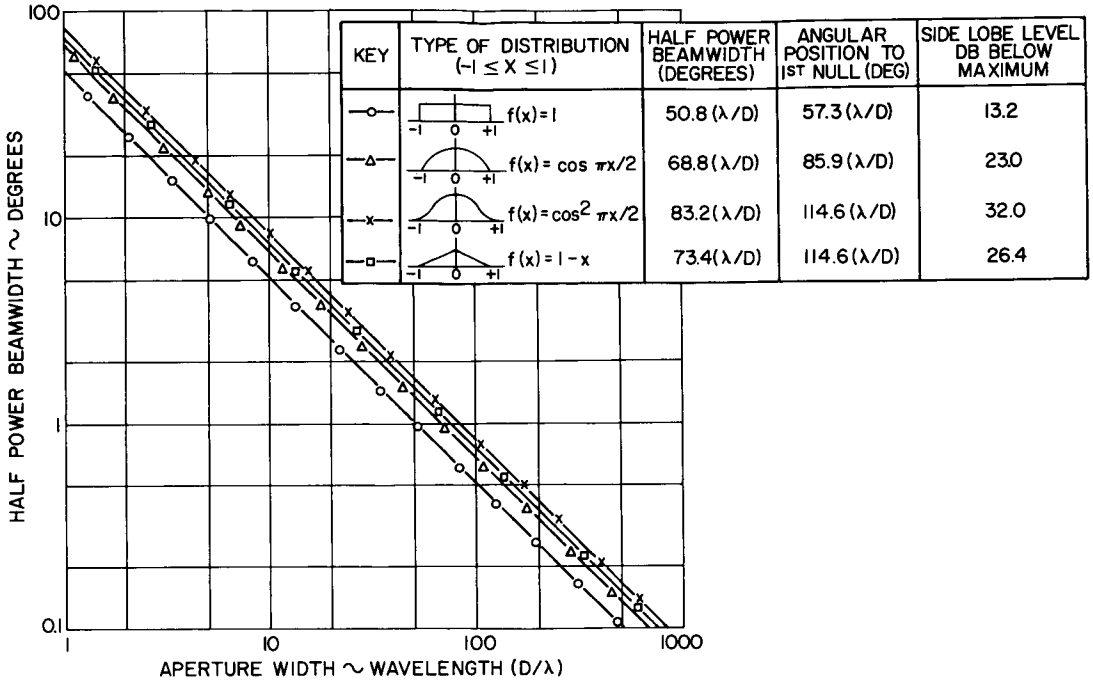


Figure 1-29. Antenna Beamwidth vs Aperture Width for Rectangular Apertures

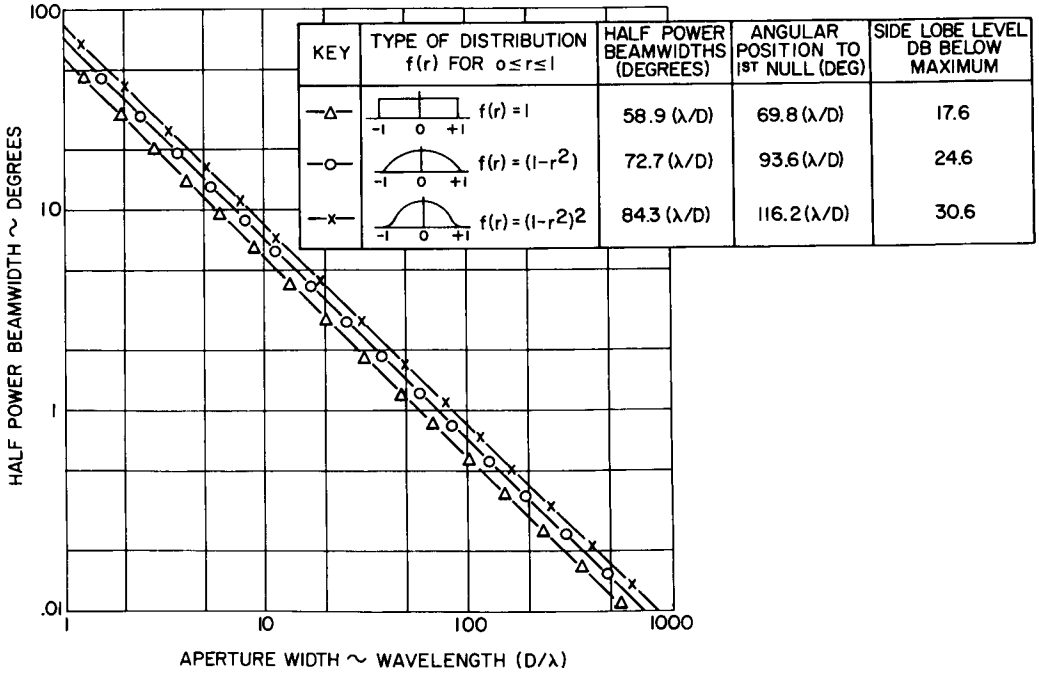


Figure 1-30. Antenna Beamwidth vs Aperture Width for Circular or Elliptical Apertures

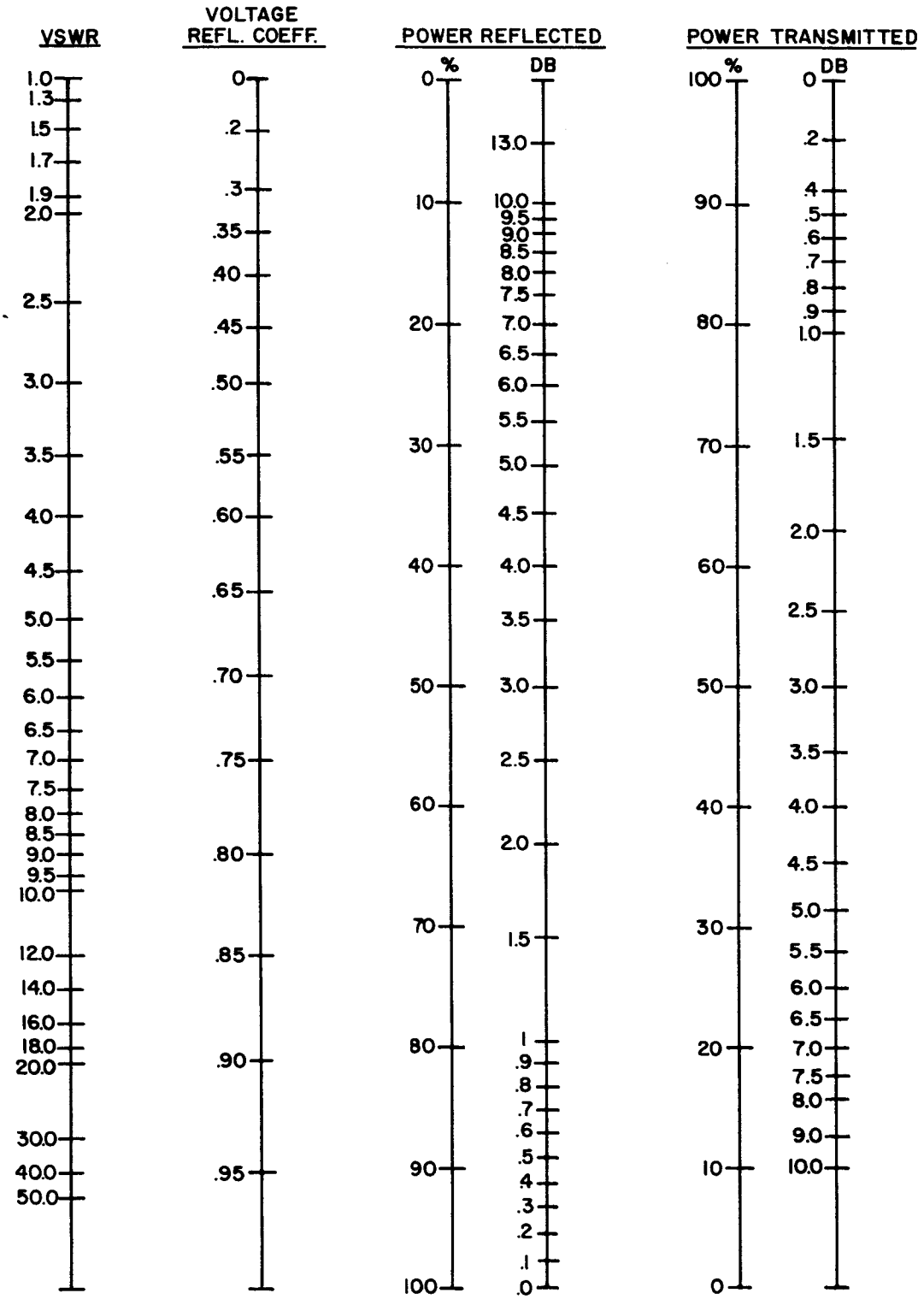


Figure 1-31. Impedance Match Characteristic

a. Spacecraft Antennas

Antennas located on a satellite should be as small as possible, light in weight, and simple. Mechanical types in which rigid elements are unfurled by springs, cables or gas pressure are suited primarily to relatively small antennas, such as the linear monopole antennas.

The design of an erectable or unfurlable antenna in space is primarily a mechanical problem, not only in mechanizing the collapsible/erectable features, but to ensure adequate microwave performance in space for the longevity of the satellite.

Surface and/or phase error tolerances of large apertures must be minimized to ensure satisfactory performance without serious degradation in the major lobe beamwidth, side lobe levels absolute gain, etc. Tolerances in the order of 1/16 to 1/32 of a wavelength will be required in general for the average antennas. The effects of random errors on the absolute gain of typical antennas is shown in Figure 1-32.

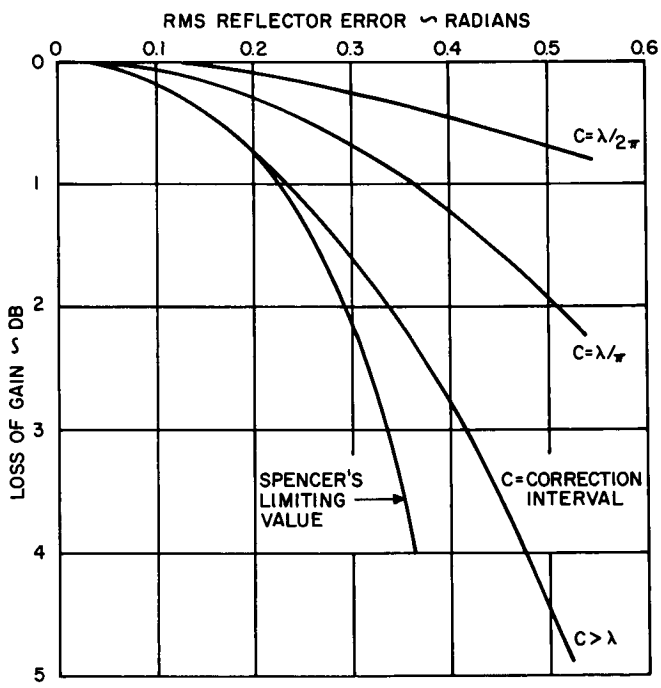


Figure 1-32. Paraboloidal Gain Loss Due to Random Errors

b. Spin Stabilized Satellite Antennas

A basic antenna consideration in spin stabilized satellites is the stabilization technique to be utilized to orient a directional beam antenna toward Earth stations. Mechanical as well as electronic techniques are feasible;

the complexity, weight, size, and reliability of one must be weighed against the other. Mechanical bearing and slip ring techniques have operated reliably in satellites for over a year, and indicate feasibility for mechanical beam steering. The complexities of the electronic scheme must be compared for each application against the generally simpler but bulkier mechanical beams steering.

Electronic schemes under investigation indicate greater insertion loss than the mechanical schemes, but generally less then 1.5 DB. Ferrite devices as well as varactor diodes are feasible switching devices.

Mechanical schemes include electrical switches with mechanically moving parts, rotating antenna feed and rotating mirrors or reflectors which in general tend to introduce less insertion loss than electrical schemes. Losses of less than 0.8 DB should be achievable. Wear, power to move mechanical parts, reliability and longevity must be weighed against the improvement in insertion loss over the electrical schene.

c. Multi-Frequency Operation

For the dual frequency requirement (Relay and Range Rate Receiver and Sensor Data Transmitter), the application of geometric optics to antenna desigr has merits, basically in that the antenna designs incorporating geometric optics are frequency independent and is applicable at all frequencies. The parabolic reflector is typical of such antenna designs, which can readily be adapted for use at many frequencies. For dual operation, a dual feed can be utilized for frequencies far removed, or a broadband feed can be displexed for frequencies closely spaced. Design curves for rectangular and circular aperture for typical aperture illumination taper are shown in Figures 1-29 and 1-30, respectively. Where side lobe levels are not important, illumination tapers providing higher side lobes levels tend to provide narrower halfpower beamwidths and higher gains. A circular aperture with a uniform or cosine taper would be most appropriate for the dual function antenna. Suitable diplexers and filters will be required to isolate the Relay Receiver and the Range and Range Rate Receiver from the Sensor Data Transmitter.

## B. SYSTEMS DESCRIPTION

### 1. Sensor Data Link

The objective of the Sensor Data Link is to provide a highly reliable communication channel from the spacecraft to the Command and Data Acquisition (CDA) station for the transmission of the video meteorological data. This section is devoted to a discussion of the basic parameters affecting the choice of appropriate transmission systems. Two significantly different approaches, analog FM and digital PCM, are discussed for comparison purposes. Primary emphasis is placed on the spacecraft requirements; the ground receiver details referred to in this subsection are covered more thoroughly in the subsection B.6.

#### a. Frequency Considerations

The choice of operating carrier frequency and consequent considerations of the type of transmitter hardware employed, is dependent upon several factors, both regulatory and technical.

The two meteorological satellites already programmed by NASA, Tiros and Nimbus, employ differing carrier frequencies for weather data transmission. The Tiros series (I, II, and III), operate at 235 MC whereas Nimbus I will operate at 1700 MC.

A considerable amount of effort has been expended by NASA to prepare telemetry and tracking facilities equipment and component parts, both ground and satellite borne at the 2300 MC band for use with the Deep Space Instrumentation Facility (DSIF) which could conceivably be utilized in this program. Examples of this are the tracking and instrumentation facilities at Goldstone, the new low-noise maser preamplifiers for use in this program and the amplitron transmitting tube for use in related satellite programs.

There is no specific band of radio frequencies specifically allocated by the Federal Communications Commission or the International Telecommunications Union (ITU) for meteorological wide band sensor data. A number of hearings have been held by both the U. S. House of Representative Committee on Science and Astronautics and the Federal Communications Commission regarding the cluttering of the radio spectrum by all types of services and the lack of a cohesive program of frequency allocations by both the USA and by international bodies, such as the ITU.

The FCC is now considering (Ref. 1-22) the following frequency band allocations for the meteorological satellite program:

(1) Two channels of 90 KC bandwidth each for digital and slowed down video transmission from the satellite to the ground in the 137 to 138 MC band. Power output shall be 50 watts maximum, and shall operate continually or on demand.

(2) Four channels of 5 MC bandwidth each (includes guard band) will be required for broad-band video transmission from the satellite to the ground. Power output shall be 50 watts maximum and initially will operate only on command. The bands 1660 to 1670 and 1690 to 1700 MC are proposed.

(3) A channel of approximately 100 MC is proposed for the transmission of a large volume of high resolution picture data during the pass from a non-synchrous satellite. The frequency band 7.2 to 7.65 KMC is proposed of this use.

Inspection of Figure 1-7 from this volume, indicates that the lowest values of equivalent antenna noise temperature, due to the contributions from atmospheric adsorption and cosmic noise, are at their lowest values between 600 MC and about 5 KMC, lying below 60°K at elevation angles greater than 10°.

In view of the above and in consideration of the availability of suitable reliable transmitter output stage devices within the next few years, it is proposed, at this time to restrict the carrier frequency range for sensor data transmission to the 1700 to 2300 MC range.

The Inter-Range Instrumentation Group (IRIG) has set a deadline for moving all telemetry communications to the 1700 MC and 2200 MC bands by 1970. This, in turn, will make available ground receiver facilities which may be utilized for use in sensor data reception for use at the CDA and MDA stations.

b. Power Amplifier Considerations

Preliminary considerations of the components available to generate RF power in the frequency range from 1700 to 2300 MC indicate several approaches. It will be shown that the RF power output requirements range from 2 to 10 watts depending upon the type of satellite system considered.

The following output state configurations will be considered:

(1) Travelling-wave tube

(2) Amplitron

(3) Voltage-tuned Magnetron

(4) Solid state driver and varactor output

1) Travelling-Wave Tube. Light-weight travelling-wave tubes (TWT) with a slow-wave helix circuit and a periodic permanent-magnet focusing system are desirable because of their large inherent power gain, large bandwidth, and high efficiency. The high efficiency is obtained by operating the collector at a voltage depressed considerably below the helix voltage. This permits reduction of the energy at which the electron beam is collected. Extreme reliability and high mean time between failure (MTBF) can be obtained with suitable design by operating the heater circuit with a low cathode-current

emission density, (less than 100 ma/cm$^2$) and an operating temperature less than 1000°C. This low operating temperature and emission density result in decreased cathode poisoning and evaporation of the cathode emissive material. Conductive cooling of the TWT collector and outer housing to the satellite structure, acting as a heat sink, is employed. The employment of optimized electron guns with excellent electron optical qualities permits focusing of the electron beam with a small magnetic field. This, in turn, allows the use of periodic permanent magnets, resulting in a low weight TWT.

Table 1-4 gives the characteristics of available TWT's suitable for use in the range 1700 to 2300 MC.

RCA has packaged suitable regulated high voltage power supplied (DC-DC converters) for use with the 10-watt TWT employed in the RELAY satellite which is approximately 9 by 6 by 3 inches and weighs 5 lb. This design can be modified for use on the SMS.

It will be noted that TWT's possess an inherent saturated gain of over 30 DB, which means that 10 milliwatts is sufficient to drive the 10 watt tube into saturation, while 2.5 milliwatts is sufficient for the 2.5 watt tube. This high power gain simplifies the driving problem considerably. Furthermore, the TWT is a well-proven device being employed in all the communication satellites launched to date: Telstar, Relay, and Syncom.

2) Amplitron. The amplitron amplifier tube currently being built at the Spencer Laboratory of the Raytheon Company is a crossed-field backward wave amplifier which possesses the following characteristics:

(1) Small size and weight

(2) High efficiency

(3) Medium bandwidth

The amplitron (Ref. 1-23) utilizes the same basic crossed-field interaction process as the cavity type magnetron and is very similar to it in appearance. Its operation is based on the interaction of a travelling RF wave with the electron stream rotating about radially from the cathode structure. When the electron angular velocity is in synchronism with the RF wave, the electrons lose energy to the RF fields at the same rate at which they accept energy from the DC field. By this means the potential energy of the DC magnetic field about the tube structure is converted to RF energy. The electrons are collected on the anode structure with an energy corresponding to their synchronous velocity. The conversion efficiency, with high magnetic fields, can theoretically approach 80 to 90 percent. However, practical structures realize conversion efficiencies of 55 to 60 percent, including filament power.

The amplitron has a non-reentrant, periodic RF structure matched to the RF input and output connectors. Consequently, with no voltage applied, or with tube failure, the tube acts as a short section of transmission line and the input driving signal will appear at the output with only a small line loss attentuation, approximately 1 DB.

TABLE 1-4

TRAVELLING-WAVE TUBE CHARACTERISTICS

| Type | Mfr. | Power Output Min. | Gain (Sat) | Freq. Range | Eff. | Weight lb | Type Magnet | Cathode Emiss-Density | Life Data |
|---|---|---|---|---|---|---|---|---|---|
| 7647 Overland Used in Radio Relay | RCA | 18 w | 35 DB | 1.7 - 2.2 KMC | 14% | 6.5 | Ferrite | 75 ma/cm$^2$ | MTBF 99% for $10^5$ hrs |
| A-1261 Modified for this freq. range | RCA | 10 w | 35 DB | 1.7 - 2.2 KMC | | 1.37 | Platinum Cobalt | 60 ma/cm$^2$ | |
| A-1228 Built for cancelled Lockheed Satellite | RCA | 11 w | 35 DB | 2.2 KMC | 20% | 6.0 | Ferrite | 75 ma/cm$^2$ | 100,000 hrs life test - 10 tubes |
| 314H | Hughes | 2 w | 33 DB | 1.5 - 3.0 KMC | 20% | 0.75 | Platinum Cobalt | 175 ma/cm$^2$ | Predicted life 40,000 hrs |
| 349H | Hughes | 10 w | 30 DB | 1.8 - 3.2 KMC | 20% | 13 oz. | Platinum | 175 ma/cm$^2$ | Predicted life 20,000 hrs |
| WJ-115 | Watkins-Johnson | 10 w | | | | | | | |
| A-1245 Used in Relay Satellite | RCA | 11 w | 33 DB | 4.05 - 4.25 KMC | 28% | 3.6 | Platinum Cobalt | 60 ma/cm$^2$ | |

There are sufficient electrons originally emitted from the cathode structure in an unfavorable RF phase, which are returned after accepting a small energy from the RF field, producing back bombardment of the cathode, and secondary emission. In order to reduce cathode overheating the filament voltage is reduced from 6.3 volts to 4 volts after a suitable preheat period.

Even though the periodic RF cavity structure is non-reentrant, in order to prevent over-all oscillation, and to act as an amplifier, the electron stream is reentrant in order to assist in the electron interaction process, resulting in improved efficiency. However, the backward-wave nature of the interaction and the electron reentry provide a feedback path which permits the amplitron to self-oscillate at a low output level with a noise spectrum when insufficient drive signal is provided. This interaction limits the stage gain, at this time, to approximately 20 DB. Figure 1-33 shows a typical voltage-current characteristic of the amplitron. With a suitable

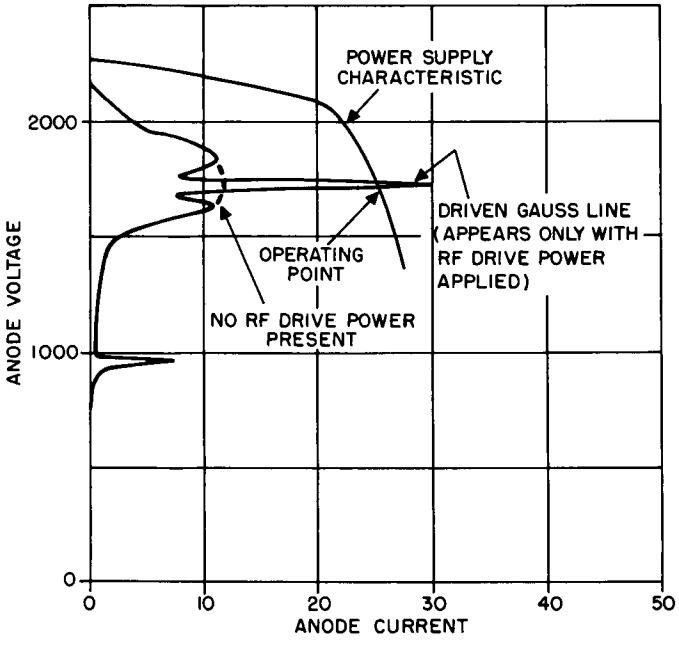


Figure 1-33. QKS 997A Amplitron Voltage - Current Characteristics

RF drive level a sharp "gauss line" or rise in anode current appears near the voltage for optimum interaction at the frequency of the drive signal, and full power output occurs, representing amplification of the drive signal. Little anode current can be drawn except at the correct voltage for interaction at the frequency of the drive signal applied. It is convenient to set this voltage with a current regulated power supply.

The voltage at which the driven gauss line portion of the characteristic appears is a function of tube geometry, the magnetic field, and

frequency. The amplitron efficiency is nearly independent of anode current and frequency.

Reliability life tests are commencing at this time. However, since the cathode is operated conservatively at a cathode emission-density of 60 ma/$cm^2$ it appears that high reliability is possible. Raytheon, based on previous experience with this type tube and cathode structure, has set as its objective an operating lifetime in excess of 10,000 hours.

The bandwidth of this tube is approximately 1 to 3 percent. Temperature, shock, and vibration tests have been performed on the amplitron tubes. Temperature variations from -40° to +89°C result in an output power variation of less than 0.2 DB.

Vibration tests indicate a minimum of resultant phase modulation, only 2° rms maximum when the tube is vibrated in each of three mutually perpendicular planes from 20 to 2000 cps at 15 g.

Successful operation has occurred after 200 g, 3 millisec shocks. Operation during the shock tests has not been monitored.

A power supply for this tube has been developed by Raytheon. It is an all solid-state DC to DC converter utilizing a magnetic amplifier with an efficiency over 75 percent. The anode supply is current regulated. Provisions are also provided for dropping the unregulated DC filament voltage from 6.3 to 4 volts after a suitable time delay. The dimensions are approximately 6-1/2 by 5-1/4 by 3-1/2 inches. Its weight is approximately 5.5 lbs.

Table 1-5 presents the nominal characteristics of available amplitrons manufactured by Raytheon Company which are suitable for space applications:

TABLE 1-5

AMPLITRON TUBE CHARACTERISTICS

| | QKS997A | QKS1200A | QKS1051 | QKS1119 |
|---|---|---|---|---|
| Power Output (Watts) | 20 | 19 | 22 | 70 |
| Gain (DB) | 20 | 20 | 20 | 20 |
| Frequency Range (MC) | 2200 to 2300 | 1700 to 2100 | 2290 to 2300 | 2290 to 2300 |
| Efficiency | 60% | 60% | 55% | 60% |
| Weight (oz) | 24 | 24 | 24 | 32 |
| Cathode Emission Density | 60 ma/$cm^2$ | 60 ma/$cm^2$ | 60 ma/$cm^2$ | 60 ma/$cm^2$ |
| Life Data-Predicted | 10,000 hrs | 10,000 hrs | 10,000 hrs | 10,000 hrs |
| Bandwidth | 1 to 3% | 1 to 3% | 1 to 3% | 1 to 3% |

3) Voltage Tuned Magnetron. A voltage tuned magnetron (VTM) is easily frequency modulated. It is necessary only to vary the anode voltage in order to change the frequency. The VTM is of the crossed-field type and similar in operation to the amplitron. However, the cavity structure is re-entrant so that self-operation is possible. The interactions in a VTM are similar to those in a high-Q magnetron in that the cathode provides an electron beam which enters into an interaction space where they are bunched and induce RF currents into the low-Q multi-cavity anode structure.

For a given tube the frequency is a function of the anode voltage and the filament voltage. The frequency of oscillation is determined primarily by the voltage between the cold-cathode post and the anode, while the modulation voltage is applied in series with this voltage. Power supply ripple must be kept to a minimum since it will appear as frequency modulation of the carrier.

Frequency pulling and power output variations, caused by load variations, can be greatly minimized by interposing a ferrite load isolator between the tube and the load or antenna.

There are several methods of maintaining the magnetron frequency with crystal oscillator accuracy, such as the phase comparison and injection locking methods. The phase comparison method mixes a portion of the magnetron output with a crystal oscillator harmonic. The output signal is amplified and fed into a phase detector and compared with the crystal oscillator output signal. The error signal is amplified and fed back to the tube for frequency correction.

The injection locking method forces the tube to oscillate at the output frequency of a crystal oscillator and harmonic generator varactor output chain. Very little power is needed for this purpose. The VTM is frequency locked by feeding the crystal controlled reference signal to the output of the tube through a ferrite load isolator to a circulator placed between the VTM and load. The insertion loss is less than 1 DB and the loss of injection power is about 2 DB. The signal required for frequency lock-in purposes can vary from 20 to 35 DB below the VTM output power. The locked-frequency range depends upon the injection power, the VTM power output, and the tube tuning sensitivity in MC/volt. Increased tube power output or tuning sensitivity decreases the locked frequency range; a larger injection signal decreases it. The VTM can be used as a frequency modulated amplifier by injection locking the tube with a signal which has been phase or frequency modulated. See Figure 1-34. The frequency deviation of the injection signal must be within the lock-in range of the VTM.

Table 1-6 presents the nominal characteristics of available VTM's.

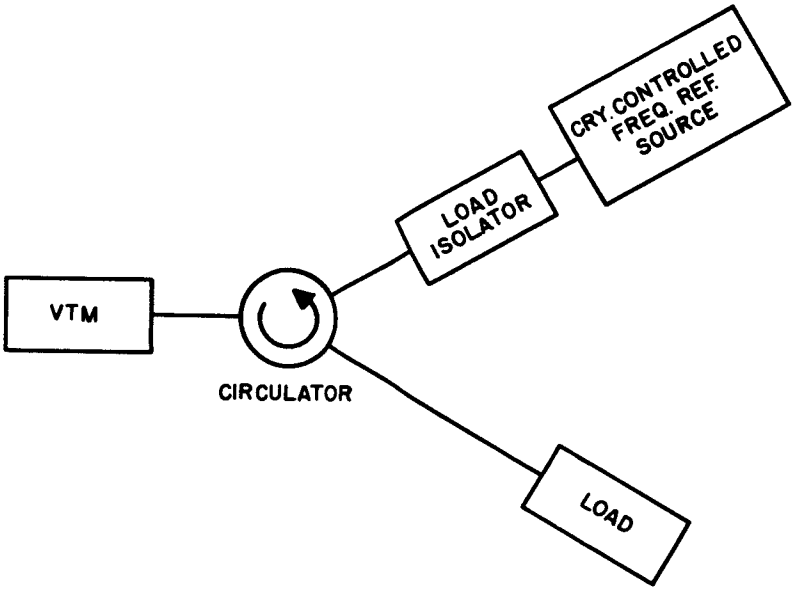


Figure 1-34. VTM Injection Frequency Locking

TABLE 1-6

CHARACTERISTICS OF VOLTAGE-TUNED MAGNETRONS

| | G-E GL-7398 | G-E 6001 | G-E ZM-6032 | G-E ZM-6000 |
|---|---|---|---|---|
| Power Output (Watts) | 2 | 2 | 7.5 | 10 |
| Tuning Sensivitivity | - | 2.6 MC/volt | 1.65 MC/volt | 1.28 MC/volt |
| Frequency Range (MC) | 2200 to 3850 | 1625 to 1700 | 2175 to 2425 | 2090 to 2410 |
| Efficiency | | 20% | 35% | 30% |
| Weight (lb) | 3.5 | 1.5 | 1.5 | 4.5 |
| Life Data | | | 3800 hours on 2 Tubes - Still in progress. Over 5% loss in RF power during test. | |

4) Solid State Output Stage. It is feasible to employ an all solid-state power output section consisting of a high power transistor amplifier stage followed by cascaded varactor diode harmonic generating stages. This output section would be driven, as would all the other output types (TWT, Amplitron, and VTM), by a crystal controlled, frequency or phase modulated, solid-state driver unit. The state of the art has progressed (Refs. 1-24 and 1-25) to the point where it is possible to generate power level outputs from 2 to 10 watts in the 1600 to 2300 MC region.

RCA and Clark Semiconductor Company are manufacturing silicon power transistors capable of producing 7 to 10 watts output, as a class C amplifer, at 100 MC. Clevite Corporation and Pacific Semiconductor Corp. have also announced transitors, for experimental use, which are capable of producing over 30 watts output at 100 MC.

High power varactor diodes manufactured by Microwave Associates, Pacific Semiconductor Corp., Bendix, and Raytheon are capable of producing the required power outputs (2 to 10 watts) up to 2300 MC, although at the upper frequency limit it may be necessary to parallel the diodes for 10 watt output. It is possible to obtain stage efficiencies of 40 to 70 percent with high quality varactor diodes operating as quadruplers for this application.

To date there has been no accumulation of life test data of high power varactor diode frequency multipliers in the upper end of the desired range.

A typical block diagram of a solid-state output channel is shown in Figure 1-35. The driver stage can be a high power silicon NPN transistor

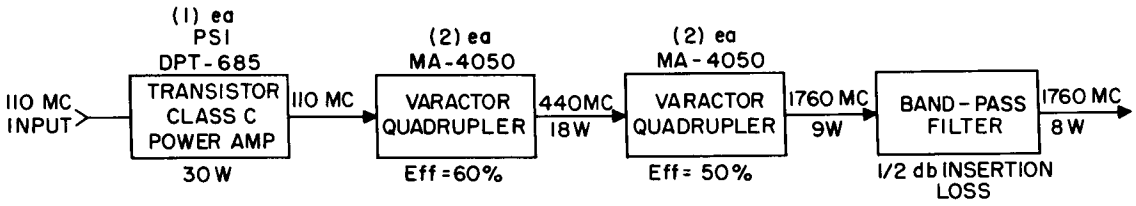


Figure 1-35. Typical Solid-State Power Output Section, Block Diagram

of the new interdigital type capable of producing 30 watts output when mounted on a suitable heat sink, with an efficiency of over 40 percent. The power gain of such a transistor will be in the region of 8 to 10.

This stage drives two varactor type quadruple harmonic generator stages. Each stage is of the shunt type configuration and employs two suitable varactors in parallel. Suitable traps and idler circuits will be used to increase the conversion frequency and prevent unwanted harmonics from appearing at the output. It is more desirable to use cascaded higher order harmonic generators such as quadruplers than cascaded doublers because of the ability to achieve higher conversion efficiency from a quadrupler than two cascaded doublers. In addition, there is less tuning circuitry involved (traps and idlers) as well as a decreased quantity of varactor diodes.

The first quadrupler (from 110 to 440 MC) will be of the lumped constant type while the last quadrupler will probably be a hybrid possessing lumped constants at the input and transmission lines at the output.

Based on the reported work (Refs. 1-24 and 1-25) it is possible to obtain conversion efficiencies of 60 percent from 110 to 440 MC and approximately 50 percent from 440 to 1700 MC.

c. Antenna Considerations

The antenna requirements for the sensor data transmitter are strongly influenced by the manner in which the spacecraft is stabilized. Where three-axis stabilization can be maintained to within a few degrees, a moderately directive antenna is permissible; but where the vehicle must be spin-stabilized, either a wide pattern or a complex microwave switching technique must be employed.

1) Three-Axis Stabilized Antenna Configuration. In order to allow for many ground stations to receive the cloud cover image data, it is desirable to provide a transmitted beam pattern equal to (or slightly greater than) the solid angle subtended by the Earth. At synchronous altitude, this angle is about 17 degrees. A parabolic antenna with a 21-degree beamwidth at the operating frequency would provide a ±2 degree tolerance to allow for minor variations in attitude stabilization. The antenna gain (assuming a 55 percent illumination efficiency) for the 21-degree beamwidth is approximately 18 DB. The antenna diameter required to provide this pattern will vary with the selected frequency from 1.5 feet at 220 MC to 1.8 feet at 1700 MC. A linearly polarized antenna feed shall be utilized so that no ambiguity in the wave front shall result when the ground station utilizes conical scan tracking techniques on the radiated signal.

2) Spin-Stabilized Antenna Configuration. Should the method of stabilization chosen involve a spinning vehicle where the spin axis is perpendicular to communication path, a linear array slot antenna might be used in preference to an omnidirectional or toroidal beam pattern with their corresponding loss in gain.

For the electronic beam stabilization approach, an array of basic elements about the periphery of the satellite surface as illustrated in Figure 1-36 can be used, electronically switching the microwave circuit to excite an aperture width of 3.3 for the 21-degree beam width required. The attitude reference for the electronic switching would be obtained from the satellites attitude sensor. The type of antennas to be utilized will depend on the frequency of operation; basic linear elements (dipole) at the on frequencies (100 to 3000 MC) range, and slots or horns at the higher frequency range (200 to 8000 MC). An array of linear elements symmetrically located about a cylindrical screen as in a Wullenweber array or with out the cylindrical screen as in a modified Adcock array (Figure 1-37) could be equally applicable utilizing either electronic or mechanical switching for beam steering.

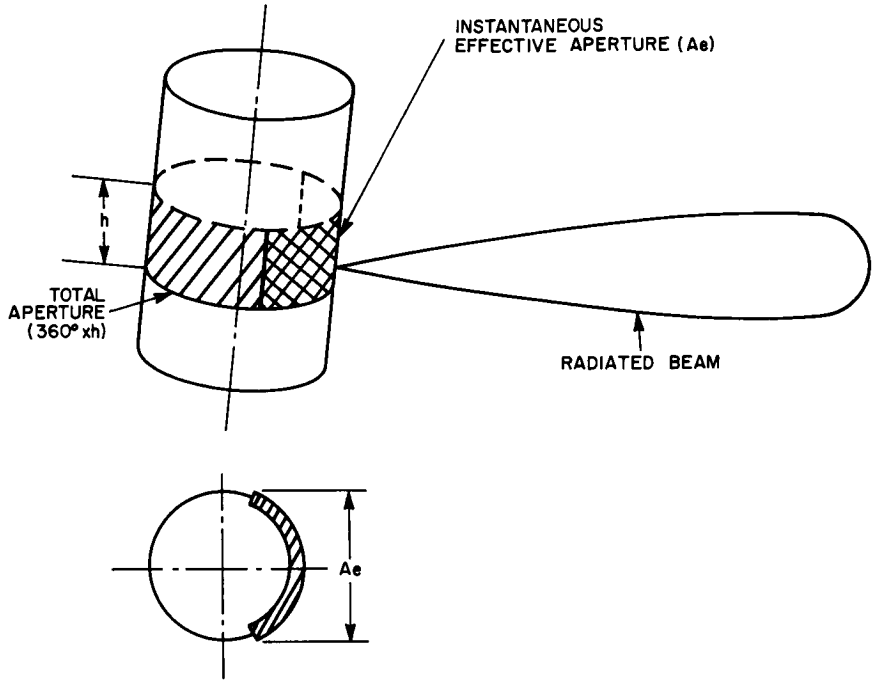


Figure 1-36. Typical Electronically Stabilized Sensor Data Link Antenna Configuration for Spin Stabilized Satellite

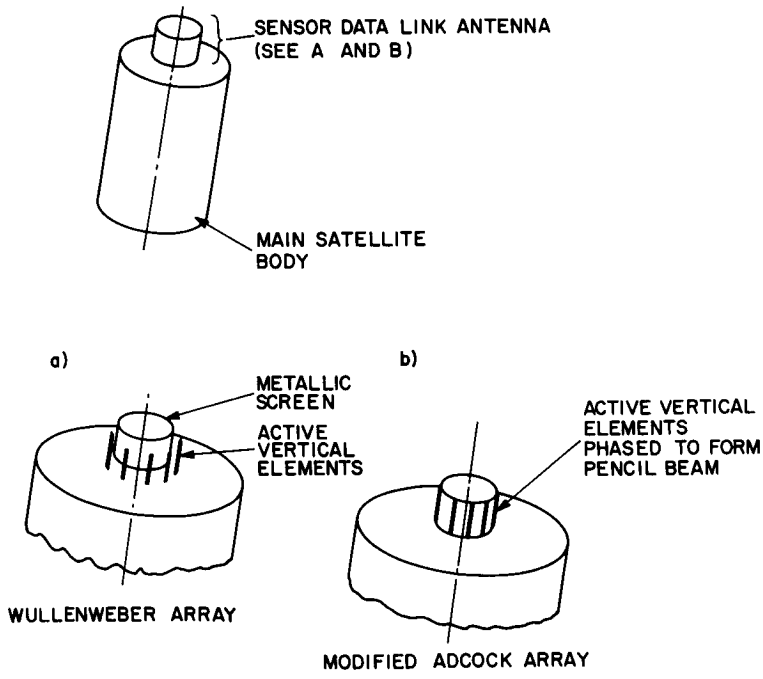


Figure 1-37. Linear Element Array for Sensor Data-Link, Antenna for Spin Stabilized Satellite

d. Modulation Methods

Many methods of modulation might be considered here, but for the sake of brevity, only two representative systems will be described; analog FM and digital PCM-Biphase.

1) FM Modulated Carrier Generation. The crystal controlled FM modulator may be of either the direct or indirect type. Both types are shown in Figure 1-38. The frequency values shown in part B of the figure are for the purpose of illustration.

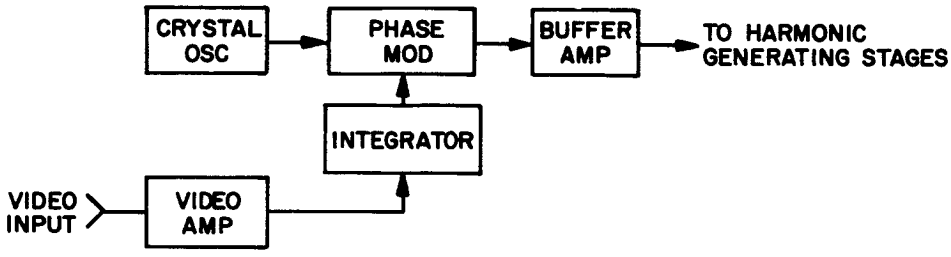


(A) - INDIRECT FREQUENCY MODULATOR

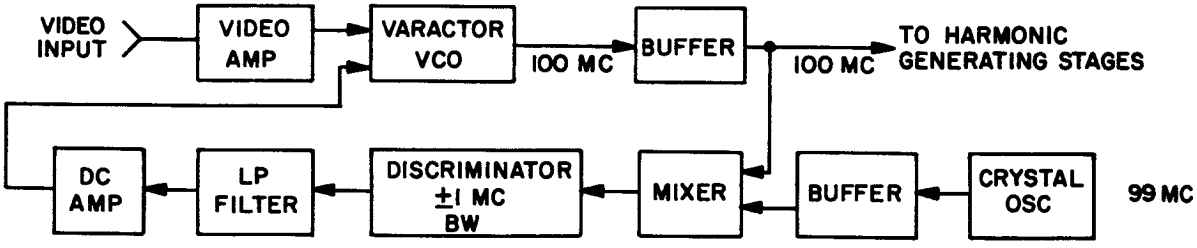


(B) - DIRECT FREQUENCY MODULATOR

Figure 1-38. FM Modulation Methods

A frequency modulated signal may be achieved by the indirect frequency modulator method even though a phase modulator is actually used. Since frequency is the rate of change of phase, similar techniques may be utilized. If the modulating signal is first integrated and then phase modulated, then the output signal is identical to that produced by conventional frequency modulation techniques. The main disadvantage of this circuit is the inability to develop large phase shifts of the carrier frequency. The limited phase deviation (usually less than 25 degrees) can be increased by frequency multiplication of the carrier. The amount of phase deviation increase is directly proportional to the frequency multiplication factor. In order to develop the desired frequency deviation (and phase shift) it will be necessary to employ a high order of frequency multiplication.

The second, and the more desirable method of FM generation, is to use the direct frequency modulator type (Figure 1-38 part B). The video

modulating voltage is used to vary the capacitance of a varactor diode placed across the tank circuit of a self-excited oscillator or VCO (Voltage Controlled Oscillator). A portion of the VCO ouput is compared against that from a reference crystal controlled oscillator, whose frequency is approximately ±1 MC different from the VCO. The beat frequency difference is fed to a conventional discriminator. The output error voltage is amplified and then fed back to the VCO. The process will continue until the error or correction voltage from the discriminator is near zero. The minimum error is defined by the closed loop gain. The open loop frequency stability of the VCO should be sufficient to maintain its carrier frequency with the capture range of the discriminator. It should be remembered that the output frequency deviation will be increased by succeeding frequency multipliers, therefore output frequency deviation from the circuit of Figure 1-38 part B should be $\frac{\delta F}{\eta}$ where $\eta$ is the order of succeeding carrier frequency multiplication.

2) PCM-Biphase Modulator. PCM Biphase modulation can be accomplished with the circuit shown in Figure 1-39. The vf-input drive is isolated

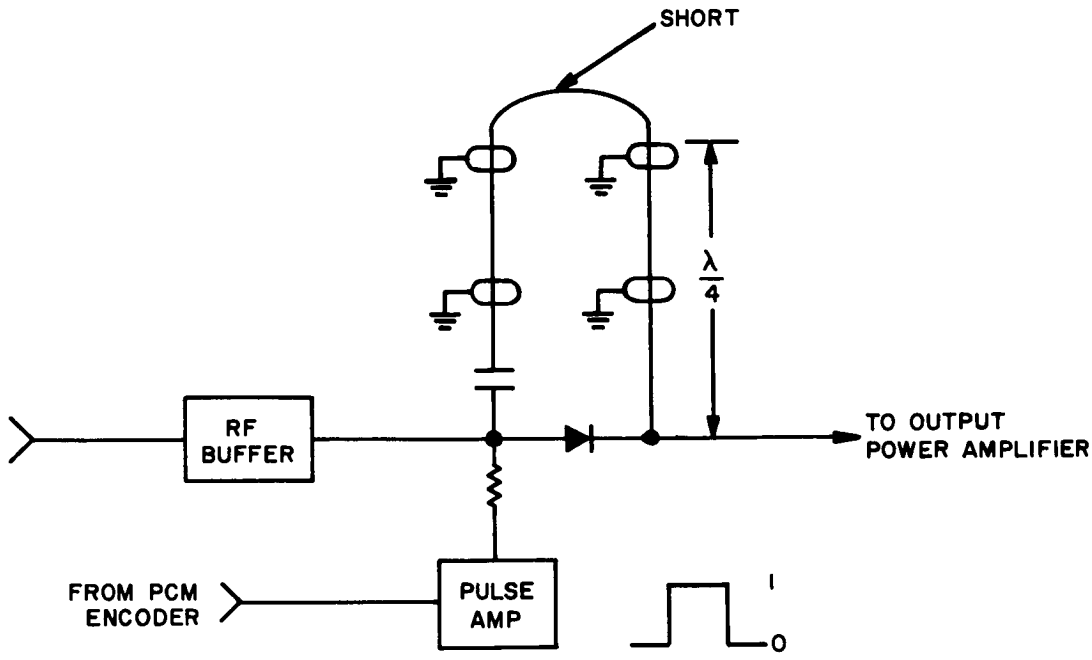


Figure 1-39. PCM Bi-Phase Modulator

from the phase modulator by means of a buffer amplifier. The phase modulator is essentially a driven diode switch which permits a 180-degree phase shift transmission line to be switched in when the input is at zero (0) or shorts it out when the input pulse is a maximum, at one (1). The 180-degree shift line is actually a re-entrant quarter-wave transmission line shorted at the far end.

The loss of sense or polarity of the return-to-zero PCM code pulses, as normally generated by propagation phase shifts, can be eliminated by utilizing a form of nonreturn-to-zero code (NRZ) wherein only the change from a zero to one or vice versa is transmitted as a 180-degree phase shift.

e. Modulation Method Comparison

Two different methods of information carrier modulation will now be compared; analog-FMFB, and digital-PCM Biphase. The system which will develop the greatest output signal to noise ratio for a given transmitter power should be seriously considered for use with the SMS.

The following parameters are common to both systems:

| | | | |
|---|---|---|---|
| (a) | Sensor output S/N | | + 40 DB |
| (b) | Required receiver S/N (for 1 DB degradation of sensor S/N) | | + 46 DB |
| (c) | Satellite antenna gain (21° at 1800 MC) | $G_T$ = | + 18 DB |
| (d) | Ground antenna gain (85 ft dia.) | $G_R$ = | + 51 DB |
| (e) | Free space plus atmospheric losses (30° elevation angle) | $\alpha$ = | - 189.5 DB |
| (f) | Fading, line polarization and incidental losses | $L_o$ = | - 13 DB |
| (g) | Receiver total effective noise temperature (NF = 1.8 DB based on parametric amplifier) | $T_e$ = | + 170°K |
| (h) | Video analog base bandwidth | $f_m$ = | 100 KC |

1) Analog - FMFB Power Budget Calculations. Basically, this type of operation achieves its high signal to noise vs carrier power ratio by utilizing a large RF carrier modulation index in order to achieve a high S/N improvement ratio above the threshold, or by obtaining a low receiver noise power system contribution by using a portion of the discriminator output (negative feedback). This output frequency modulates the local oscillator in such a way as to follow the frequency excursions of the incoming signal and thereby reduces the frequency modulation present at the intermediate frequency, thus reducing the IF bandwidth requirements and the IF modulation index. The technique is discussed in Section 1.A.4 of this volume.

a) Sample Calculation for FMFB System. An example of overall performance calculations for an analog system are as follows:

(1) In feedback FM system, a threshold C/N value corresponding to a wide deviation index is required. From Figure 1-16 a C/N of 17 DB is selected.

(2) The output S/N improvement above threshold can be determined:
S/N = Required Receiver Output S/N - Threshold C/N
= 46 DB - 17 DB = 29 DB

(3) The modulation index can be obtained from Figure 1-17,
∴ 29 DB correspond to $m_{RF}$ = 16.3

(4) The optimum feedback factor can be obtained from Figure 1-19, using 16.3 modulation index ($m_{RF}$) and output S/N = 46 DB. The feedback factor, F, is 20 DB, or a voltage ratio of 10 to 1.

(5) The IF amplifer modulation index

$$m_{IF} = \frac{m_{RF}}{F} = \frac{16.3}{10} = 1.63$$

(6) The minimum receiver IF amplifier bandwidth is $B = 2\ (1 + m_{IF}) = 2\ (1 + 1.6) = 0.52$ MC

(7) The receiver noise power, $P_n$, can be determined from Figure 1-13 for $T_e = 170°K$ and B = 0.52 MC; $P_n = 149.3$ DBW

(8) The required transmitter power can be calculated from

$$P_t = \alpha + \frac{C}{N} + L_o - G_R - G_T + P_n$$

$$= 189.5 + 17 + 13 = 51 = 18 - 149.3$$

$$= 1.2 \text{ DBW, or}$$

$$= 1.3 \text{ watts}$$

b) Power Budget Summary. A summary of this power budget is as follows:

| | |
|---|---|
| Satellite antenna gain | + 18 DB |
| Ground antenna gain | + 51 DB |
| Propagation and atmospheric losses | - 189.5 DB |
| SMS transmitter power (1.3 w) | + 1.2 DBW |
| Fading, line, polarization, etc., losses | - 13 DB |
| Receiver input power | - 132.3 DB |
| Receiver total effective noise temperature | 150°K |
| IF bandwidth | 0.6 MC |
| Receiver noise power | - 149.3 DBW |

$\therefore$ C/N = 132.3 - (-149.3) = 17 DB carrier threshold

2) Digital PCM - Biphase, Power Budget Calculations. A digital transmission system comparable to the FMFB link discussed before would utilize the most sophisticated PCM techniques available. A binary phase modulation system using synchronous detection gives promise of achieving a near optimum channel utilization.

a) Sample Calculations for PCM-Biphase System. An example of such a digital system yielding identical over-all performance comparable to the FMFB link is presented in the following sample power calculation.

(1) With a base bandwidth, $f_m$, of 100 KC, the signal must be sampled at a rate at least 200 KC.

(2) In order to preserve an accuracy of 46 DB S/N, each sample must be encoded to six (6) binary digits (Figure 1-22)

(3) The resultant pulse rate is 200 KC sample rate x 6 bits/sample = $1.2 \times 10^6$ bit/sec

(4) The practical bandwidth required to preserve a detectable wave shape is approximately equal to the bit rate, i.e., $f_m = 1.2$ MC.

(5) The IF bandwidth required for both sidebands is: $B = 2 f_m = 2.4$ MC

(6) The noise power, $P_n$, corresponding to an IF bandwidth of 2.4 MC and a noise temperature of 170°K is -142.5 DBW (Figure 1-13)

(7) The minimum C/N requirements are based upon the allowable error rate. Since the transmission time for a single frame is nearly 19 secs, and $1.2 \times 10^7$ bits are transmitted during this period, an error rate of $10^{-7}$ will, on the average, result in only one bit error per picture. The C/N ratio for a $10^{-7}$ error rate corresponds to 12 DB for the PCM-PM Local Reference.

(8) The required transmitter power can be calculated from

$$P_t = \alpha + C/N + L_o - G_R - G_T + P_n$$

$$= 189.5 + 12 + 13 - 51 - 81 - 142.5$$

$$= 3.0 \text{ DBW or } 2.0 \text{ watts}$$

b) Power Budget Summary. A summary of the power budget for the PCM system is as follows:

| | |
|---|---|
| Satellite antenna gain | + 18 DB |
| Ground antenna gain | + 51 DB |
| Propagation and atmospheric losses | - 189.5 DB |
| SMS transmitter power (2 w) | + 30 DB |
| Fading, line, etc., losses | - 10 DB |
| Antenna polarization losses | - 3 DB |
| Receiver input power | 130.5 DBW |
| Receiver total effective noise temperature | 170°K |
| IF bandwidth | 2.4 MC |
| Receiver noise power | - 142.5 DB |

$\therefore$ C/N = -130.5 - (-142.5) = 12 DB

3) Comparison of Results. Inspection of the above results for both systems indicates that the difference in transmitter power output for identical S/N outputs is negligible.

The choice of system selected should be based on the transmitter and receiver hardware complexity and reliability. If PCM were used, additional analog-digital encoding equipment would be required.

As already stated, FMFB is favored for use on the SMS based on the proven reliability and ease of instrumentation of the FM transmission system.

2. Telemetry Link

a. Telemetry Modulation Methods

The principal function of the telemetry link is the simultaneous transmission of many items of information from various subsystems of the vehicle to the ground. The process of transmitting more than one channel of information over a single link is called multiplexing. There are two general methods of multiplexing in use. One is frequency division using subcarriers. The other is time division or commutation.

1) Frequency Multiplexing. A frequency division system uses a separate subcarrier for each channel with enough spacing to provide nonoverlapping frequency intervals for the sideband structure of each channel. At the transmitter end, the subcarrier frequencies are modulated by information in each channel and added linearly into one signal which modulates the transmitter. At the receiving end, the modulated subcarrier frequencies are selected by linear frequency selective circuits, demodulated and then displayed and recorded.

2) Time Multiplexing. Instead of allotting a separate band of frequencies to each channel, a time division multiplex allots a portion of time in a cyclic sequence to each channel. The information in each channel is sampled by a commutator in cyclic serial sequence and a modulated pulse generated for each channel. These modulated pulses are then fed to the radio transmitter where they modulate a radio carrier. At the receiving end, the modulated pulses are handled in various ways. One way is to feed the pulses to a commutator which is synchro nized with the transmitter commutator. The output data can then be related to that at the transmitter. Another method is to apply a specific code to the pulse train for identification purposes.

3) Combination Frequency and Time Multiplexing. There is frequently a need for some channels to handle only slowly varying data having a narrow bandwidth and at the same time a need for additional channels to carry rapidly varying data having a wide bandwidth. These requirements can be met most efficiently by "subcommutating" a channel of a frequency or time division system. That is, a time division multiplex is used to modulate a channel of a time or frequency division multiplex which modulates the radio carrier. This makes the telemetry system more efficient in terms of spectrum utilization and power requirements.

4) Telemetry Techniques. The basic telemetry techniques in use at present are FM-FM, PAM, PDM and PCM. Each of these techniques is briefly described in the following paragraphs.

a) FM-FM. This refers to a technique of frequency modulating a transmitter with the output of one or more subcarrier oscillators, which in turn have been frequency modulated by data signals. The number of subcarrier oscillators involved is dependent upon data capacity of the telemetry system and also upon commonly accepted standards (Ref. 1-26) which govern the use of specified frequencies.

b) PAM. Pulse amplitude modulation is a method whereby many data channels are periodically sampled as to amplitude and the resultant pulse train used to modulate the carrier. If the data signals vary slowly it is not necessary that they be sampled so frequently in order to obtain an exact replica of

the input signal. The "Sampling Theorem" (Ref. 1-27) states that the sampling rate must be twice the highest frequency (Fourier component) of the original signal in order to reproduce the signal without loss of information. The accuracy of reproduction depends upon the precision with which the amplitude of the sample can be preserved through the transmission process.

c) In pulse duration modulation, a device called a keyer is inserted between a commutator and a transmitter. The purpose of the keyer is to convert constant width variable amplitude pulses to constant amplitude variable width pulses. Converting the amplitude pulses to width pulses results in a train of signal pulses whose amplitude can tolerate a considerable amount of noise without effecting data accuracy, since the data signals are now represented by the width of the pulses. Thus, the previous voltage amplitude measurements in the PAM system have become time measurements in the PDM system.

d) PCM. As in the PAM and PDM systems, data signals in the PCM system are sequentially sampled. The output of the sampler is fed to a high speed analog-to-digital encoder.

In the encoder each pulse is converted to a series of binary digits, which represent (in binary notation) the amplitude of the data signal represented by the pulse.

Since the PCM-data is transmitted in binary form, the ground station equipment is not required to recognize pulse amplitudes as in PAM. It is only necessary to recognize the presence or absence of pulses to define the data words. This can be accomplished with lesser S/N ratios than PAM or PDM. The undesirable features are the complexity of equipment and the synchronization problem.

b. Comparison of Telemetry Techniques for SMS

The basic systems in widest use for telemetry are FM-FM, PAM-FM, PDM-FM and PCM-FM. One or a combination of these systems is most likely to be used on the SMS for telemetry. Experimental data (Ref. 1-28) have been obtained comparing these systems. One such comparison is shown in Figure 1-40 for 2 percent error. The symbol definitions are as follows:

| | | |
|---|---|---|
| $S$ | = | rms carrier voltage |
| $k_i$ | = | rms noise voltage per unit root cps bandwidth |
| $B_i$ | = | information bandwidth, cps |
| $B$ | = | receiver bandwidth, cps |
| $f_s$ | = | sampling rate |

The curves indicate that PAM-FM offers the best performance for medium accuracy requirements of 2 percent based upon the criteria of spectrum utilization and required telemetry power.

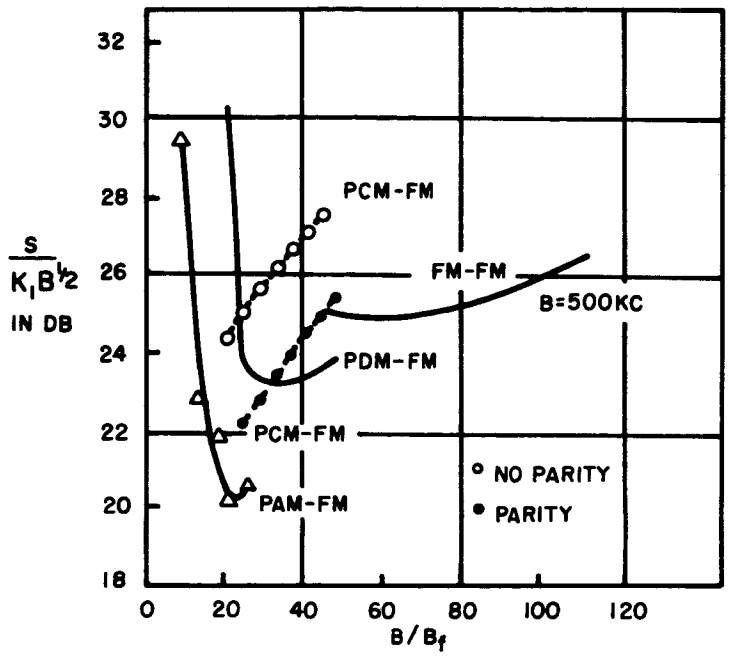


Figure 1-40. Optimized System Comparison Chart for 2% Error

Another comparison between PAM-FM and PCM-FM for higher accuracies using the same criteria is shown in Figure 1-41. This shows that the performance of the PCM-FM system is superior to the PAM-FM system where accuracies are greater than approximately 0.5 percent. It is seen that parity in the PCM-FM system results in a 2 to 3 DB threshold reduction for the range of accuracies of the chart.

From a system comparison on the basis of telemetry transmitter power and spectrum utilization, it has been concluded that PAM-FM is advantageous for medium accuracy applications and PCM-FM for high accuracy applications.

c. Error Probabilities and RMS Error in PCM-FM

Studies have been made by Aeronutronics (Ref. 1-29) and Stiltz (Ref. 1-30) to determine the probabilities of generating errors in the detection of PCM bits using an integration detector. These studies relate the bit error to the carrier-to-noise (C/N) ratio in the FM receiver IF signal. The results for the range of interest of the SMS are indicated in Table 1-7. These studies have also related the bit detection error rate to the rms error produced on samples for four or more bits per word. These results are also indicated in Table 1-7. In these studies, the deviation $\frac{f_1}{1/2\,B}$ ranged from 0.5 to 1.0 where $f_1$ is rms carrier deviation in cps and B is receiver bandwidth in cps.

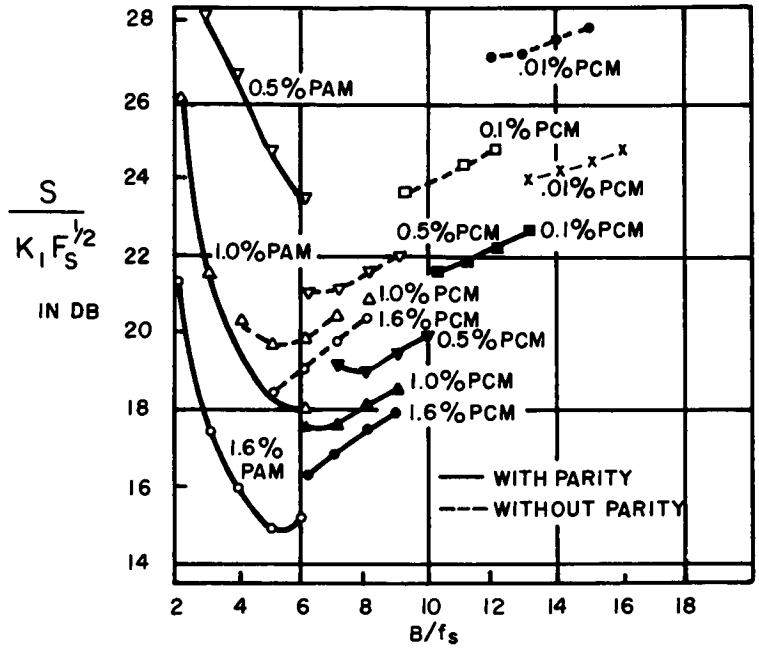


Figure 1-41. PAM-FM and PCM-FM Performance for Various Accuracies

Tests on a PCM data collection system designed by Dynatronics, Inc., utilizing a sampling detector indicate its performance falls within the limits of the results obtained by Aeronutronics.

The table indicates that for accuracies of 2 percent, the FM receiver IF C/N ratio should be approximately 8 to 12 DB. For accuracies of 0.1 percent, the FM receiver IF C/N ratio should be 12 to 15 DB. For on-off indications in telemetry, lower C/N ratios can be tolerated.

TABLE 1-7
ERROR PROBABILITY VS C/N RATIO AND RMS SIGNAL ERROR

| Telemetry Bit Detection Error Rate | FM Receiver IF C/N Ratio | Telemetry Signal Voltage Approximate RMS Error |
|---|---|---|
| 1 error in $10^6$ bits | 12 to 15 DB | 0.1% |
| 1 error in $10^3$ bits | 8 to 12 DB | 2% |
| 1 error in 10 bits | 3 to 5 DB | 20% |

d. Minimum IF Bandwidth Vs Bit Rate in PCM Telemetry

Figure 1-42 is a graph of minimum IF bandwidth vs bit rate. This is taken from the requirements specified in "PCM Telemetry Standards" Part I, Section 1 prepared by the Goddard Space Flight Center Data Requirements Systems Committee, November 1, 1962. As an example of the use of this graph, if a 200 bits per second information capacity is required the minimum IF bandwidth would be 300 cps.

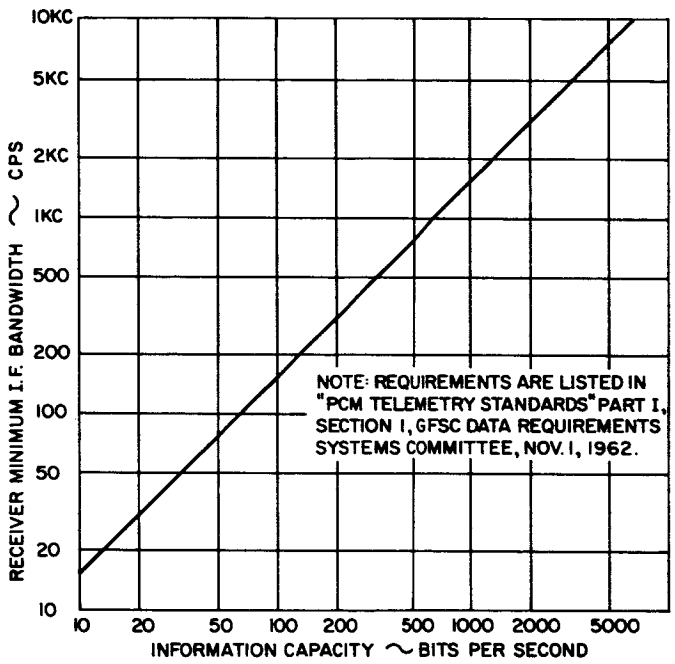


Figure 1-42. Minimum IF Bandwidth vs Bit Rate for PCM Telemetry

e. Telemetry Radio Frequency Link

The telemetry function can be divided into two classes of problems. The first is the generation, transmission and reception of radio frequency power. The second is concerned with the conversion and processing of the information, and is discussed in Section 2 of this Volume. The following paragraphs discuss the components of the telemetry RF link, the calculation of telemetry power and the selection of telemetry transmitters for the SMS.

1) Satellite Telemetry Antenna. Reliable telemetry information reception is necessary during all phases of operation of the SMS to ascertain the performance of various subsystems. Information is required during launch, orbit injection, acquisition and for station keeping. For example, temperatures of various items would be required during the launch phase and later on during station-keeping at less frequent intervals. Since tumbling might occur during any phase, an omni-directional antenna is required. For the SMS at a telemetry frequency of 136 MC this may consist of a turnstile antenna with essentially isotropic gain. The antenna would be constructed of four spring-mounted quarter wave whips (approximately 22 inches long) at 90° intervals around the satellite circumference. Each of the four whips would tend to act independently as a monopole.

The same antenna could be used for the 148 MC command receiver aboard the SMS. A duplexer system would be required for operating the antenna with both telemetry transmission and command reception.

2) Transmission Distance. The actual distance to the satellite during station-keeping is a function of the geographical location of the CDA station. However, during the launch and orbit injection phases, the SMS may be out of range of the CDA telemetry ground station. Therefore, the worldwide network of NASA tracking sites such as the Minitrack stations would be used to obtain the telemetry data. Figure 1-3 shows the distance to the SMS and the corresponding correction to the free space attenuation as a function of total subtended angle and distance from the nadir. The maximum distance between the telemetry ground station and the SMS is approximately 25,750 miles.

3) Telemetry Ground Antennas. Telemetry data will have to be received by the CDA station during station-keeping and also by various NASA tracking sites such as Minitrack stations throughout the world during the launch and orbit injection phases. Since large antennas would not be available except at the CDA station, it is desirable that the telemetry system operate with ground antennas having medium gains of 14 to 19 DB assuming a telemetry frequency of 136 MC. Such antennas are readily available from commercial manufacturers and are in use with present systems such as Nimbus and Syncom. A typical ground telemetry antenna for use with the SMS would have characteristics as listed in Table 1-8.

TABLE 1-8
TYPICAL TELEMETRY GROUND ANTENNA SPECIFICATIONS

Operating frequency 136 MC

Eight turn helical antenna

Gain, 14 DB nominal over circular isotropic

Bandwidth, 40° nominal

VSWR, 1.5 to 1 maximum

Polarization, right hand circular

Axial ratio, 1.5 DB maximum

TABLE 8-1 (continued)

Side lobe level, 10 DB down nominal

Overall length, 182-3/16 inches

Helix length, 167-3/4 inches

Diameter of helix, 28-11/16

Diameter of ground plane, 72 inches

Manufacturer, Scientific Atlanta

4) Telemetry Ground Receiver. In order to obtain best C/N ratios, it is desirable that the telemetry ground receiver have a low noise figure. However, this is not as important at telemetry frequencies of 136 MC as it is at higher telemetry frequencies of 2300 MC. This is because the antenna temperatures at 136 MC are in the vicinity of 1000°K whereas at 2300 MC they are about 20°K at a 30° elevation angle (Figure 1-7). Therefore the overall receiver noise temperature at 136 MC is determined mainly by the antenna temperature as can be seen by reference to Figure 1-14. This graph relates the overall receiver temperature $T_e$ to the antenna temperature $T_a$ for various noise figures. For example, if the receiver has a noise figure of 3 DB and the antenna temperature is 1000°K, the overall receiver temperature is 1300°K. If the antenna temperature were 20°K, the overall receiver temperature would be 310°K. The receiver noise would be lower by 1300/310 or about 6 DB at 2300 MC than that at 136 MC. If parametric preamplifiers or maser preamplifiers, having noise figures of 2 DB or less are used for telemetry at 2300 MC, the receiver noise would be reduced even further. This is discussed in subsection 1. A.

Another method of reducing receiver noise is by narrowing the reception bandwidths through the use of special demodulators such as a phase-lock detector or frequency modulation with feedback. Such methods are discussed in subsection B. 2. e. The relation between receiver noise power and bandwidth for various total effective temperatures is given in Figure 1-13.

A typical receiver for telemetry reception of the SMS at a frequency of 136 MC would be the Nems-Clarke Type 1440-2. This receiver has a noise figure of 6 DB and utilizes a phase-lock detector. Another reception method for telemetry would utilize a low noise preamplifier mounted on the telemetry antenna pedestal with the remainder of the receiver mounted at the operator's position thus minimizing the coupling loss between antenna and receiver. A typical preamplifier for this use would be a Nems-Clarke Type PR 203A. This unit has a gain of about 22 DB and a noise figure of about 4 DB.

5) Telemetry Power Calculation. It is desirable that the telemetry system accomplish its mission with maximum conservation of weight aboard the SMS. This requires that the telemetry power be a minimum consistent with other requirements such as adequate monitoring capability and reliability.

In this section, the trade-offs between telemetry power, C/N ratio, effective noise temperature and bandwidths will be considered. The bandwidth was shown to be directly proportional to information capacity in subsection 1. A. Figure 1-44 is a graph of telemetry power vs IF bandwidth for various C/N ratios. This data is based upon the following assumed values:

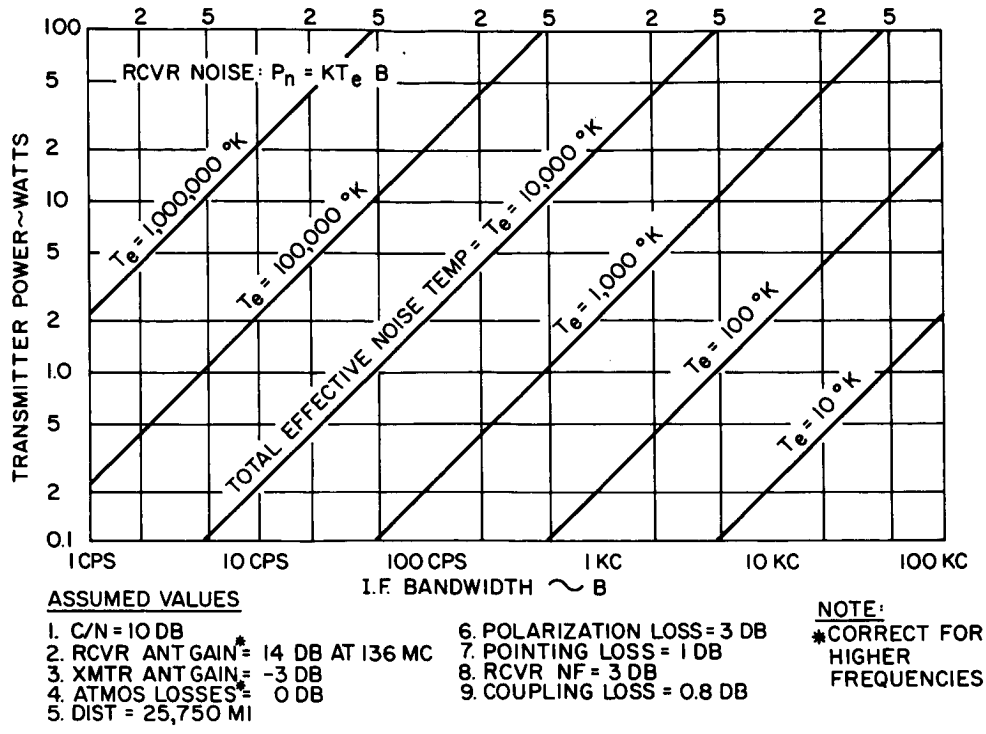


Figure 1-43. Telemetry Power vs Bandwidth for Various Effective Temperatures

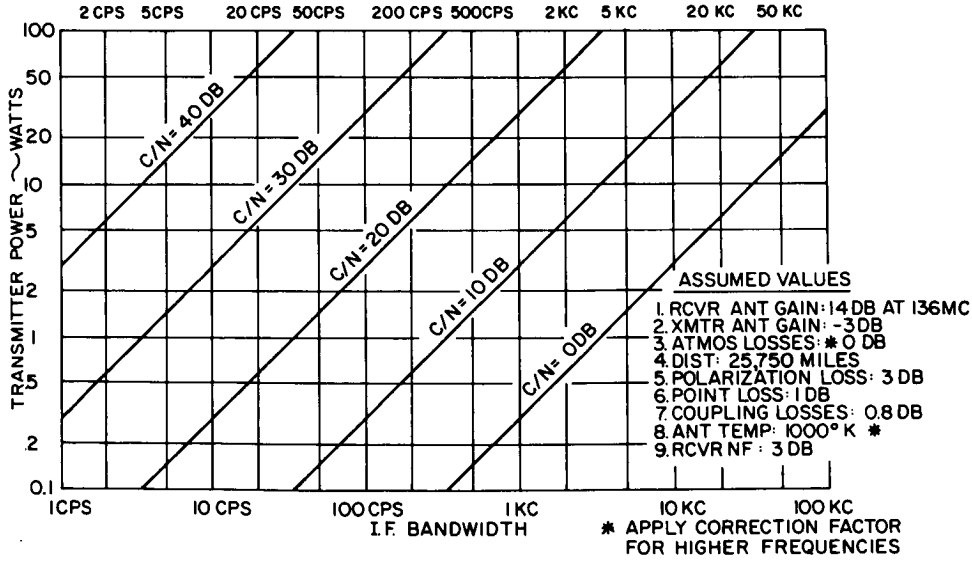


Figure 1-44. Telemetry Power vs Bandwidth for Various C/N

1) Telemetry ground antenna, axial mode helical gain, 14 DB at 136 MC

2) SMS vehicle telemetry antenna, turnstile, gain,-3 DB

3) Distance to SMS, 25,750 miles

4) Polarization loss,-3 DB

5) Coupling loss between transmitter and antenna and between receiving antenna and receiver,-0.8 DB

6) Pointing loss,-1 DB

7) Antenna temperature, 1000°K

8) Receiver noise figure, 3 DB

9) Atmospheric losses, 0 DB at 136 MC

A typical power budget calculation used in obtaining Figure 1-44 is shown in Table 1-9.

As an example of the use of this graph, if it is assumed that the telemetry system is PCM-FM and the information capacity required is 200 bits per second, then from Figure 1-42, the minimum IF bandwidth would be 300 cps. From Table 1-7 if the error rate were 1 error in $10^3$ bits corresponding to a 2% rms error in the telemetry signal voltage, the required IF C/N ratio would be about 10 DB. Therefore, referring to Figure 1-44 the minimum telemetry power required for 300 cps bandwidth and C/N=10 DB, is 0.9 watts.

It should be noted that Figure 1-44 is independent of frequency if a constant ground antenna aperture is assumed. Therefore, although the free space attenuation increases with frequency as shown in Figure 1-2, the increase in ground antenna gain would compensate for this. A slight correction for atmospheric losses at higher frequencies as in Figure 1-5, should also be applied.

Figure 1-44 assumes that the antenna temperature remains at 1000°K at all frequencies. Since the antenna temperature would ordinarily be lower than this at higher frequencies as explained in subsection B. 2. e, a correction would be necessary. The effect of decreasing the temperature is shown in Figure 1-43 which is a graph of telemetry power vs bandwidth for various total effective temperatures. It indicates that the telemetry power required is directly proportional to total effective receiver temperature. For example, if the conditions of the numerical example given previously are assumed except that the antenna temperature is assumed to be 300°K, the telemetry power required would be approximately 0.2 watts.

The effect of different ground antennas on the telemetry power required is shown in Figure 1-45. This graph shows telemetry power vs bandwidth for various ground antenna gains. For example, if a 28-foot parabolic antenna (19 DB gain at 136 MC) were used in place of an axial mode helical antenna (14 DB gain at 136 MC) for receiving telemetry, the telemetry power required would be 0.28 watts instead of 0.9 watts in the previous numerical example.

TABLE 1-9
TYPICAL TELEMETRY POWER BUDGET CALCULATION

| | |
|---|---|
| Telemetry transmitter power (2.9watts) | 4.6 DBW |
| Satellite antenna gain | -3.0 DB |
| Free space loss, 25,750 miles at 136 MC | -167.8 DB |
| Polarization loss | -3 DB |
| Pointing loss | -1 DB |
| Receiver antenna gain at 136 MC | 14 DB |
| Total coupling losses | -0.8 DB |
| Received signal power | -157 DBW |
| Receiver noise figure (Pre-amp) = 3 DB | |
| Receiver noise temperature $T_r$=290 (NF-1)=290°K | |
| Antenna noise temperature $T_a$=1000°K | |
| Total noise temperature $T_r + T_a$ = 1290°K | |
| Received noise bandwidth: 100 cps | |
| Receiver noise power (KTB) | -177 DBW |
| C/N Ratio | 20 DBW |

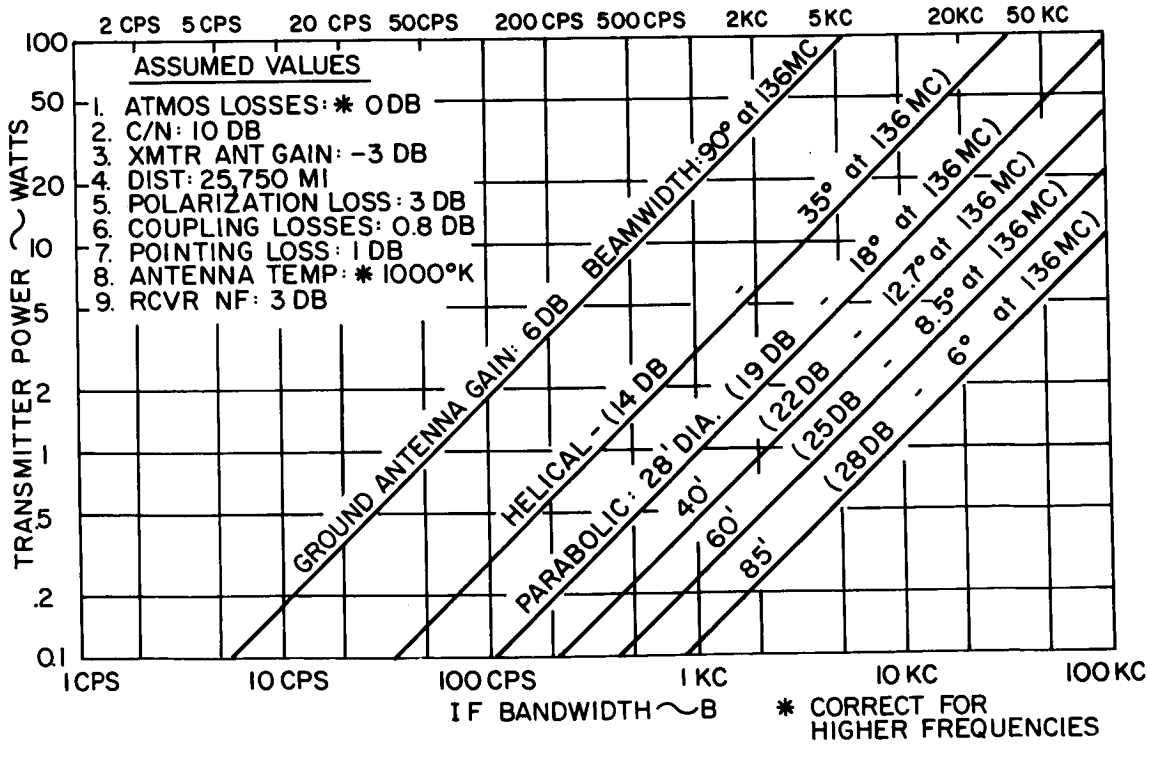


Figure 1-45. Telemetry Power vs Bandwidth for Various Ground Antenna Diameters

6) Telemetry Transmitters. For a 136 MC telemetry system, the transmitter would be solid state having either varactor frequency multipliers or transistors in their output stages. These units are readily available commercially or can be packaged to fit specific space requirements of the SMS. Table 1-10 is a listing of various units which are available for satellite operation. These are solid state units and may be used with various configurations of the SMS.

TABLE 1-10
TYPICAL TELEMETRY TRANSMITTERS

| Satellite or Unit Nomenclature | Power Output | Frequency | Weight | Volume |
|---|---|---|---|---|
| Relay | 0.25 w beacon | 136 MC | 0.65 lb | - |
| Nimbus | 0.350 w | 136 MC | - | - |
| UED type TR-11 | 0.5 w | 215-260 MC | 0.5 lb | 8.4 cu. in. |
| Tele-Dynamics Type 1054 | 1.0 w | 216-260 MC | 1.7 lb | 35 cu. in. |
| Syncom | 2 w | 136 MC | 0.5 lb | - |
| Telstar | 2 w | 138 MC | - | - |
| OSO(S-67) | 2 w telemetry mode<br>0.25 w beacon mode | 136 MC<br>136 MC | 1.0 lb | 30 cu. in. |
| Tele-Dynamics Type 1056 | 2 w | 216-260 MC | 1.7 lb | 35 cu. in. |
| UED Type TR-16 | 2.5w | 216-260 MC | 1.4 lb | 22.6 cu. in. |
| Nimbus APT | 5.5w | 136.95 MC | - | - |
| UEDType TR-17 | 5 w | 136 MC | 1.4 lb | 22.6 cu. in. |
| UED-X1065 | 10 w | 136 MC | 2.5 lb | 53 cu. in. |

Figure 1-46 is a graph of power output vs weight of various units available commercially and used aboard various satellites. This weight does not include encoding systems or the power supply system. This chart shows the general trend of increasing weight with power. To increase the telemetry transmitter power, it becomes necessary to use larger and heavier components, and more complex temperature control with larger heat sinks. All this results in an approximately linear increase in weight with telemetry power. In addition, the power supply weight increases almost linearly with the power input requirements.

7) Telemetry Transmitters for Various SMS Configurations. In Table 1-11, probable operating parameters have been selected for the telemetry system of each configuration of the SMS. These are based upon the tables and graphs previously presented in this section. Table 1-11 indicates that the power required depends on the information handling capacity. The low, medium and high capability SMS configurations will use telemetry transmitters having power outputs of 1.1, 2.2, and 4.5 watts, respectively.

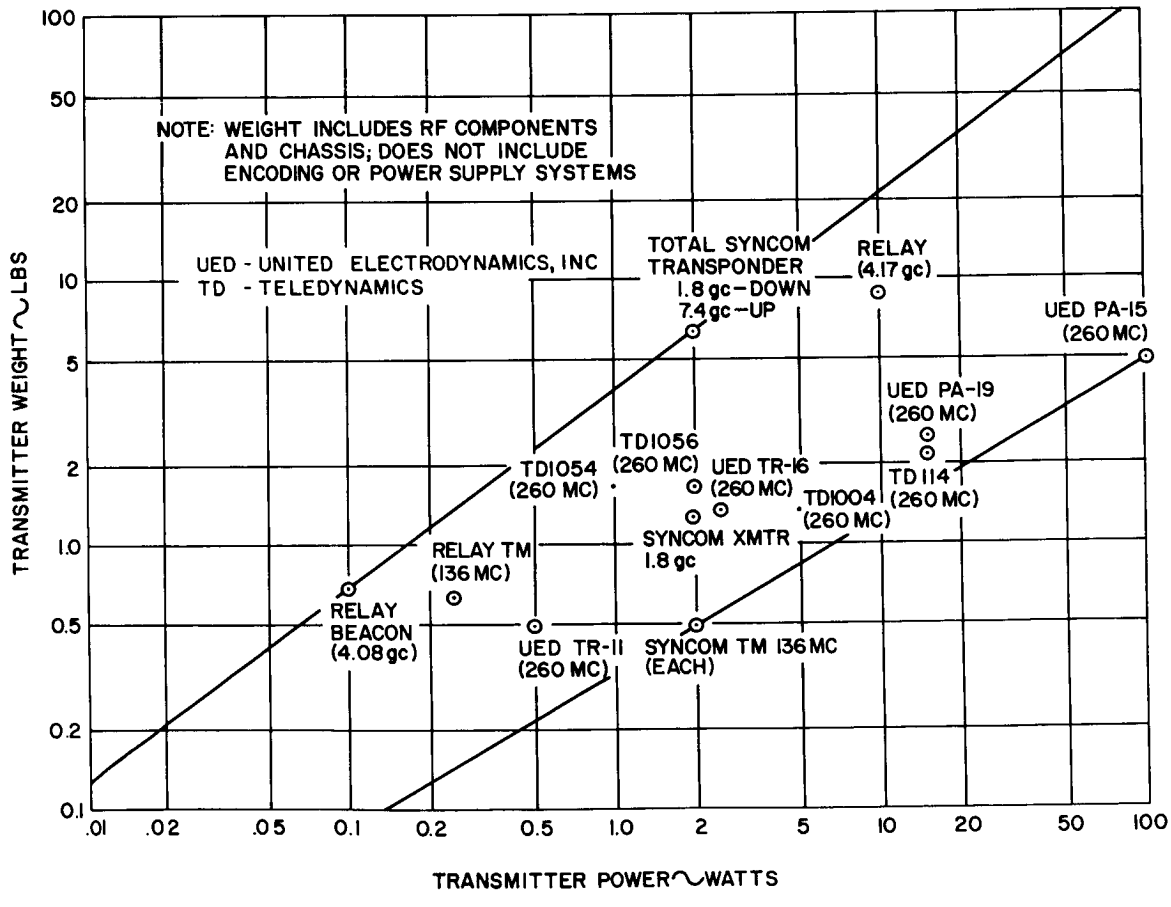


Figure 1-46. Telemetry Transmitter Weight vs Power Output

TABLE 1-11
TELEMETRY TRANSMITTER PARAMETERS

| SMS Configuration | Low Capacity | Medium Capacity | High Capacity | Notes |
|---|---|---|---|---|
| Telemetry information capacity (bits per second) | 100 | 200 | 400 | |
| Minimum IF bandwidth | 150 cps | 300 cps | 600 cps | |
| Minimum IF C/N ratio | 13 DB | 13 DB | 13 DB | |
| Minimum telemetry power required using a 14 DB gain ground antenna | 0.88 w | 1.76 w | 3.52 w | see Figure 1-44 |
| Minimum telemetry power required using a 19 DB gain ground antenna | 0.28 w | 0.56 w | 1.12 w | power reduced by 5 DB |
| Margin | 6 DB | 6 DB | 6 DB | |
| Minimum telemetry transmitter power | 1.1 w | 2.2 w | 4.5 w | |
| Suggested transmitter model to be used with SMS | UED type TR-16 Modified | UED type TR-16 Modified | UED type TR-17 | |
| Volume | 22.6cu. in. | 22.6cu. in. | 22.6cu. in. | |
| Weight | 1.4 lb | 1.4 lb | 1.4 lb | |
| Power input required | 5.0 w | 10 w | 20 w | |

8) Increasing C/N Ratios by Special Detector Methods. Methods are available in telemetry reception for increasing the C/N ratios. The increase in C/N ratio would act as an additional safety margin for operation of the telemetry system. These methods include phase-lock detectors and frequency modulation with feedback. These methods reduce the effective noise bandwidths by employing a narrowband filter in conjunction with a frequency feedback circuit. The amount of noise power bandwidth reduction depends upon the amount of feedback utilized. Figure 1-47 is a comparison (Ref. 1-31) of the threshold level and C/N ratio of ordinary discriminators and the phase-locked loop. This graph indicates the improvement in the threshold level and also shows that increases in C/N ratio from 10 to 20 DB can be obtained.

9) Telemetry Reliability. In order to achieve greater reliability, two identical telemetry units should be considered for the SMS. Only one would be operating at any one time with the other capable of being switched over in case of failure. As an additional backup, telemetry data could be used to modulate a subcarrier on the sensor data transmitter. This appears feasible since the sensor data

transmitter will be switched to an omnidirectional antenna from the directional parabolic dish during launch and orbit injection in order to enable it to work with the Goddard Range and Range Rate System. Therefore, telemetry data could be received even if tumbling occurs.

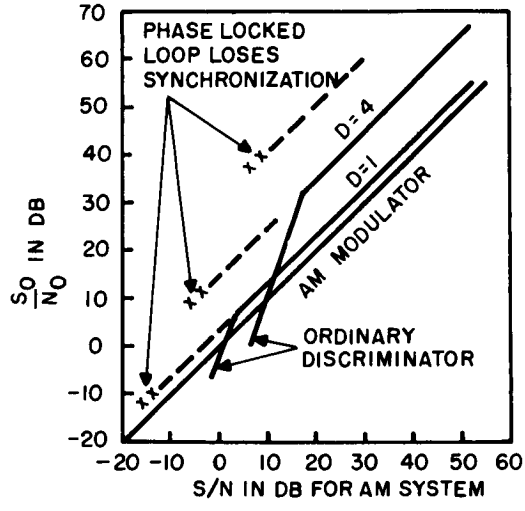


Figure 1-47. Comparison of Threshold Level and Signal to Noise of Phase-Locked Loop and Ordinary Discriminators

10) Conserving Telemetry Power. During the early phase of SMS operation such as launch or orbit injection, telemetry information will be required continuously to ascertain the operation of various subsystems. Also, as discussed in subsection 1.5.B, the telemetry transmitter may be required for VHF range and range rate measurement during this period. However, once the station-keeping position has been attained, telemetry information will be required less frequently. Therefore, the telemetry transmitter can be turned off to conserve power and telemetry data used to modulate a subcarrier on the sensor data transmitter. Alternatively the telemetry transmitter can be operated at a low duty cycle during station-keeping to conserve power.

3. Command Receiver

The purpose of the SMS command link is to transmit the required manual (or automatic) control commands from the CDA station up to the spacecraft. The command link must be so designed that the commands will be received with a high degree of reliability at anytime throughout the launch, ascent, and

injection phases of the spacecraft flight program as well as during the long period on station.

The command data to be transmitted is discussed in detail in Section 2 of this volume. Two coding techniques standardized by NASA are considered; tone digital and PCM. The most stringent power requirements are determined by the tone digital system since the peak subcarrier frequency of 11 KC requires a much wider bandwidth than the anticipated 150 bit per second data rate for the PCM system. As a consequence, the power budget illustrated herein is based upon the bandwidth requirements of the tone digital format, thereby resulting in a somewhat more conservative design.

a. System Requirements

The preliminary draft of the NASA document, Standard for Tone Digital Command Systems states that the ground transmission system used for command purposes shall be AM and operate in the 148 to 150 MC band.

The necessary system parameters can be determined as follows:

(1) The free space loss plus atmospheric losses can be found for a 30° ground elevation angle to the satellite, from Figures 1-2 and 1-3. At 148 MC this is -168 DB.

(2) The total effective receiver noise temperature is

$T_e = T_a + T_r$

$T_r = (NF-1)\ 290°K$

for a 5 DB NF receiver

$T_r = 610°K$

$T_a$ is the contribution to the satellite command antenna from galactic and cosmic noise. The hot Earth temperature (290°K) contribution can be disregarded in view of its small subtended angle from the omnidirectional antenna. The cosmic noise contribution can be obtained from Figure 1-7 and is 450°K.

The total antenna temperature is

$T_a = 450°K$

The total effective receiver temperature is

$T_e = T_r + T_a$

$= 610 + 450 = 1060°K$

(3) The receiver IF bandwidth is basically determined by several factors

(a) Highest tone digital command subcarrier frequency 11 KC

(b) Ground transmitter carrier frequency drift +0.001 percent or ±1.48 KC

(c) Receiver local oscillator frequency drift ±0.003 percent or ±3.5 KC

(d) Maximum doppler shift during transfer ellipse 0.0034 percent or 5 KC.

Based on the above factors plus a 10 percent safety factor, an IF bandwidth of 50 KC will be used.

(4) A three element helix antenna will be employed at the ground station with a gain of 20 DB over a circularly polarized isotropic source.

(5) The satellite turnstile antenna gain will be approximately - 3 DB

(6) The diplexer loss (used to suppress the telemetry transmitter output from the receiver during telemetry transmission) is in the order of -2.5 DB.

b. Power Budget Calculations

The power budget can now be calculated.

Receiver Signal Power Calculation (DB)

| | |
|---|---|
| Free space losses | -168 |
| Receiver antenna gain | - 3 |
| Transmitter antenna gain | + 20 |
| Diplexer losses | -2.5 |
| Fading Margin | - 10 |
| Transmitter power, 5000 watts | + 37 |
| Net Receiver Input Power C | -126.5 |

Receiver Noise Power Calculation

Receiver total effective noise temp. 1350°K

Receiver IF bandwidth 50 KC

Receiver noise power, from Figure 1-13 is 151.5 DBW

C/N = -126.5-(-151.5) = 25DB

c. Conclusions

This value of C/N is sufficiently high to afford a satisfactory signal level during the times when the satellite will be spinning or tumbling during the transfer ellipse phases, when a 10 DB degradiation in signal level could be expected.

The command receiver will be completely transistorized and will be of the single conversion AM superheterodyne type with a crystal controlled local oscillator. Two command receivers will be operated in parallel in order to provide redundancy and thus reliability. One suitable method of receiver output selection (employed in Syncom I) would be to provide a common AGC bus for the two receivers. The receiver with the largest AGC DC amplifier output would provide most of the audio output to the decoder by decreasing the RF gain in the other receiver.

The antenna configuration will be similar to that used in Syncom I and other satellites. The same antenna will be used by both the command and telemetry channels. Matching will be done by suitable balun matching sections and matching transformers. A diplexer will be employed to provide adequate isolation between the command and transmission systems.

The characteristics of typical command receivers which may be utilized (after modification) for the SMS are as follows:

| Manufacturer | Avco | Avco | Hughes |
|---|---|---|---|
| Model | 184003 | 183114 | Syncom |
| Frequency range | 100-150 MC | 100-150 MC | 148 MC |
| IF bandwidth | 35 KC | 35 KC | 60 KC |
| Sensitivity | 1.5uv(75%mod.) | 1.5uv(75% mod.) | - |
| Image rejection | 80 DB | 80 DB | 60 DB |
| Local oscillator stability | ± 2 KC | ± 2 KC | ±3.5 KC |
| DC voltage | 12 V | 15.6 V | -24 V |
| DC power | 170 mw | 200 mw | 500 mw |
| Weight | 1 lb | 1.5 lb | 10 oz |
| Size | 3.5x5x1 in. | 6.3 in. diam. x 1 1/8 in. high | 10 cu. in. approx. |
| Temperature range | -20 to +70°C | -20 to + 70°C | -29 to + 36°C |

4. SMS Transponder Relay System

The function of a relay system would be to rebroadcast meteorological information via the SMS to weather stations in various localities, and existing ground data receiving stations. This would minimize the use of conventional wire links and radio facilities which are presently less than adequate for this purpose.

In order to perform the relay function, special instrumentation may be required aboard the SMS. Therefore, to conserve weight it is desirable that this instrumentation utilize as much of the existing equipment already aboard the SMS (such as the telemetry and sensor data transmitter) as is possible.

In order to receive relay transmissions from the SMS, the ground station must be located in an area within line of sight of the SMS. If the SMS is located on the equator at 90° west, this area is bounded approximately by the outermost curve on Figure 1-52, where the elevation angle is 1.3°.

The type of information to be relayed via the satellite is processed meteorological data from the CDA station. This information may be in the following forms:

(1) Teletype system

(2) Black and white facsimile

(3) Nephanalysis pictures

(4) Shaded facsimile

(5) Broadband weather pictures

In the following paragraphs, the satellite transponder relay is studied from the viewpoints of bandwidth, power, antenna gains and transmission time. Two basic transponder relay systems are proposed, one using VHF and the other S-band frequency. Each of these will be compatible with the VHF telemetry system and the S-band sensor data system, respectively.

a. Characteristics of Relayed Information

Each of the information systems requires a certain baseband frequency for adequate operation. The baseband frequency is determined by the amount of time in which information need be transmitted. The less time available for transmission the greater the baseband frequency and hence the bandwidth. The bandwidth determines the noise power and therefore the power requirements of the system. The baseband frequency for the various information systems is discussed in the following paragraphs.

1) Teletype. Teletype printers having a capacity of 60 to 100 words per minute require a baseband frequency of approximately 100 cps (Ref. 1-32). High speed teletype requires a baseband frequency of approximately 750 cps.

2) Facsimile. Facsimile transmissions are available in a large variety of formats ranging from 18 x 22 inches for a meteorological map to 8 x 7 inches for a photofacsimile. The larger formats in general carry more detail and therefore contain a larger number of picture elements. Table 1-12 shows the characteristics of various fascimile systems (Ref. 1-32). For example a meteorological map contains 396 x $10^4$ picture elements while the small photofacsimile may contain only 1/8 as many elements. The baseband frequency is determined by the rate at which these picture elements are to be transmitted. In this table the baseband frequency is assumed to be one-half the number of picture elements per second. The resolution for most facsimile systems is approximately 100 lines/inch with readout times ranging up to 37 minutes. The baseband frequency ranges up to 3600 cps, enabling transmission over voice type circuits.

3) Wide Band Data. The maximum video frequency generated by a television camera is directly proportional to the rate at which picture elements are scanned along each line. The rate of scanning picture elements is given by the following formula

$$R = \left(\frac{W}{h}\right) mf\,k\,n^2 \frac{(1+b_h)}{(1+b_v)}$$

where
- $R$ = maximum rate of scanning picture elements
- $\frac{W}{h}$ = aspect ratio
- $m$ = ratio of horizontal resolution to the vertical resolution
- $f$ = Number of frames per second
- $k$ = utilization ratio
- $n$ = number of lines per frame
- $b_h$ = horizontal retrace ratio
- $b_v$ = vertical retrace ratio

Since there are two elements per cycle of a wave, the maximum video frequency

$$f_{max} = \frac{1}{2} R$$

For standard commercial television

$$\frac{W}{h} = 4/3,\ m = 0.925,\ k = 0.75,\ n = 525,\ b_h = 0.20,\ b_v = 0.08 \text{ and } f = 30$$

Therefore $R = 8.5 \times 10^6$ picture elements per second.

The maximum video frequency is

$$f_m = 4.25 \text{ MC at 30 frames per second}$$

TABLE 1-12
CHARACTERISTICS OF FACSIMILE TRANSMISSION

| | Copy size (inches) | Scanning lines per inch | Scans per minute | Total scanning time (minutes) | No. of elements | Elements per second | Base-band required (cps) |
|---|---|---|---|---|---|---|---|
| Nimbus APT | 8 x 8 | 100 | 240 | 3.33 | $64 \times 10^4$ | 3200 | 1600 |
| Meteorological Maps: | | | | | | | |
| Type 1 | 18 x 22 | 100 | 120 | 18.35 | $396 \times 10^4$ | 3600 | 1800 |
| Type 2 | 18 x 22 | 100 | 240 | 9.2 | $396 \times 10^4$ | 7200 | 3600 |
| Type 3 | 18 x 22 | 100 | 60 | 36.7 | $369 \times 10^4$ | 1800 | 900 |
| Photographs | | | | | | | |
| Type 1 | 8 x 7 | 138 | 100 | 9.66 | $107 \times 10^4$ | 1850 | 925 |
| Type 2 | 8 x 7 | 96 | 90 | 7.5 | $51.6 \times 10^4$ | 1150 | 575 |
| Type 3 | 8 x 7 | 96 | 45 | 15.0 | $51.6 \times 10^4$ | 575 | 287.5 |
| Type 4 | 8 x 12 | 100 | 100 | 12 | $93 \times 10^4$ | 1330 | 665 |
| Type 5 | 8.5 x 12 | 150 | 120 | 15 | $225 \times 10^4$ | 2500 | 1250 |

If a slow scan television system is used such as one frame in 10 seconds, the maximum video frequency would be 14.2 KC. For a 100 second readout, the maximum video frequency would be 1.42 KC.

b. Transmission Time

The transmission time of relayed facsimile pictures is an important parameter. If a time sharing arrangement is used with the sensor data transmitter, it is desirable to use as little time for the relay function as possible, to allow more time for sensor data transmission. The transmission time is determined by the number of picture elements to be transmitted. The number of picture elements is in turn determined by the required resolution and the size of the photograph. The faster that it is desired to transmit the picture, the greater the baseband frequency and hence IF bandwidth required. This in turn influences the relay transmitter power required. The general relations between these parameters are as follows:

$$\text{Number of Picture Elements} = \text{Area} \times (\text{scanning lines per inch})^2$$

The approximate relationship between the picture elements per second and the maximum baseband frequency for facsimile is:

$$\text{Maximum baseband frequency} = \frac{\text{Picture elements per second}}{2}$$

The relationship between transmission time and baseband is given in Figure 1-48 for various facsimile pictures. The larger pictures such

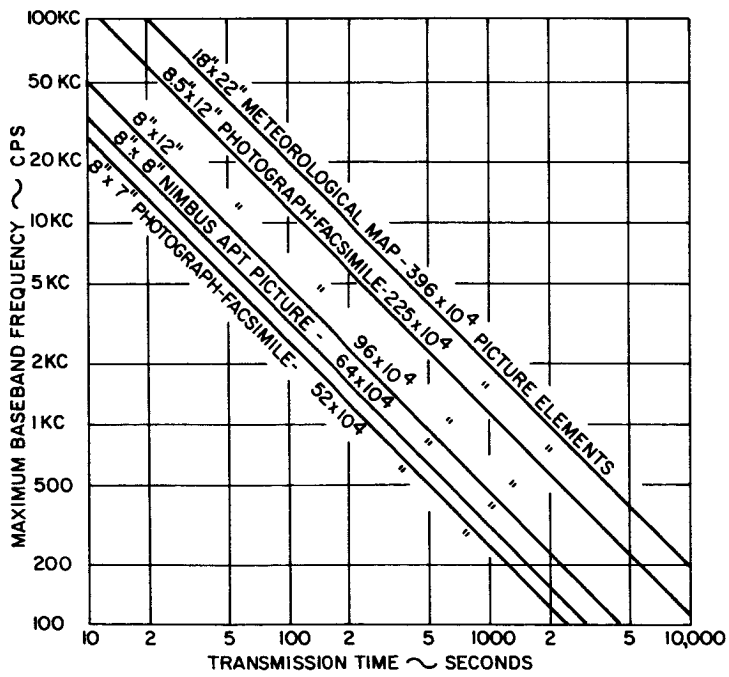


Figure 1-48. Relay Baseband Frequency vs Transmission Time for Facsimile Pictures

as 18 x 22 inch meteorological maps have correspondingly many more picture elements and hence take a longer time to transmit for given maximum baseband frequency. To illustrate the use of this graph, if the 8 x 8 inch Nimbus APT picture is transmitted in 200 seconds, the baseband is 1600 cps maximum. If it is desired to transmit the Nimbus APT picture at a baseband frequency of 160 cps, the transmission time would be 2000 seconds.

The relation between the baseband frequency and the IF bandwidth depends upon the modulation method. If the 1600 cps baseband is used to amplitude modulate a subcarrier of 2400 cps which in turn frequency modulates the 136 MC carrier with a deviation index of 2, the IF bandwidth (see subsection A) needed is

$$\begin{aligned} BW &= 2\,(1 + D)\,f_m \\ &= 2\,(1 + 2)\,4000 \\ &= 24 \text{ KC.} \end{aligned}$$

where $BW$ = IF bandwidth (containing 99 percent of the energy)
$D$ = modulation index = 2
$f_m$ = highest modulating frequency
= 1600 + 2400 = 4000 cps

c. Signal To Noise Ratio

For high grade photofacsimile transmissions with photographically processed recordings, the rms noise level into the facsimile receiver should be at least 35 to 40 DB (Ref. 1-32) below the maximum picture carrier. In black and white transmissions the copy appearance is not important but good legibility is necessary. The noise can be much higher than for tone pictures depending on the size of the lettering of the copy. For 12 point boldface characters, the rms noise should not be less than 10 DB below the signal level into the facsimile receiver.

d. Types of Relay Repeaters

The information to be relayed will not be processed in the SMS, therefore, a repeater would be used on board the SMS. The function of the repeater would be to receive a modulated carrier coming up from the CDA ground station, change the carrier frequency, amplify the new carrier, and rebroadcast it to the MDA ground stations. There are many types of repeater systems available (Ref. 1-38) and they are discussed in the following subsections. Refer to Figure 1-48A.

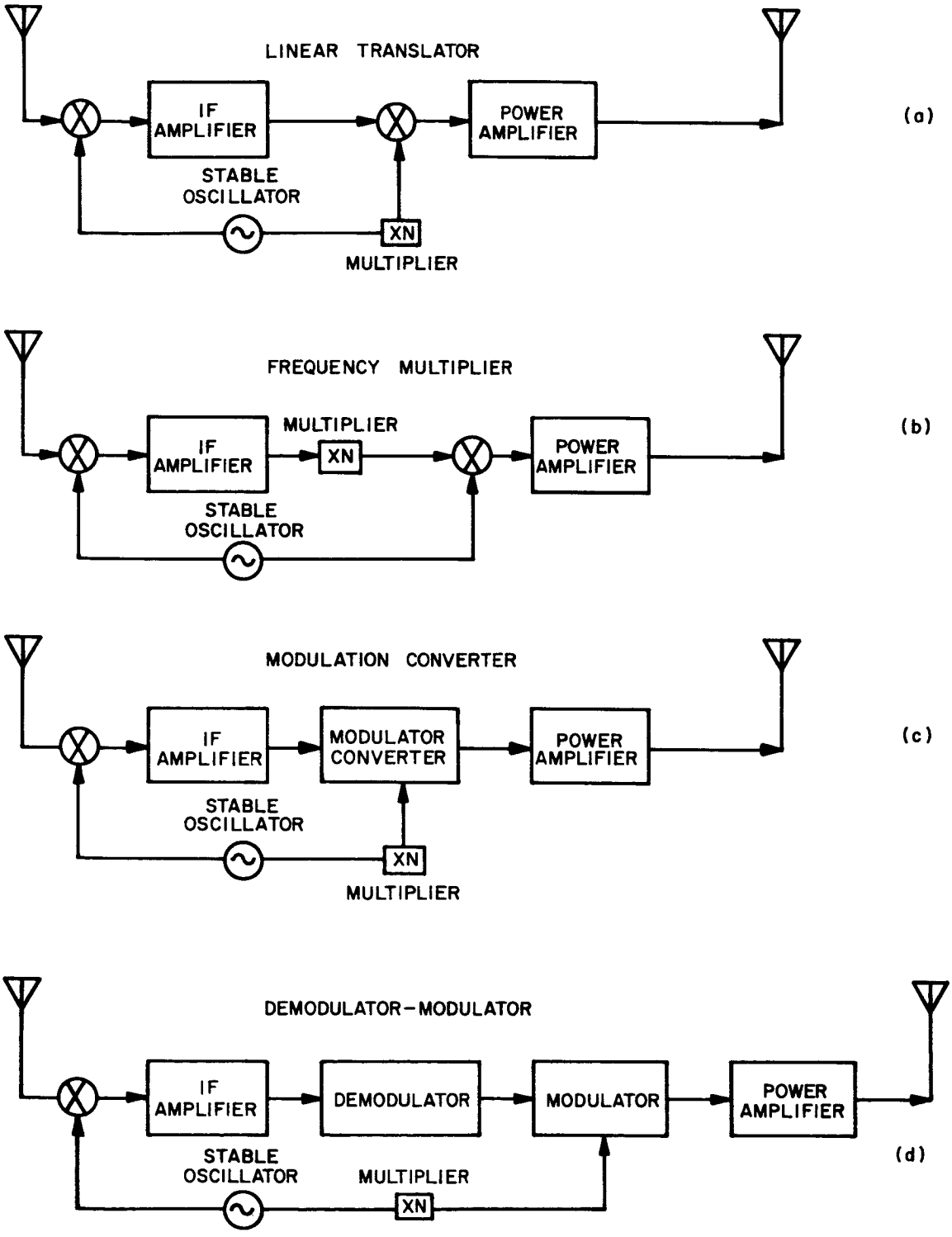


Figure 1-48A. Types of Relay Repeaters

1) Linear Translater. The linear translater simply performs a frequency translation on the incoming signal spectrum before retransmission. The input signal is heterodyned with a stable oscillator to produce an IF signal. The IF signal is then heterodyned with a multiple of the stable oscillator frequency and the output fed to a power amplifier.

2) Frequency Multiplier Repeater. The frequency multiplier repeater reduces the received signal to an intermediate frequency and then multiplies it to the transmitted frequency. The frequency deviation is also multiplied by the same factor and the RF bandwidth occupancy increased. The frequency multiplier is therefore useful in matching a high power narrowband ground transmitter (e.g.a. Klystron) to a low-power wideband satellite transmitter (e.g. a traveling wave tube). The multiplier is suitable only for FM or PM signals.

3) Modulation Converter. The modulation converter changes the input modulation form. It has been proposed specifically for converting single sideband (SSB) transmissions to FM. The conversion can be accomplished by inserting at the satellite receiver a strong local carrier along with the stack of SSB telephone channels. The weak frequency modulation of the carrier that results is then enhanced (after limiting) by frequency multiplication. Both amplitude and frequency stability of the inserted carrier are vital. The former determines the ultimate frequency occupied by SSB signals.

4) Demodulator-Modulator Repeater. This type reduces the information to baseband, operates on it and then allows it to modulate the satellite transmitter. Having been designed for one type of modulation, this repeater is inflexible in changing to another type. The ability to process the baseband signals may be important in processing equipment but will, in general, be an additional burden on the satellite.

e. S-Band Transponder Relay

One method of providing the relay function in the SMS vehicle is by use of an S-band transponder system. The transmitter and antenna portions of the transponder would be the sensor data transmitter and the sensor data antenna already aboard the SMS. An S-band receiver would have to be incorporated on the SMS to receive the relayed messages from the ground. A block diagram of the system is shown in Figure 1-49. Since the relay is used only when the

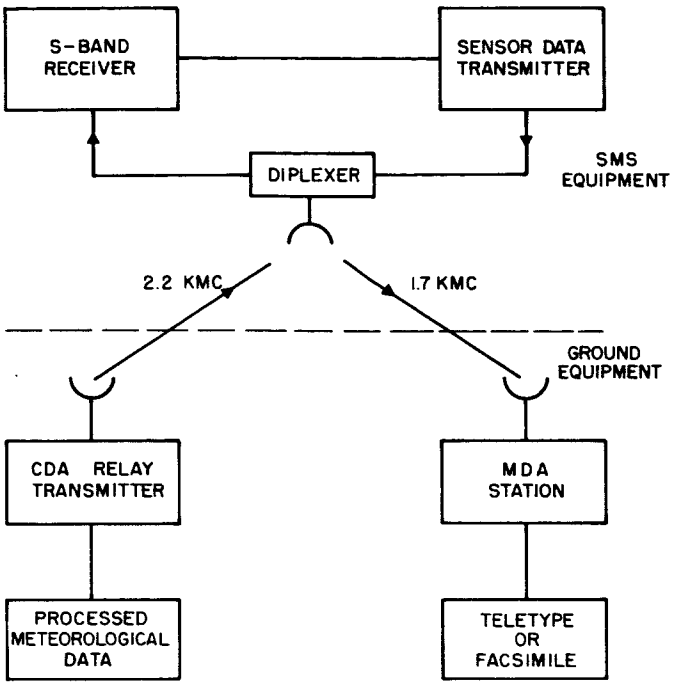


Figure 1-49. S-Band Transponder Relay

SMS is in its station-keeping position, the sensor data antenna would be pointed toward the Earth. The S-band receiver would weigh approximately 3 lb and require a power input of approximately 3 watts. This receiver, made frequency coherent, would be the same as required with the S-band RARR system discussed in subsection B-5. Therefore both the relay function and the range and range rate measurement function could be performed with the same transponder, i.e., the S-band receiver and the sensor data transmitter.

The power budget and power requirements for the down link are the same as those of the sensor data transmitter. The sensor data transmitter can be time multiplexed or frequency multiplexed for the relay function and sensor data function. The power requirements depend upon the bandwidth and C/N ratio required. These considerations for the sensor data transmitter are given in subsection B-1. Baseband frequencies of up to 100 KC could be used with this S-band relay.

A typical power budget for the S-band relay is shown in Table 1-13. The data being relayed is assumed to be an 18 x 22 inch meteorological map (type 1 of Table 1-12). The baseband frequency range is 1800 cps amplitude modulating a subcarrier of 3600 cps. The composite signal frequency modulates a carrier of 2200 MC. The 2200 MC carrier is transmitted to the spacecraft receiver. This demodulates the carrier obtaining the composite signal. The composite signal is then used to modulate the sensor data transmitter in a frequency multiplexing arrangement. The power level is assumed to be 1 watt.

TABLE 1-13
TYPICAL POWER BUDGET FOR S-BAND RELAY

A. Ground to Spacecraft Link

| | |
|---|---|
| Ground transmitter power -1 KW at 2200 MC | + 30 DBW |
| Ground antenna gain<br>85 ft dia. parabolic dish | + 53 DB |
| Free space loss<br>2300 MC at 25,750 miles | -192 DB |
| Spacecraft antenna gain | + 19 DB |
| Received signal power | - 90 DBW |
| S-band relay receiver noise figure (NF) = 5 DB | |
| S-band relay antenna temperature ($T_a$) = 400°K | |
| S-band receiver temperature ($T_r$ = 290 (NF-1)) = 620°K | |
| Total effective temperature ($T_e = T_a + T_r$) = 1020°K | |
| S-band relay receiver bandwidth = 600KC | |
| S-band relay receiver noise power | -140 DB |
| Miscellaneous losses | - 5 DB |
| Received C/N ratio | + 45 DB |

B. Spacecraft to Ground Link

| | |
|---|---|
| S-band relay output (1 watt) | 0 DBW |
| Satellite antenna gain (1.75 foot diameter) | + 17 DB |
| Free space loss (1700 MC at 25,750 miles) | -190 DB |
| Miscellaneous losses | - 3 DB |
| Ground antenna gain (28 foot diameter) | + 41 DB |
| Received signal | -135 DB |
| Receiver noise figure (Pre-amp NF) = 3.5 DB | |
| Receiver noise temperature ($T_r$ = 290 (NF-1))= 350°K | |
| Antenna noise temperature ($T_a$) = 100°K | |
| Total noise temperature ($T_e = T_r + T_a$) = 450°K | |
| Baseband = 0 to 1800 cps | |
| Subcarrier frequency 3600 cps | |
| Highest modulation frequency ($f_m$) = 1800 + 3600 = 5400 cps | |
| Deviation ratio (D) = 2 | |

TABLE 1-13

B. Spacecraft to Ground Link (continued)

| | |
|---|---|
| RF spectrum bandwidth (BW=2 (1 + D) $f_m$) = 32,400 cps | |
| Receiver noise bandwidth (B) = 50 KC | |
| Receiver noise power (N) = $KT_eB$ | -155 DBW |
| Carrier to noise ratio (C/N) | 20 DB |
| Output signal to noise ratio | 27 DB |

The relay S-band ground station would consist of a 28 foot diameter parabolic dish, receiver and facsimile recorder. The antenna would be fixed in direction and pointed toward the SMS eliminating expensive gimbal structures. The receiver front end could be a tunnel diode S-band receiver having a noise figure of 3.5 to 4 DB. The receiver output would be fed into the facsimile recorder.

f. VHF Transponder Relay

Another approach toward satisfying the relay function is to utilize the command receiver and telemetry transmitter as a transponder. A block diagram of this system is shown in Figure 1-50. No additional equipment

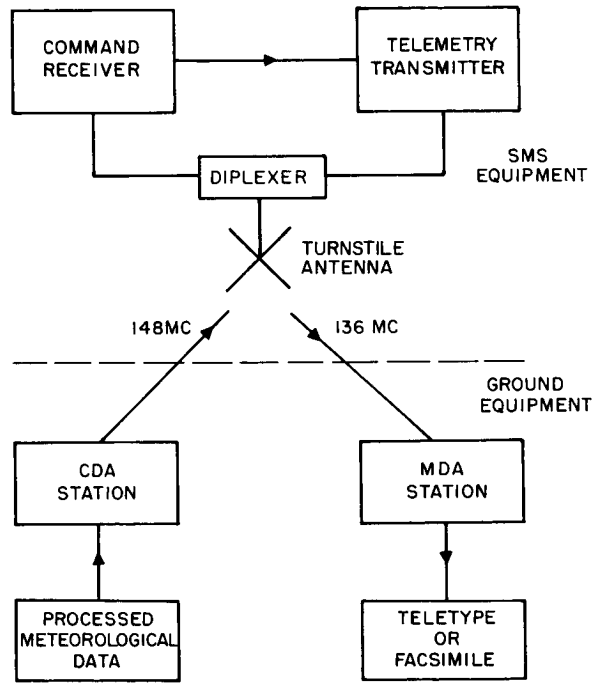


Figure 1-50. VHF Transponder Relay

would be required aboard the SMS. In addition, if the transponder were made frequency coherent as described in subsection B.5, it can be employed in the range and range rate tracking system. The disadvantage of a VHF relay system is the limited bandwidth available (up to several kilocycles). This imposes a limitation on the rate at which information can be transmitted. Therefore, a low information rate system such as single channel teletype could be used or, if facsimile is used, it may require a longer time to transmit a complete picture. A typical power budget is shown in Table 1-14.

TABLE 1-14
TYPICAL POWER BUDGET FOR VHF RELAY

A. Ground to Spacecraft Link

| | |
|---|---|
| Ground transmitter (5 KW at 148 MC) | 37 DBW |
| Ground antenna | 20 DB |
| Free space loss (25,750 miles at 136 MC) | -167.8 DB |
| Receiver (command and telemetry) antenna gain | - 3 DB |
| Miscellaneous losses | - 10 DB |
| Received carrier power | -123.8 DB |
| Receiver noise figure = 5 DB | |
| Receiver noise temperature (290 (NF-1))= 620°K | |
| Antenna temperature = 1000°K | |
| Total effective temperature = 1620°K | |
| Receiver noise bandwidth = 35 KC | |
| Receiver noise power (KTB) | -151.0 DB |
| Receiver carrier to noise ratio | 27.2 DB |

B. Spacecraft to Ground Link

| | |
|---|---|
| Spacecraft (telemetry) transmitter (Power at 136 MC 2.5 W) | + 4.0 DBW |
| Satellite antenna gain | - 3.0 DB |
| Free space loss (136 MC at 25,750 miles) | -168.5 DB |
| Receiver antenna gain | + 19 DB |
| Miscellaneous losses | - 10 DB |
| Received carrier power | -158.5 DB |
| Receiver noise figure (NF) = 3 DB | |
| Receiver noise temperature ($T_r$ = 290 (NF-1)) = 290°K | |
| Antenna noise temperature ($T_a$) = 1000°K | |
| Total noise temperature = $T_r + T_a$ = 1290°K | |
| Receiver IF bandwidth = 1 KC | |
| Receiver noise phase-locked bandwidth = 100 cps | |
| Receiver noise power (KTB) | -177 DBW |
| Carrier to noise ratio | + 18.5 DB |
| Output signal to noise ratio for deviation index of 2 | + 29 DB |

5. Satellite Beacon and Tracking

A prime requirement for successful operation of the SMS is an accurate knowledge of position and velocity during launch, orbit injection, and station-keeping. These measurements are needed for the following purposes:

(1) For time and guiding the orbital injection operations

(2) For detecting and measuring later drifts of the orbit beyond acceptable limits in order to have a basis for corrective commands

(3) For obtaining reference coordinates of cloud pictures and other meteorological data

In order to perform the tracking function, special instrumentation will be required aboard the SMS. Therefore, to conserve weight it is desirable that this instrumentation utilize as much of the existing equipment already aboard the SMS (such as the telemetry and sensor data transmitters) as is possible.

a. SMS Launch and Orbit Injection Path

The placement of the SMS will probably be accomplished in a number of stages. These stages include launch, parking orbit, orbit injection by transfer ellipse, and final apogee motor impulse. Each of these stages will be discussed in relation to the beacon and tracking considerations for the SMS.

1) Launch and Parking Orbit Phase. The SMS propulsion vehicle will be launched from Cape Canaveral and directed into a parking orbit. The parking orbit is assumed circular and at an altitude of approximately 100 miles. The plane of the parking orbit will be approximately 28 degrees from the equatorial plane.

2) Transfer Ellipse Phase. When the SMS is in its parking orbit, a rocket motor will be ignited to bring it into the transfer ellipse phase. The initiation of the transfer ellipse will occur at the longitude of approximately 172° W and at the equator. Figure 1-51 is the computed transfer ellipse (Hohmann Ellipse) characterization. (Ref. 1-33). It shows the altitude of the SMS as a function of time. The SMS is expected to reach synchronous altitude in approximately 5-1/2 hours after leaving the parking orbit. The figure also shows the position of the SMS in the transfer ellipse relative to coordinates on the Earth's surface. The graph shows that approximately 5-1/2 hours after leaving 172°W longitude at the equator, the SMS will be at 90°W longitude at the equator. The vehicle will then be at the apogee of the transfer ellipse.

3) Apogee Phase. When the SMS has reached the apogee of the transfer ellipse, an apogee motor will be ignited. This will place the SMS in the required synchronous orbit.

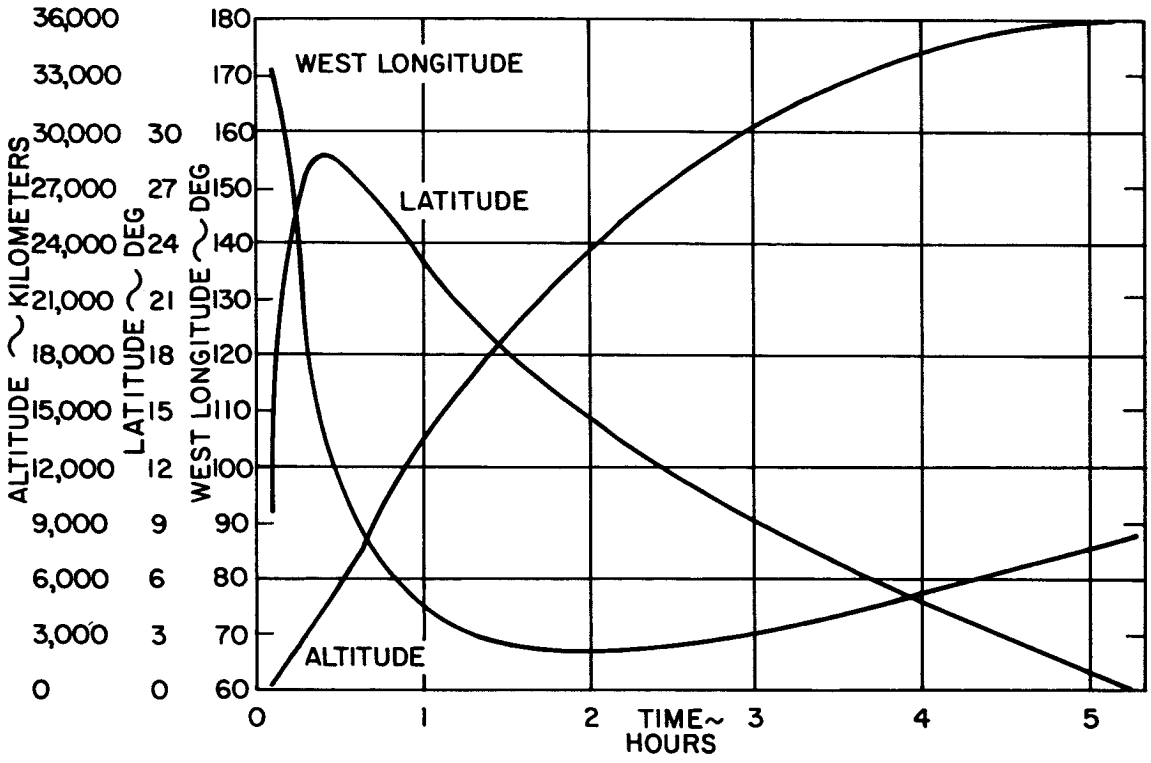


Figure 1-51. SMS Transfer Ellipse Characteristics

4) Stationkeeping. During stationkeeping, it is expected that maximum drift in the SMS will be the following:

| | |
|---|---|
| Maximum angular drift: | ±5 degrees longitude |
| | ±5 degrees latitude |
| Maximum altitude drift: | ±300 miles |

5) Tracking Angle of Elevation. Figure 1-52 shows the angle of elevation of SMS in its stationkeeping position as observed from various geographical locations on the Earth's surface. The chart indicates that in areas such as Europe and most of Africa, the SMS would be below the horizon so that a CDA or tracking station could not be established there. At fringe areas such as Fairbanks, Alaska the SMS would be very low on the horizon (approximately 4 degrees elevation) making it an unsuitable location for the CDA or tracking station. However, almost all of Canada, the U.S., and South America would be suitable for tracking.

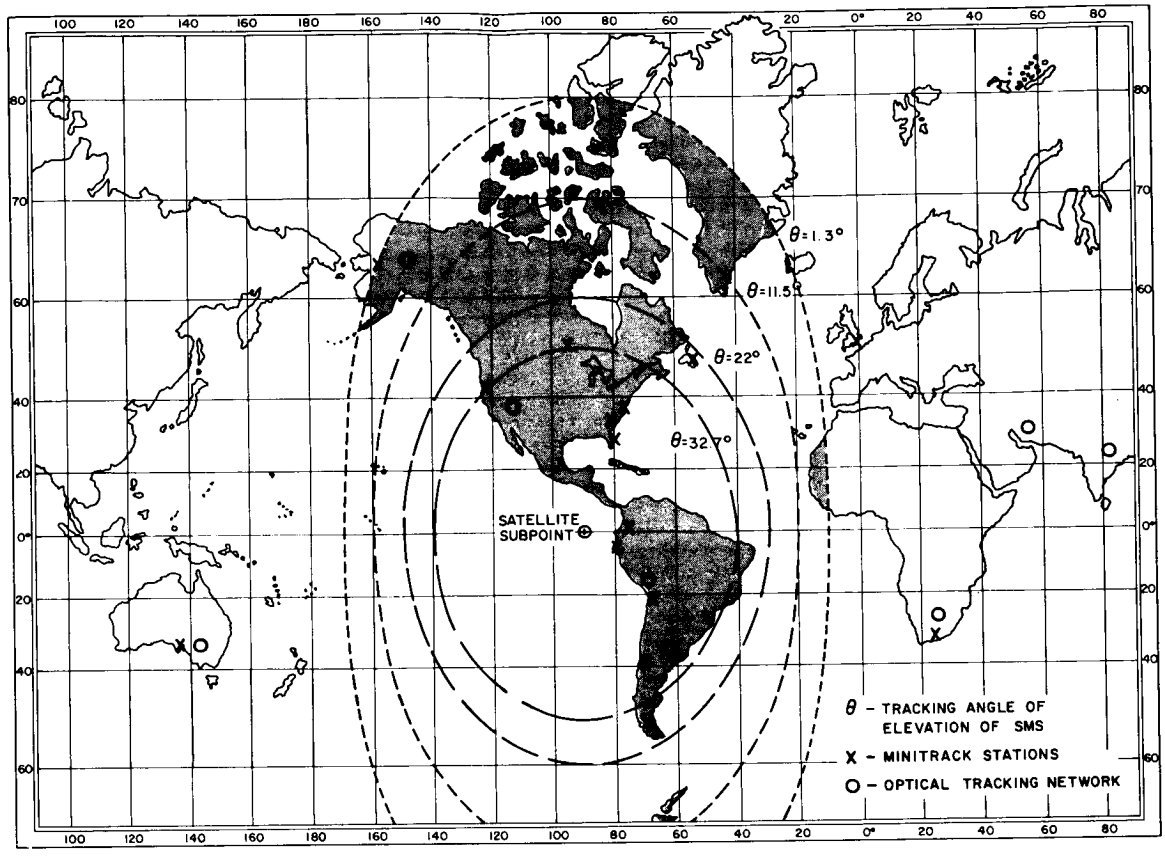


Figure 1-52. SMS Coverage Map

6) Tracking Requirements. The tracking requirements for the SMS will vary for each phase of operation. During the launch and parking orbit phase, it is desirable to determine the orbital parameters such as period, eccentricity, inclination, etc. During the transfer ellipse, it is desirable to measure the trajectory parameters such as position and velocity. When the SMS is in its stationkeeping position, angular position may be adequate. Each of these phases may therefore require a different method of tracking. These methods are discussed in subsequent paragraphs.

b. Goddard Range and Range Rate System (RARR System)

The basic function of the RARR system is orbital or trajectory determination of spaceborne vehicles. The method of trajectory determination is based upon the precise determination of range and range rate from one or more ground stations. The general system used in determining range and range rate is illustrated in the simplified diagram of Figure 1-53. In the RARR system, the ground transmitter, modulated by ranging sidetones, sends a signal to the

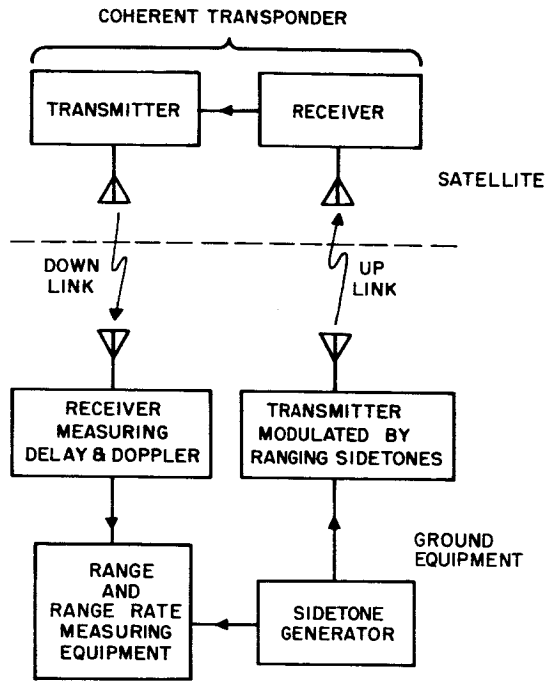


Figure 1-53. Goddard Range and Range Rate System

satellite transponder which re-transmits the signal back to the ground. The phase delay in the sidetones is used for measuring range. The transponder is frequency coherent throughout so that the doppler shift frequency is preserved and re-transmitted resulting in an accurate measure of range rate. The ground stations of the RARR system are designed to be transportable.

1) Range Measurement. Range measurements are accomplished using the basic sidetone technique with frequencies of 8, 32, 160, 800 cps; 4, 20, 100, and 500 KC. The highest frequency is selectable between 500, 100, and 20 KC, and is used to determine the finest increment of range, with the lower frequency tones used to remove range ambiguities. The range tones are phase modulated onto the ground transmitter carrier frequency and transmitted to the transponder. The transponder retransmits these tones, maintaining ranging tone phase coherence. The ground receiver compares the phase of the received ranging tones with the transmitted ranging tone phase, to determine range between the tracking station and the satellite.

2) Range Rate Measurement. The relative velocity (radial) between an observer on Earth and a satellite causes the familiar doppler shift in frequency of an RF signal received from the satellite. The amount of shift is given by

$$f_d = -\frac{\dot{r}f}{c}$$

where $f_d$ = shift in frequency received from the transmitted frequency in cps

$f$ = transmitted frequency in cps

$\dot{r}$ = relative velocity between receiver and transmitter in meters/sec.

$c$ = velocity of light = $3 \times 10^8$ meters/sec.

The doppler shift is, therefore, proportional to the carrier frequency and to the relative velocity.

Range rate or satellite velocity relative to the tracking station is determined by measuring the received doppler cycles per unit time, to determine the average velocity or range rate over that time interval. In order to determine the doppler frequency, it is necessary to maintain frequency coherence of the ground transmitter frequency through the transponder and back to the ground receiver. There the returned frequencies are compared against a coherent sample of the ground transmitter frequency.

3) Transponder Systems. The RARR system is capable of operation with two types of coherent transponders aboard the space vehicle, one being at VHF frequencies (136 MC) and the other at S-band frequencies (2300 MC). These units are intended to be compatible with the normal command-telemetry system or alternatively S-band transponder used in communication satellites. Due to bandwidth allocation limitations, the VHF system uses a maximum sidetone frequency of 20 KC, whereas the S-band system uses a maximum sidetone frequency of 100 KC. The lower sidetone frequency has lower accuracy. The doppler shift at VHF frequencies is proportionately less than that at S-band frequencies. For example, if the satellite had a velocity of 4 meters/sec, relative to the tracking station, the doppler shift at 136 MC would be 1.81 cps whereas at 2300 MC it would be 30.7 cps. The higher frequency shift can be measured with greater precision.

The VHF system is, therefore, less accurate than the S-band system and is intended for low weight satellites where the command-telemetry system can be adapted for RARR measurements.

4) Equipment Accuracy. The following listing gives the approximate equipment accuracies of each system:

| RARR System | VHF | S-Band |
|---|---|---|
| Equipment accuracy (approximate) | | |
| Range | ±75 meters | ±15 meters |
| Range rate | ± 1 meter/sec. | ±0.1 meter/sec. |
| Operating distance | 150 to 60,000 Nautical miles | 150 to 60,000 Nautical miles |
| Frequency - up links | 148 MC | 2271 MC |
| Frequency - down links | 136 MC | 1705 MC |
| Highest sidetone frequency | 20 KC | 100 KC |
| Down link power | Up to 4 watts | Up to 2 watts |

| RARR System | VHF | S-Band |
|---|---|---|
| Down link antenna gain | 0 DB | 0 DB |
| Ground antenna beamwidth | 17° | 2.5° |
| Ground antenna tracking accuracy (approximate) | 1° | 0.1° |

The VHF RARR system is not favored for future applications because a wide bandwidth is required for accurate measurements (up to 500 KC). This may not be available for allocation several years hence, so that the S-band system would be preferable.

5) RARR Station Locations. The location of RARR stations being planned for the next few years are at:

| | | Longitude | Latitude |
|---|---|---|---|
| (1) | Carnarvon, Australia | 113° 27' 02" W | 24° 30' 0" S |
| (2) | Rosman, North Carolina | 277° 15' 0" W | 35° 10' 0" N |
| (3) | Johannesburg, South Africa | 28° 14' 28" W | 26° 1' 57" S |

6) Proposed SMS Range and Range Rate Transponders. The choice of transponder, either VHF or S-band, would be determined by compatibility with presently existing equipment aboard the SMS as well as weight and power requirements. For a low capability vehicle where weight and power conservation is of utmost importance, the VHF RARR system can be incorporated into the normal VHF command and telemetry system. This is shown in block diagram of Figure 1-54. This diagram shows a 148 MC signal with sidetone modulation up to 20 KC

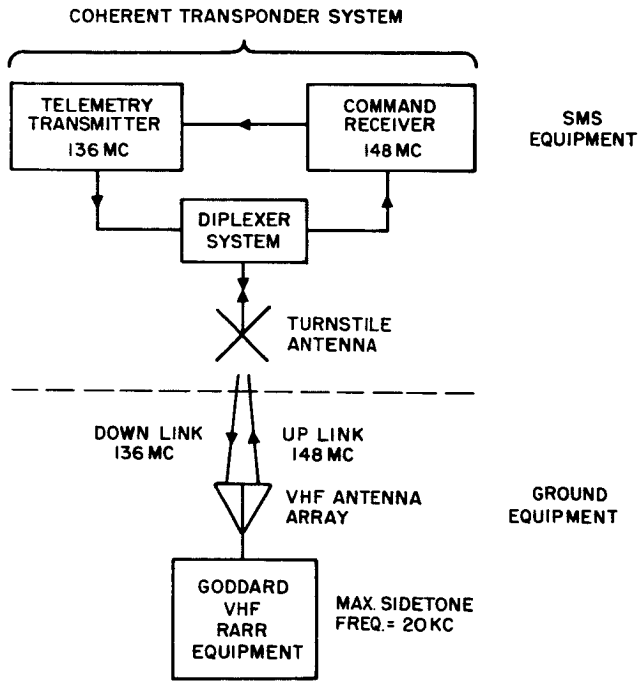


Figure 1-54. VHF Range and Range Rate System

being sent from the ground station to the command receiver aboard the SMS. The command receiver and the telemetry transmitter are arranged as the coherent transponder. The sidetone phase delay and doppler frequency change are then measured by the ground station providing range and range rate data. The major requirement for compatibility in the SMS would be to make the command and telemetry units frequency coherent throughout. This would involve increased circuit complexity, but would not increase the weight significantly. Goddard Space Flight Center is developing a coherent VHF transponder of 4 watts total output. It will weigh 4 to 5 lbs.

For the medium or high capability SMS, the S-band RARR system can be incorporated utilizing the sensor data transmitter. This is shown in Figure 1-55. Here the sensor data transmitter is made a part of the coherent

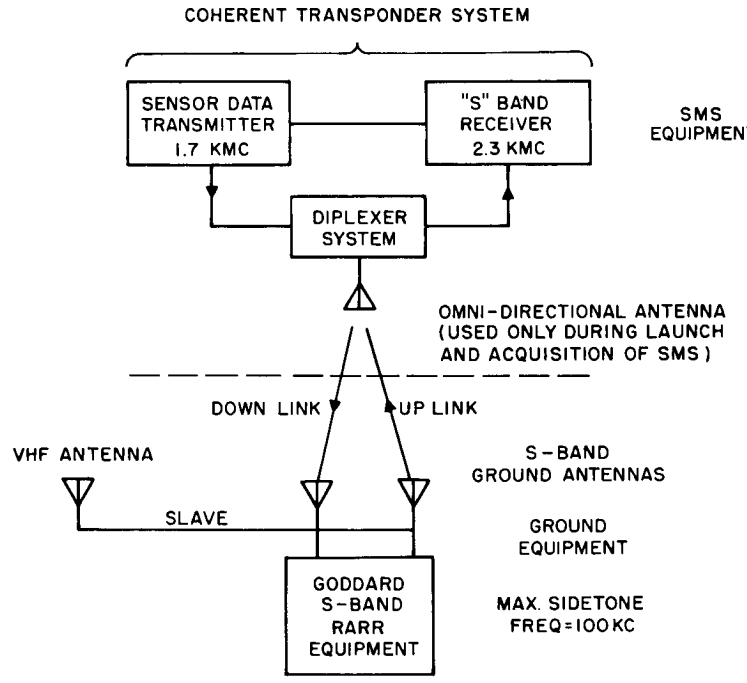


Figure 1-55. S-Band Range and Range Rate System

transponder. An additional S-band receiver would be required to complete the transponder. An S-band omni-directional antenna would also be required. This would be switched to the output of the sensor data transmitter during the launch and acquisition phase when range and range rate measurements are most important and when sensor data is not required. When the SMS assumes its proper operating station, the sensor data transmitter can be switched to its directional antenna.

The S-band receiver and the omni-directional antenna would not add an appreciable amount to the weight or power required. Also the S-band receiver could be used in a transponder relay for facsimile or teletype. This is discussed in subsection B.4. A coherent S-band transponder having an output of 0.65 w at 1700 MC has been developed for the EGO satellite. It weighs 8 lbs and the power input is 28 w.

For a medium or high capability SMS, the VHF RARR system could be employed as a back-up for the S-band RARR system. Therefore, if the latter failed in some manner such as losing coherency or the S-band receiver failed to function, the VHF system could function to supply range and range rate data, although at reduced accuracy.

7) VHF Beacon. After launching of the SMS, it is necessary that the Goddard RARR ground stations as well as the Minitrack Stations acquire and track the satellite. One mode of the operation is to extract range, range rate, and angular data from the S-band portion of the RARR system while utilizing the VHF receiving system for the initial antenna acquisition function. The relatively broad beamwidth (approximately 16 degrees) of the VHF ground antenna locks on to a 136 MC beacon aboard the SMS. The S-band ground antenna (approximately 2.5 degrees beamwidth) is slaved to the VHF ground antenna as shown in Figure 1-55 and proceeds to track the SMS, extracting range, range rate, and angular data.

Another mode of operation would involve only a VHF RARR transponder. Then the VHF ground antenna would acquire and track the beacon directly, extracting range and range rate data.

The 136 MC beacon aboard the SMS can be the telemetry transmitter signal unmodulated. This beacon would also be used for Minitrack Tracking stations.

When the telemetry transmitter is used in the beacon mode, reduced power output can be used to conserve power. A typical power budget would be as follows:

| | |
|---|---|
| Transmitter power (0.25 w at 136 MC with no modulation) | -6 DBW |
| Satellite antenna gain | -3 DB |
| Free space loss (25,750 miles @ 136 MC) | -167.8 DB |
| Receiving antenna gain (Minitrack 136 MC tracking antenna) | +15 DB |
| Miscellaneous losses | -5 DB |
| Received signal power | -166.8 DBW |

Receiver noise figure (Pre-amp) = 3 DB

Receiver noise temperature ($T_r = 290\,(NF-1)$) = 290°K

Antenna noise temperature ($T_a$) = 1000°K

Total noise temperature ($T_e = T_r + T_a$) = 1290°K

Receiver noise phase-locked tracking bandwidth = 10 cps

| | |
|---|---|
| Receiver noise power ($N = KT_eB$) | -187 DBW |
| Carrier to noise ratio | +20.2 DB |

8) Tracking with RARR Stations. Computations have been performed (Ref. 1-33) to determine path of the SMS during the transfer ellipse phase. Calculations were made to determine the path as seen from each of the three planned RARR stations given in section 5. The results indicated that the only facility capable of tracking the SMS during the transfer ellipse would be at Rosman, N. C. The results are given in Figure 1-56 which shows azimuth

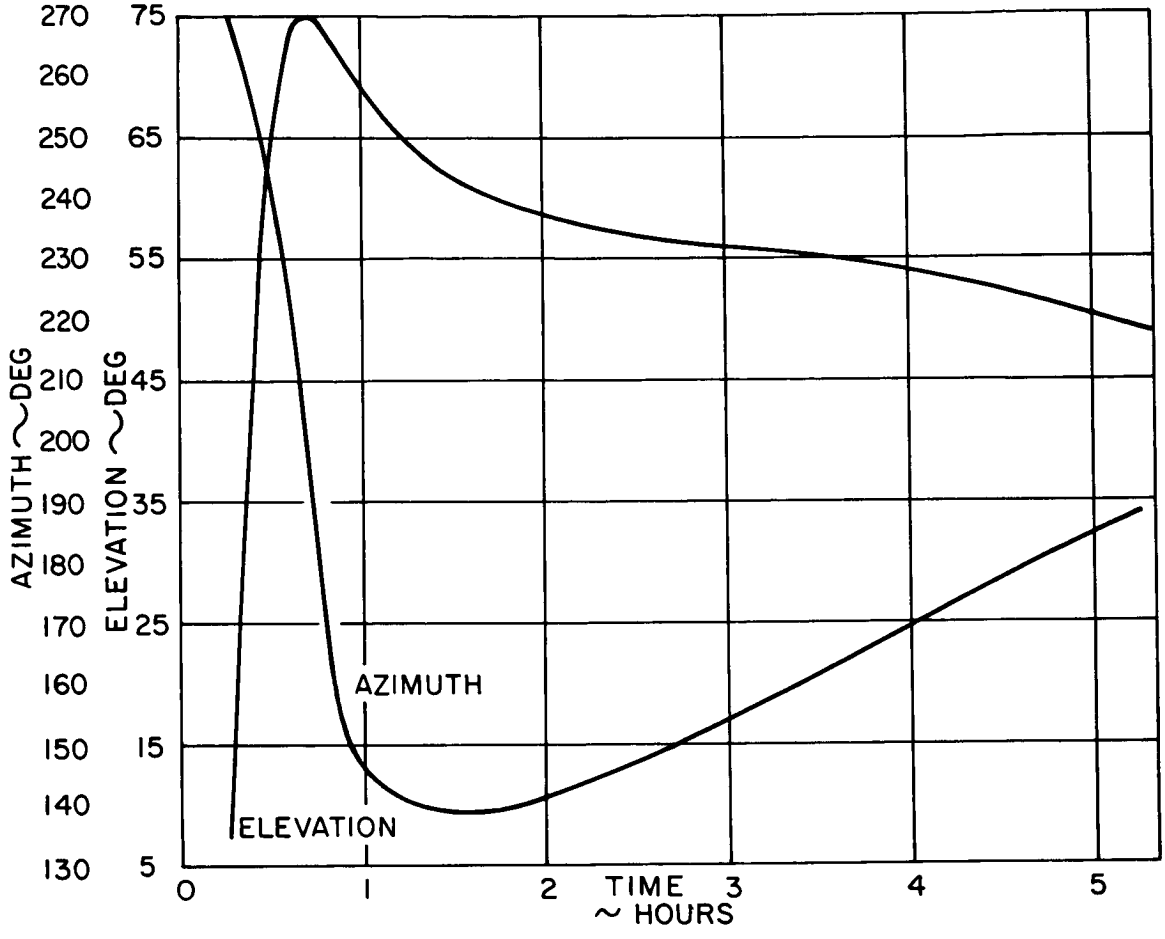


Figure 1-56. SMS Tracking Azimuth and Elevation Data During the Transfer Ellipse (as seen from Rosman, N.C.)

and elevation and Figure 1-57 which show slant range and range rate as measured from this station. This station would be capable of tracking the SMS approximately 16 minutes after it left the parking orbit and would follow it for the 5-1/2 hour period until it reached its final position. It is seen that slant range varies from approximately 5000 kilometers to a maximum of 36,000 kilometers. Range rate varies from approximately - 2 kilometers/second to +4 kilometers/second.

c. Minitrack Tracking Stations

These stations are general purpose tracking sites with telemetry reception capability. They are intended for tracking satellites with low circular orbits. They operate at VHF frequencies such as 108 and 136 MC and measure only angle using an interferometer technique. Their accuracy is about 10 seconds of arc. The Minitrack network would be used to track the SMS when

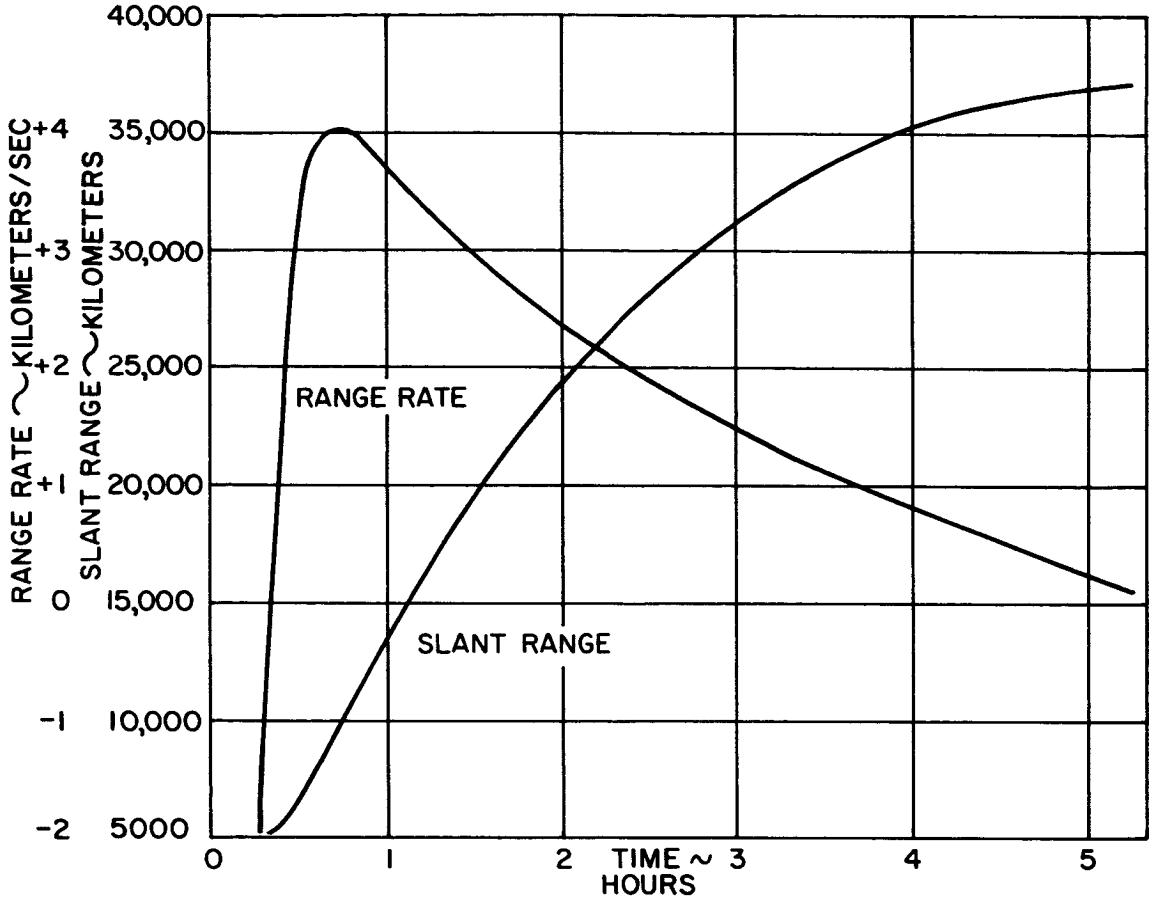


Figure 1-57. SMS Tracking Range Rate and Slant Range During the Transfer Ellipse (as seen from Rosman, N.C.)

it is in its parking orbit of 100 miles and for initial phases of the transfer ellipse. The location of the Minitrack stations is given in Figure 1-52. They are as follows: Woomera, Australia; College, Alaska; Goldstone, California; East Grand Forks, Minnesota; St. Johns, Newfoundland; Blossom Point, Maryland; Rosman, North Carolina; Fort Myers, Florida; Quito, Ecuador; Lima, Peru; Santiago, Chile; Antofogasta, Chile; Winkfield, England; Johannesburg, South Africa.

d. CDA Station Tracking

Another method of tracking the SMS during stationkeeping is to utilize the large parabolic antenna used for sensor data reception at the CDA station. The angular position of the SMS can be found by manual scanning with this antenna for maximum signal strength. Alternatively a rotating reflector can be mounted on the antenna to obtain conical scanning. The accuracy of the angular position would then be a fraction of the half power beamwidth. Figure 1-58 is a graph of approximate tracking accuracy versus ground antenna size. This is based upon the tracking accuracy equal to 1/20 of the half power beamwidth, a figure which is normally attainable in conically scanned tracking antennas.

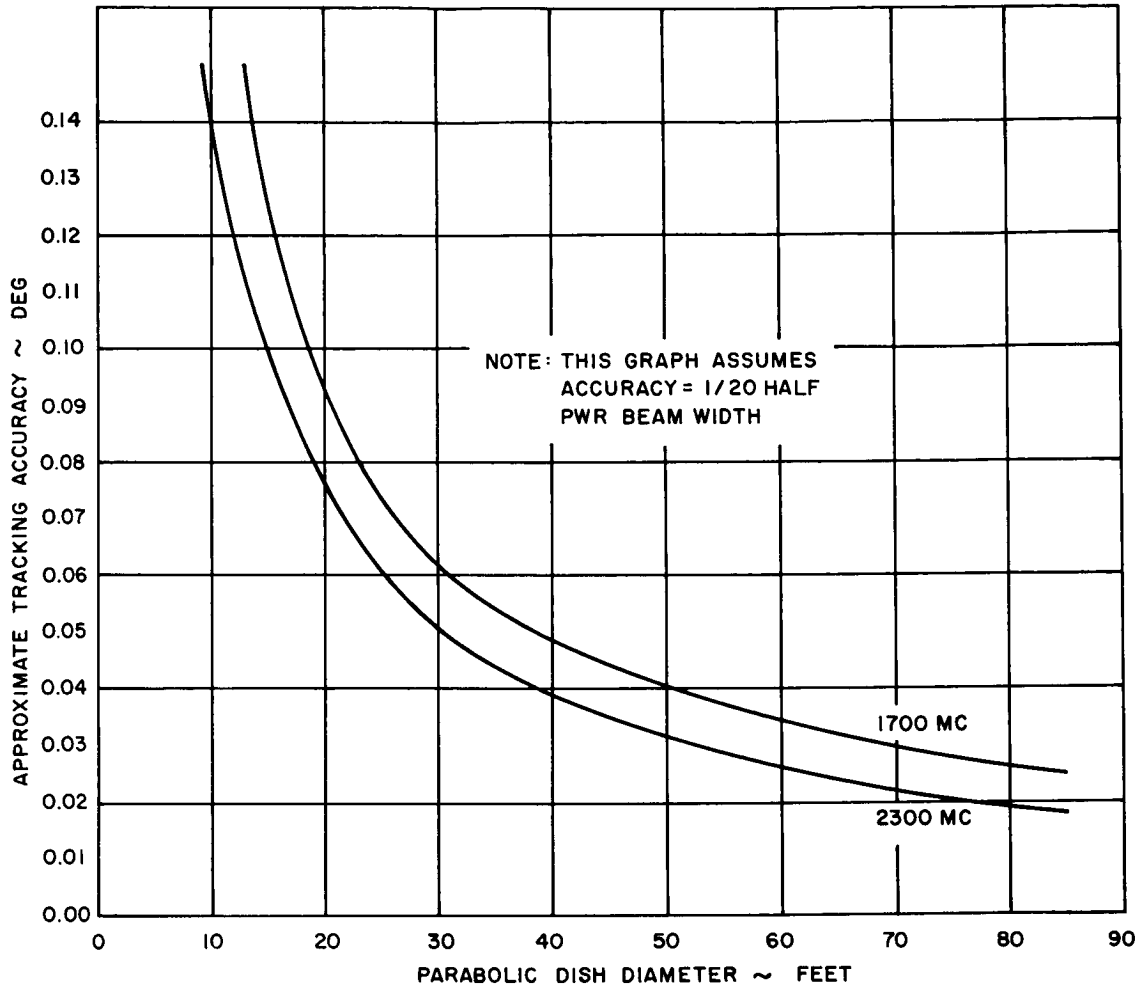


Figure 1-58. Tracking Accuracy vs Antenna Diameter

e. Transportable Angular Tracking Stations

Transportable tracking stations have been developed for tracking and commanding a synchronous communication satellite (Syncom). These can be modified for tracking the SMS during launch, orbit injection, and for station-keeping. The modifications would involve changing the frequencies. The pertinent characteristics of these units are shown in Table 1-15.

TABLE 1-15

CHARACTERISTICS OF TRANSPORTABLE ANGULAR TRACKING STATION FOR SYNCOM

(1) 30-foot parabolic antenna mounted on two military type semi-trailers

(2) Entire system transportable in C-124 and C-133 type aircraft

(3) Capable of assembly to operation in 2 days

(4) Servo and tracking system in 6 van-mounted racks

(5) Capable of automatic acquisition and tracking of satellite

| Characteristic | Specification Value |
|---|---|
| Tracking accuracy | ±0.057 degrees |
| Static reflector tolerance | 0.035 inch |
| Lock-on-time | 3 seconds maximum |
| SUPERHIGH FREQUENCY TRANSMISSION | |
| 7100 to 7800 MC Syncom - 7362 MC | |
| 20 KW average power, circular polarization | |
| Gain | 54 ± 1 DB |
| Main side lobes | 22 DB minimum |
| Beamwidth | 0.31 ± .05 degrees |
| VSWR | 1.25 maximum |
| Coalignment to UHF Beam | ± 0.02 degrees |
| ULTRA HIGH FREQUENCY RECEPTION | |
| 1700 to 1900 MC, Syncom - 1815 MC | |
| 100 milliwatts, adjustable linear polarization | |
| Gain | 42 ± 1 DB |
| Main side lobes | 23 DB minimum |
| Beamwidth | 1.3 ± 0.14 degrees |
| VSWR | 1.3 maximum |
| Crossover | 0.7 to 1.3 DB |
| S/N with a 1 cps bandwidth | 50 DB minimum |
| Allowable error | |
| 0 to 30 mph mean wind | 0.057 degrees |
| 31 to 45 mph mean wind | 0.128 degrees |
| Mean time between failures | 224 hrs |
| Life expectancy | 10 years |
| Minimum tracking velocity | 0.01 deg/sec maximum |

The transportable angular tracking station may be improved by the following means:

(1) A maser preamplifier can be added to reduce noise error and improve tracking accuracy.

(2) The antenna can be mounted on a fixed base to raise the system mechanical resonance point and permit the use of greater servo bandwidth to improve tracking accuracy.

(3) A 45-foot diameter reflector can be used in place of the 30-foot reflector to obtain greater RF gain.

(4) A Cassegrain reflector can be added to improve RF performance.

f. Ionospheric Refraction Effects

A major source of error in all satellite tracking schemes at VHF frequencies is ionospheric refraction. Atmospheric ionization is mainly caused by solar radiation so that maximum errors occur on the day side of the Earth and appreciably less refraction occurs on the night side. Studies (Ref. 1-34) have been made to determine the error angles caused by ionospheric refraction. Figure 1-59 shows the results for a satellite with a 200-mile decaying orbit during the daytime. The graph shows that at a frequency of 100 MC the elevation angle

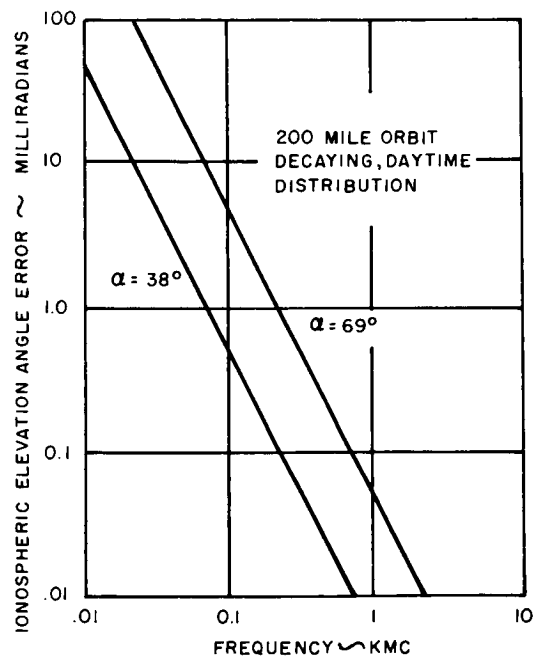


Figure 1-59. Refraction Error vs Frequency

error is in the order of several milliradians. At higher frequencies above 500 MC, the error is negligible.

Another study (Ref. 1-35) has been made to determine the refraction contribution to doppler shift for navigation satellites. Table 1-16 indicates the results of these studies.

TABLE 1-16

TYPICAL REFRACTION CONTRIBUTIONS TO THE DOPPLER SHIFT

| Frequency (MC) | Vacuum term (cps) | First order term (cps) | Second order term (cps) |
|---|---|---|---|
| 50 | 1250 | 10 | 0.5 |
| 100 | 2500 | 5 | 0.08 |
| 200 | 5000 | 2.5 | 0.01 |
| 500 | 12,500 | 1 | - |

The table indicates the doppler shift error varies from approximately 1 percent at 50 MC to less than 0.01 percent at 500 MC. The error in range rate would be correspondingly reduced.

In using the VHF RARR system, it is possible to take into account ionospheric refraction since the errors are systematic and the variations in the ionosphere are fairly well known. However, this would involve complex computations as compared to using an S-band RARR system. Therefore, the S-band system is preferable.

It is possible to reduce ionospheric error at VHF frequencies through the use of several frequencies transmitted simultaneously. The first order error can then be computed and taken into account. This is the method used in navigation satellites such as Transit.

g. Optical Tracking Methods.

Another method of obtaining tracking information to establish the spatial position of the SMS is by optical cameras. Cameras are currently the most accurate method of fixing the position of a satellite in space. An accuracy of better than several seconds of arc can be obtained. Typical cameras that can be used for tracking the SMS are the Baker-Nunn, the Recording Optical Tracking Instrument (ROTI), and the Telescopic Photographic Recorder (TPR). These can also be used to check the accuracy of the electronic devices. These cameras can only be used at dawn and dusk and (of course) only in clear weather.

A network has been set up which is known as the NASA/Smithsonian Astrophysical Observatory Optical Tracking Network. It consists of twelve Baker-Nunn cameras. These are located in various places throughout the world between latitude 33°N and 33°S and all at places of good visibility. The locations of several stations are given in Figure 1-52. They are in Africa, South America, Nevada, and Australia. Therefore during stationkeeping of the SMS, at least one of these areas should have clear enough weather to view the satellite during most of its operating life.

6. Command Data Acquisition Station

The ground station complex at the Command Data Acquisition station will provide facilities for the following functions:

(1) Sensor data reception from the satellite

(2) Command data transmission to the satellite

(3) Telemetry data reception from the satellite

(4) Relay data transmission to the satellite

Other facilities such as ground command encoding, ground telemetry decoding, image display and recording will not be treated in this report.

NASA has stated that a completely new CDA station will be constructed solely for use with the SMS, since the demands for its use will be so great that no existing station could afford to devote 100 percent of its time to this program in view of the other deep space and scientific satellite programs scheduled for the 1967 time period. A block diagram of the CDA communications system is presented in Figure 1-60.

a. Antenna Considerations

The heart of the CDA station will be the antenna, used primarily for sensor data reception.

Consideration has been given to two different size antennas for this purpose: 60 and 85 feet diameter parabolic antennas. The 85-foot antenna will provide 3 DB higher gain than that obtained from the 60-foot unit. It has been shown, that the cost of a typical parabolic antenna with an equatorial mount varies with the 2.7 power of the antenna diameter. (See Figure 1-61.) Thus the cost of an 85-foot antenna will be approximately twice that of a 60-foot antenna (Ref. 1-36). In spite of this, it is proposed that the 85-foot antenna be used on several counts:

(1) The additional cost is only a small portion of the cost for the entire satellite system.

(2) The additional 3 DB gain is an added safety factor against communication system degradation.

(3) The growing use of 85-foot antennas for satellite tracking purposes has resulted in a greater know-how in this size of antenna design and construction and should ultimately result in a corresponding decrease in antenna cost.

The 85-foot antenna system will be designed to operate in the 1700 to 2300 MC range because of technical and allocation considerations previously discussed in subsection B.1.

It is possible to instrument the antenna with either a Cassegrainian feed or with the more conventional method of locating the feed at the focal point. Despite the added complexity it may be desirable to utilize a Cassegrainian

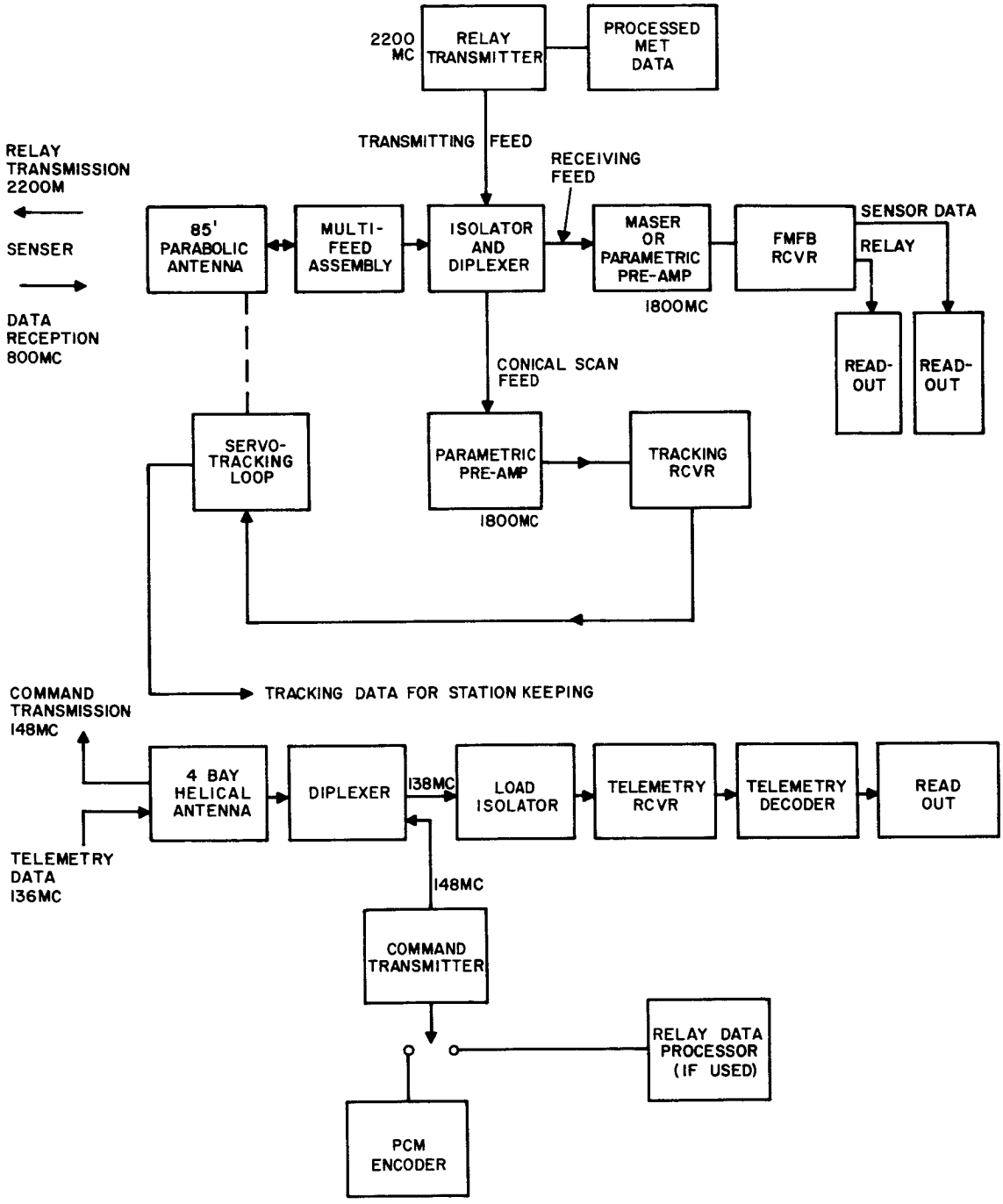


Figure 1-60. CDA Communications, Block Diagram

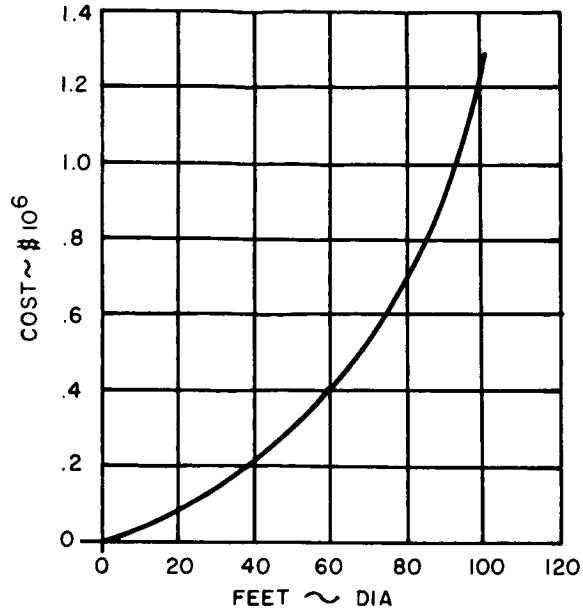


Figure 1-61. Approximate Cost of Parabolic Antenna with Equatorial Mount

feed to take advantage of the reduced side lobe amplitude and consequent reduced hot earth pickup via the side lobes.

Composite feeds will be used for both simultaneous sensor data reception from the satellite and relay data transmission to the satellite. Suitable diplexers and isolators will have to be provided to assure sufficient isolation of the receiver from the transmitted signal. In addition a conical scan feed mechanism should also be provided so that the ground station can track the satellite during stationkeeping. Tracking angle measurements for stationkeeping can be obtained from digital shaft encoders tied to the azimuth and elevation tracking servos. The antenna beam width of 0.35 degrees should allow for angular tracking accuracies of a fraction of this value, i.e., better than 0.02 degrees.

b. Sensor Data Receiver

In order to decrease the over-all receiver noise temperature, a low noise parametric or helium-cooled maser preamplifier assembly should be mounted as close to the receiver feed mechanism as possible in order to decrease line losses with their associated noise temperature increases.

The maser type most commonly used (manufactured by Microwave Electronics Corporation) employs two ruby crystals in a three-level travelling wave maser structure. A microwave pump oscillator is employed to convert the inherent microwave absorption in the slow travelling wave structure into emission or gain (Ref. 1-37). This maser has an electronic tuning range of 75 MC, and a gain of

approximately 30 DB with a 15 MC bandwidth. It is possible to get wider bandwidths at the expense of reduced gain. Cooling is done by means of a helium compressor type refrigerator developed by A.D. Little, called the Cryodyne. The refrigerator contains a heat engine. In order to cool helium by Joules-Thompson expansion, the temperature must be reduced to about 15°K by means of three expansion pistons. The helium does work on the piston and becomes cooled. The final stage is an expansion valve which produces liquid helium at 4.2°K. The liquid helium is circulated around the pipes at the lower portion of the refrigerator to cool the maser.

The characteristics of a suitable maser front end manufactured by Microwave Electronics Corp., is as follows:

| | |
|---|---|
| Frequency | 1.7 KMC |
| 3 DB bandwidth | 15 MC |
| Tuning range | 75 MC |
| Gain | 30 DB typical, (25 DB minimum) |
| Maser noise temperature alone | 8° K, typical, (12°K maximum) |
| Pump frequency | 11.7 KMC approximately |
| Pump power | 50 mw, typical, 100 mw, maximum |
| Operating temperature | 2.5°K |
| Weight | Less than 250 lbs |

A parametric amplifier can be used in place of the maser amplifier with a consequent increase in noise temperature from about 10°K to 190°K. This degradation may not be serious in view of the excellent C/N and S/N ratios present at the receiver as is pointed out in subsection B.1.

There are several types of parametric amplifiers but the most common and efficient type is one utilizing a semi-conductor varactor diode as the nonlinear reactive element. The voltage sensitive varactor diode converts energy from a pump frequency to a signal frequency by interaction with an idler circuit tuned to the difference frequency. The diode appears as a negative resistance at both the idler and signal frequencies and affords amplification of the input signal frequency. Since the diode is a reactive device it generates very little noise itself. The major source of noise originates in the idler circuit. For this purpose its frequency is made as high as possible in order to reduce the noise contribution. It is possible to reduce this noise considerably by cooling the idler circuit with liquid oxygen, nitrogen or helium. However, this is rarely done due to the refrigerator complexity.

This parametric amplifier is of the one-port variety and, therefore, affords fail-safe operation. If the parametric amplifier should fail, straight through operation will result, with minimal insertion loss and little noise contribution. The new noise figure will be just slightly larger than the noise figure of the succeeding stage.

Gains of 20 DB and bandwidths of 5 to 10 percent are available in the frequency range from 800 MC to 7 KMC. This type of amplifier is nominal in price compared to a maser although its noise figure is poor in comparison.

The characteristics of a typical S-band uncooled parametric amplifier, produced by Airborne Instruments Laboratory, are as follows:

| | |
|---|---|
| Frequency range (fixed-tuned) | 2200 to 2300 MC |
| Amplifier noise figure* | 2.5 DB maximum<br>2.0 DB nominal |
| Type | One port |
| Gain | 20 DB |
| Weight | 10 lbs |
| Pump | Internal |

* The noise figure quoted is a system noise figure and is based on a second stage noise figure not exceeding 8 DB.

The sensor data receiver shall incorporate the FMFB features discussed in subsection B.1. It can be of the double conversion superheterodyne type with the frequency tracking loop connected from the discriminator output to the VCO input, as previously described (Ref. 1-14).

The video output of the receiver is fed to either a demodulator where the relay subcarrier is stripped from the sensor data modulation (if employed), or a video processor, where the sensor data video information and the relay data information (if present) can be read out on a video recorder or other suitable displays.

The sensor data receiver (ground receiver) should possess the following basic characteristics:

| | |
|---|---|
| Modulation type | FMFB |
| Receiver type | Double conversion superheterodyne |
| Frequency range | 1700 to 1900 MC |
| Bandwidth | > 25 MC |
| Receiver effective noise temperature | 170°K |

c. Command Transmitter

The command transmitter could be of conventional construction and design. The ground encoder (discussed in Section 2) will prepare the proper digital format for acceptance by the command transmitter. The power budget previously estimated for the SMS command receiver was based on a transmitter output of 5 KW.

The antenna system for this transmitter should consist, in order to meet the power budget requirements, of a 3-bay helical antenna, with a suitable bed-spring type reflector suitably attached to a polar mount assembly so that 360 degree azimuth and 180 degree elevation angle coverage are provided. It is possible to share this antenna with a ground telemetry receiver by the use of a suitable diplexer and associated circuitry.

The servo control mechanism for this antenna will be controlled by the GSFC computer and given the same pointing data as the 85-foot sensor data antenna since both are pointing at the SMS.

The transmitter (ground command) characteristics are as follows:

| | |
|---|---|
| Frequency range | 148 to 150 MC |
| Modulation type | AM (pulse modulated) |
| Percent modulation | 75 (maximum) |
| Power output | 5 KW |
| Modulation frequency range | 50 cps to 15 KC |
| Carrier frequency tolerance | ±0.001 percent |
| Harmonic suppression | >60 DB |

d. Telemetry Receiver

The telemetry receiver should share the use of the 3-bay helical antenna employed for command transmission. This will minimize the amount of equipment used and simplify the tracking and pointing problem. Suitable diplexers and filters will be employed so that the command transmitter signal is attenuated sufficiently to avoid any receiver performance degradation.

A conventional telemetry receiver will be used at the CDA station. It should contain a phase-lock loop front end in the event the added signal tracking sensitivity is required during the station acquisition phase, when the SMS is either spin stabilized or is tumbling and the received signal may be degraded.

The characteristics for a suitable telemetry receiver are as follows:

| | |
|---|---|
| Modulation type | FM |
| Frequency range | 136 to 137 MC |
| Noise figure | 3.5 DB |
| Input impedance | 50 ohms |
| Image rejection | > 65 DB |
| IF rejection | > 85 DB |
| RF bandwidth | 2 MC |
| IF bandwidth | Variable from 10 KC to 500 KC |
| Phase-lock loop bandwidth | 50 cps to 500 cps |
| Video amplifier response | 10 cps to 150 KC |

e. Relay Transmitter

In accordance with the relay consideration discussed previously in subsection B.4, two methods of transmitting relay data (narrow and wideband) were proposed.

The narrow band channel employing the command and telemetry links on a time-shared basis is suitable for reception at modified Nimbus APT stations. The wide band channel at S-band employs the sensor data transmission link but requires the addition of a ground transmitter and a spacecraft receiver.

The additional equipment required at the CDA station is minimal for the narrow band relay; therefore, this report will cover only the wide band channel transmitter. The power budget previously calculated for the relay ground to space link (subsection B.4) for a medium or high capability satellite, indicates that a transmitter power of 1 kilowatt would be sufficient to develop an output signal to noise ratio in the satellite relay receiver large enough so that the weather data being retransmitted would not be degraded.

The transmitter proper should be of the conventional FM type capable of developing the required power without undue distortion. The output stage might be a klystron amplifier or other suitable type. The output of this transmitter would be sent to the transmitting feed on the 85-foot antenna for transmission to the SMS.

The relay transmitter (for a medium or high capability ground relay transmitter) characteristics are as follows:

| | |
|---|---|
| Frequency range | 2200 to 2300 MC |
| Transmission modulation type | FM |
| Modulation frequency range | 20 to 100 KC |
| Power output | 1 KW |
| Carrier frequency tolerance | 0.001 percent |
| Harmonic suppression | 60 DB |

7. Multiple Data Acquisition Stations

The function of the multiple data acquisition (MDA) stations will be to receive both raw and processed meteorological data from the SMS. These stations will be economical stations scattered over the Earth. In order to receive transmissions from the SMS, these stations must be located within line of sight of the SMS. If the SMS is located on the equator at 90°W, the area of possible sites is bounded by the outer most curve in Figure 1-52 where the elevation angle is 1.3 degrees.

Two possible types of MDA stations are to be recognized. One is within the SMS system. Its functions are to receive from the SMS both direct raw meteorological data, and relayed processed meteorological data. These stations will serve global and regional weather centers.

The second type will consist of the Nimbus APT ground stations. These will be emplaced and operating before the SMS system is built. Some of them will be at locations which will never have equipment of the first type. The objective is to include in SMS system provisions for relaying processed meteorological data into these stations, with minimum additions or modifications to them. Approximately 50 to 150 Nimbus ground stations with this equipment are contemplated.

a. Direct Sensor Data Reception

In order to receive sensor data from the SMS at the MDA stations it would be necessary to have S-band (1700 MC) receiving equipment. The receiving equipment at these stations would consist of an antenna, receiver, recorder and possibly data processing equipment. Much of this would be similar to equipment at the CDA station.

The antenna would be a fixed parabolic dish permanently pointed toward the SMS thus avoiding the expense of a gimbal structure and servo system. A fixed parabolic antenna 30 feet in diameter would have a gain 41 DB. The position of the feed would be slightly movable to track the variations of ±5 degrees of the angular position of the SMS. This antenna would be much less costly than the 85-foot diameter CDA antenna.

The receiver would be a frequency modulation type with feedback (FMFB) as described in subsection B.6. The highest baseband frequency $f_m$ of sensory data is 100 KC. Using a deviation index of 20, the RF spectrum bandwidth is

$$BW = 2(1 + D)f_m$$

where

$BW$ = RF spectrum bandwidth
$D$ = modulation index
$f_m$ = baseband frequency

For $D = 16.3$ and $f_m = 100$ KC, $BW = 3.46$ MC. The use of 20 DB of feedback in the FMFB receiver reduces the effective modulation index to 1.6. Therefore, the noise bandwidth is

$$BW_N = 2\ (1 + 1.6)\ 100,000 = 520 \text{ KC}$$

where

$BW_N$ = noise bandwidth

The output of the receiver would be fed into a video recorder capable of recording frequencies up to 100 KC. The data can then be processed at the MDA station or sent to a centralized processing station.

A power budget for a typical MDA station utilizing the equipment is indicated in Table 1-17. The power budget is similar to that indicated in subsection B.1 except that a safety factor of 10 DB due to miscellaneous losses has been sacrificed.

TABLE 1-17

MDA STATION DIRECT SENSOR DATA RECEPTION POWER BUDGET

| | |
|---|---|
| SMS sensor data transmitter power (1.3 w at 1700 MC) | +1.2 DBW |
| Satellite antenna gain | +18.0 DB |
| Free space and propagation losses | -189.5 DB |
| Ground antenna gain | +41 DB |
| Antenna polarization loss | -3 DB |
| Receiver carrier power | 132.3 DBW |
| Receiver total effective noise temperature = 150°K | |
| Receiver noise bandwidth = 0.52 MC | |
| Receiver noise power ($KT_eB$) | -149.3 DBW |
| Carrier to noise ratio | 17 DB |
| Output S/N ratio | 46 DB |

b. Processed Meteorological Information

In order to receive processed meteorological data at the MDA station from the SMS, it is necessary to relay such data via a transponder aboard the satellite. Such relays were discussed in subsection B. 4. The information may be in any of the following forms:

(1) Teletype

(2) Black and white facsimile

(3) Nephanalysis charts

(4) Tone value facsimile

(5) Cloud cover pictures which have been processed and annotated.

The relay system may be at VHF frequencies (utilizing the command-telemetry system)or at S-band frequencies (utilizing an S-band receiver and the sensor data transmitter). The data can be transmitted at a high rate with a wide bandwidth or at a low rate with a narrow bandwidth. The VHF relay system is suitable for narrow bandwidths up to several kilocycles, while the S-band relay system is more adaptable to wideband data up to several hundred kilocycles. The considerations relating to information rate and bandwidth have been fully discussed and typical power budgets for each of the relay systems are shown in subsection B. 4.

c. Nimbus APT Ground Station

A third type of ground station in addition to the CDA and MDA stations, would be the Nimbus APT ground station used in a VHF relay system. The relay would use a 148 MC ground transmitter at the CDA to transmit the information to be relayed to the command receiver on the SMS. The command receiver would demodulate the carrier obtaining the relayed information data. This data would then be used to modulate the telemetry transmitter operating at 136 MC. The Nimbus APT ground station would then be used to receive the relayed information data. The problems involved in utilizing these ground stations in such a system is discussed in the following paragraphs.

1) Characteristics of Nimbus APT System. The automatic picture transmission (APT) system as used in Nimbus is composed of two subsystems: a satellite camera and transmission subsystem and ground receiving and recording subsystem.

The satellite camera is a storage vidicon system capable of long duration storage and a very slow readout rate (200 seconds). It takes wide angle pictures and transmits them in real time to the ground station at 136 MC. The ground station consists of helical antenna, receiver and facsimile equipment. The system is designed for local weather observation and forecasting applications. The pertinent characteristics of the Nimbus APT system are given in Table 1-18 and a block diagram of the ground station is shown in Figure 1-62.

TABLE 1-18

NIMBUS AUTOMATIC PICTURE TAKING SYSTEM CHARACTERISTICS

Transmitter Aboard Nimbus

Construction: Solid State

Modulation: FM

Frequency = 136.95 MC

Deviation = ±10 KC

Output power = 5.5 watts (approximately)

Resolution = 700 lines

Gray scale = 7 steps with change in density of 0.12 between steps

Readout time = 200 seconds

Baseband modulation = 0 to 1600 cps

Subcarrier frequency = 2400 cps

Operational Ground Receiving Stations

Antenna: 8-turn helix designed for 136 MC

Beamwidth = 34 degrees

Gain = 14 DB

TABLE 1-18

NIMBUS AUTOMATIC PICTURE TAKING SYSTEM CHARACTERISTICS (CONT'D)

| | |
|---|---|
| Pre-Amplifier: | 2 stage RF amplifier |
| | Noise figure = 4.5 DB |
| | Gain = 23 DB |
| | Bandwidth = 5 MC |
| Receiver: | Tuning Range = 130 to 140 MC |
| | IF bandwidth = 50 KC |
| | Noise bandwidth with phase-lock demodulator = 20 KC (maximum) |
| Antenna Temperature: | Assumed to be 1000°K |
| | Deviation on FM = 10 KC |
| | Deviation ratio = 10000/2400 + 1600 = 2.5 |
| | Normal S/N = 9 DB |
| | Safety margin = 12 DB |
| | Minimum Total S/N = 21 DB |

2) Nimbus APT Power Budget. The following is an estimate of the Nimbus APT power budget. It is based upon a maximum distance between the Nimbus and the APT ground station of approximately 2000 miles:

| | |
|---|---|
| Transmitted power | +7 DBW |
| Transmitter antenna gain | -3 DB |
| Free space loss (2000 miles at 136 MC) | -145 DB |
| Receiver antenna gain (including polarization and other losses) | +10 DB |
| Received signal power | -131 DBW |
| Receiver noise figure = 4.5 DB | |
| Receiver temperature ($T_r$) = 290 (NF-1) = 500°K | |
| Antenna temperature ($T_a$) = 1000°K | |
| Total noise temperature ($T_e$) = 1500°K | |
| Receiver noise power (20 KC bandwidth) | -155 DB |
| Carrier to noise ratio (C/N) | 24 DB |

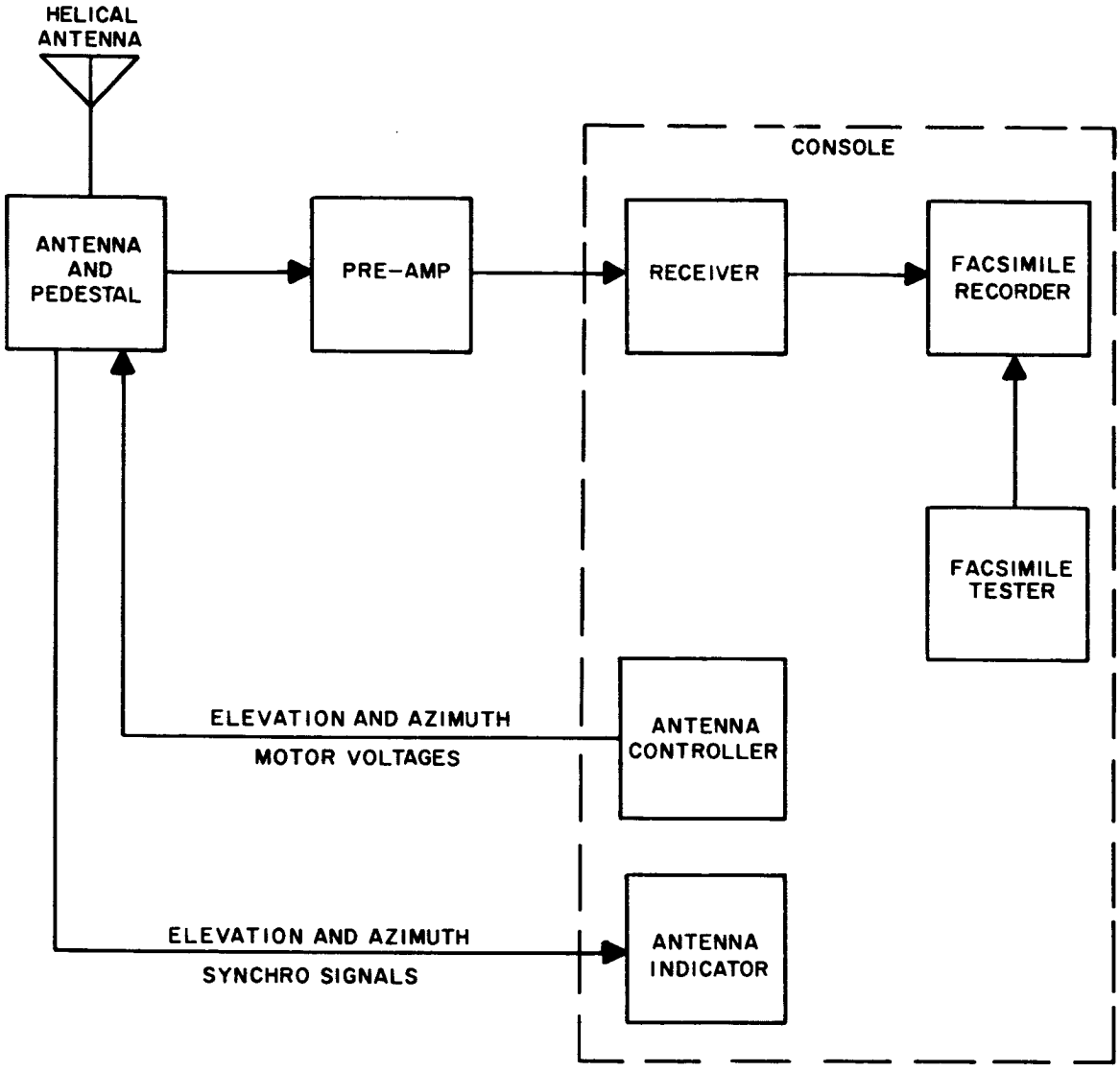


Figure 1-62. Automatic Picture Transmission Ground Station, Block Diagram

3) Application of APT Stations to SMS. Since the maximum SMS distance of 25,750 miles is approximately one order of magnitude greater than the maximum Nimbus distance of 2000 miles, the free space loss is increased by approximately 22 DB. Therefore, in order to utilize the APT ground stations, it is necessary to make up for this increased loss. This can be

accomplished by attempting to increase the radiated power by increasing the SMS transmitter power or using a larger antenna with greater gain. Alternately, modifications to the APT ground station may be required such as decreasing the information rate by narrowing the bandwidth and hence increasing the readout time. These alternatives are described in the following sections.

a) Satellite Power vs Distance. The Nimbus APT system is designed to operate at a maximum distance of about 2000 miles with a satellite transmitter power of approximately 5 watts.

Figure 1-63 is a plot of transmitter power required for other distances between the satellite and the APT ground station. This graph is based upon using the same signal to noise ratio shown in the power budget given previously for the Nimbus APT system. At the maximum synchronous distance of 25,750 miles, a transmitter output of 650 watts is required if the same S/N ratio is to be maintained as on the original Nimbus APT system. This power requirement is obviously impractical for the SMS. An attempt can be made to reduce this power requirement by increasing the transmitter antenna gain. Figure 1-63 also shows the amount of transmitter power required with different aperture antennas.

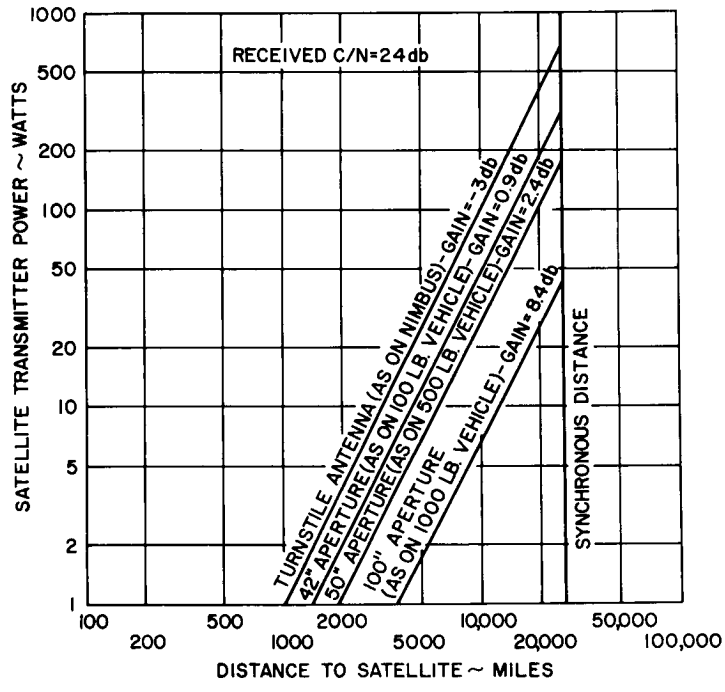


Figure 1-63. Satellite Transmitter Power vs Distance (Using Nimbus APT Ground Station, Frequency = 136 MC)

For example 43, 50, and 100-inch aperture antennas (either parabolic dishes or axial mode helical antennas) would result in transmitting antenna gains of 0.9, 2.4 and 8.4 DB, respectively. This would reduce the transmitter power requirements at the synchronous distance to 320, 175, and 44 watts, respectively.

The aperture size is determined by the dimensions and weight of the SMS vehicle. Larger vehicles can utilize larger aperture antennas. It has been estimated that 100, 500, and 1000 lb vehicles will be large enough to mount antennas with apertures of 42, 50, and 100-inch, respectively. These antennas could be of the parabolic or the helical type at the operating frequency of 136 MC. The helical antenna could be a spring-loaded or pop-out type which is extended when the SMS is in its stationkeeping position and faces toward the Earth. Since the relay would only be used when the SMS is in its operational position, a directional antenna could be tolerated.

The above analysis indicates that it is impractical to use the Nimbus APT ground stations unmodified for a 100-or 500-lb SMS relay, since the transmitter power required even with the largest practical antennas, is 320 and 175 watts, respectively. For a 1000-lb vehicle utilizing a 100-inch pop-out helical antenna, a transmitter of 44 watts output would be required.

b) Modifying the APT Ground Station. An alternate method of attempting to use the APT system for the SMS relay is to modify the ground station rather than the satellite equipment. This modification would consist of decreasing the rate at which information is transmitted by narrowing the bandwidth of the receiving system. The transmission time would be correspondingly increased. The various methods of modifying the ground station are discussed in the following sections.

Narrowing the APT Bandwidth

The present bandwidth is 20 KC. The baseband maximum frequency carrying the picture information is 1600 cps and the subcarrier frequency is 2400 cps. The modulation index is 10000/(1600 + 2400) = 2.5. A narrower bandwidth can be obtained by using a baseband maximum frequency of 160 cps. In place of modulating a subcarrier of 2400 cps, the 160 cps would be used to frequency modulate the 136 MC carrier directly with a deviation index of 2. The RF spectrum would be

$$\text{RF BW} = 2\ (1 + D)\ f_m \quad \text{(See subsection A.)}$$
$$= (2)\ (3)\ (160) = 960 \text{ cps}$$

Using a bandwidth of 1.5 KC, the gain in signal to noise ratio would be approximately 12 DB. At the receiver, the 2400 cps subcarrier could be reinserted by having the 0 to 160 cps baseband frequency amplitude modulate a 2400 cps oscillator. The composite signal would then be fed into the facsimile machine. The resolution of the lowered baseband frequency system would be approximately 1/10 that of the original system.

This method would involve changes in the circuit of the APT receiver with no changes to antenna or facsimile recorder. A switch could be incorporated to perform this change-over from normal operation.

For black and white pictures, the S/N ratio required is much less than that for tone value photographs, as indicated in subsection B. 4. Therefore, the modified Nimbus APT ground station could receive black and white nephanalysis or meteorological maps with a smaller S/N ratio than indicated in the previous power budget.

A standard meteorological map of 18 x 22-inch dimensions could be reproduced in sections with the 8 x 8-inch APT format. For example, nine APT pictures could be used for one weather map. The transmission time for the nine pictures would be a minimum of 1900 seconds. This method is in effect a slowing down of the readout time as indicated in Figure 1-48.

Another method of reducing readout time is by changing the speed of the facsimile machine used with the APT system. This would involve changing gear ratios.

Experiments could be conducted of the present Nimbus APT system to determine the effect on picture quality of decreasing the baseband frequency carrying the picture information and increasing readout time.

Changing the Ground Antenna Gain

Another method of making up the loss due to the increased distance is to raise the ground antenna gain. The ground antenna gain of 14 DB could be increased by utilizing a multi-element array in place of the helical antenna. The array would be fixed in direction since the SMS would be stationary relative to the ground station. The use of such an array would increase gain by 6 to 8 DB. An additional increase would be necessary to overcome the 22 DB loss if the same carrier to noise ratio is to be maintained as in the original APT.

Changing Frequency of Operation

The frequency of operation could be increased by utilizing a new antenna on the same APT pedestal mount. The new antenna could have a greater gain than the original unit. The receiver could be modified for the higher frequency by utilizing a frequency converter. Both of these modifications would be major and amount to a complete change in the APT ground station equipment except for the facsimile recorder.

## C. REFERENCES


1-1 Mathwich, H. R., "Space Communications System Design Nomographs," IRE Trans, CS-10 No. 1, March 1962

1-2 Hogg, D. C., "Effective Antenna Temperature Due to Oxygen and Water Vapor in the Atmosphere," Journal of Applied Physics, September 1959

1-3 Bean, R. R., and Abbott, R., "Oxygen and Water Vapor Absorption of Radio Waves in the Atmosphere," Geofisica Pura E Applicato, Milano, 1957

1-4 Pearlman, S., "Concerning Optimum Frequencies for Space Communications," IRE Trans., CS-7, September 1959

1-5 Weisbrod, S., and Anderson, L. J., "Simple Methods for Computing Tropospheric and Ionospheric Reactive Effects on Radio Waves," Proc., IRE, October 1959

1-6 Schulkin, M., "Average Radio-Ray Refraction in the Lower Atmosphere," Proc., IRE, August 1952

1-7 Forward, L., and Richey, F., "Effects of External Noise on Radar Performance," Microwave Journal, December 1960

1-8 Haydon, G. W., "Technical Consideration in the Section of Frequencies for Communications," NBS Report No. 7250, December 1, 1962

1-9 Hansen, R. C., "Low Noise Antennas," Microwave Journal, June 1959

1-10 Menzel,, D. H., "The Radio Noise Spectrum," Harvard University Press, 1960

1-11 Ko, H. C."The Distribution of Cosmic Radio Background Radiation," Proc., IRE, January 1958

1-12 Rohde, U. L.,"Very Low Noise Transistor Amplifiers in the UHF Band Using the Parametric Conversion Mode", Journal British IRE, September 1962

1-13 O'Neil, J., "Some Microwave System Design Considerations," Electrical Design News, December 1962

1-14 Ruthoff, C. L., "FM Demodulator with Negative Feedback," Bell System Technical Journal, July 1961

1-15 Enole, L. H., "Decreasing the Threshold in FM by Frequency Feedback," Proc., IRE, January 1962

1-16 Bedrosian, E., "Power-Bandwidth Tradeoff for Feedback FM Systems: A Comparison with Pulse Code Modulation," Rand Report RM-2787-NASA, October 1961

1-17 Nichols, M. H., and Rauch, L. I., "Radio Telemetry, "Second Edition, John Wiley and Sons, 1954

1-18 Johnston, N. A., " A Brief Review of Some of the Properties of PCM," Republic Aviation Corp., Internal Memo No. 530.057.22, July 2, 1962

1-19 Baghdady, L., "Lectures on Communication System Theory," McGraw-Hill Book Co., 1960

1-20 Weaves, C.S., "A Comparison of Several Types of Modulation," Trans, IRE, Communication Systems, March 1962

1-21 Fisch, J., "Modulation Techniques for Wide Band Microwave Transmission Systems," Republic Aviation Corp., Internal Memornadum, MSD-530-502, RAC-998, 26 October 1962

1-22 FCC Docket 13522, "Preliminary Views of the U.S.A., for Frequency Allocations for Space Radio-Communications," Attachment to Second Note of Inquiry, Adopted May 17, 1961

1-23 Raytheon Report, "Amplitron Amplifiers for Space Communications," Report BR-2367, Raytheon Co., 1962

1-24 Martin, J. C., "Low Loss Frequency Multipliers of Higher Order and Power in the UHF Range," AIEE Winter Meeting, 1962

1-25 Luettgenau, G., "A Practical Approach to the Design of Parametric Frequency Multipliers," Report No. 9846-0002-MU-000, Pacific Semiconductors Inc., 1961

1-26 GSFC Data Requirements Systems Committee, "Pulse Frequency Modulation Telemetry Standards," Part I Telemetry Standards, Section 2, November 1, 1962

1-27 Nichols, M.H., and Rauch L.I., "Radio Telemetry," John Wiley and Sons, 1954

1-28 Link, W.E., and Eatough, C.D., "Experimental Optimization and Evaluation of Telemetry Systems, IRE Trans., Space Electronics and Telemetry, Vol. SET-8, September 1962

1-29 Aeronautics Publication No. U-743, "Telemetry System Study," Aeronutronics Division, Ford Motor Co., December 1959

1-30 Stiltz, H.L., "Aerospace Telemetry," Prentice Hall, 1961

1-31 Gilchriest, C.E.,"Phase-Locked Loop as a Discriminator or Tracking Filter," IRE Trans., Telemetry and Remote Control, Volume TRC-4, June 1958

1-32 Henney, K., "Radio Engineering Handbook," Fifth Edition, McGraw-Hill, 1959

1-33 Pines, S., and Wolfe, H., "Interplanetary Trajectory by the Enke Method Programmed for the IBM 707 and 7090," Republic Aviation Corp., Report No. RAC 656-451, December 12, 1960

1-34 Millmann, G.H., "An Analysis of Tropospheric, Ionospheric, and Extraterrestial Effects on VHF and VHF Propagation," General Electric Co., Technical Information Series Report No. R56EMH31, October 1956

1-35 Guier, A., and Weiffenbach, L., "A Satellite Doppler Navigation System," IRE Proc., Vol. 48 No. 4, April 1960

1-36 Foldes, P., "AGAD Conference on Low Noise Electronics," Pergamon Press, 1961

1-37 DeGrasse, R.W., "The Travelling Wave Maser," Microwave Electronics Corp., Technical Memo No. 6, 1962

1-38 Space Data Handbook, Space Technology Laboratories, Inc., Redondo Beach, Calif., 1962

# SECTION 2 - DATA HANDLING

Three channels are used to transmit data utilized by the SMS vehicle. Sensor data will be transmitted to the ground via the sensor link, telemetry data will be transmitted to the ground via the telemetry link, and command data will be sent up to the SMS via the command link.

This section discusses the data-handling portion of each of the links as it is handled within the vehicle. The data-handling portions of the sensor and telemetry links occur between the sources of the data (sensors, transducers) and the respective transmitters. The data-handling portion of the command link occurs between the on-board receiver and the actuators. The organization of the data for ease of interpretation, and the quantity of information needed to implement the various functions is discussed. The various aspects of the information handling capacity of the channels and the trade-offs of analog versus digital communication are covered in the Communications Section of this report.

## A. SENSOR DATA SYSTEM

This section deals with possible digital data handling techniques that might be applied to the raw video output of the cloud-cover imaging sensor prior to the subsequent transmission of this data to the ground. The techniques discussed herein have as their object the enhancement of picture quality and/or the elimination of redundancy to cause a reduction of bandwidth.

### 1. Overall Description

Video data as generated in the SMS is available first as an analog voltage. It is sometimes worthwhile to convert this data to a digital form, usually PCM, and transmit it in this form. This is the case when an unfavorable signal to noise ratio is expected, such as when transmitting from outer space, or when many quantized levels are needed. An explanation of analog-to-digital conversion is given in the later section on telemetry. In particular, the "over-under" method is applicable here where the bit rate is especially high.

In brief, the "over-under" method of conversion from analog to digital involves a series of successive trials which bracket in on a sample analog voltage. A voltage equal to half the full range is compared with the sample. If the sample is lower, a voltage of one-quarter range is tried. If in the first trial the sample has been higher, then a value of three-quarter range would be tried next. In this way the sample is approximated by the generator which automatically has the appropriate binary code as the generator input.

A rate of 100,000 picture elements per second will be assumed for the remainder of this discussion since it is not out of line with present plans for SMS. This requires a bit stream of 500,000 bits/second to achieve a maximum of 32 quantized levels from black to white. Actually some of the code groups (or levels) must be used for line and frame synchronization.

The system as presently conceived does not require any extensive storage. The block diagram, Figure 2-1, shows the output of the video sensor

coming to the data converter where it will be sampled, quantized and encoded. No further storage is required since the system is capable of operating at the speed of data flow.

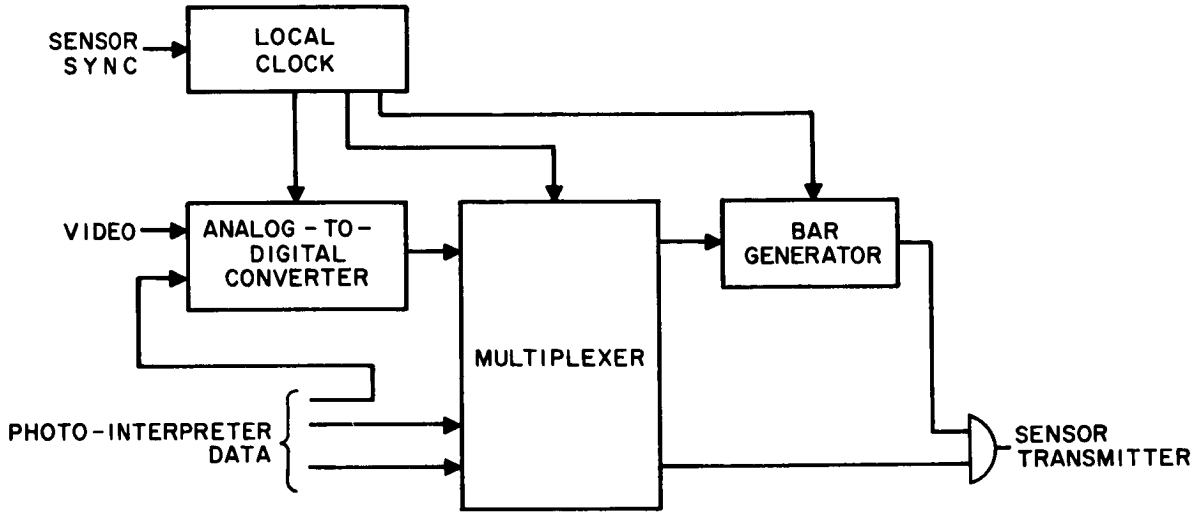


Figure 2-1. Sensor Data Handling System

The final determination as to whether data should be encoded or transmitted in analog form is left to the study of communications and the power versus frequency requirements for satisfactory transmission.

2. Error-Correcting Codes

It is conceivable that error-correcting codes might be valuable for a digital transmission even though parity bits are not, since error-correcting codes allow for restoration of the data and actually carry with them a fair degree of redundancy which makes possible satisfactory operation with a less favorable signal to noise ratio. Also, analysis of the nature of communications problems from a synchronous satellite may show that interruptions in the form of bursts are to be expected at some predictable rate, and of some likely duration. Burst-error correcting codes can be utilized to cover specifically the most common errors anticipated. They do require a sizeable penalty in hardware carried in the vehicle.

3. Coordinate Delta-Encoding

A basic approach to cutting down on the bandwidth required for transmission of information is through the method known as delta-modulation. In its various forms, it relies on the a priori knowledge that a given picture element will not usually be very different from its neighbors. Various treatments are given in the literature which depend on the final goal of the restored picture. In some cases, deterioration occurs in the high frequencies, or edges. In other cases the relatively smooth slow transitions become run through with contour lines.

These effects are not necessarily objectionable, and there are schemes for minimizing undesired features. A method is suggested below which, as usual, depends on the probable similarity of neighboring points for its saving in bandwidth. To keep down the circuit requirements, each element is compared with its most recent (in time) neighbor rather than attempt to compare it with its surrounding (in both X and Y coordinates) neighbors.

The technique of band compression which is explored does not cause any loss in resolution. Two variations are presented. The saving in bandwidth comes about by assumptions concerning the topology of the pictures to be reproduced. These assumptions remain to be proven.

Qualitatively, it is assumed that cloud-cover pictures will resemble terrestrial contour maps rather than maximum resolution checkerboard patterns. If a scan-line does not cross more than a certain percentage of contour lines relative to the total number of elements per line, a savings can be effected in bandwidth, with no sacrifice in the accuracy of the contour positions and values.

The first method calls for the examination of successive picture elements in scanning. When a change is observed, the coordinate of the point along the line is transmitted along with the absolute value of the new point. This system clearly becomes useful when the number of new values is low enough so that the extra space needed for coordinate representation is available.

The second method is the same as the first except that instead of transmitting the coordinate of the point, the distance from the previous point is given. This effects a greater saving, and comes about because points which are close (and consequently more frequent) have smaller differences; as they grow fewer the space between them increases faster than the need for space to express the larger difference. This method, then, has a variable word length and a field must be set aside to call out the word length.

In both systems buffer storage is needed for accommodating occasional peak loads.

Detailed explination:

$n$ = number of bits for quantization

$p$ = number of picture elements/line, also number of lines (for square aspect)

$T$ = time for transmission of one picture, (seconds)

$F$ = bit rate for straight digital transmission, also $\frac{np^2}{T}$

$r$ = number of lines/mile

$C$ = coverage (sq mi) = $\frac{FT}{nr^2}$

$f$ = bit rate based on statistical assumptions

$\log_2 p$ = number of bits to determine element position on a line

$n + \log_2 p$ = number of bits to specify location and absolute value of corrected element

$$\% \text{ correction} = \frac{n}{n + \log_2 p} \text{ for break-even} \qquad (2\text{-}1)$$

Break-even point is the point beyond which it is more economical to send the complete picture than the corrected one. This exists because of the additional bits that are required per picture element in the correction system to locate the corrected element.

For the same resolution, coverage, total picture, and transmission time, a lower frequency f can be used if it is known that on the average, there will be no more than some maximum percent correction.

$$\% \text{ correction} = \frac{n}{n + \log_2 p} \times \frac{f}{F} \qquad (2\text{-}2)$$

The average for which this is assumed is based on the total storage provided so that the accumulated corrections can be held until transmitted at the lower frequency.

An example that might be appropriate for SMS

$n$ = 5 (32 levels maximum)

$T$ = 10 seconds

$p$ = $10^3$ picture elements/line

$\therefore$ $F = 500 \times 10^3$ bits/sec

<u>For method 1:</u>

% correction for break-even:

$$\frac{n}{n + \log_2 p} = \frac{5}{5 + \log_2 10^3} = \frac{5}{5 + 10} = 33.3\%$$

$$\% \text{ correction} = \frac{n}{n + \log_2 p} \times \frac{f}{F} \qquad (2\text{-}2)$$

$$\% \text{ correction} = \frac{1}{3} \times \frac{f}{F} \quad \text{(See Figure 2-2)}$$

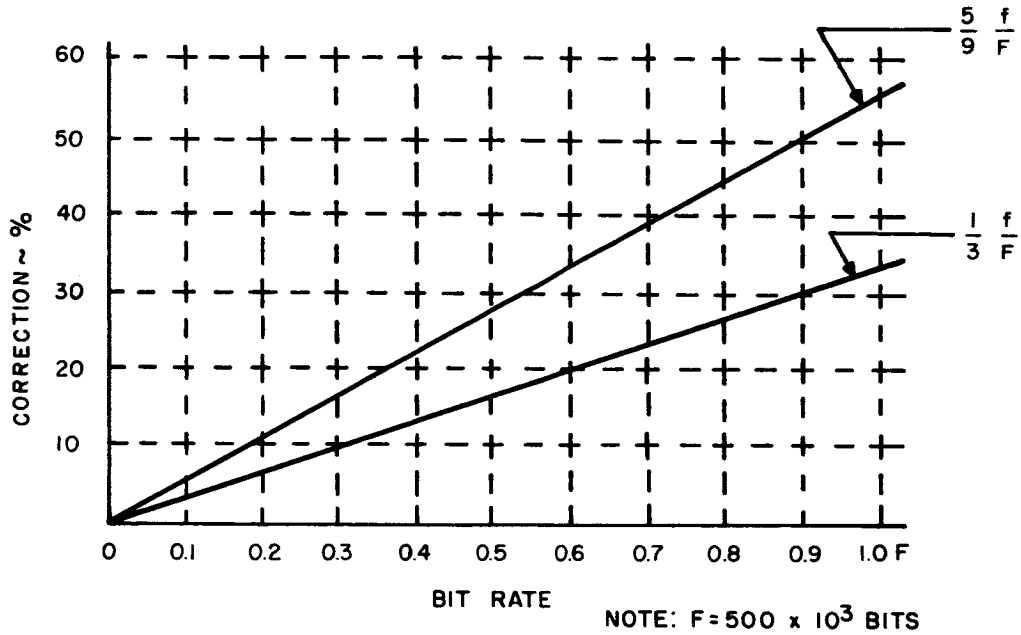


Figure 2-2. Correction Capability vs Frequency

For method 2:

Since $p = 10^3$, assume that a line will be treated in quarters; therefore, up to 8 bits may be needed to designate the change in coordinate to the new point. Three bits are then needed to call out the word size. Consequently, since $n = 5$, the total word is $3 + 5 + w$, or $8 + w$ where $1 \leq w \leq 8$.

$w = \log_2 d$ where d is distance (number of picture elements) from last correction.

The break-even point is

$$\frac{n}{8 + \log_2 d}$$

where $8 + \log_2 d \leq 5d$ (the closest packing of corrections on the average that can be tolerated).

$\therefore$ d = 2 (to the nearest integer)

and $\frac{5}{8+1} = \frac{5}{9}$ or 55%

$$\% \text{ correction} = \frac{n}{8 + \log_2 d} \times \frac{f}{F} \qquad (2\text{-}3)$$

$$\% \text{ correction} = \frac{5}{9} \times \frac{f}{F} \quad \text{(See Figure 2-2)}$$

The curves of Figure 2-2 show what savings may be effected in bandwidth depending on the percentage of corrections in the pictures.

The coordinate delta-system pictured in the block diagram, Figure 2-3, is a one point store which is used to hold the previously scanned point so that it may be compared successively with the latest one. Figure 2-3 further shows that the output of the sensor is converted to digital data. It might be feasible to use an eight-level coordinate-delta followed by the new absolute analog representation of the element. The conversion to a digital (binary) system followed by an appropriate amount of storage is also shown in the figure. The number of registers needed in this storage is based on the expected peak load which may occur. The bank of storage acts as a reservoir for data coming in at a high clock rate and leaving at a low rate.

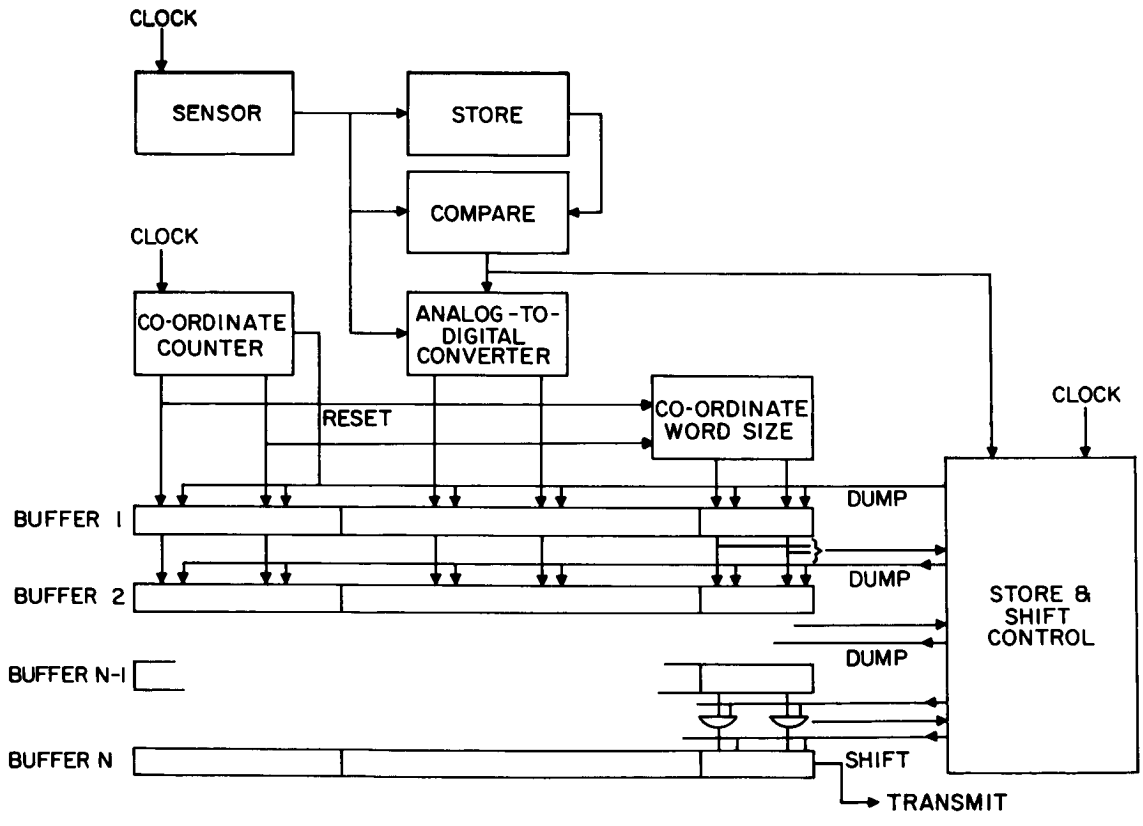


Figure 2-3. Coordinate Delta System

A peak load may occasionally overflow the system. If this happens, there will be no accumulation of error beyond one-quarter line, and in most cases, there will be no accumulation at all. Only the overflowed points will be in error at that time. At the end of the excess demand, when memory space becomes available, the coordinate-delta, which has been accumulating in the coordinate counter, will not, in general, have overflowed the counter, and so the restored service will carry the correct coordinate. Occasionally, when the demand is so severe that the counter is overrun, the rest of the quarter-line will be displaced.

The system, as shown, uses storage in the form of successive dumps followed at the end by a shift-register. Alternatively, the registers may all be shift-registers, with a control system keeping tabs on the sequence and status of each.

Figure 2-4 is a logical drawing of the coordinate word-size unit. It is suggested that contour maps of varying terrain will have configurations which are not very different from the contours to be expected in the photographs of the SMS. An empirical check should be made of the assumptions in this discussion. Samples can be scaled to the resolution being checked. The accumulation of data would be too tedious for a manual task, so it is suggested that a device similar to a curve-tracer be used to automatically scan the maps and record the number of transitions.

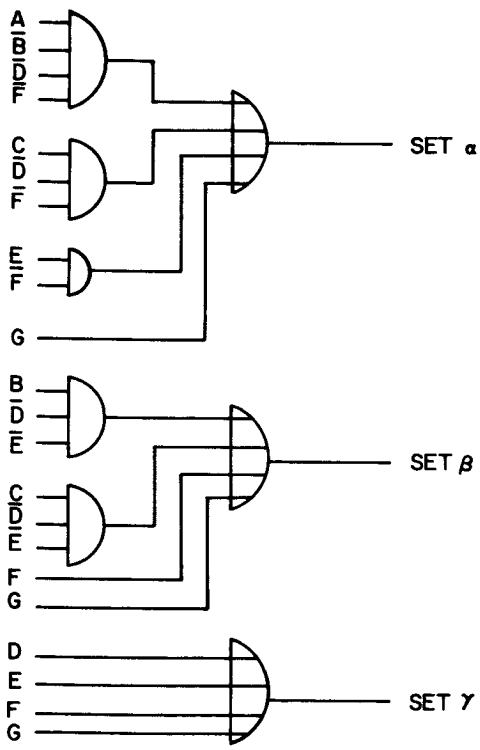


INPUT: A-G = OUTPUT OF CO-ORDINATE COUNTER

OUTPUT: α,β,γ = 3 BIT NUMBER CORRESPONDING TO POSITION OF MOST SIGNIFICANT BIT IN THE INPUT.

TRUTH TABLE (X = DON'T CARE)

| A | B | C | D | E | F | G | α | β | γ |
|---|---|---|---|---|---|---|---|---|---|
| 1 | 0 | 0 | 0 | 0 | 0 | 0 | 1 | 0 | 0 |
| X | 1 | 0 | 0 | 0 | 0 | 0 | 0 | 1 | 0 |
| X | X | 1 | 0 | 0 | 0 | 0 | 1 | 1 | 0 |
| X | X | X | 1 | 0 | 0 | 0 | 0 | 0 | 1 |
| X | X | X | X | 1 | 0 | 0 | 1 | 0 | 1 |
| X | X | X | X | X | 1 | 0 | 0 | 1 | 1 |
| X | X | X | X | X | X | 1 | 1 | 1 | 1 |

Figure 2-4. Coordinate Word Size

4. Photointerpreter Data

It may prove worthwhile to transmit the picture in its analog form. This of course results in considerable saving in hardware at the data-processing section. In any event, whether the video data is transmitted in analog or in digital form, some digital information will be required. This information is for photo-interpreter use and consists primarily of cogent data which is obtainable only on board the vehicle, and secondarily of data which could be dubbed in on the ground, but carries greater validity if transmitted with the original picture. Such items as mirror coordinates, iris diaphragm setting and frame sequence might be included. Information which could be dubbed in includes such items as the date and time the picture was taken, vehicle and camera identification, and (possible) lens selection.

The display of the data may be in binary form, that is, in the shape of spots on a line at the bottom of each picture. It is assumed that the pictures will be utilized by trained personnel to whom this form of display will not present any technical hardship; consequently, the inclusion of elaborate character-generation equipment on board the vehicle would be unnecessary. A high degree of redundancy will be used in this transmission since the information is more sensitive to misinterpretation if mistakes are transmitted, and since there is physical space for considerable information. It is also desirable from the point of view of the interpreter to have spots (or bars) which can easily be seen with no special equipment. Figure 2-1 shows the multiplexing of this information with the video data, and the spot-generating system needed.

A ground-based character generator can be added at any time to the ground station. This would be done if it should prove worthwhile to eliminate a coded form of information and to substitute instead standard characters for the photointerpreter's benefit. The character generator would be controlled by the data transmitted from the vehicle and would require no changes or extra facilities in space vehicle equipment.

5. Heat Budget Sensor Data

The output from the heat budget sensor will be in the form of 10,000 picture elements which are to be read out in a 10-second period. The exact description of this system is to be found in Section 4 of Volume 3. The precision to be transmitted is one part in 512. This requires nine bits per picture element. The total frequency requirement is 9000 bits/second. The output of this sensor is to be read out once every half-hour. There are two such sensors whose data is grouped on a point to point basis. To avoid large storage, the data from these two sensors will be interleaved. The entire bit stream, now 18,000 bits/sec, will be transmitted to the ground station via the sensor transmitter. This will be accomplished by sharing the channel with the video sensors. The video sensors will have the use of the channels for most of the half-hour period. The heat budget sensors will be cut in for the necessary time (about 15 seconds) every half hour. This action can be accomplished via programming from the ground or under operator control.

### 6. Summary

It is estimated that a digital system would weight 9.1 lb, occuply 283 cu. in., and require 6.7 watts. This estimate is based on comparison with similar systems analyses including a Republic study made of the Orbiting Solar Observatory.

The type of circuitry generally considered has been solid state miniaturized components varying from cordwood welded module construction to microminiaturized circuitry (presently becoming available in the form of integrated units or miniature assemblies).

## B. COMMAND DATA SYSTEM

### 1. Overall Description

The command system allows a ground operator to control certain actions on board the vehicle. In its entirety, the system consists of a ground console upon which commands are entered, a ground transmitter and antenna system for beaming commands to the vehicle, an on-board receiver and antenna system, a data-handling system for routing the commands to the proper control points, and finally, the various actuators which carry out the commands. Incidental to the overall system are command verification procedures and storage devices which may be needed.

The following part of the report will be concerned with that section of the command system in the vehicle which follows the receiver and continues through to the actuators. This is shown diagrammatically in Figure 2-5.

In contrast to other orbiting satellites, no bulk storage and timed programming of commands is necessary in the SMS. Because it will be in synchronous orbit, the SMS vehicle will always be in contact with the ground station. The only memory needed in the command system is that which is required to maintain an instruction until it is rescinded. This will probably be a flip-flop associated with each instruction having this requirement, except where specialized actuating equipment already accomplishes this.

### 2. Tone Digital System

In the pre-orbital period following the launching of the vehicle, the command system used will be compatible with the NASA standard Tone Digital Command System which can then be used to control the vehicle from many stations around the Earth.

The tone digital command system is described in NASA-GSFC document, "Part II-Command Standards-Section 2-Tone Digital Command Standards." The system has an upper limit of 70 commands based on the use of a four-out-of-eight code. The possibility exists of using this system for a much higher number of commands by allowing the system to function in several modes, that is, each instruction code can have several interpretations. This can be done without altering the basic structure of the ground stations. The ground station

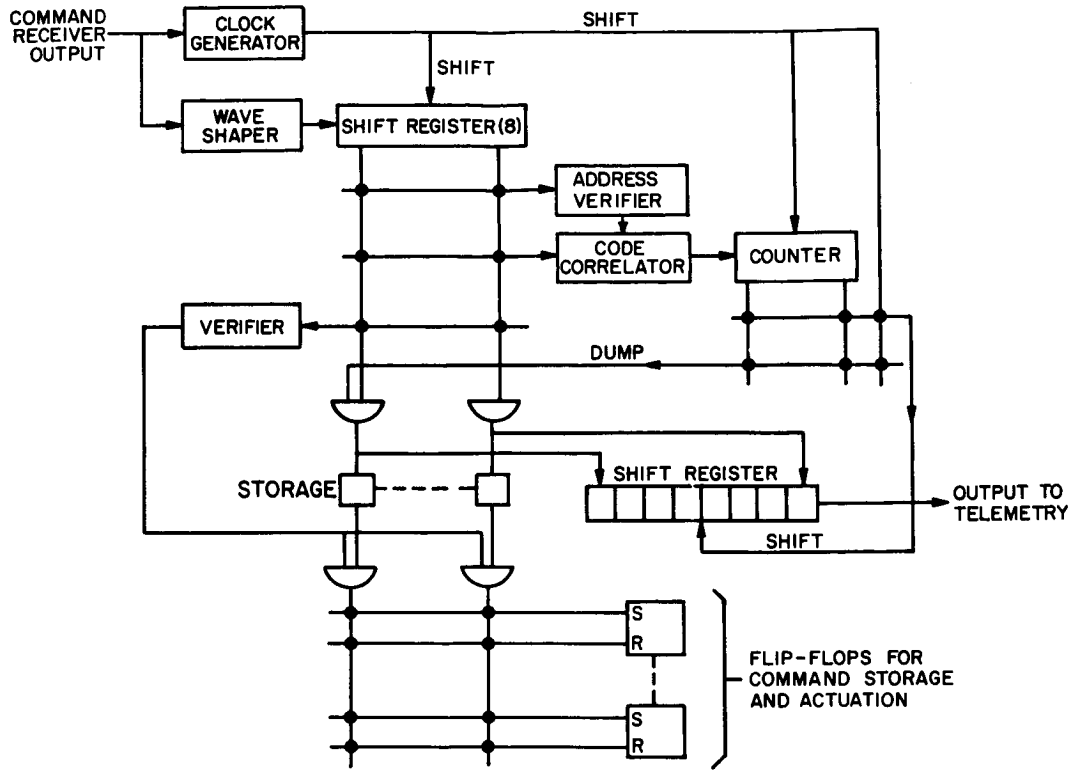


Figure 2-5. PCM Command System

consoles are equipped to handle four commands in one transmission. The first of these commands can be interpreted as a mode number. This is a function only of the on-board equipment and does not require modification of existing ground station facilities. By using two modes which double the function of all the command codes except the mode numbers themselves, 136 commands could be achieved. Many variations suggest themselves, most of which differ only in the final design details. Among the more important ones which should be considered are the use of several instructions for redundancy in mode switching, the possibility of assigning a block of codes for critical commands regardless of the mode, and the possibility of an automatic reversion to a basic mode after a fixed time interval. These have in common the property of minimizing the effects of a failure.

Table 2-1 shows a possible format using a fixed block of 30 critical commands and three modes, with four instructions for each of the mode-switching functions, for a total of 150 instructions. Command verification as described below will be used in this system.

TABLE 2-1
FORMAT OF TONE DIGITAL COMMAND SYSTEM USING THREE MODES.

| | |
|---|---|
| 1. | Command Mode 1 |
| 2. | Command Mode 2 |
| 3. | Command Mode 3 |
| 4. | Command Mode 1 |
| 5. | Command Mode 2 |
| 6. | Command Mode 3 |
| 7. | Command Mode 1 |
| 8. | Command Mode 2 |
| 9. | Command Mode 3 |
| 10. | Command Mode 1 |
| 11. | Command Mode 2 |
| 12. | Command Mode 3 |
| 13. | Instruction 13 |
| | to |
| 30. | Instruction 30 |

| | Mode 1 | Mode 2 | Mode 3 |
|---|---|---|---|
| 31. | Instruction 31-1 | Instruction 31-2 | Instruction 31-3 |
| | to | to | to |
| 70 | Instruction 70-1 | Instruction 70-2 | Instruction 70-3 |

3. Control Command

The command system under consideration would handle continuous control commands through a closed loop involving the ground station operator and a return path via the telemetry link. Two bits are used to start a control command. One indicates direction (left-right) and the other "on" or "off". The drives on all the controls will be slow enough so that the operator will be able to easily observe the response and bring the reading, as telemetered, to a desired value despite the transmission delay in the loop. It may be necessary to have two speeds, a control speed and a slewing speed, for some of the functions which may have a wide range as well as a close accuracy requirement.

The alternative to this method would be the transmission to the vehicle of the absolute value to which a control is to be set. The penalty for this method in extra equipment is very high. It is necessary to store the value of the command and perform comparisons in the vehicle which determine the actual driving signals for the equipment involved. Since such a system is used where very rapid response to the command is required, it follows that the comparisons must be frequent and rapid, and the decisions controlled by good closed-loop design to prevent hunting and other adverse effects which an operator (and a slow rate) would prevent. An on-board computer can sometimes be used where there are many such loops. The computer would be time-shared, and would function as a sampled data system at a rate appropriate for each loop. It appears that there is no requirement for such a control system on the SMS vehicle.

Where command requirements dictate a capacity in excess of 70 (or 136) commands available with the tone digital system, consideration should be given to a PCM command system.

4. PCM Command System

A PCM command system, as described below, can handle 256 commands and can be readily modified to much higher capacity as the design of the vehicle progresses. The system is designed around ground verification of a command before execution. The command as stored will be transmitted to the ground via the telemetry link and will require a return command coded as an execute command for transfer to the actuating controls. The actual verification can be accomplished by the operator or can be automatically programmed by ground equipment.

a. Verification

Verification of commands to be carried out will be required of all positive action commands, that is, all those which will initiate an action. If verification is required on "halt" type commands, an unfortunate situation may develop. This situation is due to failure where it may not be possible to stop some previously initiated action. One solution is to dispense with the verification of "halt" type commands. Another is to have a general "halt" command which shuts down all action and is used only in an emergency, after which actions required can be started up again.

b. Detailed Description

As shown in Figure 2-5. the detected signal from the receiver is introduced to two circuits: one for generating clock pulses, and the other for modifying the form of the "ones" and "zeros". The form of the detected signal is shown in Figure 2-6. A 50% duty cycle pulse is used to represent a "one" and

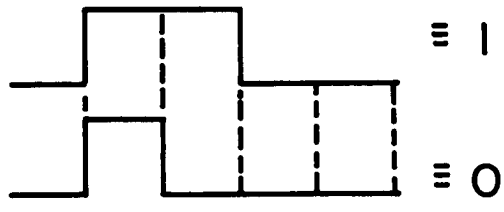


Figure 2-6. Pulse Configuration

a 25% duty cycle pulse is used to represent a "zero". The leading edge of these pulses always occurs at the beginning of the pulse period and will therefore be the basis for generating a clock pulse. The circuit that generates the clock is basically a differentiator followed by a monostable multivibrator. This is shown in block form in Figure 2-7. It will be more convenient to introduce the informa-

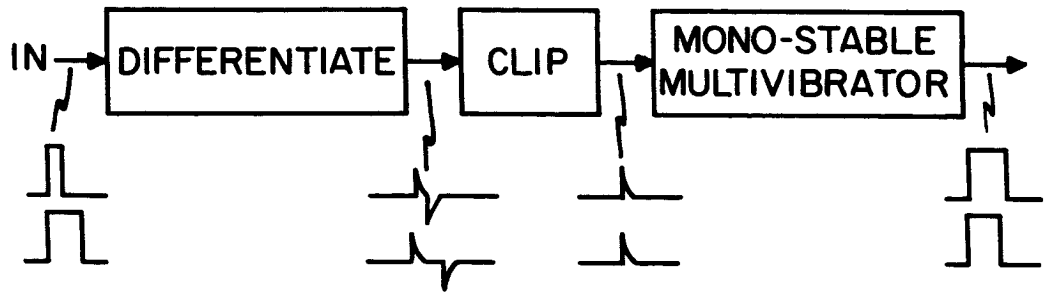


Figure 2-7. Clock Generator

tion into the shift register in the form of "pulse" or "no pulse" for "one" or "zero". This is accomplished at the block labelled "Wave Shaper" in Figure 2-5 and is expanded in block form in Figure 2-8.

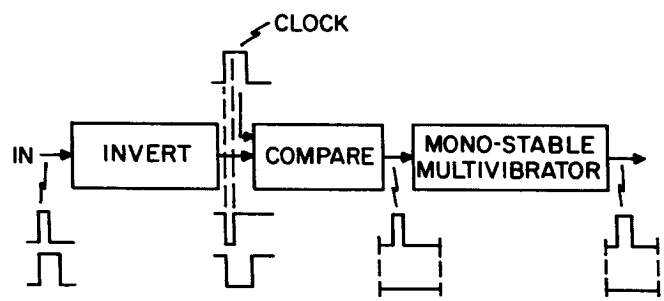


Figure 2-8. Pulse Generator

The inverter is followed by a comparison with the clock pulse. Coincidence occurs only for the "zero" case. This is used to generate a pulse which will inhibit the next clock pulse and result in a pulse for "one" and no pulse for "zero."

The generated clock pulses are used to shift the information into an eight-bit shift register. This goes on continually if information is being received.

To properly decode commands which are received, it is necessary to first ascertain the position of the bits of information relative to the start of a command code. For this purpose, use will be made of a "Barker" or pseudorandom code, which is an arrangement of bits which has a high cross correlation for the correct position and zero or negative for all the possible translated (offset in time) positions. Even with occasional mistakes within the code, it is probable that successful synchronization will be achieved. A seven-bit code will be used, and Figure 2-9 shows the circuit for carrying out the detection and synchronization shown in the block diagram. The synchronization is implemented by resetting a counter which is then used to "tick off" the next eight pulses and dump them into a register where

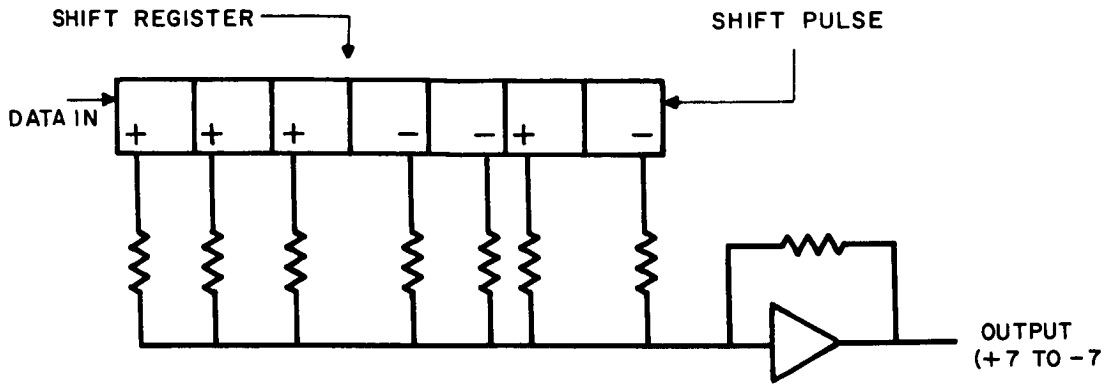


Figure 2-9. Code Correlator

they will be sorted until verified. When they are dumped into this storage, they are also dumped into a shift register and, in synchronism with the telemetry, are transmitted to the ground.

When verification is completed, either by the operator or by automatic means, an "Execute" signal is transmitted. If no transmission has occurred between these instructions, synchronization will be automatic. It is possible to arrange for the retransmission of the Barker code, if desired, to resynchronize. Close study of the details of the design will show which courses are preferable in a great many possible variations without materially altering the configuration and the resultant data. In any case, the receipt of the "Execute" signal will result in the stored command being gated through to a bank of flip-flops which will hold these commands until rescinded. There are as many of those flip-flops as there are functions to be carried out. On-off type commands may be decoded into the "Set" and "Reset" of a single flip-flop. Proportional commands, which require an indication of direction as well as state, will require at least two flip-flops. It may be necessary to augment this system somewhat to provide for security. A unique address code is assigned to the vehicle and is detected in much the same way that a command is detected. However, the logic of the vehicle is such that the address must be received just ahead of the command to be executed. Its function is to unlock the command system for a short time duration, during which it will admit a command. This is similar to the tone digital command system which has an address code as part of its structure.

5. Programming

Regardless of the particular system, verification of the actual performance of a function will be obtained from the telemetry where the result of the action called for will be observed. Proportional commands will be monitored this way by an operator who will control the progress of a command towards its

new setting. As previously stated, based on the particular command it may be desirable to have two or more speeds, such as a slewing and a slow speed for directing a control. A more sophisticated control station based on automating this concept is shown in Figure 2-10.

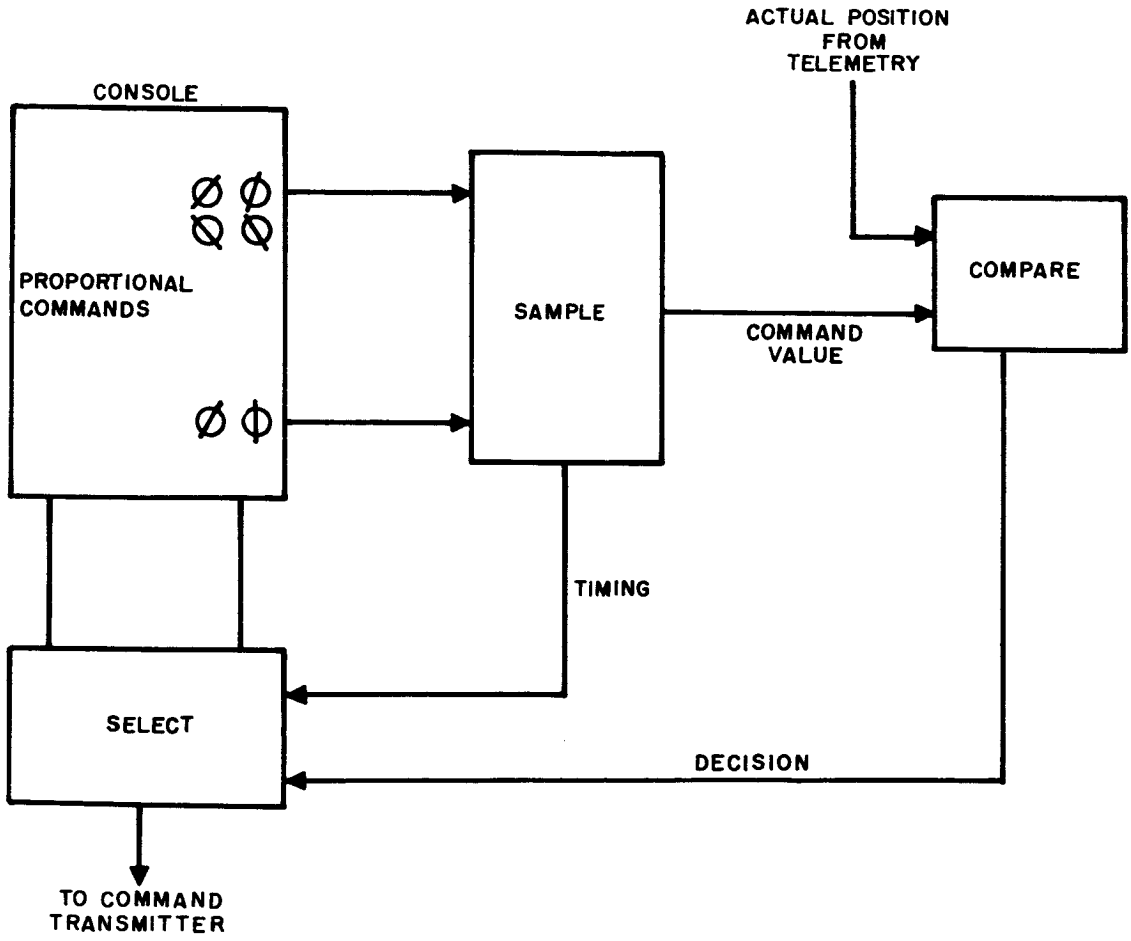


Figure 2-10. Ground Station Control of Proportional Commands

With no additional burden on the vehicle borne equipment, the values of the new proportional commands can be set up on the control console, and when the initial command setting up direction and action is verified, a ground-based computer can take over the function of monitoring the progress of the control towards its goal, making decisions as to changes of speed and implementing these as necessary.

6. Summary

Because instructions will generally be sent on an operator-controlled basis, the basic command link data rate need not be very great. Even if ground computer control is instituted, most of the actions do not require extremely precise timing. Following this reasoning a bit rate was selected which will make the verification link via the telemetry somewhat simpler. For the medium- performance vehicle, the rate illustrated here will be 128 bits/second. Table 2-2 lists the command requirements for the SMS vehicle.

The Tiros command system is a relatively simple one and it was possible to use the tone command system. This system used up to seven tones to command the various instructions. The immunity of the tone command system to false commands by extraneous systems is very poor; consequently, it is no longer recommended.

In contrast, the tone digital system has a much greater immunity against interfering signals. This system is recommended by Goddard Space Flight Center (GSFC) for simple on-off commands. This report has shown that it is possible to use such a system for the SMS vehicle even though a larger number of signals may be required than the original tone digital command system was designed to handle. Also, the use of on-off signals as timing controls for proportional commands has been discussed. The tone digital system is compatible with the command consoles at the GSFC Satellite Instrumentation Network stations.

If it does not prove feasible to use the tone digital system for more than the initially designed 70 commands, it is still desirable to make use of the final feature of its compatibility with the GSFC stations. This is possible if the tone digital system is used for the pre-orbital phase and is then held in reserve for a backup system while a PCM system takes over.

Generally, GSFC recommends the use of PCM for instruction command systems. PCM is used in the Nimbus, OGO, and other satellites where a command must be stored in the vehicle for later action based on a real-time clock. While the SMS vehicle does not have this requirement because of its synchronous orbit, it does have a rather large number of commands which a PCM structure can easily handle. GSFC presently plans to implement two PCM systems at several of its stations. One, the OGO system, has a bit rate of 128 bits/second and would meet the requirements of the SMS vehicle. (The other, the OAO system, has a 1000 bits/second rate which is considerably higher than that required here.) The verification procedure in the OGO system could be used in the SMS if the suggested method should prove to have insufficient advantage to warrant additional hardware. It involves sending the instruction word and following it with the same word in complement form. The two transmissions can then easily be checked for agreement.

It is estimated that the size of the SMS command system data handling will be 210 cu. in., the weight will be 8.8 lb, and the power requirement will be 9.8 watts.

TABLE 2-2

SMS COMMAND REQUIREMENTS

| Command | Number of Commands |
|---|---|
| Heat Budget Sensor: | 1 |
| On | 1 |
| Off | 1 |
| Reference Temperature 1 - Readout | 1 |
| Reference Temperature 2 - Readout | 1 |
| Reference Temperature 3 - Readout | 1 |
| Signal 1 (non-scan) | 1 |
| Signal 2 | 1 |
| Reference Temperature 1 (re-check) - Readout | 1 |
| Reference Temperature 2 (re-check) - Readout | 1 |
| Reference Temperature 3 (re-check) - Readout | 1 |
| Spare | 1 |
| Attitude Control: | |
| Acquisition & Re-Acquisition - initiate | 1 |
| Earth Track Command - initiate | 1 |
| Attitude Control - | |
| Roll On-Off; cw-ccw | 2 |
| Pitch On-Off; cw-ccw | 2 |
| Yaw On-Off; cw-ccw | 2 |
| Dump Command 1 | 1 |
| Dump Command 2 | 1 |
| Dump Command 3 | 1 |
| Station Keeping 1 | 1 |
| Station Keeping 2 | 1 |
| Rate Gyro Start 1 | 1 |
| Rate Gyro Start 2 | 1 |
| Rate Gyro Start 3 | 1 |
| Rate Gyro Stop 1 | 1 |
| Rate Gyro Stop 2 | 1 |
| Rate Gyro Stop 3 | 1 |
| Velocity Correction | 2 |
| Spare | 2 |
| Spare | 1 |
| Spare | 2 |
| Spare | 1 |
| Spare | 2 |
| Spare | 1 |
| Power Supply: | |
| Array-Secondary | 2 |

| Command | Number of Commands |
|---|---|
| Power Supply (continued) | |
| Spare | 2 |
| Spare | 1 |
| Communication: | |
| Primary DC Transmitter | 2 |
| Data Transmitter Subcarrier to Telemetry Encoder | 2 |
| Data Transmitter Subcarrier to Relay Rcvr Output | 2 |
| DC Transmitter | 2 |
| Modulation Input to Transmitter | 2 |
| Switch to unmode mode for beacon operation | 2 |
| Override switch from omni-to directional | 2 |
| Spare | 2 |
| Spare | 2 |
| Spare | 2 |
| Cloud Picture Sensor: | |
| Target voltage - increase - decrease | 2 |
| Beam Current - increase - decrease | 2 |
| Multiplier Voltage - increased-decrease | 2 |
| Photocathode Voltage - increase - decrease | 2 |
| Scan Mirror - X cw-ccw | 2 |
| Scan Mirror - Y cw-ccw | 2 |
| Light Density Filters, Angle cw-ccw | 2 |
| AGC increase-decrease | 2 |
| Lens Aperture increase-decrease | 2 |
| Shutter | 2 |
| Occulting Mask | 2 |
| Bandwidth Control increase-decrease | 2 |
| Spare | 2 |
| Spare | 2 |
| Spare | 2 |
| Spare | 2 |
| Spare | 2 |
| Spare | 2 |

## C. TELEMETRY SYSTEM

The function of the telemetry unit is to relay to the ground the status of various critical functions in the vehicle which are considered important. Some of the data points are selected because of the action which can be taken from the ground via the command link. Others for which no action can be taken are neverthless important because the information provides data concerning the general behavior of the vehicle as related to the original design estimates and serves as a guide to determine causes of failures.

A block diagram of a typical telemetry system is given in Figure 2-11. The input points, labelled "digital points" and "analog points" come from transducers which are located at the sources of the quantities to be measured. The information is organized by the body of the equipment into a predetermined format and is sent on to the transmitter which transmits it to the ground station. In the ground station, the data thus received can be interpreted as readings of the measurements required. This discussion will concern primarily the flow of data leaving the transducers, through the equipment shown and up to the input to the transmitting equipment. The Communications Section of this report covers the transmission link. The transducers will be selected by the designers of the various equipments to best convert the quantity to be monitored to a compatible electrical signal. Ground station equipment is not covered.

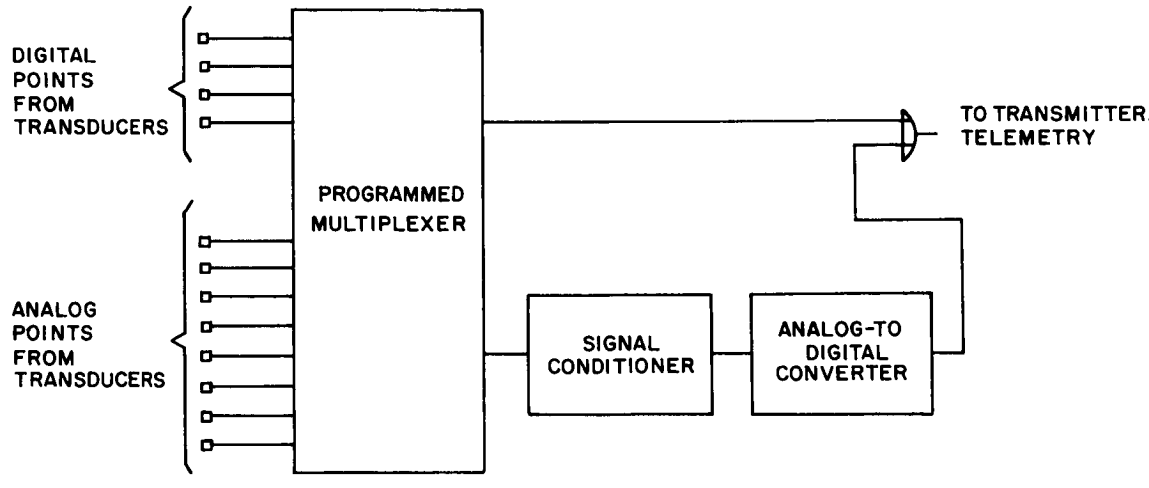


Figure 2-11. Telemetry Data Handling

The study in the Communications Section shows that for the precision requirements of this vehicle (in some cases, 0.1%) a PCM system is the most satisfactory. PCM systems are generally gaining in favor for the reasons previously discussed. The high rate section of the Nimbus satellite telemetry which is of the same order of magnitude as the system to be discussed, uses PCM transmission.

The relatively high rate of transmission needed in some satellites stems from the fact that they must store data during an orbit and transmit the entire store in a relatively short time period when they are located favorably with respect to a ground station. The SMS will be in a synchronous orbit and therefore does not require any bulk storage. The data rate is relatively high because of the number of points and the frequency of monitoring.

A listing of the points of interest for a representative system in the SMS vehicle is given in Table 2-3. The requirements for each point are given in the form of required precision, sampling rate, and the resultant bit rate for a PCM system. The estimated precision together with the sampling rate based on the highest frequency of interest, amplitude, and pertinent comments are included.

The nature of the points being measured varies considerably. Typically, in some cases a voltage is to be monitored, in others a shaft position, or, the output of a transducer measuring a quantity such as temperature. The transducer output may be in analog voltage form or it may be in digital code. All of the quantities must be converted to digital code prior to transmission. A solid-state converter is used. The block diagram for such a unit is shown in Figure 2-12. This diagram shows an "over-under" type of converter which successively brackets the desired value until it reaches as close an approximation as possible.

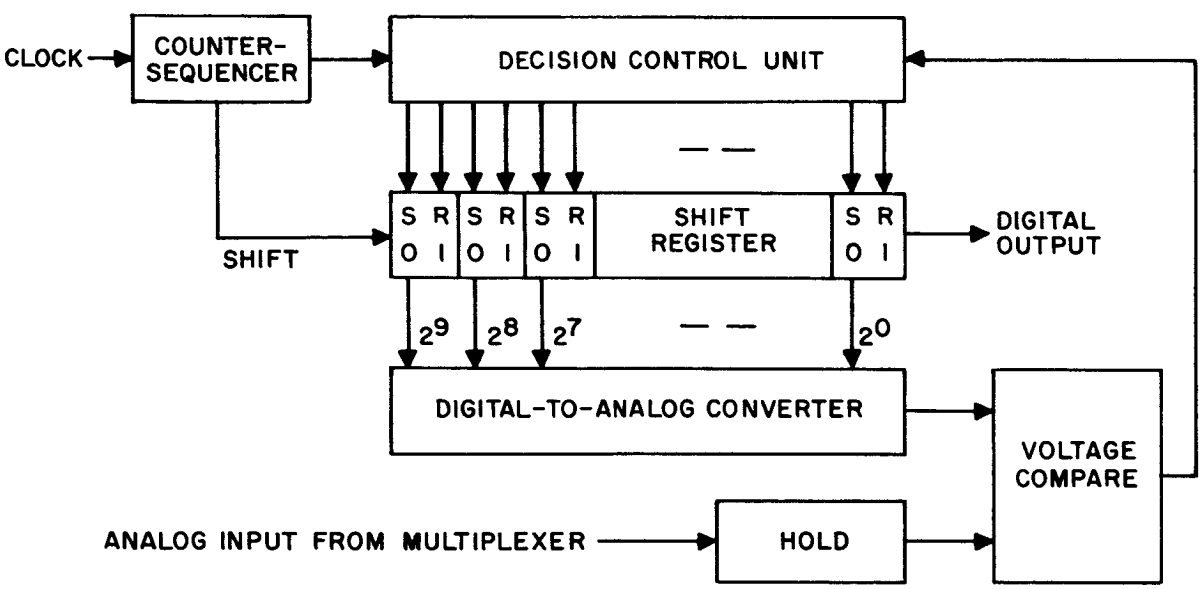


Figure 2-12. Analog-to-Digital Converter

TABLE 2-3

REPRESENTATIVE REQUIREMENTS FOR TELEMETRY-SMS

| Item | Precision % | Precision Bits | Sampling Rate | Bit Rate | Comments |
|---|---|---|---|---|---|
| Attitude Control | | | | | |
| 1. Rate Gyro | 1 | 7 | 4/sec | 28/sec | 0-10°/sec; acquisition-continuous |
| 2. Rate Gyro | 1 | 7 | 4/sec | 28/sec | 0-10°/sec; acquisition-continuous |
| 3. Rate Gyro | 1 | 7 | 4/sec | 28/sec | 0-10°/sec; acquisition-continuous |
| 4. Cold Gas Solenoid | | 1 | 2/sec | 2/sec | On-Off; continuous |
| 5. Cold Gas Solenoid | | 1 | 2/sec | 2/sec | On-Off; continuous |
| 6. Cold Gas Solenoid | | 1 | 2/sec | 2/sec | On-Off; continuous |
| 7. Control Field (reaction wheel) | 1 | 7 | 1/min | 7/min | 0 to ±26 VAC; continuous-Earth track |
| 8. Control Field (reaction wheel) | 1 | 7 | 1/min | 7/min | 0 to ±26 VAC; continuous-Earth track |
| 9. Control Field (reaction wheel) | 1 | 7 | 1/min | 7/min | 0 to ±26 VAC; continuous-Earth track |
| 10. Fixed Field (reaction wheel) | 10 | 4 | 1/hr | 4/hr | 26 VAC fixed; Earth track |
| 11. Fixed Field (reaction wheel) | 10 | 4 | 1/hr | 4/hr | 26 VAC fixed; Earth track |
| 12. Fixed Field (reaction wheel) | 10 | 4 | 1/hr | 4/hr | 26 VAC fixed; Earth track |
| 13. Tachometer (reaction wheel) | 1 | 7 | 1/min | 7/min | 0.125 rpm; continuous-Earth track |
| 14. Tachometer (reaction wheel) | 1 | 7 | 1/min | 7/min | 0.125 rpm; continuous-Earth track |
| 15. Tachometer (reaction wheel) | 1 | 7 | 1/min | 7/min | 0.125 rpm; continuous-Earth track |
| 16. Horizon Scanner Output Head | 1 | 7 | 1/2/sec | 3.5/sec | 0 to ±35; continuous |
| 17. Horizon Scanner Output Head | 1 | 7 | 1/2/sec | 3.5/sec | 0 to ±35; continuous |
| 18. Horizon Scanner Output Head | 1 | 7 | 1/2/sec | 3.5/sec | 0 to ±35; continuous |
| 19. Roll | 1 | 7 | 1/2/sec | 3.5/sec | 0 to ±5; continuous-Earth track |
| 20. Pitch | 1 | 7 | 1/2/sec | 3.5/sec | 0 to ±5; continuous-Earth track |
| 21. Logic Signals | | 1 | 2/sec | 2/sec | On-Off; Acquire and re-acquire |
| 22. Logic Signals | | 1 | 2/sec | 2/sec | On-Off; Acquire and re-acquire |
| 23. Logic Signals | | 1 | 2/sec | 2/sec | On-Off; Acquire and re-acquire |
| 24. Logic Signals | | 1 | 2/sec | 2/sec | On-Off; Acquire and re-acquire |
| 25. Logic Signals | | 1 | 2/sec | 2/sec | On-Off; Acquire and re-acquire |
| 26. Logic Signals | | 1 | 2/sec | 2/sec | On-Off; Acquire and re-acquire |
| 27. Sun Sensor | 0.1 | 10 | 2/min | 20/min | 0 to ±90; continuous |
| 28. Sun Sensor | 0.1 | 10 | 2/min | 20/min | 0 to ±90; continuous |
| 29. Sun Sensor | 0.1 | 10 | 2/min | 20/min | 0 to ±90; continuous |
| 30. Sun Sensor | 0.1 | 10 | 2/min | 20/min | 0 to ±90; continuous |
| 31. Sun Pitch | 0.1 | 10 | 2/min | 20/min | 0 to ±90; acquisition |
| 32. Sun Yaw | 0.1 | 10 | 2/min | 20/min | 0 to ±90; acquisition |

TABLE 2-3

REPRESENTATIVE REQUIREMENTS FOR TELEMETRY-SMS (Cont'd)

| Item | Precision % | Precision Bits | Sampling Rate | Bit Rate | Comments |
|---|---|---|---|---|---|
| Attitude Control (continued) | | | | | |
| 33. Sun Logic Signals | | 1 | 2/sec | 2/sec | On-Off; Continuous during acquisition |
| 34. Sun Logic Signals | | 1 | 2/sec | 2/sec | On-Off; Continuous during acquisition |
| 35. Sun Logic Signals | | 1 | 2/sec | 2/sec | On-Off; Continuous during acquisition |
| 36. Sun Logic Signals | | 1 | 2/sec | 2/sec | On-Off; Continuous during acquisition |
| 37. Gas Pressure Reservoir | 5 | 5 | 2/sec | 10/hr | 0-3000 psi; continuously-once/hr. |
| 38. Gas Pressure Regulator | 5 | 5 | 2/sec | 10/hr | 0-50 psi; continuously-once/hr. |
| 39. Electronics | 5 | 5 | 1/2/sec | 2/5/sec | 0-10 V; continuous |
| 40. Electronics | 5 | 5 | 1/2 sec | 2.5/sec | 0-10 V; continuous |
| 41. Electronics | 5 | 5 | 1/2 sec | 2.5/sec | 0-10 V; continuous |
| 42. Electronics | 5 | 5 | 1/2 sec | 2.5/sec | 0-10 V; continuous |
| 43. Electronics | 5 | 5 | 1/2 sec | 2.5/sec | 0-10 V; continuous |
| 44. Electronics | 5 | 5 | 1/2 sec | 2.5/sec | 0-10 V; continuous |
| 45. Electronics | 5 | 5 | 1/2 sec | 2.5/sec | 0-10 V; continuous |
| 46. Electronics | 5 | 5 | 1/2 sec | 2.5/sec | 0-10 V; continuous |
| 47. Electronics | 5 | 5 | 1/2 sec | 2.5/sec | 0-10 V; continuous |
| 48. Electronics | 5 | 5 | 1/2 sec | 2.5/sec | 0-10 V; continuous |
| 49. Electronics | 5 | 5 | 1/2 sec | 2.5/sec | 0-10 V; continuous |
| 50. Electronics | 5 | 5 | 1/2 sec | 2.5/sec | 0-10 V; continuous |
| Video Sensor | | | | | |
| 51. Target Voltage | 0.25 | 9 | 1/sec | 9/sec | 0-3 V |
| 52. Beam Current | 1 | 7 | 1/sec | 7/sec | 100:1 |
| 53. Multiplier Voltage | 2 | 6 | 6/hr | 36/hr | 5:1 |
| 54. Photocathode Voltage | 2 | 6 | 6/hr | 36/hr | 5:1 |
| 55. B+ | 1 | 7 | 6/hr | 42/hr | |
| 56. B+ | 1 | 7 | 6/hr | 42/hr | |
| 57. B- | 1 | 7 | 6/hr | 42/hr | |
| 58. B- | 1 | 7 | 6/hr | 42/hr | |
| 59. Scan Mirror - X | 2 | 6 | 1/sec | 6/sec | |
| 60. Scan Mirror - Y | 2 | 6 | 1/sec | 6/sec | |
| 61. Light Density Filters, Angle | 1 | 7 | 1/sec | 7/sec | |
| 62. Horizontal Scan Current | 5 | 5 | 6/min | 30/min | |
| 63. Vertical Scan Current | 5 | 5 | 6/min | 30/min | |

TABLE 2-3

REPRESENTATIVE REQUIREMENTS FOR TELEMETRY-SMS (Cont'd)

| Item | Precision % | Precision Bits | Sampling Rate | Bit Rate | Comments |
|---|---|---|---|---|---|
| Video Sensor (continued) | | | | | |
| 64. AGC | 1 | 7 | 1/sec | 7/sec | |
| 65. Lens Aperture | | 2 | 6/min | 18/min | Multi-position |
| 66. Shutter | | 2 | 6/min | 18/min | Multi-position |
| 67. Bandwidth Control | 5 | 5 | | | |
| 68. Magnetic Focus Coil | 5 | 5 | | | |
| 69. Alignment Current | 5 | 5 | | | |
| 70. Set Up Program | 5 | 5 | | | |
| Communications | | | | | |
| 71. #1 AGC Monitor-Command Rcvr. | 5 | 5 | 2/hr | 10/hr | Orbit |
| 72. #2 AGC Monitor-Command Rcvr. | 5 | 5 | 2/hr | 10/hr | Orbit |
| 73. Demod. Output to Decoder - Rcvr. | 5 | 5 | 2/hr | 10/hr | Orbit |
| 74. #1 AGC Monitor-Relay Rcvr. | 5 | 5 | 2/hr | 10/hr | Orbit |
| 75. Demod. Output to Decoder - Rcvr. | 5 | 5 | 2/hr | 10/hr | Orbit |
| 76. Video Input-Sensor Data Xmitter | 5 | 5 | 2/hr | 10/hr | Orbit |
| 77. RF Drive - P.A. #1 Xmitter | 5 | 5 | 2/hr | 10/hr | Orbit |
| 78. HV Drive - P.A. #1 Xmitter | 1 | 7 | 2/hr | 14/hr | Orbit |
| 79. Common Output - RF Power Out | 5 | 5 | 2/hr | 10/hr | Orbit |
| 80. Temp. Check - P.A. #1 Xmitter | 5 | 5 | 2/hr | 10/hr | Orbit |
| 81. Xmitter Power Out. - Telemetry | 5 | 5 | 2/hr | 10/hr | Orbit |
| 82. Encoder Out. to Xmitter In., Telemetry | 5 | 5 | 2/hr | 10/hr | Orbit |
| 83. Thermal - Out. Xmitter Telemetry | 5 | 5 | 2/hr | 10/hr | Orbit |
| 84. Indicate Horizon Sensor Ant. Sw. | | 1 | 2/hr | 2/hr | Orbit |
| 85. #1 AGC Monitor-Command Rcvr. | 5 | 5 | 4/min | 20/min | Launch and Pre-orbit |
| 86. #2 AGC Monitor-Command Rcvr. | 5 | 5 | 4/min | 20/min | Launch and Pre-orbit |
| 87. Demod. Output to Decoder - Rcvr. | 5 | 5 | 4/min | 20/min | Launch and Pre-orbit |
| 88. #1 AGC Monitor - Relay Rcvr. | 5 | 5 | 4/min | 20/min | Launch and Pre-orbit |
| 89. Demod. Output to Decoder - Rcvr. | 5 | 5 | 4/min | 20/min | Launch and Pre-orbit |
| 90. Video Input-Sensor Data Xmitter | 5 | 5 | 4/min | 20/min | Launch and Pre-orbit |
| 91. RF Drive - P.A. Xmitter, Data | 5 | 5 | 4/min | 20/min | Launch and Pre-orbit |

TABLE 2-3

REPRESENTATIVE REQUIREMENTS FOR TELEMETRY-SMS (Cont'd)

| Item | Precision % | Precision Bits | Sampling Rate | Bit Rate | Comments |
|---|---|---|---|---|---|
| Communications (continued) | | | | | |
| 92. HV Drive - P.A. Xmitter, Data | 1 | 7 | 4/min | 28/min | Launch and Pre-orbit |
| 93. Common Output - RF Power Out | 5 | 5 | 4/min | 20/min | Launch and Pre-orbit |
| 94. Temp. Check - P.A. Xmitter, Data | 5 | 5 | 4/min | 20/min | Launch and Pre-orbit |
| 95. Xmitter Power Out - Telemetry | 5 | 5 | 4/min | 20/min | Launch and Pre-orbit |
| 96. Encoder Out to Xmitter In. | 5 | 5 | 4/min | 20/min | Launch and Pre-orbit |
| 97. Thermal - Out Xmitter, Telemetry | 5 | 5 | 4/min | 20/min | Launch and Pre-orbit |
| 98. Indicate Horizon Sensor Sw. | | 1 | 4/min | 4/min | Launch and Pre-orbit |
| Power Supplies | | | | | |
| 99. Primary Battery | 1 | 7 | 1/5/sec | 1.2/sec | Acquisition |
| 100. Primary Battery Temp. | 1 | 7 | 1/min | 7/min | Acquisition |
| 101. Solar Array | 1 | 7 | 1/min | 7/min | Acquisition |
| 102. Solar Array Temp. | 1 | 7 | 1/min | 7/min | Acquisition |
| 103. Secondary Battery | 1 | 7 | 1/5/sec | 1.2/sec | Track |
| 104. Secondary Battery Temp. | 1 | 7 | 1/min | 7/min | Track |
| 105. Solar Array | 1 | 7 | 1/5/sec | 1.2/sec | Track |
| 106. Solar Array Temp. | 1 | 7 | 1/min | 7/min | Track |
| 107. Charging Current Monitor | 1 | 7 | 1/5/sec | 1.2/sec | Track |
| 108. Array Orientation | 1 | 7 | 1/5/sec | 1.2/sec | Track |
| 109. Spare | 1 | 7 | 1/5/sec | 1.2/sec | Track |
| 110. Spare | 1 | 7 | 1/min | 7/min | Track |
| 111. Spare | 1 | 7 | 1/min | 7/min | Track |
| Heat Budget | | | | | |
| 112. Shutter Operation | | 2 | | | On Command |
| 113. On-Off | | 2 | | | On Command |
| 114. Reference Temp. 1 | 0.2 | 9 | | | On Command |
| 115. Reference Temp. 2 | 0.2 | 9 | | | On Command |
| 116. Reference Temp. 3 | 0.2 | 9 | | | On Command |

TABLE 2-3

REPRESENTATIVE REQUIREMENTS FOR TELEMETRY-SMS (Cont'd)

| Item | Precision % | Precision Bits | Sampling Rate | Bit Rate | Comments |
|---|---|---|---|---|---|
| Data Handling | | | | | |
| 117. Check Point | 5 | 5 | 1/min | 5/min | Continuous |
| 118. Check Point | 5 | 5 | 1/min | 5/min | Continuous |
| 119. Check Point | 5 | 5 | 1/min | 5/min | Continuous |
| 120. Check Point | 5 | 5 | 1/min | 5/min | Continuous |
| 121. Check Point | 5 | 5 | 1/min | 5/min | Continuous |

The converter consists of an analog-to-digital converter and ten inputs. This corresponds to the maximum precision requirement in the telemetry list. This unit can code to a precision of 0.1% ($1/2^{10} = 1/1024$). When a voltage is to be encoded, a sample (which is held constant for the coding period) is compared to the output of the analog-to-digital converter. The most significant input is energized first, causing the output of the analog-to-digital converter to assume half of its reference voltage as output. If this should, on comparison, prove to be smaller than the sampled voltage, the next most significant input is energized with the first one left on. This combination gives 75% of the reference voltage. If the first comparison had proved too big, the next most significant voltage would have been energized with the first one turned off. This would have resulted in an output of 25% of the reference voltage. In this way, successive comparisons bracket the sampled value. When the ten comparisons are completed, the status of the ten inputs is actually the binary code, which is then sent on the telemetry transmitter.

The previously described "over-under" unit requires only 10 clock periods to encode a sample to ten places. This is particularly useful where time is important. In a unit such as this, the pulse rate is slow enough to consider a simple counter scheme which offers a savings in hardware even though its basic clock rate must be considerably faster. Such a system is illustrated in Figure 2-13. In this system a simple binary counter runs in sequence from 1 to 1024. Its output goes into an analog-to-digital converter which will then have a stepped sawtooth waveform as an output. This waveform is compared with the sample to be encoded. When the comparison goes through a null, the counter is stopped and the status of the counter is read out. This corresponds to the code being sought. This counter must be capable of running through its entire count in one sample time, which means it must be about one hundred times as fast as the "over-under" unit. This places the basic frequency at about 40 KC, which does not call for special circuitry.

It is clear from the above that the range of the analog-to-digital system depends on the reference voltage used. Wherever possible this same voltage is used as reference for the transducers which will generate the voltage to be encoded. This eliminates errors due to different standards and also may eliminate scaling factors. Typically, potentiometers that sense shaft positions can be supplied with this same reference. Where this is not possible, the voltages must be scaled to the appropriate reference or else accept a loss in precision if the full range of the monitored value is less than the full range of the converter.

As shown in Table 2-3 the sampling ranges and the precision requirements for the various points vary widely. There are points for which a simple on-off check is to be made no more than every few minutes. There are others where data with 1% precision must be checked four times a second. The final data rate of the telemetry system is a composite of these requirements. Data is arranged in a format consisting of words and blocks of words (called frames). The basic frame rate is selected as the rate which is in agreement with the most data. Beyond that, the few items requiring monitoring at a greater frequency are repeated several times in each frame, or super-commutated. The data for which a much slower rate is satisfactory can be sent out on alternate or fewer frames, or sub-commutated. It is clear that sub-commutated data can time-share a common location within the frame structure and that these items can be separated out correctly as long as the starting point and the sequence are known at the receiving station.

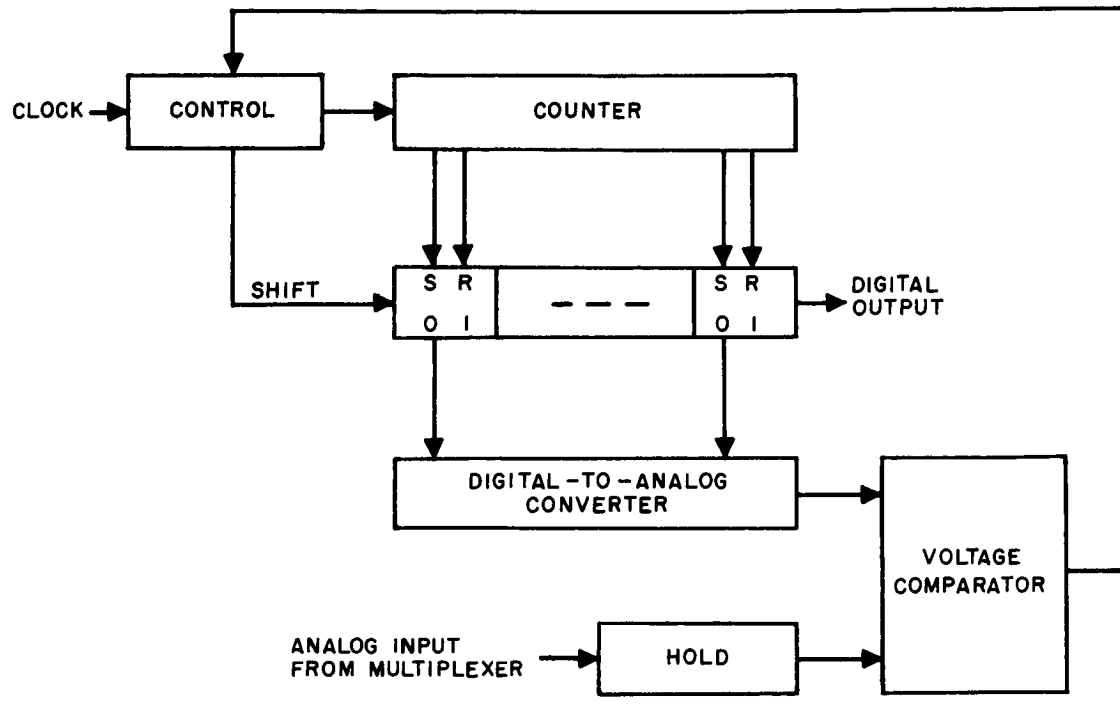


Figure 2-13. Analog-to-Digital Converter, Sawtooth Type

The function of the multiplexing unit in the telemetry system is to arrange all the data in series in the predetermined sequence following the frame format. Figure 2-11 is a block diagram of the telemetry system which shows the key position of the multiplexer. All inputs to be monitored go via the multiplexer to the analog-to-digital converter where necessary, or directly to the transmitter where possible. The format is controlled by a wired-in program.

A summary of the tabulated telemetry requirements is shown in Table 2-4. The results of this summary show that for the complete system, a bit rate of 200 bits/second is required. With provision for spares and other contingencies at this stage of a design estimate, a figure of 400 bits/second is used.

TABLE 2-4 SUMMARY OF TELEMETRY REQUIREMENTS

| Total Sampling Rates: | per second | per minute | per hour |
|---|---|---|---|
| | 226 | 907<br>or 16/sec | 176<br>or 1/sec |

226 + 16 + 1 = 243 pulses per second

In addition, if command verification is to be accomplished by playback of the command via the telemetry link, 10 pulses every one-quarter second will be assigned for this purpose.

This brings total to:

$$243 + 4(10) = 283 \text{ pulses/second}$$

This figure is for a maximum capability vehicle, with no attempt made to carefully review requirements to sort out those needed only prior to acquisition and those needed only in orbit.

Where digital transducers such as code wheels are used, it is possible to save a considerable amount of harness wiring by having the portion of the multiplexing which serializes the output located at the site of the measurement. This usually entails having a counter at the site which is controlled by a clock pulse from the main multiplexer. This counter must start up at the right time and scan the digits in the correct sequence and timing. For the most stringent requirement, 10 bits, in the SMS, a four stage counter would be needed. A single line could be used to send a burst of ten successive clock pulses to the counter which would then serialize the output of the code wheel. An automatic reset would occur after a pre-set time by using a mono-stable multivibrator. The serialized output is sent to the main multiplexer via a second line. This unit would otherwise require ten lines for the output. The extra equipment in the form of a four-stage counter with its power and space requirement must be weighed against the weight of the harness involved. Some of these decisions must be reserved until the actual design of a vehicle has progressed far enough to determine the lengths of the harnesses. No savings can be obtained with most analog transducers since the output is already on one line.

A block diagram of the local multiplexing is depicted in Figure 2-14. This diagram actually shows a further extension of the above remarks; hence, an ultimate system is displayed. Here only two wires are used to handle all the digital telemetry. The "clock" line is actually directed to each local counter in turn by addressing it. It then delivers the necessary number of pulses. The output (since each unit is addressed in sequence) can all be on one line. There is now an additional hardware requirement in the form of addressing units. Again, the decision to adopt such a scheme must come about in a late stage of design.

Although the telemetry requirements become progressively simpler as the vehicle under consideration has its performance requirements reduced, no great savings accrues to the vehicle in terms of size, weight, and power. Units such as the analog-to-digital converter discussed above do not undergo any significant changes and the counters, programmers, and other such units will only lose the equivalent of one flip-flop each if their capabilities are cut in half. The signal conditioner may show the greatest effects of reduction in requirements.

From a systems point of view, it is important to recognize that the requirements for telemetry change as the vehicle proceeds from launch to final station acquisition. Table 2-3 clearly illustrates this point. In point of fact, however, little gain in hardware can result from this situation. The only gain is the possibility of utilizing the sensor channel for back-up telementry after acquisition. The additional complication in trying to generalize the multiplexing equipment for different functions will more than offset any gain due to a savings in basic equipment.

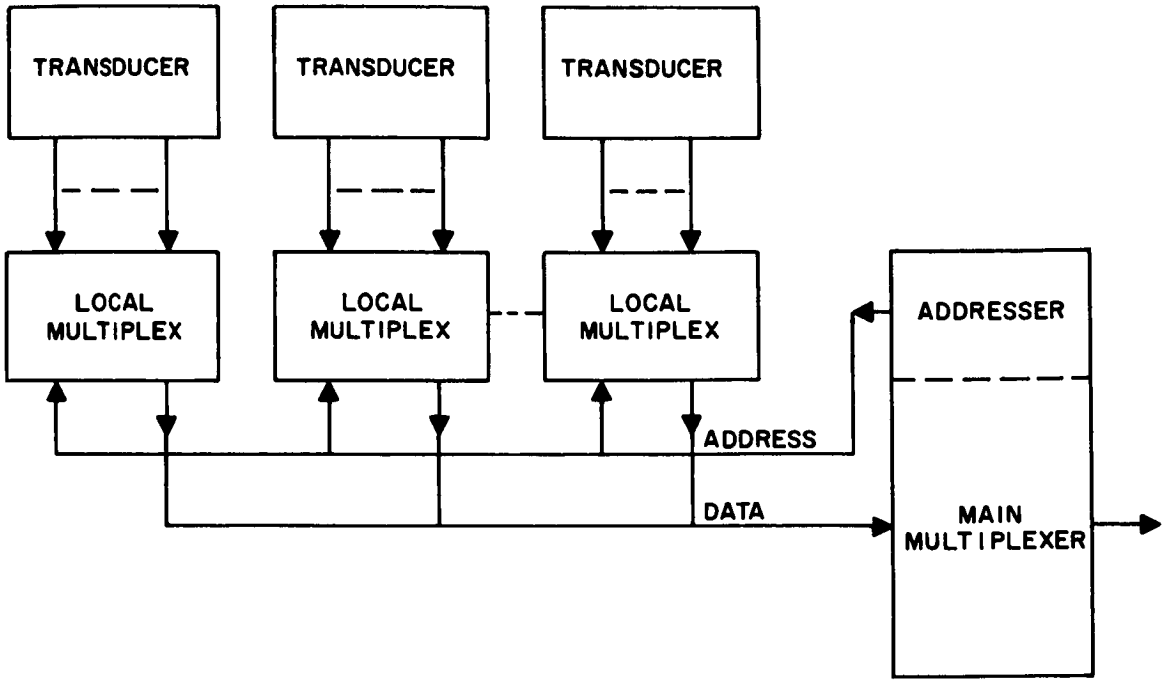


Figure 2-14. Two-Wire System Based on Local Serializing

Error-correcting codes could be used in the telemetry to introduce redundancy which would serve to enhance a signal even with a poor signal to noise ratio. They of course require a greater bit rate, but can be tailored to suit the most probable error. Alternatively, an orthogonal code can be used. This is detected by correlating the input with each of the possible codes. The correlation is zero for all except the correct one. A decision unit is used to detect the greatest output. When noise is present the wrong outputs will not all be zero, but will probably be considerably smaller than the correct output. All of these systems add some complexity to the basic encoding and can only be justified if the trade-off against power offsets the additional weight and power of the extra coding equipment.

It is estimated that the weight of a telemetry unit with the basic requirements summarized in Table 2-3 will be 17 lb. This is based on the availability of similar systems and the studies made for future availability. The size will be 663 cu in. and the power requirement is 17 watts. Cutting back on the performance requirements of the vehicle causes little change in telemetry equipment because a basic requirement for stabilization must still be met. The biggest change is estimated in the signal conditioning circuitry. The reduced weight will be 13.2 lb; the reduced volume, 496 cu in.; and the reduced power, 11.6 watts.

Subsection 2B, contains a discussion concerning the verification of commands by repeating them over the telemetry link. As seen in Table 2-3, there already is a group of data requiring a repetition rate of four times per second. This cycle will be used to repeat the command, when a command is called for.

It is not now necessary to select a particular word size or format except in the general terms already discussed. This selection bears only on the final design of the multiplexer without affecting the trade-off considerations which are the prime concern in this report.

## SECTION 3 - POWER SYSTEM STUDY

### A. INTRODUCTION

The power system study will review the various power generation and energy storage devices that are applicable to a Synchronous Meteorological Satellite (SMS).

The mission objectives set up criteria for establishing the overall vehicle requirements. These in turn determine the design parameters of the electrical systems such as communications, stabilization and control, sensors, etc., all of which require electrical power. In view of the differences in individual system load requirements trade-off areas must be evaluated in terms of the overall vehicle configuration to achieve the optimum power system design. Thus it is essential that the power system requirements be established concurrently with the other vehicle system parameters.

Following the descriptions of each of the available power systems, the pertinent characteristics for space applications are summarized. Certain techniques are ruled out on the basis that they will not be available during the procurement time of this system. Other techniques that are sufficiently developed or that indicate sufficient promise in the next few years have been recommended for active support so that they may be incorporated in the system program schedule.

### B. DESCRIPTION OF POWER SYSTEMS

#### 1. Solar Power

The total solar radiation closely approximates the radiation from a black body at 5785°K. At distances greater than a few million miles from the Sun, the incident solar energy density varies inversely with the square of the distance from the sun. The solar radiation above the Earth's atmosphere is usually taken as 2 cal/cm$^2$/min or 130 watts/ft$^2$. This number is based upon a mean solar distance from the Earth of 149.6 x 10$^6$ km. However, the Earth's orbit is eccentric, thus the solar radiation above the Earth's atmosphere varies from about 126 to 134 watt/ft$^2$.

##### a. Solar Thermoelectric Power System

A thermoelectric converter consists of many thermocouples connected in series and parallel to provide the required load voltage and current. The three interrelated thermoelectric effects are:

(1) Seebeck effect

(2) Peltier effect

(3) Thompson effect

The Seebeck effect describes the voltage that is produced when there is a difference in temperature between the junctions of the dissimilar materials. The Peltier effect describes the heat evolved at the junctions of a thermocouple when current from an external source is pumped around the circuit. The Thompson effect describes the heat evolved <u>within</u> the thermoelectric material

that occurs when current flows through the thermocouple and it depends upon the rate of change of the Seebeck coefficient (volts/°K) with temperature which is usually assumed to be zero in most thermoelectric considerations. Hence, the Thompson effect is usually disregarded. Metallic thermocouples have never found practical use as thermoelectric converters because the conversion efficiency is only a few tenths of a percent. However, the development of semiconductor thermoelectric materials has tremendously increased the conversion efficiency.

The basic configuration of a solar powerplant that utilizes a thermoelectric converter based on Seebeck's principle is shown in Figure 3-1. In this system, the collected solar energy is focused by a circular-parabolic collector on the target located in the focal plane of the collector which serves as the hot junction. The thermocouples are embedded in the walls of the target. A heat transfer medium transports the unconverted thermal energy from the thermoelement cold junction to the radiator where it is radiated into space.

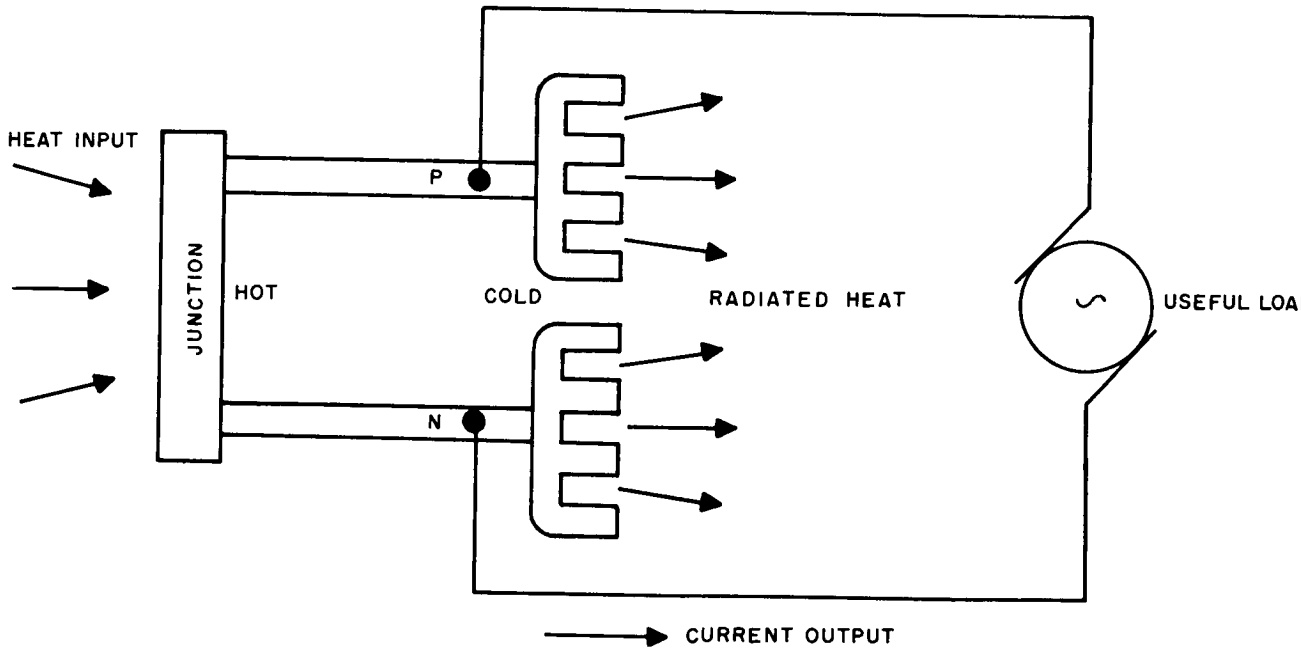


Figure 3-1. Solar Thermoelectric Configuration

When heat energy is supplied to the hot junction so that the hot junction temperature $T_h$ exceeds the cold junction temperature $T_c$, current will flow through the load as shown in Figure 3-1.

Assuming that the total solar power available is approximately 125.5 watt/ft$^2$ and the effective collector-target efficiency is 50 percent, the heat power available at the thermocouple hot junction is 62.7 watts/ft$^2$ of collector area. If the converter efficiency is assumed to be 6.7 percent, the collector area required to furnish 500 watts of electrical power is

$$\text{Collector area} = \frac{500}{0.067} \times \frac{1}{62.7} = 119 \text{ ft}^2$$

Since the Sun is almost a point source, subtending 32 minutes of arc, the form of the collector is usually parabolic. If the ratio of the aperture to the focal length is not too large, a spherical shape can be used to approximate the parabola. Where it is desirable to concentrate the Sun's energy along a line target of thermal-to-electrical converter instead of a circular target, a trough which is parabolic in cross section can be used.

The number of thermocouples that must be connected in series to develop the required voltage, $V_L$, across a matched load is given by

$$N_s = \frac{2V_L}{S\Delta T}$$

where $V_L$ = load voltage

$S = |S_p| + |S_n|$ = the sum of the absolute value of the Seebeck coefficients for p-type and n-type thermocouple legs, Volts/°K

$\Delta T = T_h - T_c$

The area presented by this string of thermocouples is

$$A_s = N_s (A_n + A_p)$$

where $A_n$ and $A_p$ are the cross section areas of the thermocouple legs.

The length of each thermocouple leg is given by

$$L = \frac{A_s K \Delta T}{P_e}$$

where K = average value of thermal conductivity of the thermoelectric material, watt/cm °K

$P_e$ = electric power supplied to the load, watts

$$= \frac{Z\Delta T}{4}$$

Here Z, the figure of merit of the thermoelectric material, is given by

$$Z = \frac{(|S_p| + |S_n|)^2}{\left[(\rho K)_p^{1/2} + (\rho K)_n^{1/2}\right]^2}$$

where $\rho$ = electrical resistivity, ohm-cm.

The weight of the thermoelectric material is obtained from the product of the volume and density, that is, $A_s$ LD.

The matched load efficiency of the thermoelectric generator is

$$\eta_m = \frac{Z\Delta T}{3\,T_h + T_c + S/Z}$$

To date , the best materials on which data has been obtained are bismuth telluride ($Bi_2Te_3$) and lead telluride (PbTe). Table 3-1 shows the theoretical efficiencies that may be obtained with these converters.

TABLE 3-1
THEORETICAL THERMOELECTRIC CONVERTER PERFORMANCE

| $T_h$ (°C) | $T_c$ (°C) | Thermoelectric Material | $Z \times 10^{-3}$ | $\eta_m$% |
|---|---|---|---|---|
| 600 | 100 | PbTe | 0.67 | 6.71 |
| 600 | 200 | PbTe | 0.69 | 5.45 |
| 600 | 300 | PbTe | 0.58 | 3.54 |
| 300 | 100 | $Bi_2Te_3$ | 2.0 | 6.57 |
| 300 | 200 | $Bi_2Te_3$ | 2.0 | 3.23 |

PbTe thermoelectric material has been used successfully in SNAP thermoelectric converters with a hot junction temperature of 600°C. However, sublimation of the PbTe molecules occurs at temperatures above 500°C (approx.) and becomes a significant process, limiting service life above 650°C. Figure 3-2 (Curve 4 ) gives the solar thermoelectric power system weight versus power output for currently available systems and for future approximations.

b. Solar Thermionic Power System

The essential features of a thermionic converter, as shown in Figure 3-3, consists of two electrodes separated by a vacuum. If the cathode is maintained at a sufficiently high temperature, electrons will be emitted. A portion of the emitted electrons will be collected by the anode, pass through the load, and return to the cathode. If the anode material is properly selected and its temperature is much lower than the cathode temperature, the electron flow from the anode-to-cathode will be much less than the electron flow from cathode-to-anode.

A space charge builds up near the cathode surface, presenting a retarding barrier, and limiting the electron flow. The space charge may be sufficiently reduced by making the electrode spacing a few thousandths of an inch. Another method of reducing the space charge is to inject positive ions into the inter-electrode space by introducing cesium vapor between the electrodes. The ions form a gaseous plasma and neutralize the space charge.

The Fermi level is defined as the highest occupied energy level in a metal at absolute zero. At higher temperatures, a few electrons will have higher energies in accordance with Fermi-Dirac statistics.

Thermal energy added at the cathode enables some electrons to overcome the work function and any unneutralized space charge to reach the anode. Upon arrival at the anode they fall to the anode Fermi level, the excess energy

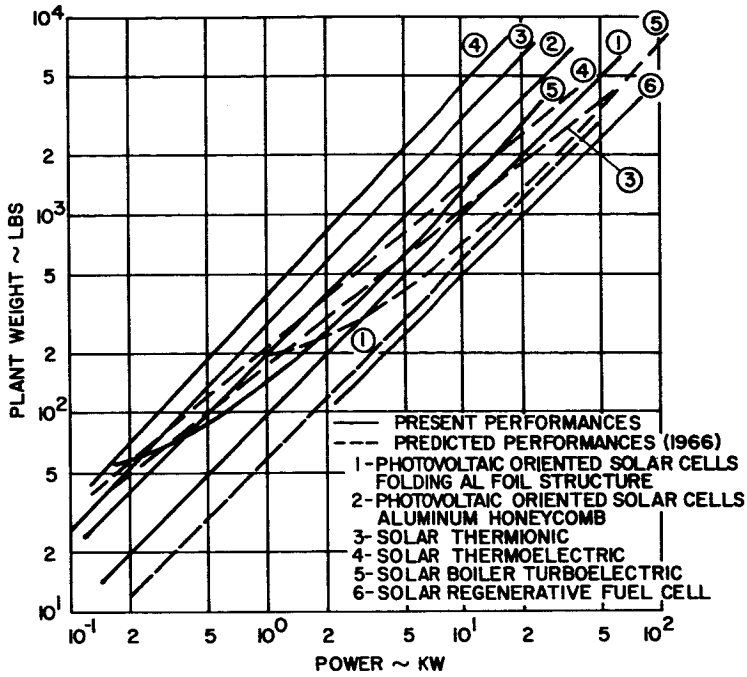


Figure 3-2. Solar Power Source Weight vs Power Output

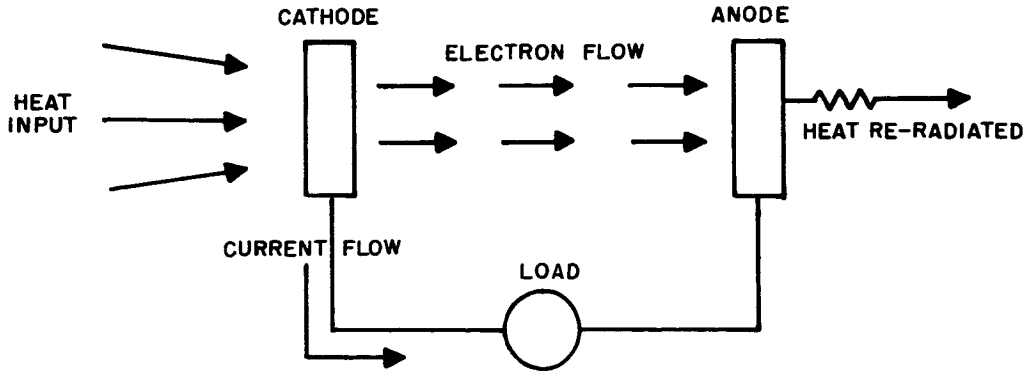


Figure 3-3. Solar Thermionic Converter

given up appearing as heat. The output voltage available is the difference in Fermi levels, which in the absence of space charge would equal the difference in anode and cathode work functions.

The conversion efficiency of a thermionic converter depends upon the particular materials selected for the cathode and anode and the temperature differential between cathode and anode. The efficiency varies nearly exponentially with the emitter temperature which indicates that thermionic converters are essentially high temperature devices.

Table 3-2 illustrates the theoretical performance of a thermionic converter consisting of a barium-impregnated tungsten cathode and a nickel anode thinly coated with barium and strontium oxides. From this table it is apparent that the heat source must operate at temperatures exceeding 1200°K if thermionic converters are to have conversion efficiencies greater than 10 percent. However, if long periods of operation are to be obtained, the cathode must be made quite thick and allowed to ablate. It does not appear with the present state of the art that one year of operation could be obtained in this manner, since the ablated material will condense on the cooler parts and cause other problems such as distortion and shorting. It can be stated however that if a breakthrough in the field of high temperature materials should occur, such that a nuclear heat source can be used and the thermionic emitter operated at high temperatures for extended periods, thermionic converters would become excellent power conversion devices since, theoretically, a tungsten diode operated at 3400°K would yield a conversion efficiency of about 39 percent.

TABLE 3-2
THEORETICAL THERMIONIC CONVERTER PERFORMANCE

| Cathode Temp (°K) | Current Density (amp/cm$^2$) | Heat-Power Input to Cathode (watts/cm$^2$) | Heat-Power Removed from Anode (watts/cm$^2$) | Electrical Power Output (watts/cm$^2$) | Efficiency $\eta$ (%) |
|---|---|---|---|---|---|
| 1173 | 0.1 | 2.32 | 2.25 | 0.07 | 3.02 |
| 1209 | 0.5 | 3.26 | 2.91 | 0.35 | 10.7 |
| 1238 | 1.2 | 4.68 | 3.84 | 0.84 | 17.9 |
| 1293 | 2.6 | 7.92 | 5.96 | 1.96 | 24.7 |
| 1343 | 5.2 | 15.52 | 8.88 | 3.64 | 29.1 |
| 1403 | 9.0 | 19.69 | 13.39 | 6.3 | 32.0 |

c. Solar Cells (Photovoltaic)

Semiconductor (silicon) solar cells consist of p-type and n-type silicon. The n-type has an excess electron due to the doping of the silicon with a material that has five electrons in the valence orbit. The p-type has a lack of electron, or hole, due to the doping of this cell with a material having three electrons in the valence orbit.

When light from the Sun impinges upon the surface of the solar converter, it is mainly absorbed with a resultant displacement of electron hole

pairs. The light energy in the form of photons breaks the valence bonds in the silicon crystal liberating electrons from the n-type material and the positive holes from the p-type material. The result is that an external voltage is built up causing current to flow through a load. Another energy conversion process is the photoelectric effect in which electrons are emitted from a surface into a vacuum where they are collected by a transparent electrode. Both of these conversion techniques are quantum devices where individual photons from the Sun (or other light source) cause quantum transitions in a metal or semiconductor to release charge carriers for electrical current flow in an external circuit. These are to be contrasted to the thermionic and thermoelectric devices which are heat rather than light engines.

In all conversion techniques that operate on a quantum basis, devices in normal operation can use only that radiation which has a frequency above a threshold value. In the case of a silicon cell, the threshold frequency corresponds to photons with just enough energy to lift an electron from the valence band to a conduction band. Excess photon energy above the threshold value is not efficiently used. Longer wavelengths are largely transmitted through the cell. An optimization is made, where the Sun is assumed to radiate like a black body at 6000°K. It turns out that the optimum threshold wavelength is about 11,000 angstroms, and the corresponding efficiency is 44 percent. This figure applies to any quantum process with unit quantum yield regardless of whether it physically corresponds to a photoelectric, photovoltaic or photochemical conversion technique.

Modern p on n solar cells are manufactured by a process first involving melting hyper-pure silicon. A very small amount of pure arsenic is introduced into the melt to convert the silicon into an n-type semiconductor. A single crystal, normally about 6 inches long and 1 inch diameter, is then grown about a "seed" crystal. The crystal is cut into wafers and subsequently heated to just below its melting point in an atmosphere containing boron trichloride. Boron diffuses into the silicon at a temperature near 1000°C, creating a surface p-type of semiconductor. Finally the boron is etched from the back surface. The thickness of the p-layer is determined by the time of exposure to the boron atmosphere. This p-n potential barrier must be close to the surface where solar photons are absorbed. In practice, a depth of one micron is satisfactory for efficient energy conversion. One electrical connection is made to this thin diffused region and another to the etched region to give a positive and negative terminal, as shown in Figure 3-4.

Typically, each silicon solar cell (1 x 2 x0.05 cm) yields about 1/2 volt and 50 ma when exposed to sunlight at 0°C.

A more radiation resistant cell, the n on p cell, is made by diffusing phosphorous into the surface of a p-type silicon crystal so as to make an n-type layer on the surface. Details on the solar cell performance degradation due to radiation effects will be found in subsection C.

The theoretical overall efficiency of conversion for a silicon solar cell is about 20 percent. Solar cells are available commercially in quantity with overall solar conversion efficiencies up to 14 percent.

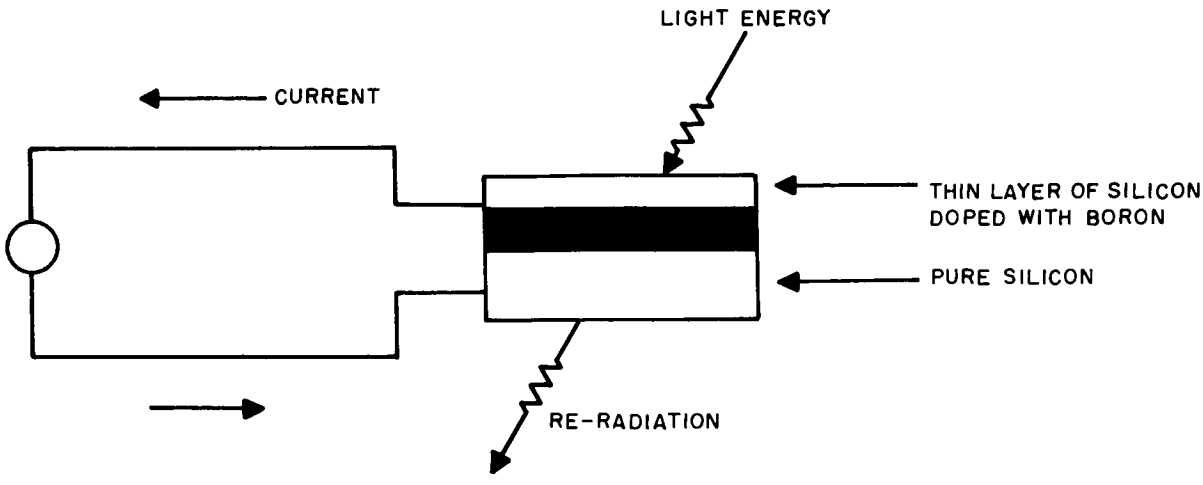


Figure 3-4. Solar Cell Diagram (Photovoltaic Effect)

At room temperature, the difference between the theoretical and the obtainable efficiency is due mainly to the following losses in the energy conversion processes:

(1) Surface reflection of the incident energy

(2) The conversion material responds to only a portion of the solar spectrum

(3) Recombination of the generated current carriers within the cell

(4) Dissipation of electrical energy due to the internal resistance of the cell

In general, an elevation in temperature results in reduced efficiency of solar cells. Typical curves of voltage versus current of an individual silicon solar cell at various temperatures are shown in Figure 3-5. Table 3-3 shows the various photovoltaic materials and the best room temperature efficiencies to date.

TABLE 3-3
SOLAR CELL EFFICIENCY

| Material | Energy Band-gap (EV) | % Efficiency |
|---|---|---|
| Si | 1.1 | 15 |
| GaAs | 1.35 | 10 |
| CdS | 2.4 | 8 |
| CdTe | 1.45 | 4 |
| InP | 1.25 | 3 |
| Se | 1.0 | 1 |
| GaP | 2.35 | 1 |

Usually, the higher the semiconductor band-gap, the less is the efficiency reduction with elevation of temperature. Thus the efficiency degradation with temperature of silicon cells is approximately twice that of GaAs. It has been observed that the loss in output power ranges from 0.24 to 0.55 percent per °C rise in temperature of the silicon solar cell (see Figure 3-6). As a result, at 100°C, a silicon cell's efficiency is only 50 percent of the value at 0°C while a GaAs cell's efficiency is 80 percent of its 0°C value. GaP having a large band-gap is even better than GaAs in this respect. However, CdS does not behave like a wide-gap semiconductor and has a temperature dependence resembling silicon.

A suggestion for improving the efficiency of sunlight conversion is to use sunlight concentrators, such as parabolic reflectors or possibly a light-weight Fresnel lens, to increase the sunlight by as much as a factor of four. Thus, by choosing a solar cell material having a suitable band gap, a net gain in electrical output of perhaps two could be obtained.

Another suggestion is based on the fact that some cells (such as silicon) are fairly transparent to photons carrying less energy than the band gap. Consequently, one could stack one cell beneath another, with the lower cells having progressively smaller band gaps to absorb some of the energy transmitted through earlier cells. A ten layer cell has been estimated to have a potential efficiency of 86 percent. Thus far, because each layer produces a different voltage, combinations of interconnections have prevented practical realization of this approach.

The details of the solar cell array design are described in sub-section F. The assumed solar cell parameters will be based upon the use of silicon solar cells having a conversion efficiency of 12 percent. The design will also take into consideration the degradation of solar cell efficiency with ±100°C temperature variation from 0°C. As noted before, the efficiency for silicon cells goes down about 50 percent with a 100°C rise in temperature. Thus it will be necessary to assume that the efficiency of solar energy conversion is only 6 percent though the cells used are of the 12 percent type at 0°C.

Since the solar power available at the Earth, and with slight variation at the synchronous orbit, is 130 watts/ft$^2$, the solar cell output will yield 6 percent of 130 or 7.8 watts/ft$^2$. Reducing this figure 4 percent to include the loss of solar cell area due to contact "shingling", it can be assumed that the power density of the solar cell array is 7.5 watts/ft$^2$.

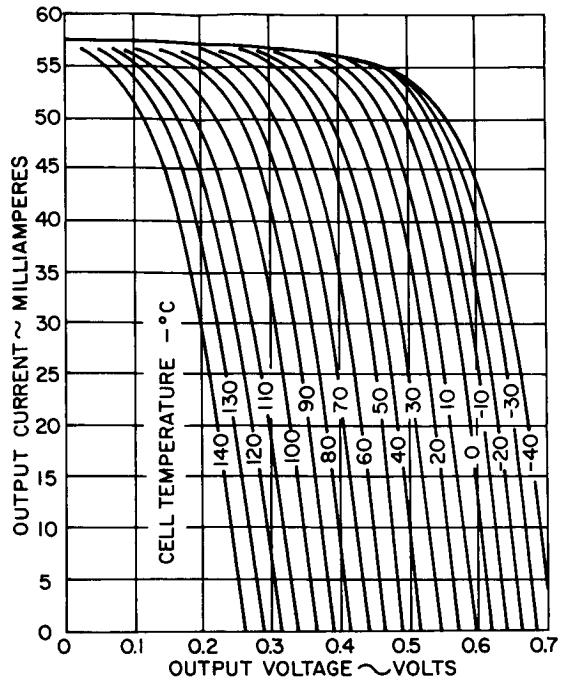


Figure 3-5. Effect of Temperature on Current-Voltage Characteristic of Solar Irradiated Cell (1 x 2 cm)

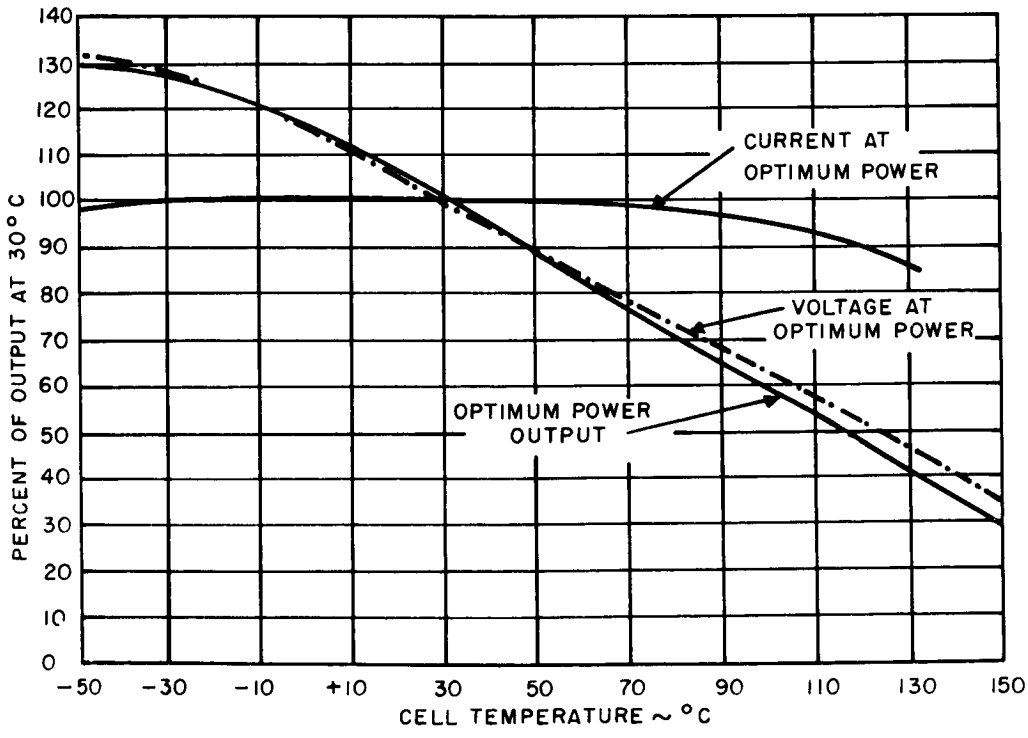


Figure 3-6. Typical Variation of Voltage-Current at Optimum Power with Temperature

The weight of the solar cell array, which includes the protective quartz glass top, the bonding layers, solar cells and the honeycomb base, (as shown in Figure 3-7) is assumed to be 1.5 lbs/ft$^2$. Thus the specific power of the solar array is essentially 5 watts/lb.

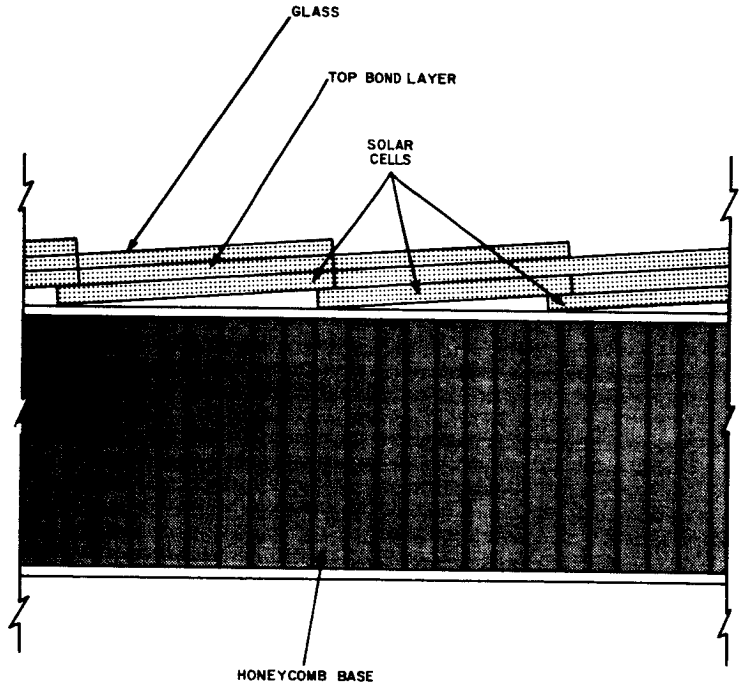


Figure 3-7. Cross Section of Paddle Segment

A summary of the advantages and disadvantages of solar cells follows:

Advantages

(1) Long life expectancy once array is erected in space.

(2) Separate radiator is not required.

(3) Cells are presently available.

Disadvantages

(1) An oriented array is required for supplies furnishing over 100 watts.

(2) Wiring, assembly and test of a large number of cells poses a severe problem.

(3) The silicon cells are brittle and cannot be flexed. This imposes restrictions on the construction of the array.

(4) The array must be erected in space without damaging the cells or wiring.

(5) The efficiency of the cells decreases with temperature.

(6) Cells in each string must be matched for electrical performance.

(7) Cells must be adequately protected from micrometeorite and radiation damage.

A possible solution to the problems of complexity and weight may be found in the development of large area thin-film photovoltaic cells. They are light, flexible, and easily manufactured. Though of low efficiency, their lightness and large area capacity greatly reduce the complexity and cost of power generation. At the present state of the art, thin-film CdS solar cells are 2 percent efficient and have a specific power output of 14 watts per pound. The drawback in their use at present is that their reliability is low, especially for extended periods of time, and they are readily susceptible to humidity and corrosive environments.

d. Photoemissive Cathode Power System

The appeal of a photoelectric emissive converter is that it is a large-area device which is low in cost and light in weight. In operation, a photoemissive substance is directly exposed to sunlight and the electrons given off are collected by a grid. A load is connected between the photoemitter and the collector, and power is developed, thus completing the conversion of the solar radiation into electricity.

The operation involves collection by a field which is produced by a difference in work function between the emitter and the collector. The lowest work function material is the collector, while the emitter is somewhat higher in work function. An ideal collector-emitter combination is AgOCs which has a work function of 0.75 eV and $Cs(NaK)_3Sb$ which has a work function of 1.55 eV. This combination gives a maximum voltage per cell of about 0.8V.

The basic limitation of the photoemissive device is its long wavelength threshold. Well over 50 percent of the solar photons cannot cause the emission of an electron in even the best photoemitter. Only 13 percent of the Sun's spectrum in the outer atmosphere would yield a quantum efficiency greater than 10 percent. The longer wavelengths contribute negligibly. It is concluded that a top conversion efficiency of about 1.5 percent of solar energy can be achieved with this method.

There are two ways in which this efficiency can be improved:

(1) Devise a wavelength converter so that the total energy in the solar spectrum is composed of photons of energy greater than the threshold level of 2.4eV.

(2) Devise more efficient photoemitters with thresholds at shorter wavelengths.

Progress in this field has been sporadic. The breakthroughs have been due to empirical experimentation rather than that of basic understanding. Many problems exist and experts in the field do not anticipate the kind of improvement required to provide a photoemissive device of even 10 percent overall efficiency.

e. Photochemical Power System

The photochemical cell is based on the principle that light energy impinging upon an organic acid causes a molecular rearrangement to produce an isomer of the compound. If a cell containing this isomerized compound is connected to a cell containing the un-isomerized compound, electrical energy will be produced due to a chemical concentration gradient.

A proposed cell is shown in Figure 3-8. Containers A and B contain a dye, proflavine plus a reducing agent, ascorbic acid or thionine plus iron or another photosensitive substance. A platinum electrode immersed in the system will acquire a potential which differs when illuminated by light from what it would be in a dark solution.

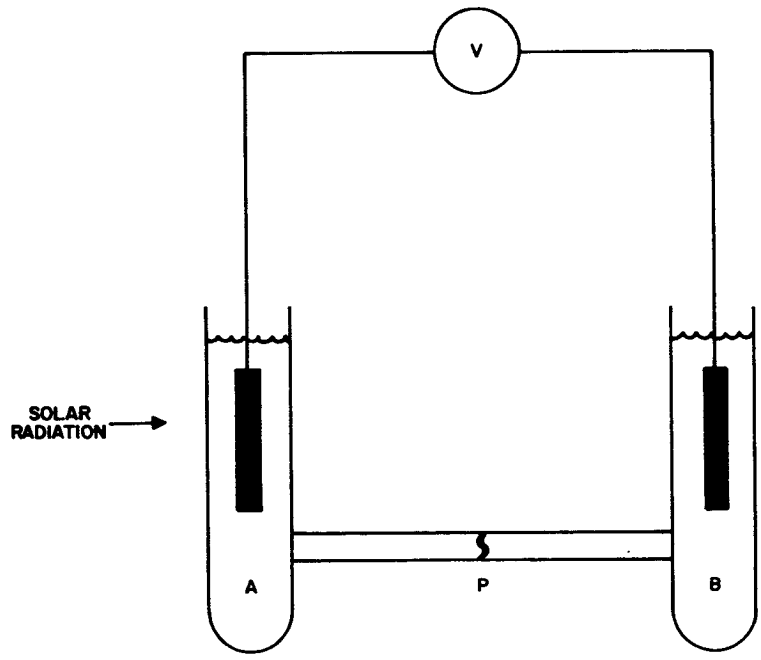


Figure 3-8. Photochemical Cell

In the diagram, A is exposed to the incident radiation with side B shielded. Photochemical isomerization of the acid occurs in container A regardless of current being drawn from the cell. The longer the cell is irradiated before power is drawn, the larger is the amount of power that is available. The concentration of hydrogen ions on side A is greater than that on side B. Electron transfer occurs through the external wire by electrochemical reactions at the electrodes because of the hydrogen in concentration gradient. Electrical neutrality is maintained by diffusion of the anion from A to B through the porous plug, P.

A typical output derived from such a system is a dark potential of 0.046 volt and photo-induced potential of 0.385 volt. For a cross-sectional cell area of 45 $cm^2$, short circuit currents of over 50 ma have been drawn for very short intervals, and currents exceeding one milliamp have been obtained for periods exceeding 1000 minutes. Thus, $\frac{(0.385-0.046)(50)}{45} = 0.376$ $mw/cm^2$ = max. photochemical output. The Sun's incident power is 140 $mw/cm^2$. Therefore the conversion efficiency is $\frac{0.376}{140} = 0.0027 = 0.27$ percent.

Many factors influence the photo-induced potential, such as the pH factor, the dye, the reducing agent, and the temperature and polarization of the electrodes.

The efficiency of conversion of solar energy into electrical energy is dependent upon

(1) The percentage of the incident energy absorbed, "a".

(2) The fraction of the photon energy used to bring about the desired process. For a photochemical process any excess energy possesed by the photon is converted to heat. This is the ratio of the free energy change, $\Delta F$ to the incident energy $E_\lambda$ in K cal/mole of quanta.

(3) The collection efficiency, that is, the percentage of the electo-active species formed reaching the electrode. For a photochemical reaction this would correspond to the quantum efficiency, $\phi$.

Thus, the energy conversion efficiency, $\eta$, may be represented as

$$\eta = a\,\phi\,\frac{\Delta F}{E_\lambda}$$

Here $\Delta F = nF\,E_\phi$, where $E_\phi$ is the photopotential, n is the number of electrochemical equivalents per mole, F is the Faraday charge constant, 96,500 amp-seconds.

The maximum power available is determined by

$$P = a\,\phi\,\Delta F\,I_\phi$$

where $I_\phi$ is the incident light intensity in moles of quanta per sec per $cm^2$.

There is much basic work yet to be done in the study of photochemical phenomena and on devising schemes for extracting power effectively. Among the chief problems of concern are the stability and reversibility of the system, decay of the potential with time as a function of exposure time to light, search for processes with higher quantum efficiencies than those presently available, and minimizing electrochemical polarization losses at the electrodes. Furthermore, the efficiencies produced are much less than 0.25 percent and life operation is presently of only a few hundred hours duration.

f. Solar Regenerative Fuel Cell

This type of device utilizes solar energy to decompose a chemical byproduct of a fuel cell to produce the fuel for the cell. The fuel cell is a device which produces electrical energy from chemical energy. Figure 3-9 shows a schematic of this type of system and Figure 3-2 (Curve 6) shows the system weight as a function of the power output. An electrochemical reaction between lithium metal and hydrogen gas produces electrical current. The reaction produces lithium hydride which is decomposed by solar energy to regenerate the lithium and hydrogen.

The fuel cell-solar energy system thus makes use of two sources of energy. These are the exothermic energy available from the reaction of the stored reactants of the fuel cell system and the energy available as radiant energy to reconsititute the products of the reaction to the original form.

The fuel cell differs in one major respect from other closed or open cycle systems. The fuel cell is not Carnot-limited and theoretically can achieve 100 percent efficiency. Fuel cells using hydrogen-oxygen have been reported with efficiencies of 60 to 70 percent. The major disadvantages in this system are that it does not as yet have the extended time reliability and it is too heavy a system for low power operations.

g. Solar Turboelectric Power System

The solar turboelectric system is shown schematically in Figure 3-10. Solar energy is utilized to heat a liquid metal fluid which goes through a conventional cycle of heating, compression, expansion, and cooling. A turbine drives the generator to produce electrical power.

It is essentially a simple system and can be made to approach the Carnot efficiency, which is the theoretical limit between any two given temperatures. The principal disadvantages are related to the life problem. These disadvantages are the use of corrosive liquid metals as working fluids and the necessity of using rotating components in the conversion system.

Although the turboelectric system is most attractive in the megawatt range, it is also competitive in the low power level (below a few kilowatts). This is due to the fact that proportional weight savings do not accrue when the power requirement is reduced, because the necessary structure, plumbing, condenser preheat equipment, start-up equipment, boiler, and alternator have an irreducible minimum weight associated with them. Its disadvantages also include the interruptions in operation caused by shadows, the need for large collector areas and suntracking systems, the difficulty of temperature control and possible environment degradation or damage to the collector surfaces. Figure 3-2 (Curve 5) plots the total plant weight as a function of electrical power output, assuming full time sunlight operation.

The Sunflower is a mercury Rankine solar power converter designed to supply 3 KW while in an Earth orbit for a period of one year. The system consists of a 32-ft paraboloidal solar collector, a boiler-heater Li-H storage unit, a turbine alternator and a radiating condenser. The estimated weight of a system

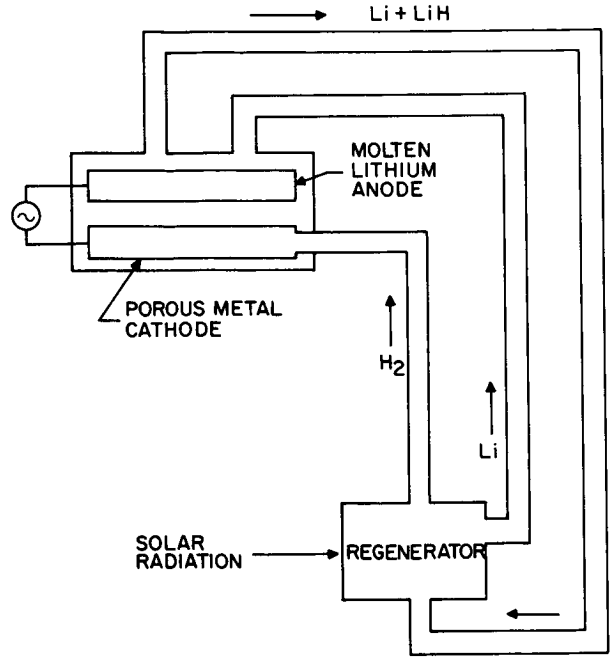


Figure 3-9. Solar Regeneration Fuel Cell

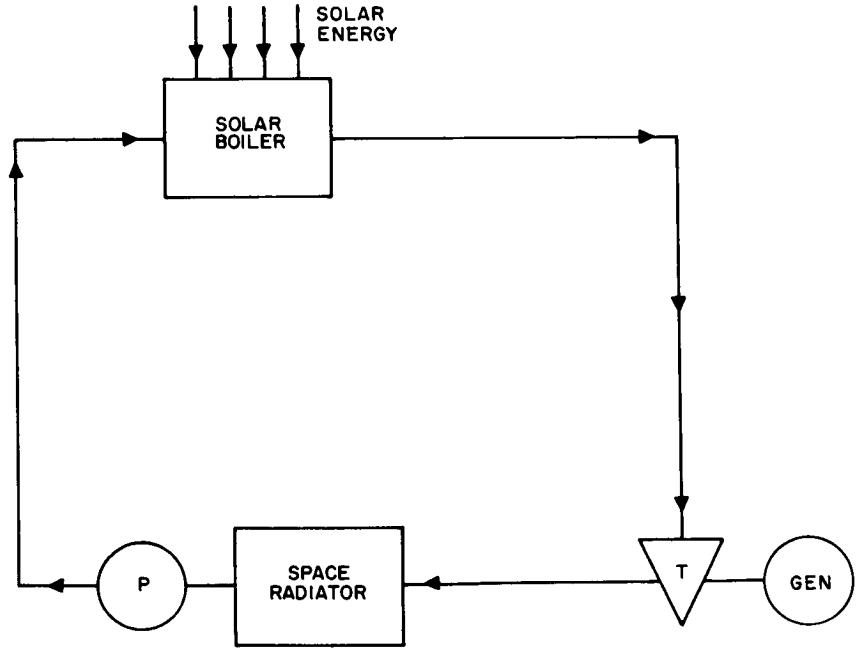


Figure 3-10. Solar Turboelectric System

capable of providing 1/2 KW at a synchronous orbit altitude with a maximum shade period of 70 minutes is approximately 200 pounds.

h. Thermal Storage System

If solar energy is used, an energy storage system must be provided to satisfy the vehicle power requirements while the satellite is passing through a dark period. In addition to electrochemical storage systems, considerable research is now being devoted to the development of thermal energy storage systems such as that obtained from the latent heat of a phase change, e.g., heat of vaporization. The only practical thermal system at present is that based upon the latent heat of fusion. Several elements and compounds having high heat-of-fusion and melting temperatures have been studied. Lithium hydride has a storage capacity of approximately 350 watt-hrs/lb.

However, the weight of the lithium-hydride accounts for only 25 to 30 percent of the total weight of the storage system. Hence the storage capacity is reduced to the range from 88 to 105 watt hrs/lb. If the thermal-to-electrical energy converter has an efficiency of 10 percent, the effective electrical output capacity of the system is only 8.8 to 10.5 electrical watt hrs/lb.

2. Nuclear Power

a. General

Utilizing nuclear energy as the thermal source, the conversion of nuclear energy to electrical energy can be accomplished by the following methods:

(1) Nuclear thermoelectric

(2) Nuclear thermionic

(3) Nuclear turboelectric

Nuclear energy sources include fission and fusion reactors and radioisotopes. However, fusion reactors are far beyond the present state of the art. Similarly, radioisotopes are expensive and are not readily obtainable in sufficient quantities. Hence, for 10 KW or larger systems, only nuclear fission reactors are used. For smaller power units either fission reactors or radioisotopes are used.

A nuclear power supply for space vehicle applications is composed of three major subsystems,

(1) Nuclear heat source

(2) Power conversion system

(3) Heat rejection system

The power conversion cycle determines the operating temperature of the other two. The details of the cycle, for example the working fluid, are a function of the operating temperature. The radiator area and weight are a function of the

cycle cold temperature. The reactor size, weight, and concept are a function of temperature because of the operating temperature limitations of the applicable core materials. In order to minimize the weight of the heat rejection system, it is necessary that the conversion system operate at a high sink temperature and recover a maximum fraction of Carnot efficiency. Since the waste heat of a cycle must be radiated to space, the area requirement and hence the weight associated with the heat rejection system is, for a given power level, proportional to the fourth power of the cycle cold temperature and inversely proportional to the cycle conversion efficiency. At low powers, the reactor size is independent of power because of the minimum critical size requirements. Therefore, the conversion efficiency affects only the size of the radiator and the conversion equipment.

Since the reactor and shield are the dominant weight of nuclear power systems at low power, the conversion efficiency of the cycle cold temperature is not so important at low powers as it is at high powers. At higher power levels, however, the radiator becomes the dominant weight item of the system. Consequently, for the higher power systems there is a great incentive to achieve high efficiency and high heat rejection temperatures to minimize the weight of the radiator. In the fission process the nucleus absorbs a neutron and the resulting compound nucleus becomes unstable and breaks up into two or more parts of more or less equal mass, called fission fragments. Most of the fragments are radioactive and emit beta particles and gamma rays. From the point of view of the utilization of nuclear energy, the importance of fission lies in two facts. First, the process is associated with the release of considerable amounts of energy and second, the reaction initiated by neutrons is also accompanied by the liberation of neutrons. It is thus possible, under proper conditions, for the process to be self-sustaining and for energy to be generated continuously, once the fission reaction has been started.

The large energy release in fission is associated with the fact that the products of the reaction have an appreciably smaller total mass than that of the nucleus undergoing fission plus the neutron causing fission. Because of the equivalence of mass and energy, the considerable decrease in mass in the fission reaction must be accompanied by the liberation of a large amount of energy. The fission of 1 gram of U-235 per day would yield roughly 1 megawatt of power.

The leakage radiation from a nuclear reactor represents approximately 6 percent of the total reactor power. The two components of the leakage radiation for which shielding must be provided are neutrons and gamma rays. Neutrons are most effectively slowed down by light atoms, such as hydrogen. Heavy atoms, such as lead, provide the most effective shielding against gamma rays. Various separation schemes make it possible to isolate the nuclear power system 100 to 200 feet from the payload, and by applying the cone-apex shadow effect, reduce the weight of the shield considerably.

b. Nuclear Thermoelectric Power System

A nuclear thermoelectric system is similar to the solar thermoelectric system except that the heat source is a nuclear reactor instead of solar radiation. Figure 3-11 shows a diagram of one type of nuclear thermoelectric

system (for low power levels) where the fluid is heated in the reactor, and flows through a converter and radiator. The heated fluid from the reactor flows through the tubes containing the semiconductor elements in the converter and radiator unit. Connections are made to the semiconductor elements for the electrical current generated.

The reactor employs a homogenous fuel moderator of zirconium hydride containing U-235. For minimum weight, the reactor is reflected by beryllium and controlled by variation of the effective reflector thickness by means of angular rotation of two semicylindrical beryllium drums.

Figure 3-12 shows another type of nuclear thermoelectric system (for high power levels) wherein the thermoelectric elements are placed directly on the surface of the reactor, elminating the coolant loop illustrated in Figure 3-11. Fins are required to radiate the waste heat to space. The system shown in Figure 3-13 is the SNAP-10A system which is designed to deliver 300 watts of power for one year. The above system could be utilized with a radioactive isotope source.

The Seebeck (thermoelectric) effect offers advantages of static operation and high reliability potential. However, the temperature limits and the conversion efficiency of current converter materials limits the usefulness of thermoelectric conversion systems to relatively low power levels. The basic PbTe material (discussed in solar thermoelectric) has a theoretical conversion efficiency of about 15 percent of Carnot and is limited to a peak hot-junction temperature of about 800°F by sublimation. However, other practical engineering considerations, such as thermal impedance and electrical contact resistance, limit the net efficiency of practical devices to about 10 percent of Carnot. The reactor-thermal conversion efficiency is approximately 20 percent. Therefore the nuclear thermoelectric system will have a net efficiency of about 2 percent. At low power thermoelectric outputs, the specific power is about 1 watt/lb.

c. Nuclear Thermionic Power System

This type of system is similar to the solar thermionic system except that nuclear energy is again the heat source. For low power levels, the converters are placed on the outer surface of the reactor core while for high power levels, large emission surface areas are required so that reactors of this type would be comprised of an array of converter-fuel elements which would be utilized inside the core, i.e., the reactor and power conversion system become one and the same.

Figure 3-14 shows a simple schematic with the converters mounted on the outside of the core. The waste heat absorbed by the coolant would be rejected in a space radiator. Figure 3-15 shows an arrangement for the converter elements to be housed directly inside the reactor core.

Two types of thermionic converters are possible, as noted in the solar thermionic discussion, the vacuum diode and the space charge neutralized cesium diode. Each is characterized by its means in neutralizing the negative interelectrode space charge. In the vacuum diode the electrode spacing is made of the order of a few thousandths of an inch. In the cesium diode, space charge

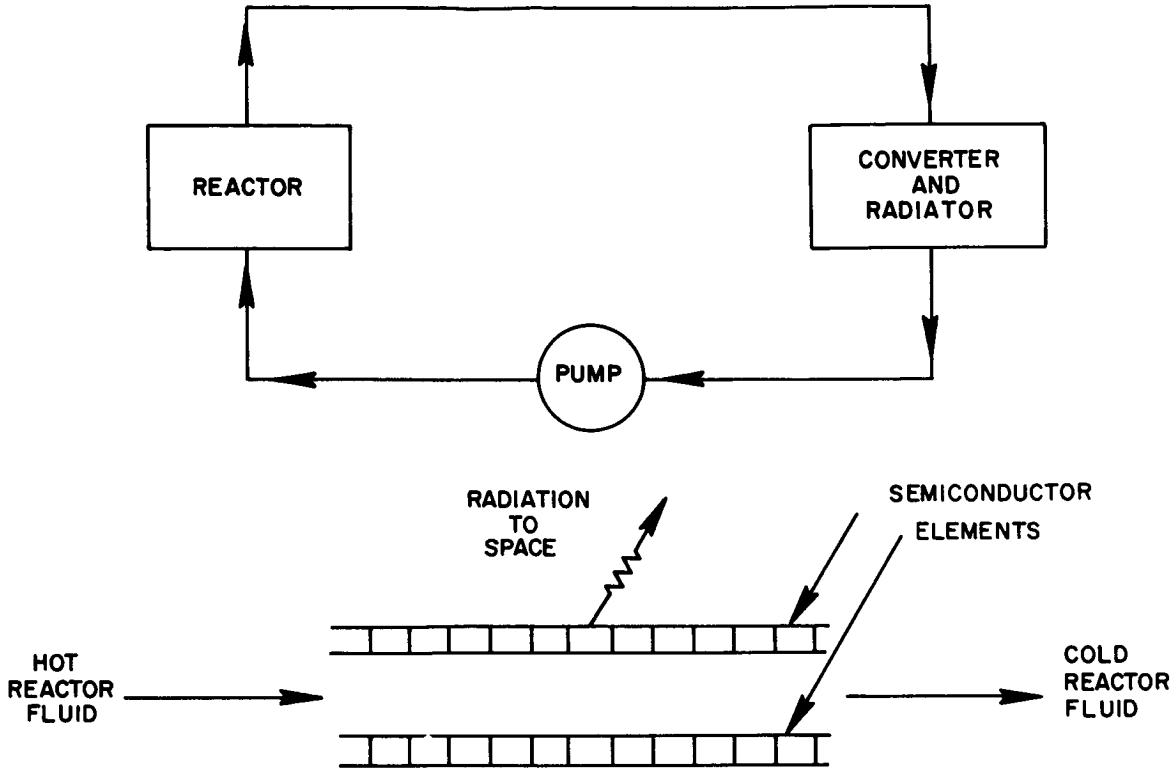


Figure 3-11. Nuclear Thermoelectric System

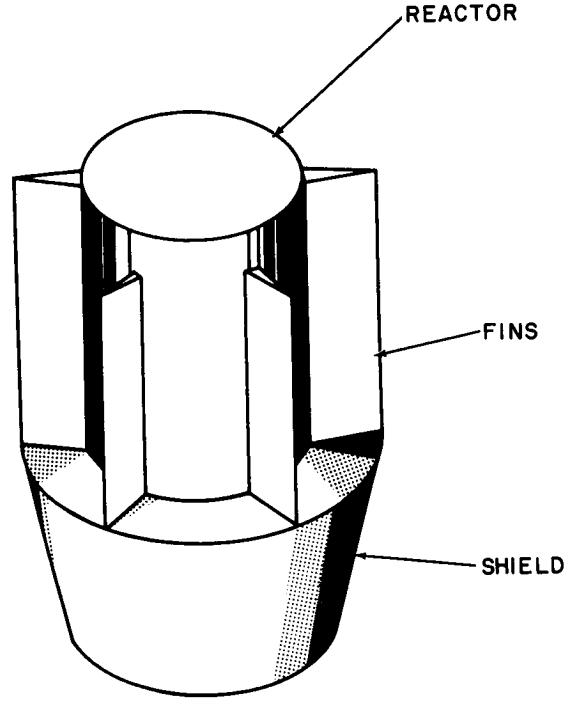


Figure 3-12. High Power Nuclear Thermoelectric System

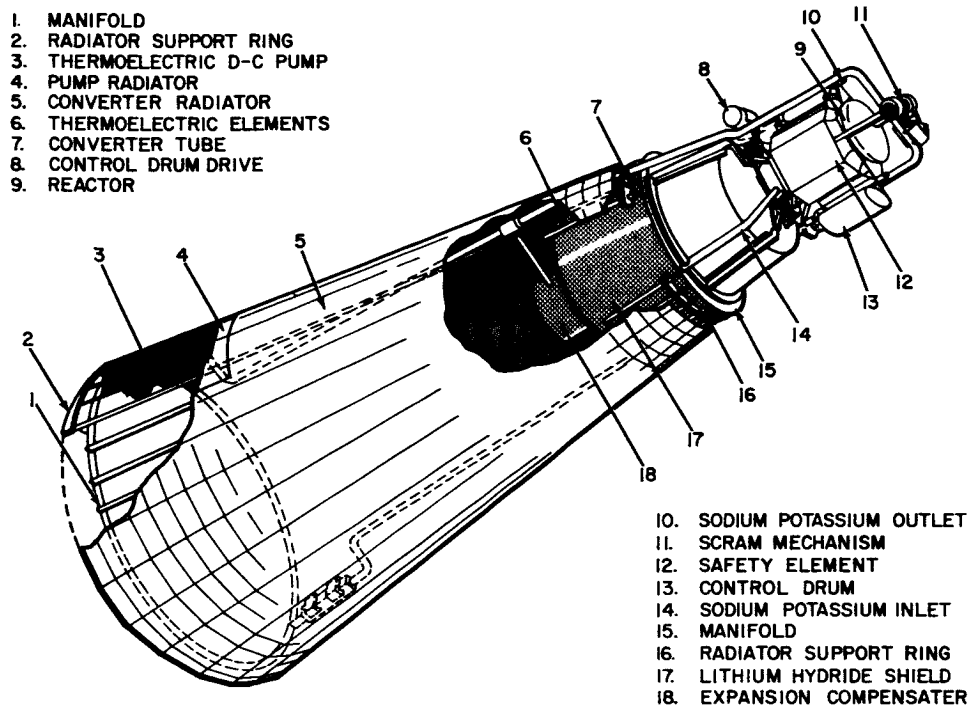


Figure 3-13. SNAP-10 System

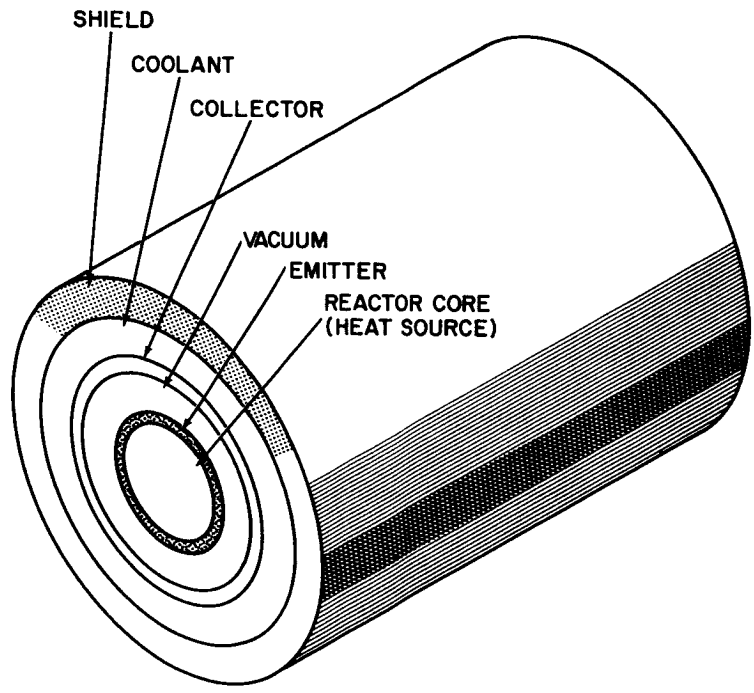


Figure 3-14. Nuclear Thermionic System

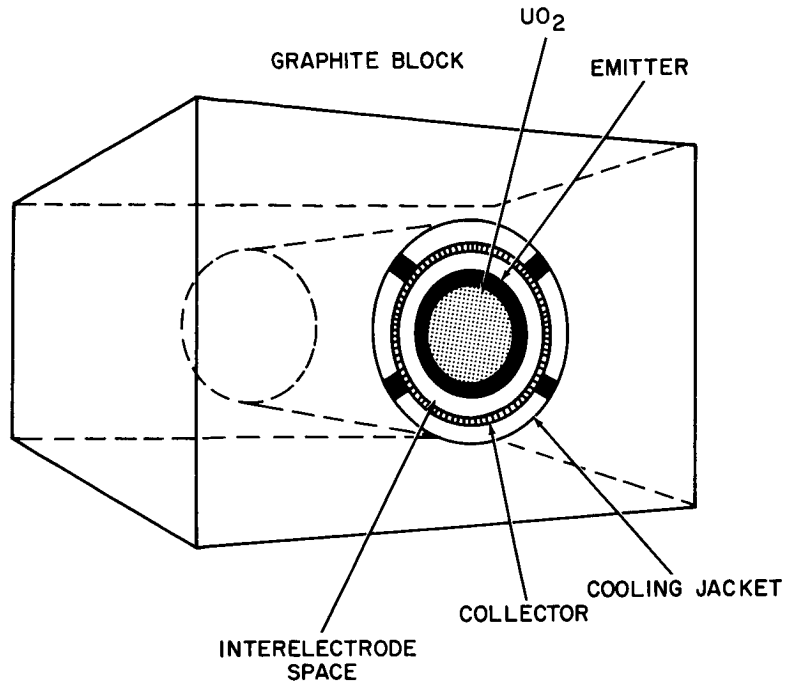


Figure 3-15. Nuclear Thermionic System (Elements Inside Core)

neutralization is accomplished by injecting positive cesium ions into the space between the electrodes, and the spacing requirements becomes far less stringent. The required temperature and actual measured efficiencies for these diodes are given in Table 3-4.

TABLE 3-4
NUCLEAR THERMIONIC CONVERTER EFFICIENCY

| Type | Emitter Temp. | Collector Temp. | Observed Efficiencies |
|---|---|---|---|
| Vacuum diode | 1600 to 1900°F | 700 to 1100°F | 2 to 4 % |
| Cesium diode | 2600 to 3500°F | 1100 to 1400°F | 12 to 14% |

For reactor application, the cesium diode appears most practical and efficient. The specific power output for a nuclear thermionic system utilizing a radioactive isotopic source is approximately 1.74 watts/lb.

d. Nuclear Turboelectric Power System

The nuclear turboelectric system is essentially a conventional power plant with the combustion chamber replaced by a nuclear reactor or a radioisotope source. Figure 3-16 is a schematic diagram of this system. A liquid metal, such as NaK-78, flows through the reactor and is heated. The liquid

metal transfers its heat to another fluid, such as mercury, in a heat exchanger. The mercury is expanded through a turbine and is cooled by rejecting its heat to space through a space radiator. The mercury condensate is returned to the boiler by a feed pump. The work output of the turbine is used to drive the generator which generates electrical power for the pump. All of the rotating components, the NaK pump, turbine, generator, and mercury pump are mounted on a single, common shaft which rotates at 40,000 RPM. The entire assembly is enclosed in a hermetically sealed housing.

The turboelectric nuclear space power system will probably utilize a Rankine cycle because it offers a high conversion efficiency, operates at relatively low source temperatures, and rejects waste at relatively high temperatures. The Brayton cycle appears unattractive for space application because of its lower fraction of Carnot efficiency, higher reactor temperature requirements and larger radiator demands. The Rankine cycle operates on a Carnot efficiency of 25 percent and a conversion efficiency of 40 percent of Carnot, resulting in an overall system efficiency of 10 percent. Figure 3-17 (Curve 1) shows that the nuclear turboelectric (mercury Rankine cycle) power system weight for a 1 KW output is 420 pounds. This is an equivalent specific power of 2.38 watts/lb. Unfortunately, the system is minimum weight limited because of the reactor and plumbing and therefore there is no linear relationship which decreases the total system weight with decreasing power requirements.

e. Summary of SNAP Systems

The basic objective of the Systems for Nuclear Auxiliary Power (SNAP) program is to develop auxiliary power sources for both space and ground applications over a broad power range. The basic principles of their operation are essentially those which were described in the previous three subsections, b, c, and d.

Nuclear power units offer unique advantages for space applications, including compactness, long life, elimination of need for secondary batteries and Sun orientation requirements. In addition, nuclear surfaces are relatively impervious to the hazards of space environments such as Van Allen radiation, solar flares and the impingement of micrometeorites.

1) SNAP Reactor Power Systems. Compact reactors and power conversion equipments for space application have been under development for a number of years under AEC, NASA and DOD sponsorship. Three SNAP reactor projects are now programmed for early orbital flight testing. These are the 500 watt SNAP-10A, the 3 KW SNAP-2, and 30/60 KW SNAP-8 systems. Advanced space systems capable of producing hundreds of kilowatts with extension into the megawatt range with specific powers of 50 to 200 watts/lb., such as the SNAP-50 and SPUR, are now under study.

The various reactor and system characteristics are shown in Table 3-5.

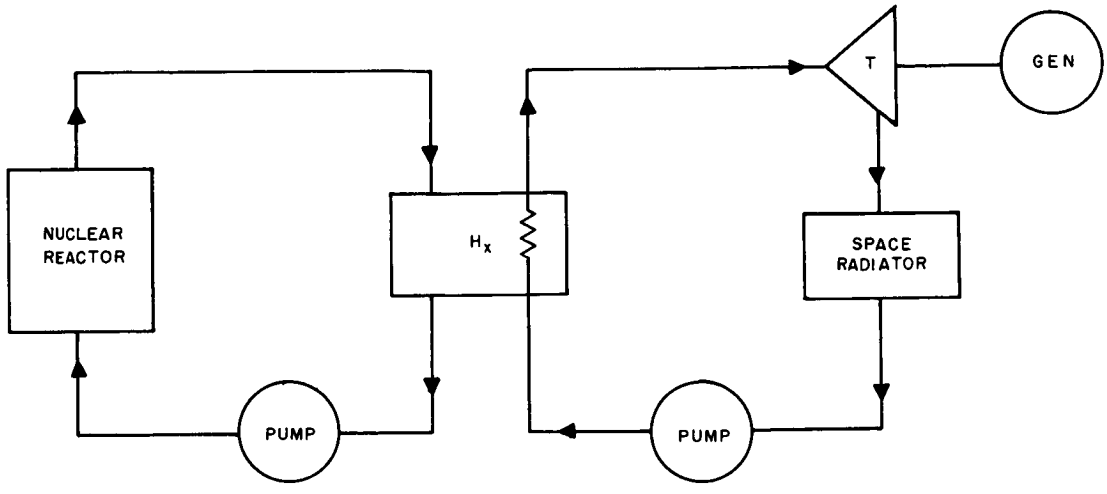


Figure 3-16. Nuclear Turboelectric System

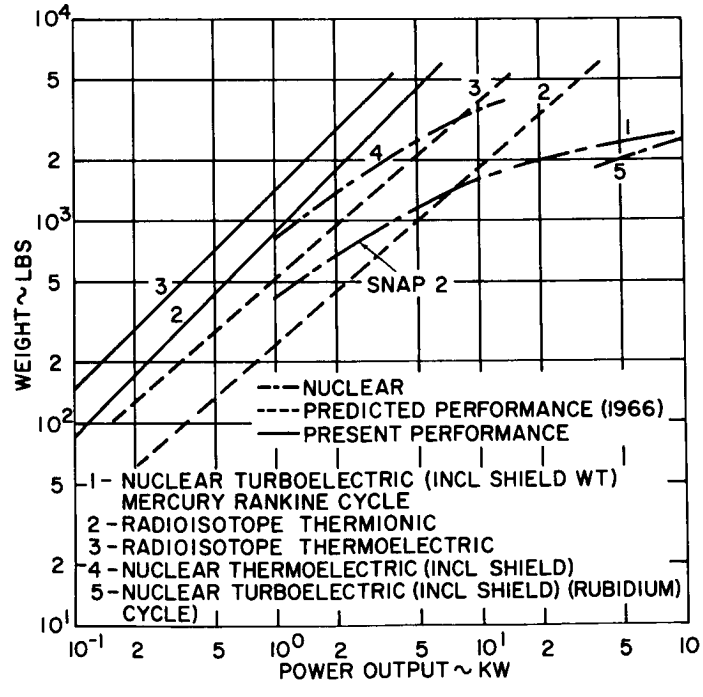


Figure 3-17. Nuclear Power Source Weight vs Power Output

TABLE 3-5
SNAP REACTOR SYSTEM PARAMETERS

| Parameter | SNAP-10A | SNAP-2 | SNAP-8 |
|---|---|---|---|
| Output, KWE | 0.5 | 3 | 30-60 |
| Thermal, KW | 30 | 50 | 600 |
| Efficiency, % | 20 | 6 | 10 |
| Power conversion | Thermoelectric (Ge-Si) | Rankine (Hg) | Rankine (Hg) |
| Minimum life, yr. | 1 | 1 | 1 |
| (U-ZrHx) Reactor size, in. | 16 x 14 dia. | 16 x 14 dia | 19 x 15 dia |
| Core volume, $ft^3$ | 0.3 | 0.3 | 0.48 |
| Power density, $Mw(th)/ft^3$ | 0.099 | 0.165 | 1.25 |
| Reactor wt, lb | 250 | 250 | 400 |
| Fuel moderator rods, number | 37 | 37 | 211 |
| U-235,Kg | 4.3 | 4.3 | 7.0 |
| $N_H$, H atoms/$cm^3$ | $6.5 \times 10^{22}$ | $6.5 \times 10^{22}$ | $6.0 \times 10^{22}$ |
| Atomic burnup, % | 0.02 | 0.03 | 0.23 |
| Max temp, °F | 1050 | 1300 | 1450 |
| O.D., in. | 1.25 | 1.25 | 0.56 |
| Heat flux, $Btu/hr/ft^2$ | 10,200 | 17,000 | 55,000 |
| Neutron flux, $n/cm^2/sec$ | $1.8 \times 10^{11}$ | 3.1 x 10 in. | $2.3 \times 10^{12}$ |
| Radical reflector, in. | 2.3 Be | 2.3 Be | 3 Be |
| Be control drums | 4 (start up) | 4 | 6 |
| Reactor coolant | NaK-78 | NaK-78 | NaK-78 |
| Temp out, °F | 990 | 1200 | 1300 |
| Temp in, °F | 880 | 1000 | 1100 |
| Hg boiling temp, °F | - | 930 | 1070 |
| Hg condensing, °F | - | 600 | 700 |
| Hot junction temp, °F | 930 | | |
| Radiator temp, °F | 615 | 600 | 700 |
| Radiator area, $ft^2$ | 62.5 | 120 | 400 |
| $Ft^2$/KWE | 125 | 40 | 13 |

TABLE 3-5 (cont'd)

| Parameter | SNAP-10A | SNAP-2 | SNAP-8 |
|---|---|---|---|
| System shielded wt, lb* | 950(875) | 1480(1350) | ~ 3000 |
| System unshielded wt, lb | 525 | 750 | 1500 |
| Reactor wt, lb | 270 | 290 | 500 |
| Shield wt, lb | 225 | 300 | 1050 |
| Specific power, watts/lb | 0.95 | 4 | 20 |
| Available | 1964 | 1965 | 1967 |
| Responsible agency | AEC | AEC | AEC/NASA |
| System prime contractor | Atomics Int. | Atomics Int. | Aerojet General |
| Power conversion sub-contractor | RCA | Thompson R. W. | Aerojet General |
| Reactor associate contractor | - | - | Atomics Int. |
| Flight test agency | A. F. | A. F. | NASA |
| Flight test assoc. cont. | Lockheed | Lockheed | - |

* Recent information indicates these weights may be revised to the values shown in parentheses.

The SNAP-50 is a 300 KWE power system and has a UC type reactor (operating at 2000°F). The power conversion is a Rankine (Rb) turbo-generator. The specific radiator area is 3 $ft^2$/KWE, and the system specific power output is 50 watts/lb. It is scheduled to be available in 1970.

The SNAP-Research system is a 3000 KWE power system and also operates with a fast UC type reactor (operating at 3500°F). The power conversion is a thermionic type. The specific radiator area is 1/2 $ft^2$/KWE and the system specific power output is 200 watts/lb. It is scheduled to be available in 1975.

2) SNAP Radioisotopic Power Systems. Radioisotopic power relates to the generation of heat by absorption of electromagnetic and particle radiations emitted by a carefully sealed source of radioisotopes. The heat is then partially converted into electricity by a thermoelectric or thermionic conversion device as explained previously, with the remainder of the heat radiated to the external environment.

The radioisotopic SNAP program has been oriented toward supplying the need for small, compact, lightweight and reliable power supplies for space applications. After preliminary selection of the most promising isotopes is made on the basis of comparing the mission life with the isotopic radioactive half-life, the choice of the radioisotopic fuel is dictated primarily by considerations involving availability and shielding requirements. Regarding availability, it is noteworthy that the lack today is not in quantities of radioisotopes, but rather in

facilities to separate, purify and process the active materials into forms useful for power application.

Table 3-6 shows the SNAP Generator Specification (without shielding) for the isotopic sources. Table 3-7 lists the radioisotope heat sources. Promethium 147 is readily available as a fission product. It emits a weak beta, 0.22 Mev maximum energy, and decays with a half-life of 2.6 years. The Pm-147 by itself would require practically no shielding; however, as it is formed by fissioning of U-235 it undergoes nuclear reactions to form Pm -146 and Pm - 148, both of which emit high energy gammas. Pm - 148 has a 42 day half-life and can be virtually eliminated by storing the reactor waste for about 2 years after encapsulation. Pm - 146 will be present however because of its 2 year half-life. It is this isotope which determines the shielding requirements. An estimated weight breakdown of a 500-watt shielded system using Promethium - 147 is approximately 280 lbs.

One of the most significant factors in establishing the practicality of isotopic power for space applications is the assurance that can be provided for the radiological safety of operation systems employing such devices. Failures may occur at any of the four fundamental phases; launch, ascent, orbital injection, re-entry (orbital decay or re-entry before the design lifetime of the satellite).

At present it is estimated that the isotope capsules can withstand launch pad fire and explosion resulting from booster malfunction and will survive impact resulting from guidance or upper stage failures during the ascent phase because of the protection afforded by the surrounding vehicle structure. At completion of the mission the capsule will ultimately re-enter the atmosphere and will burn up at altitudes greater than 100,000 ft. Complete burn up and dispersion into micron-sized particles can be assured by careful design of the fuel form. If necessary, small amounts of a metallic matrix may be added to the basic fuel to enhance its burnup properties.

3. Chemical Power

The use of solar energy for the primary energy source imposes a need for a method of energy storage to operate the equipment during dark periods of orbit. Since the power from the solar input is from a photovoltaic cell system, the use of an electrical storage system, as opposed to thermal or mechanical ones, is indicated in most applications.

The conversion of chemical energy to electrical energy will be discussed for the following devices:

(1) Primary batteries

(2) Secondary batteries

(3) Fuel cell

(4) Chemical turbines

TABLE 3-6
SNAP GENERATOR SPECIFICATION

| | SNAP 1A | SNAP 3 | Satellite | SLLG[a] | HLLG[b] | SPG[c] | TIPS[d] |
|---|---|---|---|---|---|---|---|
| Design power (watts) | 125 | 3 | 14.5 | 19 | 13 | 100 | 5 |
| Design life (constant power) | 1 yr | 90 d | 5-10 yr | 6 mo | 2 mo | 6 mo | 3 mo |
| Weight (lb) | 200 | 4 | 11.9 | 16.6 | 6.2 | 77 | 0.9 |
| Initial thermal input (watts) | 6500 | 70 | 260 | 655 | 370 | 7500 | 120 |
| Fuel nuclide | Cerium144 | Polonium210 | Plutonium238 | Curium242 | Curium242 | Curium242 | Curium242 |
| Half-life | 285 d | 138 d | 86 yr | 163 d | 163 d | 163 d | 163 d |
| Quantity | 880,000c | 2300c | 475g | 6.3g | 3.1g | 70g | 1g |
| Voltage | 28 | 3 | 3 | 3 | 3 | 28 | 0.7 |
| Efficiency: Thermoelectric | 6.75 | 6.0 | 6.54 | 6.51 | 5.4 | 5.2 | 4.6 |
| Efficiency: Overall device | 4.7 | 5.75 | 5.5 | 4.8 | 5.2 | 5.0 | 4.2 |
| Hot junction T, °F | 1050 | 1050 | 900 | 1000 | 1400 | 1000 | 2240 |
| Cold junction, T, °F | 335 | 300 | 235 | 370 | 458 | 490 | 1110 |
| Outer shell length (in) | 34 | 5.5 | 7 | 8.4 | 6 | 21.5 | 2 |
| Diam. (In) | 24 | 4.75 | 12.5 | 7.5 | 2.75 | 19.5 | 2 |
| Radiation emission | Beta (22 roentgens) (per hr. at 100 ft from bare core) | Alpha (5.3 Mev) | Neutrons and gamma (1.5 mrem per hr. at 1 meter) | Neutrons and gamma (125 mrem per hr. at 1 meter) | Neutrons and gamma | Neutrons and gamma | Neutrons and gamma |

(a) Soft Lunar Landing Generator

(b) Hard Lunar Landing Generator

(c) Space Probe Generator

(d) Thermionic System

TABLE 3-7
RADIOISOTOPE HEAT SOURCES

| Isotope | Strontium 90 | Cerium 144 | Promethium 147 | Polonium 210 | Curium 244 |
|---|---|---|---|---|---|
| Half-life (yrs) | 28 | 0.78 | 2.6 | 0.38 | 18 |
| Power density (watts/$cm^3$) | 1.16 | 24.5 | 2.22 | 1200 | 27 |
| Availability (annual KW) | Adequate | Excellent | Adequate | Fair | Inadequate |
| Shielding required | Pb, 6 in. | Pb, 12. in. | Pb, 2 in. | Minor | Pb, 0.5 in. (30 in water) |
| Cost (dollars per thermal watt) | 45 | 15.0 | 168 | 640 | $<$ 1600 |

a. Primary Batteries

In a primary battery the chemically reacting parts require renewal or replacement. In a secondary or storage battery, the chemical reactions being reversible, the chemical conditions are restored after partial or complete discharge by sending electric current into the cell.

All batteries have the following four essential parts in common:

(1) The anode, a reducing agent

(2) The cathode or depolarizer, an oxidizing agent

(3) The electrolyte, a material that permits ionic conduction between anode and cathode

(4) The separator, a material that physically separates anode and cathode but permits ions to move between the electrodes

Figure 3-18 which is a common (Leclanché) dry cell (used for flashlights) shows that it consists of a carbon cathode, zinc anode, a solution of

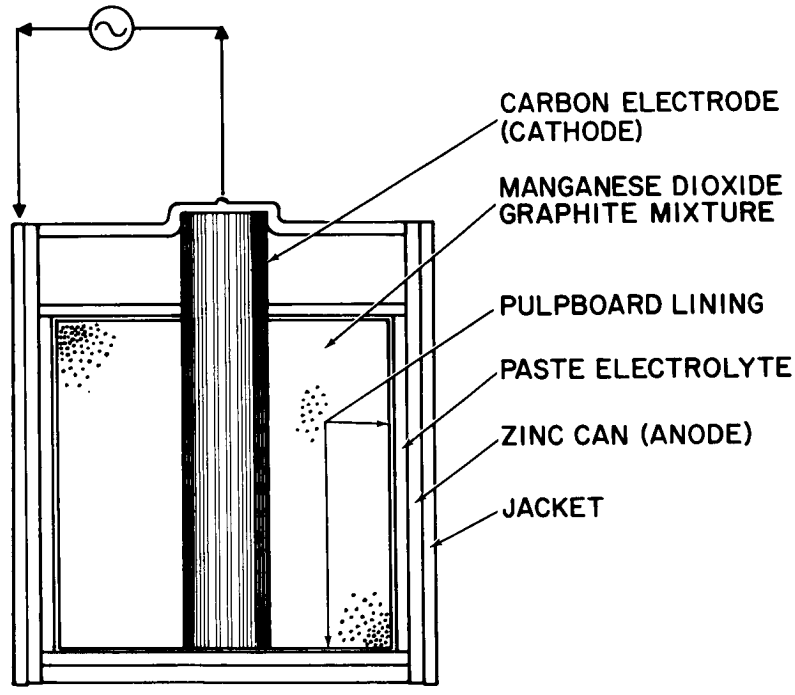


Figure 3-18. Primary Battery

zinc chloride and an ammonium chloride electrolyte. In this cell the paste is the electrolyte material as well as the separator between the anode and cathode. The manganese dioxide acts as a depolarizer.

Another type is the zinc-mercuric oxide dry cell which has three

times the capacity of the Leclanché dry cell. The anode is amalgamated zinc strip coiled into a spiral with cellulosic strips separating adjoining layers. The cathode is a mixture of red mercuric oxide and 5 percent graphite. The electrolyte is potassium hydroxide saturated with zinc oxide. The practical output is 45 watt-hrs per pound. Cell voltage is 1.3 volts. The system has good shelf life; the capacity decreases sharply below 50°F. At 0°F, the capacity is almost zero.

Silver-zinc batteries are available as both primary and secondary batteries. The cathode is silver oxide and the anode is zinc. The electrolyte is aqueous potassium hydroxide. The primary type battery is activated just before use because shelf life is limited to 8 to 14 hrs. This is the result of deterioration of the separators. The output is as much as 40 to 75 watt-hours per pound. Compared to a zinc-mercuric oxide battery, it is less compact, but it is also capable of high rate pulse discharge because it has a low internal impedance. The primary silver-zinc system is used when power is required for a short period (e.g., during initial orbital acquisition) and it is well advanced in its development and reliability.

b. Secondary Batteries

The five types of secondary batteries which comprise the bulk of the storage battery types are:

(1) Lead-acid battery (automotive battery)

(2) Nickel-iron or Edison battery (heavy duty industrial applications)

(3) Nickel-cadmium battery (long service life)

(4) Silver-cadmium battery (long service life)

(5) Silver-zinc

The Lead-Acid cell has low cost, high voltage per cell, good capacity and life. However it is also relatively heavy, has only average low temperature characteristics and cannot remain discharged too long without being damaged. The latest development in this type allows sealing of the battery, preventing evaporation and avoiding the need for continual addition of distilled water.

The Nickel-Iron cell is extremely rugged and reliable and can operate at very high temperatures. The main disadvantages are water consumption during charge and a 15 to 20 percent monthly drop in capacity on charged stand.

The Nickel-Cadmium cell comes in two cell constructions; pocket plate for heavy duty use and sintered plate for high rate applications. It is rugged, has long life, can be overcharged, performs well at low temperatures and can be hermetically sealed. It consists of a nickel-oxide anode, a cadmium metal cathode, a separator between plates, and an aqueous potassium hydroxide electrolyte.

In the pocket type, the active nickel and cadmium materials are held in perforated flat or round tubes held in a plate frame, and the separator is made of plastic rods or an open plastic grid between alternate plates.

In the sintered plate construction, the active materials are held in a highly porous thin flat plate made by sintering nickel powders onto a screen or onto a perforated flat plate electrode support. Cellulosic or polymeric woven or unwoven sheets are used as the separator material between the closely packed sintered plates. This construction results in a high rate of discharge capability. Among the sintered plate varieties, the hermetically sealed type is of importance in space applications. It functions in such a manner that when it becomes completely charged, oxygen evolved at the nickel anode is transferred to the cadmium cathode where it is recombined.

The cycle life of sealed nickel cadmium cells is quite high, depending upon the percentage of discharge. Figure 3-19 shows the cycle life of sealed nickel-cadmium cells as related to percent of the discharge. The theoretical specific energy is 95 watt-hrs per pound. Figure 3-20 shows that about 12 watt-hrs per pound are obtained for a discharge rate of 1 hour, and 17 watt-hrs per pound are obtained for a discharge rate of 10 hours. However, if a percentage discharge of 67 percent is used, a specific energy of only 8 watt-hrs per pound is realizable (for 1 hour discharge rate). Failures occur because of overheating, separator and electrode degradation, electrode corrosion contamination, structural defects and leaks.

The batteries must supply energy for peak load periods when the capability of solar cell panels is exceeded. For a long-life power system, this requires on the order of 20,000 charge-discharge cycles. The depth of discharge should therefore be held to about 10 percent. For the SMS mission, there is superimposed the requirement for battery power when the vehicle is in the Earth's shadow. This occurs on 82 days of the year, with the maximum time in any one orbit being 66 minutes. For this limited number of cycles a greater depth of discharge, up to 65 percent, may be used. Consideration should be given in the design and operation of the satellite to the desirability of completely recharging the batteries immediately after the spacecraft emerges from the Earth's shadow and before resuming meteorological observations.

The Silver-Cadmium secondary battery consists of a cathode of silver oxide, an anode of cadmium metal, and an electrolyte of aqueous potassium hydroxide. The major attraction of the silver-cadmium system is its increased specific energy. The theoretical energy output is 150 watt-hrs per pound. In working sealed units, 24 watt-hrs per pound can be achieved for full discharge. For a 67 percent discharge, 14.5 watt-hrs per pound can be obtained. The major shortcomings of the silver-cadmium systems are limited cycle life and deterioration of separators at elevated temperatures. (A most extensive cycle life testing of sealed silver cadmium cells is being conducted by the Air Force. This includes the evaluation of two hundred and twenty 15 ampere-hour cells and six 28 volt batteries. Two cycles will be used; a two hour cycle with 85 minute charge and 35 discharge, and a 24 hour cycle with 22 hours and 48 minutes charge and 1 hour and 12 minutes discharge. Depth of discharge will be 25, 50, and 75 percent at -10, 5, 25 and 50°C. The batteries will be tested at 25°C. These tests are currently underway but no data are available at this time.)

Table 3-8 is a summary of the state of the art of the primary and secondary battery characteristics as applicable to satellite energy-storage system.

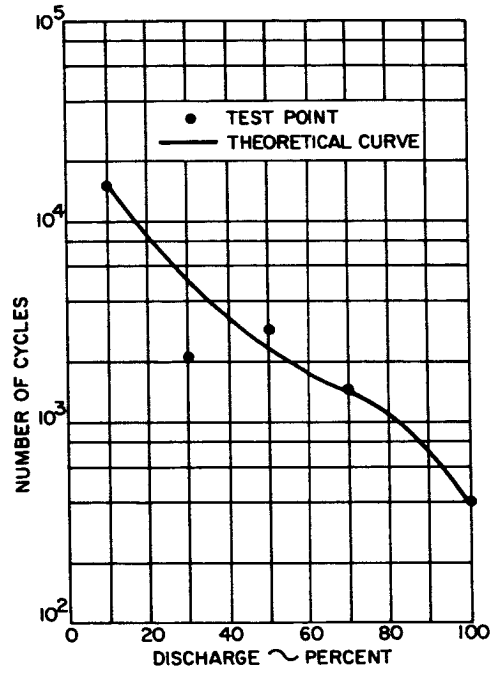


Figure 3-19. Cycle Life of Sealed Nickel Cadmium Cells

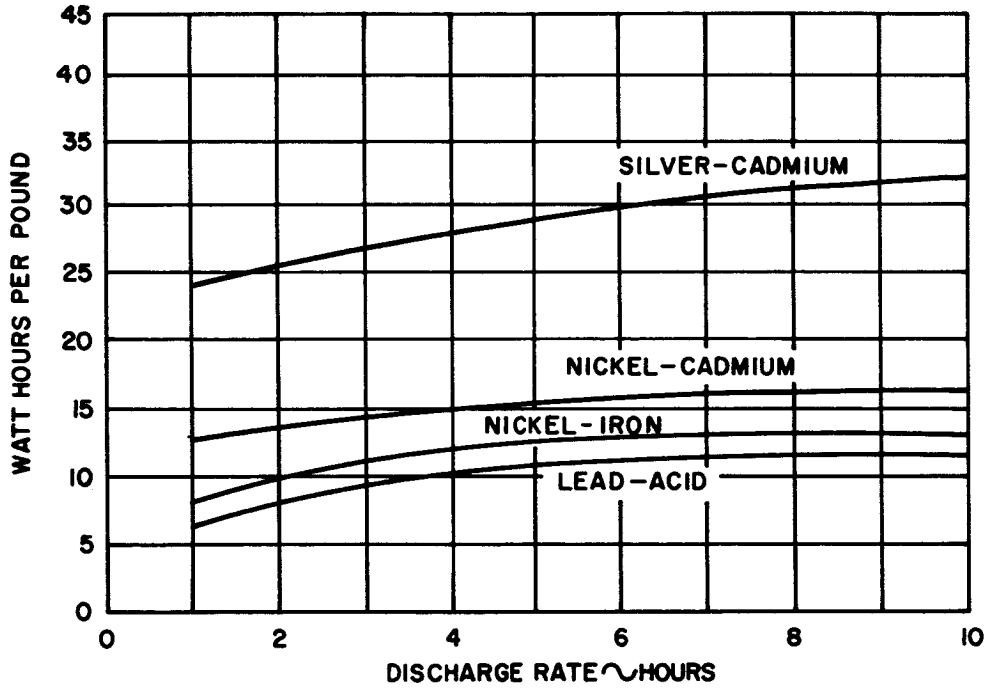


Figure 3-20. Energy vs Unit Weight for Various Batteries

TABLE 3-8

BATTERY STORAGE SYSTEMS

| | | Type | Anode | Electrolyte | Cathode | Nominal Voltage of Basic Cell | Watt-hours / lb * | Watt-hours / cu-in. * | Voltage Regulation | Service Duty | Discharge Rate | Service Temperature (Dry Cells) | Cycle Life (Secondary Cells) | Watts-hours dollar |
|---|---|---|---|---|---|---|---|---|---|---|---|---|---|---|
| PRIMARY | Ready(dry) | Leclanche' | Zn | $ClNH_4$ $MnO_2$ $Cl_2Zn$ | C | 1.5 | 10 | 1 | Fair | Interm't | Low | 30 to 90F | | 2-50 |
| | | Mercury | Zn | KOH | HgO C | 1.34 | 30 | 5.0 | Good | Interm't | Low | 50 to 160F | | 0.7-14 |
| | | Alkaline dry cell | Zn | KOH | $MnO_2$ | 1.5 | 47 | 2.2 | Good | Light | Low | 40 to 90F | | 33 |
| | | Magnesium cell | Mg | MgBr | $MnO_2$ | 2.0 | 50 | 3.3 | Fair | Light | Low | | | 28 |
| | Reserve (wet) | Lalande | Zn | NaOH CuO | CuO | 0.8 | 20 | 0.94 | Good | Light | Low | | | 57 |
| | | Air cell | Zn | NaOH $O_2$-C | CuO | 1.4 | 20 | 2.0 | Good | Light | Low | | | 75 |
| | | Water-activated cuprous-chloride | Mg | Water CuCl | CuCl | 1.2 | 21 | 2.1 | Good | Light | Low | | | |
| | | Water-activated silver-chloride | Mg | Water AgCl | AgCl | 1.4 | 47 | 5.0 | Good | Heavy | High | | | |
| | | Silver-zinc | Zn | KOH | AgO | 1.5 | 70 | 5.6 | Good | Heavy | High | | | |
| SECONDARY | | Lead-acid | Pb | $H_2SO_4$ $H_2O$ | $PbO_2$ | 2.0 | 12 | 1.1 | Fair | Light | Med | | 200-2000 | 20 |
| | | Nickel-iron (Edison) | Fe | KOH | $NiO_2$ | 1.2 | 13 | 0.7 | Good | Medium | Med | | over 2000 | 5.7 |
| | | Nickel-cadmium (Jungner) | Cd | KOH | $NiO_2$ | 1.25 | 17 | 1.9 | Good | Heavy | High | | over 2000 | 2 |
| | | Silver-zinc | Zn | KOH | AgO | 1.5 | 59 | 4.4 | Good | Heavy | High | | 10-400 | |
| | | Silver-cadmium | Cd | KOH | AgO | 1.1 | 32 | 2.6 | Good | Heavy | High | | 300-1000 | 2 |

* Energy/weight and energy/volume ratios correspond to 10-hr discharge rate for secondary batteries.

Figures 3-20 and 3-21 show the energy versus unit weight and energy versus unit volume for the various secondary battery systems described (temp approx 85°F). Figure 3-22 shows the capacity versus temperature characteristics for the various primary and secondary batteries. It should be noted that these curves are based on a slow (350 hr) discharge rate. Thus for nickel-cadmium at 25 through 75°F, the capacity is approximately 17.5 watt-hrs per pound. At either end the capacity falls off.

Table 3-9 shows the secondary cell discharge rate characteristics as a function of temperature.

The Silver-Zinc rechargeable battery provides the greatest energy per unit weight and volume in the rechargeable battery field. It has extremely low resistance, can provide high or low rate discharges and can be left in the discharged state for long periods.

The components of the silver-zinc secondary battery are similar to those of the silver-zinc primary battery except that the separator must be considerably thicker to prevent the transfer of silver and to prevent shorts caused by separator deterioration. The realizable specific energy is from 20 to 50 watt-hrs per pound, depending on the rate of discharge. At high temperatures, the capacity is lower because of increased self discharge. Where the highest energy capability is needed for only a limited number of cycles, a vented silver-zinc cell is the best choice.

Approximately 100 cycles can be achieved at a low rate of discharge, and approximately 20 cycles can be achieved at high rates. Failure occurs from the deterioration of the separator and from shorting.

For space applications, hermetic sealing is necessary. This is difficult because the zinc reacts with the electrolyte to form hydrogen, and in addition, the recombination of the oxygen generated is not completely successful in this system. Sealed cells have been made that can be operated at low rates but will not tolerate any overcharge.

c. Fuel Cells (Degenerative type)

The distinguishing factor and primary disadvantage of degenerative fuel cells is that the fuel supply must be replenished if an extended period of operation is to be obtained.

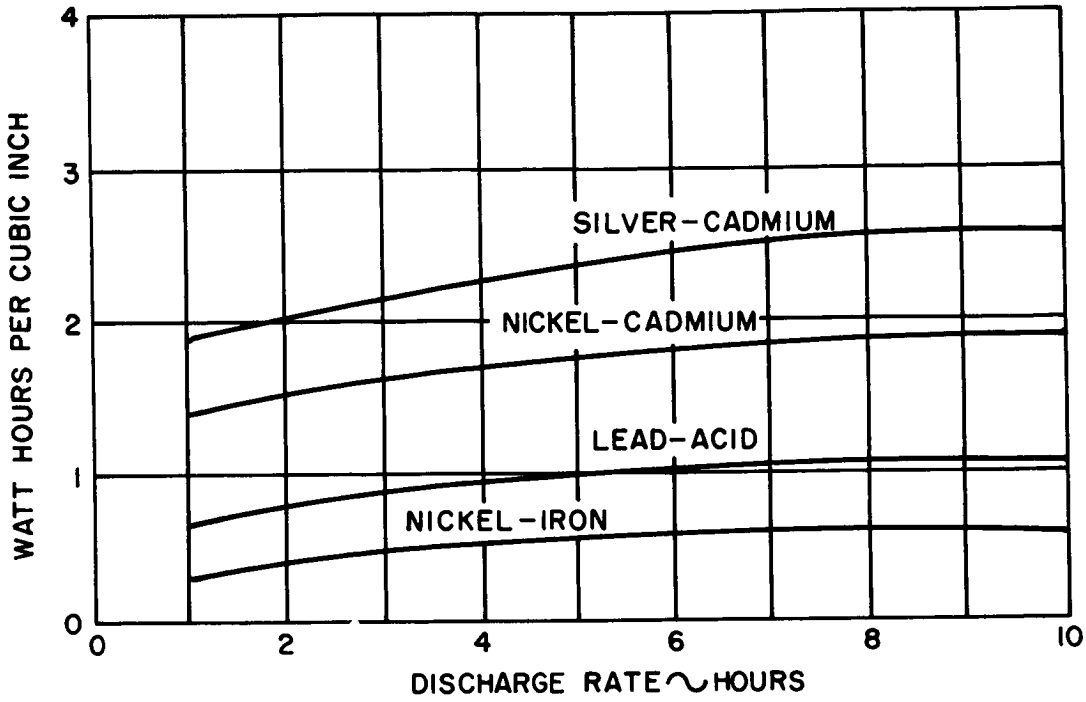


Figure 3-21. Energy vs Unit Volume for Various Batteries

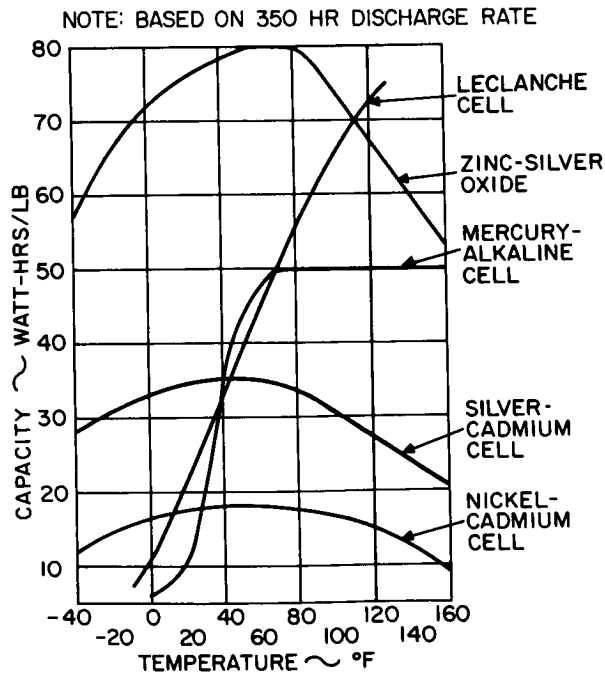


Figure 3-22. Capacity vs Temperature for Various Batteries

TABLE 3-9
SECONDARY CELL TEMPERATURE-DISCHARGE CHARACTERISTICS

| | Temperature (°F) | Discharge Rate (hours) | Lead-Acid | Nickel-Cadmium (Pocket Plate) | Nickel-Cadmium (Sintered Plate) | Edison (Nickel-Iron) | Silver-Zinc | Silver-Cadmium |
|---|---|---|---|---|---|---|---|---|
| Watt-hours per pound (Based on an Allowable Voltage Drop of 20 percent) | 80 | 5 | 11.4 | 6 | 15 | 15 | 52.8 | 24.6 |
| | | 1 | 8.4 | 4.8 | 11.6 | 9.5 | 45.8 | 19.8 |
| | | 0.25 | 6.8 | 2.9 | 9.9 | --- | 39 | 15.6 |
| | 0 | 5 | 5.4 | 4.2 | 11.5 | --- | 39.4 | 20.9 |
| | | 1 | 3.9 | 3.1 | 9.9 | --- | 33 | 16.6 |
| | | 0.25 | 2.9 | 1.7 | 8.7 | --- | 24.6 | 12.1 |
| | -40 | 5 | 3.7 | 3.2 | 9 | --- | --- | 10.7 |
| | | 1 | 2.5 | 2.4 | 8.4 | --- | --- | 7.7 |
| | | 0.25 | 1.5 | 0.9 | 5.3 | --- | --- | --- |
| Watt-hours per cubic inch (Based on an Allowable Voltage Drop of 20 percent) | 80 | 5 | 0.83 | 0.47 | 1.08 | 1.16 | 3.36 | 1.57 |
| | | 1 | 0.61 | 0.38 | 0.84 | 0.73 | 2.92 | 1.26 |
| | | 0.25 | 0.49 | 0.23 | 0.72 | --- | 2.48 | 0.99 |
| | 0 | 5 | 0.39 | 0.33 | 0.83 | --- | 2.51 | 1.33 |
| | | 1 | 0.28 | 0.24 | 0.72 | --- | 2.1 | 1.06 |
| | | 0.25 | 0.21 | 0.13 | 0.63 | --- | 1.67 | 0.77 |
| | -40 | 5 | 0.27 | 0.25 | 0.65 | --- | --- | 0.68 |
| | | 1 | 0.18 | 0.19 | 0.61 | --- | --- | 0.49 |
| | | 0.25 | 0.11 | 0.07 | 0.38 | --- | --- | --- |

Technical feasibility has been shown in the following systems

(1) Low temperature (50 to 150°F), low pressure (1 to 50 psi) hydrogen-oxygen or air fuel cells

(2) Mid-temperature (400 to 600°F), high pressure (400-1000 psi) hydrogen-oxygen or air fuel cells

(3) Low temperature fuel cells using hydrocarbon fuels and oxygen.

(4) High temperature (400 to 1000°F) fuel cells at low pressure using hydrocarbons and air

1) Hydrogen-Oxygen Type. The theoretical capability of this system is 1400 watt-hrs. per pound. In a prototype, 500-watt fuel cell, 50 watt-hrs. per pound were achieved. The weight per kilowatt-hour is approximately 100 pounds with the fuel, consisting of hydrogen and oxygen, weighing 13 pounds per kilowatt-hour.

To illustrate the operation, Figure 3-23 shows the hydrogen-oxygen, liquid electrolyte cell (low temperature and low pressure or medium temperature and high pressure).

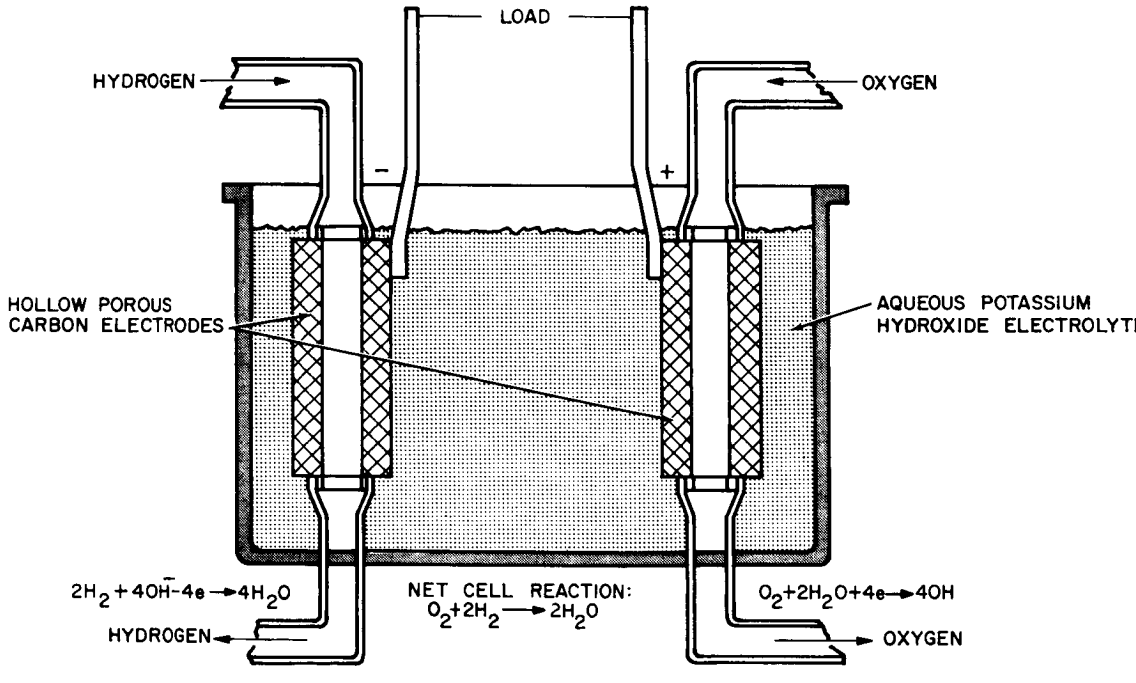


Figure 3-23. Hydrogen-Oxygen, Liquid Electrolyte Fuel Cell

At the present, practical high-energy operation can be obtained only with pure hydrogen and oxygen. The major shortcomings of this system are fuel storage problems and flooding of electrodes.

2) Ion Exchange Membrane Fuel Cell Type. Two types of ion exchange fuel cells have been reported. One is a low temperature, low pressure, hydrogen-oxygen fuel cell in which a wet ion exchange membrane is used as the electrolyte. Porous electrodes with proper catalysts are in contact with the membranes, and hydrogen and oxygen are introduced to opposite sides. Ionic conductivity through the cell is obtained by the mobile hydrogen ions in the membrane matrix.

This type of cell has been under development as a compact, lightweight, portable, power pack for military personnel. The hydrogen source is a bora-hydride-acid generator which produces moist hydrogen gas suitable for use in the cell.

The other type of ion exchange fuel cell uses hydrogen as the fuel gas and an aqueous bromine-bromide electrode as the oxidant. The aqueous solution is reported to overcome the harmful effects associated with the drying of the membrane.

Because of the low specific energy available, low operating current, and mechanical problems associated with the exchange fuel cell, it does not appear to be outstanding for use as a primary electrical power source for space vehicles and satellites.

Table 3-10 is a summary of available fuel cell characteristics under various temperature and pressure operations using different fuel systems. It includes both the degenerative and regenerative systems.

d. Chemical Turbines

Chemical systems are those using fuels such as hydrazine, liquid hydrogen-oxygen and a mechanical-to-electrical converter such as a turbine generator. Chemically-fueled systems are lighter than solar or nuclear power systems at power levels from 2 to 5 kilowatts for missions lasting to several hundred hours. Because of their safety, compactness, and current availability, chemical systems will be used for even longer missions than would be justified from weight considerations alone.

Many types of chemical systems are under development. These include hydrazine-fueled turbomachines and cryogenic systems using engines fueled by liquid hydrogen and oxygen. Studies have been conducted to determine the proper place in the power-duration spectrum for various types of power plants. Zwick and Zimmerman find chemical systems to be superior (in terms of weight) for power levels in excess of 1 horsepower for missions less than 50 hours long. Howard and McJones find chemical systems superior for missions lasting from 50 to 200 hours, depending on the power level required.

Other propellant systems which have been used in open cycle secondary power systems are solid propellants, ethylene oxide, propyl nitrate, and bipropellants such as hydrogen peroxide-hydrazine, hydrogen peroxide-diesel fuel, etc. Ethylene oxide, propyl nitrate, and the solid propellants are not considered suitable for long duration applications.

TABLE 3-10
FUEL CELL CHARACTERISTICS

| Type | Fuel | Oxidant | Electrode | Electrolyte | Operating Temperature | Operating Pressure | Open Circuit Voltage Theoretical | Open Circuit Voltage Measured | Current Density (Amp/Sq Ft) | Output (Watt-hour/lb) | Output Cu. Ft. Per KW | Output Lbs. Per KW | Percent Efficiency thermal to electric | Remarks |
|---|---|---|---|---|---|---|---|---|---|---|---|---|---|---|
| Ion-Exchange Membrane | Hydrogen | Oxygen or Air | Activated Metal | (Solid) Ion-Exchange Membrane | 50°F above ambient -65° to +165°F | Atmospheric | 1.1 | 1 0.8v@ 10ma | 22 @ 0.8v | 100 (measured) | 3.5 to 5 | 250 to 500 | 60@15 to 20 amp /sq ft | National Carbon Co. and GE-AAT Dept. developing construction relatively simple. |
| Redox | Liquified Fuel | Oxygen or Air | Porous Metal | Liquids | 70 to 85°C | Approx. Atmospheric | ~1 | - | 200 | 1200 with air 1600 with pure oxygen | 5 | 50 to 75 | - | Units have been operated for three-month periods without interruption. Has definite weight and size advantage over Hydrogen-Oxygen Type Cells, G.E. and Lockheed. |
| Carbox | HCO-Petroleum Hydrocarbons (Kerosene) | Oxygen or Air | Porous Metal | Fused Carbonate | 500 to 800°C | Atmospheric | ~1 | 0.7 | 60 | - | - | - | 64 | Being developed by Patterson-Moos and Pittsburgh Cons. Coal Co. |
| Hydrox | Hydrogen | Oxygen | Porous Metal | - | 200 to 250°C 400 to 500°F | 10 to 55 Atm. 400 to 600psi | 1.1 | 1.0 | up to 1000 | - | 0.25 to 1.2 | 40 to 90 | - | 1500 hr-life possible. Work by Patterson-Moos. |
| Thermal Regenerative | Hydrogen | Group I Metals | Fuel Metal & Nickel | Fused Group I Chlorides | 608 or 1004°F | 200 to 500mm Hg absolute | 0.75 | 0.72 | 245@0.72v with lithium | ~5 | - | - | Carnot: 40 | Operated non-regeneratively for 2 weeks. Operating temperature depends upon fuel. (MSA Res. Corp.) |
| Solar Regenerative | Nitric Oxide | Chlorine | Carbon-Disk | Liquid nitrosyl chloride | 70°F | 15 psig | 0.21 | 0.21 | 2@0.1v | - | - | - | - | Development by Sundstrand Aviation. |
| Low Temp.-Pressure | Hydrogen | Oxygen | Specially Processed Carbon | 12 molar Solution of KOH | 70 to 150°F | 1 to 5 atmos. | 1.2 | 1.12 | 100@0.95v and 140°F, and oxygen @ 5 atm. | 1620 | 3.5 to 5 | 250 to 500 | 75 | Being developed by Union Carbide Consumer Products Co. |

## 4. Microwave Transmitted Power

During recent years, studies and experiments on the feasibility of transmitting power by means of focused microwave beams have been conducted. Superpower amplitron tubes have been built and tested. A microwave heat exchanger for incorporation into a gas turbine engine has been designed and demonstrated, and studies of a high-altitude platform design have been made. The platform design program has been given the code name of Ramp. In the Ramp system, it is planned that power will be transmitted from an antenna on the ground to an array mounted on a rotary-wing platform. The microwave energy will be guided to a heat exchanger where it will be converted to heat. This exchanger will supply power to operate a closed-cycle gas turbine. The gas turbine will drive a large compressor which will pump air through the blade ducts and out the jet tips to turn the rotor.

The system of focusing beams has been more widely used in the optical than in the microwave field. In the normal microwave antenna, focusing is used to transfer energy from the reflector to the feed device. Studies have been made of numerous antenna systems that use focusing principles to approximate the far-zone pattern at a convenient site in the near zone. There have been numerous discussions of focused antennas for certain power transfer applications. Optical principles applicable to efficient focused antenna systems have been established in detail.

In the Ramp system, a large portion of the energy transmitted by the ground antenna appears at the focal plane within the focal spot. In an optically perfect, uniformly illuminated system, approximately 84 percent of the radiated energy would be focused within this spot. However, aberrations and distortions introduced by the atmosphere degrade the system. As much as 98 percent of the energy can be confined to the focal spot by tapering the illumination of the transmitting reflector. This results in a larger focal spot. For a pair of antennas, the coupling is such that uniform illumination would result in approximately 78 percent of the radiated energy being intercepted by the receiving antenna. For the case of tapered illumination, receiving apertures of the same diameter would result in intercepting more energy. The improvement in the proportion of intercepted energy is the result of the increase of the major lobe energy caused by sidelobe reduction and the change caused by tapering the distribution of energy across the focal spot. The diameter of the focal spot is given by

$$D_A = K\lambda R/D_T$$

where

| | | |
|---|---|---|
| $D_A$ | = | spot diameter |
| $R$ | = | distance to the antenna |
| $D_T$ | = | diameter of the transmitting antenna |
| $\lambda$ | = | wavelength |
| $K$ | = | an illumination factor |

The illumination factor, K, is as follows:

(1) K = 2.00 for uniformly illuminated rectangular apertures

(2) K = 2.44 for uniformly illuminated circular apertures

Typical antenna parameters for the Ramp system are as follows:

(1) Transmitting aperture diameter, $D_T$, 350 feet

(2) Platform altitude, R, 65,000 feet

(3) Wavelength $\lambda = 1/6$ foot (6 kilomegacycles)

(4) Focal spot diameter, $D_A$, 75 feet

Efforts to determine the best combination of weight, power, and cost for the Ramp system have led to a design for a receiving aperture diameter of 50 feet. This aperture, if properly centered on the axis of a 350-foot diameter transmitting antenna, would intercept 75 percent of the transmitted energy (89 percent of the focal spot energy). A realistic overall efficiency figure would be approximately 32 percent if both the transmitting and the receiving antennas are approximately 65 percent efficient.

These techniques when applied to a 24-hour synchronous satellite, however, appear to be impractical as can be seen by the following calculation. Assuming the following parameters:

(1) The transmitting antenna is 5000 feet in diameter and is uniformly illuminated

(2) The receiving antenna is 80 feet in diameter ($D_R$)

(3) The efficiencies of the transmitting antenna and the receiving antenna, $\eta_T$ and $\eta_R$, are each 65 percent

(4) The wavelength is 1/6 foot

The diameter of the focal spot (which encloses 84 percent of the transmitted power) is then:

$$D_A = K\lambda R/D_T$$

$$= 2.44 \times \frac{1}{6} \times \frac{22,300 \times 5280}{5000} = 9,600 \text{ feet}$$

The ratio of power received by the satellite to the power transmitted (if the energy is uniformly distributed over the focal spot area) is

$$\frac{P_r}{P_t} = \left[\frac{D_R}{D_A}\right]^2 \eta_T \, \eta_R \, (0.84)$$

$$= \left[\frac{80}{9600}\right]^2 (0.65)\,(0.65)\,(0.84)$$

$$= 24.5 \times 10^{-6} = 0.0025 \text{ percent}$$

Therefore, in order to obtain 500 watts at the satellite, 20.4 megawatts would be required even with a 5000-foot diameter transmitting antenna. Because methods for generating and transmitting this amount of power at microwave frequencies are not available at present, this method appears to be impractical.

5. Summary Of Power Sources And Energy Storage Systems

The pertinent characteristics of the power systems discussed in the power study are summarized in Table 3-11. The approximate power level and the mission duration most suitable for each type of power system are given. Also shown are the relative weights of each of the systems in their present state of development. With respect to relative weights, it should be noted that ratings are not directly comparable but differ with the two types of power systems available. In one type, such as the primary battery, the total energy is self-contained. In the other type, such as the solar thermionic system, energy is continuously obtained from the Sun. Therefore, these two systems cannot be compared directly unless the period during which solar energy is available is specified for a particular mission. The major advantages and disadvantages of each power system are also given.

Figure 3-24 indicates, generally, the uses for various power systems in terms of power level versus mission duration. The many other factors that influence the choice of a power system for a specific mission are not taken into account in this figure.

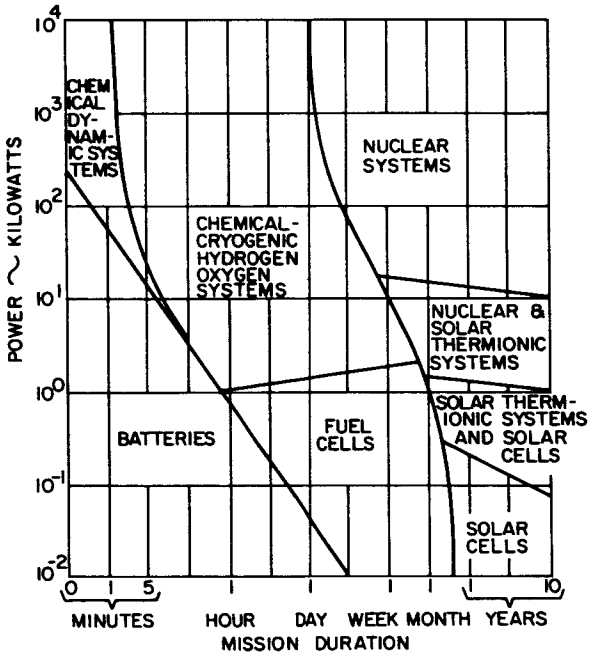


Figure 3-24. Application of Space Power Systems

TABLE 3-11
POWER SYSTEM CHARACTERISTICS AND APPLICATIONS

| Power System | Power Level | Mission Duration | Relative Weight | Advantages | Disadvantages | Availability |
|---|---|---|---|---|---|---|
| Solar cell, nickel-cadmium batteries, nonoriented | Less than 100 watts | Greater than 1 month | 1000 to 2000 pounds per kilowatt | No orientation system required | Only about 25 percent of solar cells used at a time | Currently available |
| Solar cell, nickel-cadmium batteries, Sun-oriented | 100 to 1000 watts | Greater than 1 month | 250 to 1500 pounds per kilowatt | -- | Sun-seeker orientation system required | Currently available |
| Primary batteries | Less than 10 kilowatts | Less than 3 days | 45 to 80 watt-hours per pound | Simplicity | Limited energy capacity | Currently available |
| Fuel cells | Less than 1 kilowatt | Less than 6 months | 50 to 100 watt-hours per pound | -- | Operation is relatively complex | Under development; available in 1 to 3 years |
| Solar Thermionic & Thermoelectric systems | 0.1 to 20 kilowatts | Greater than 1 month | 100 to 300 pounds per kilowatt | No fuel need be carried | Large size, difficult to launch and deploy | Under development;available 1 to 2 years |
| Nuclear Radioisotope systems | 0.5 to 100 kilowatts | Greater than 1 week | 40 to 800 pounds per kilowatt | Low weight of fuel required; solar energy not required | Large weight required for radiation shielding; radiation hazard; complex control | Under development;available in 2 to 5 years |
| Chemical systems | Greater than 2 kilowatts | Less than 300 hours | 100 to 500 watt-hours per pound | Currently available; compactness | Fuel requirement prohibitive for long missions | Currently available |
| Microwave transmission systems | Less than 10 kilowatts | Indefinite | -- | No fuel need be carried | Large receiving antenna required; limited altitude, approximately 20 miles | Under development |

Combinations of solar cells and nickel-cadmium batteries appear to be most suitable when about 1 kilowatt is required for several months or more. Nonoriented solar cell systems are useful for power levels below approximately 100 watts because the weight of the cells, which are not fully used, is not excessive. Oriented solar cell arrays appear to be more practical in terms of weight for power levels greater than about 100 watts.

It appears to be most advantageous to use primary batteries when power is required for relatively short intervals of time. The use of storage batteries without a means of recharging them does not appear to be practical for long duration missions. For example, if 500 watts are continuously required for 30 days, a total energy of approximately 360,000 watt-hrs is needed. Even if silver-zinc batteries with an output of 50 watt-hrs per pound were used, a total battery weight of 7200 pounds would be required. A solar cell system with an output of 500 watts would weigh approximately 250 pounds. Therefore, it appears to be more efficient to use a solar cell system for this relatively short mission. For longer missions, such as the one assigned to the synchronous satellite, the use of a solar cell system would result in an even greater comparative weight saving.

On the basis of the current state of development and on demonstrated cycle life, nickel-cadmium batteries appear to be the best overall choice. There is evidence that silver-cadmium cells cannot in general accept as high charging rates as nickel-cadmium cells. The silver-zinc cells do not warrant strong consideration for the synchronous orbit application because of relatively short cycle life.

Fuel cells, such as the hydrogen-oxygen type, would be the lightest for mission situations in which several hundred watts are required for several days. Although these devices are relatively complex in operation, when they are fully developed, such fuel cells could become competitive with battery and solar cell systems.

Solar thermionic systems appear to be a good choice when power levels from 0.1 to 20 kilowatts are needed for no more than several weeks. At power levels above approximately 1 kilowatt, solar cell panel arrays, i.e., solar voltaic systems, become excessively heavy as compared to the concentrators used in solar thermionic systems. Therefore, the use of thermionic systems is more efficient. The disadvantages of thermionic systems are that the concentrators are large and that the electrical conversion systems (such as boiler-turbines) are complex. Design of a solar concentrator is difficult because it must be stowed during launch and it must be deployed with a considerable amount of accuracy once in orbit. However, thermionic systems are safer to operate than nuclear systems.

Nuclear power systems offer the best prospects for situations in which power levels from 0.5 to more than 100 kilowatts are needed for several months to several years. They offer long life and elimination of Sun-orientation requirements. In addition, nuclear systems are relatively impervious to the hazards of space environment such as Van Allen radiation, solar flares, and micrometeoroids,

The principal disadvantage of nuclear systems for small power applications is the large weight associated with shielding the payload against radiation. In addition, a complex control system is needed for the reactor and a heavy heat dissipation system is required. At higher power applications, although the initial weight penalty is great, it is competitive with other power systems for extended periods of use. It has been estimated that at the 500-watt level a reactor system weighs approximately 950 pounds while an isotopic thermionic system would weigh approximately 285 pounds. The isotopic system thus appears competitive to the solar-battery system in this range. There is an additional factor which must not however be overlooked. Whereas the nuclear reactor can be turned on once the vehicle has achieved orbit, the isotopic system must be in operation at all times. There are, therefore, the hazards of radioactivity and heat dissipation with which the ground crew must contend.

Chemical power systems appear to be most suitable for short duration missions lasting several hundred hours or less during which power levels of 2 kilowatts or greater are required. The advantages of these systems are that they are safe, compact, and currently available. For long missions, the amount of chemical fuel required becomes prohibitive. They appear to be most useful as auxiliary power sources when high power is required for short duration missions.

Microwave power transmission does not appear to be worthy of consideration for the 24-hour synchronous satellite because the large distance involved results in extremely poor efficiencies.

## C. SPACE RADIATION EFFECTS ON SOLAR CELLS AT SYNCHRONOUS ORBIT

The composition of outer-space radiation is both electromagnetic and charged-particle in nature. Electromagnetic radiation arises from the Sun and other stars, which emit energy in the wavelength region from gamma rays to the infrared. The charged-particle radiation can be divided into three main categories:

(1) galactic cosmic rays (energetic atomic nuclei)

(2) solar flares

(3) Van Allen radiation

Particular attention is centered on the radiation effects on solar cells, semiconductors, and organic materials because they comprise a large portion of the systems used in space vehicles and at the same time have properties that are most readily susceptible to radiation damage.

It has been repeatedly confirmed that the major reaction in polymers, whether produced by electrons, protons, X-rays, or gamma rays, depend primarily on the total energy absorbed (unit of absorbed dose is the rad, i.e., 100 ergs of absorbed energy per gram of material). In the Van Allen belts, the energy absorbed by a material bombarded by protons and electrons will occur as a result of the high energy particles producing excitations and ionizations in the material. Absorbed energy will be proportional to the energy of the bombarding particles, the number of particles per unit area, the time of exposure, and the electron density of the material.

1. Cosmic Rays

Solar cosmic rays are high energy charged particles, mostly protons, with a varying number of heavier nuclei which are accelerated in solar flares and propagate out into space. It is believed that the particles are accelerated to high energies in local magnetic fields near sunspots by an electromagnetic mechanism.

2. Solar Flares

The solar flare itself may be thought of as an explosion on the surface of the Sun in which high energy protons and electrons are ejected. The energy spectrum of protons ranges from a few Mev to energies greater than 15 Bev. The electron energy spectrum goes up to 100 Mev. Fluxes as well as energies and duration vary from event to event but have been measured to be $10^4$ times that of normal cosmic ray radiation and are thought to reach $10^6$ protons/cm$^2$ - sec for large solar flares. Flares usually last two or three days and reach their maximum flux 5 to 10 hours after occurring. Occurrences of these flares are random.

3. Van Allen Belt (Natural and Artificial)

The natural Van Allen belt consists actually of two zones, the inner zone reaching its peak at about 2000 miles from the Earth and the outer zone at about 10,000 miles, both centered about the geomagnetic equator. Beyond the peak of the outer zone the radiation diminishes steadily, so that at 40,000 miles no significant radiation intensity exists.

The inner natural zone has been called the proton zone, but it does have its share of low energy electrons. In the inner zone there are two components, a hard one, made up of protons of intensity, $\phi = 4 \times 10^4$ p/cm$^2$ - sec. for threshold energy, E>40 Mev. The electron intensity, $\phi = 2 \times 10^9$ e/cm$^2$-sec. for E>20 Kev; $\phi = 10^8$ e/cm$^2$-sec for E>200 Kev; $\phi = 10^7$e/cm$^2$-sec for E>600 Kev; $\phi = 10^6$e/cm$^2$-sec for E>1 Mev.

The outer natural zone, i.e., the electron zone, also has its share of protons but their intensity is small. The protons in the outer zone for E>60 Mev.have an intensity $\phi < 10^2$ p/cm$^2$- sec; for E<30 Mev, $\phi$ is insignificant. The electron intensity for E>20 Kev, $\phi = 10^{11}$e/cm$^2$-sec and for E>200 kev, $\phi < 10^8$ e/cm$^2$-sec.

As a result of the high altitude nuclear tests performed over Johnston Island on July 9, 1962, and also of Russian and U.S. high altitude tests after that date, a high flux rate of energetic electrons (in the region above 1 Kev) were more or less permanently trapped at altitudes from as low as 200 miles to as high as 12,000 miles and possibly beyond. This "artificial" electron radiation belt can cause silicon solar cells in the proton zone to deteriorate at a much greater rate than was previously expected as a result of protons in the "natural" Van Allen radiation belt. It is estimated that the electron flux rate for altitudes less than 12,000 miles has increased by a factor of approximately 225 times; thus for the inner zone, $E > 1$ Mev, $\phi = 2.25 \times 10^8$ e/cm$^2$ - sec. and not $10^6$ e/cm$^2$ - sec.

4. Radiation Sensitivity of Silicon Solar Cells

The degradation of solar cell short circuit currents is often characterized by the dosage required to reduce the short circuit current to 75 percent of its initial value. Figures 3-25 and 3-26 present the energy dependence of the radiation damage in terms of the integrated flux required to produce a 25 percent decrease in short-circuit current of a typical p/n silicon solar cell. The ordinate in both figures can be suitably modified for more radiation-resistant cells. Thus for the n/p as shown in comparison with the p/n in Figure 3-27, the n/p cell can tolerate an accumulation of $4.3 \times 10^{14}$ electrons/cm$^2$ as compared to $0.8 \times 10^{13}$ electrons/cm$^2$ for the p/n, i.e., an improvement factor of 54 times. Further tests indicat that the n/p cell can tolerate four times the integrated proton flux as compared to the p/n cell.

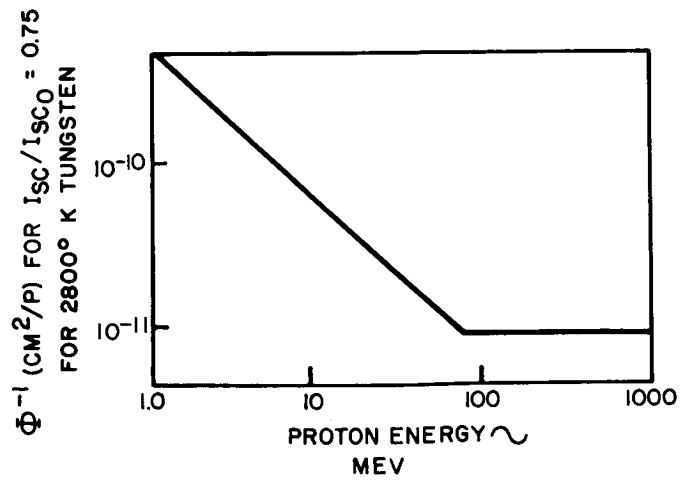


Figure 3-25. Proton Radiation Effects on Solar Cells

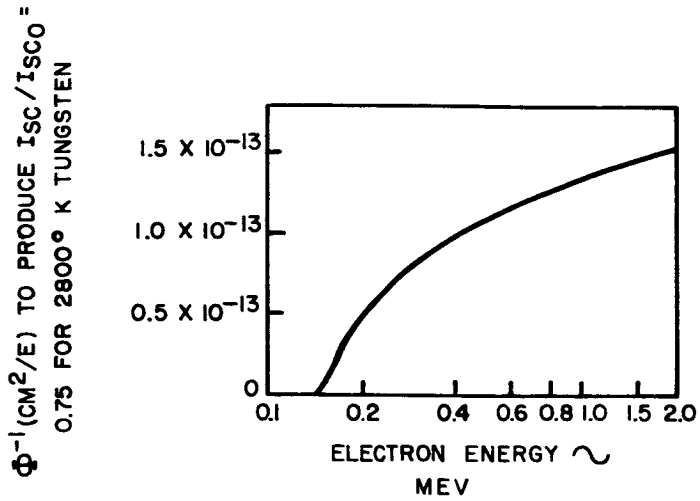


Figure 3-26. Electron Radiation Effects on Solar Cells

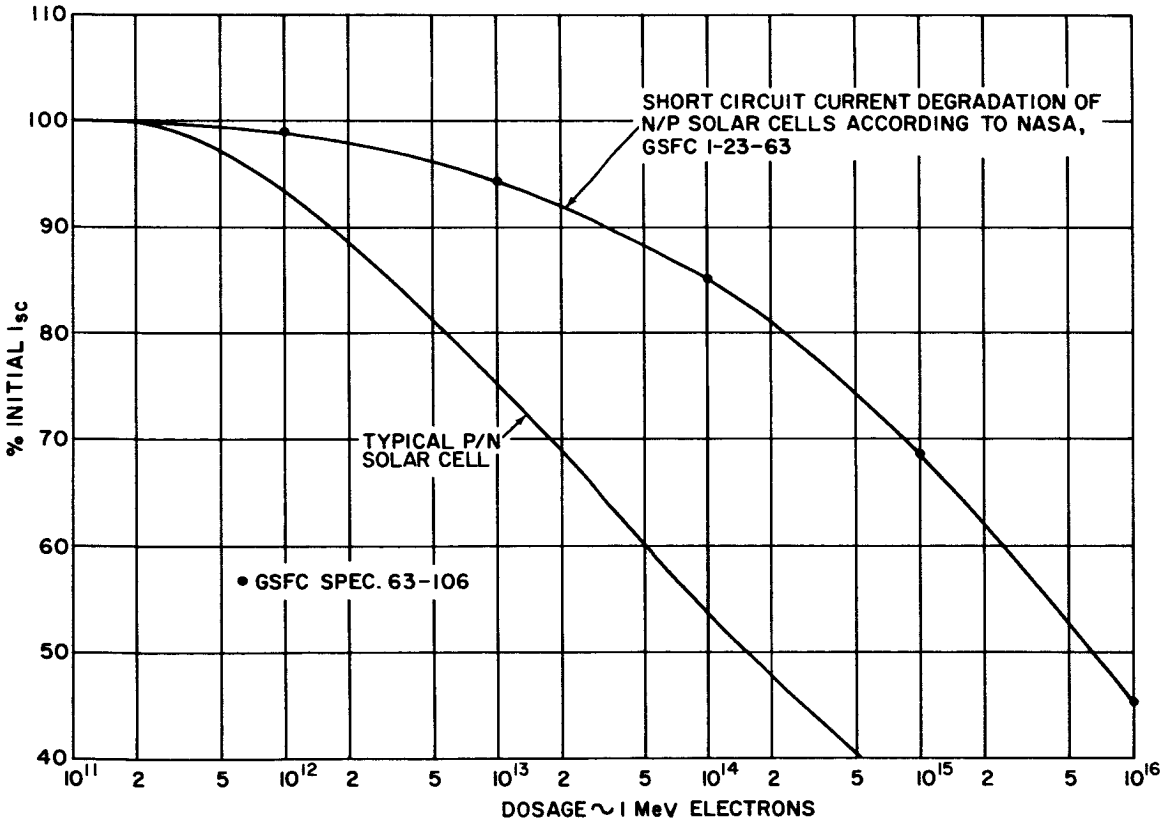


Figure 3-27. Comparison of Electron Energy Radiation Effects on p-n and n-p Solar Cells

Below about 1 Mev, radiation damage in solar cells becomes limited by the decreasing range of the protons. Radiation damage at very low proton energies has not been investigated.

The energy required to displace a single silicon atom from its lattice position is 12.9 electron volts. It requires an electron of 145 Kev in order to transfer this energy to the silicon atom. (Similarly, a 100 electron volt proton has sufficient energy to accomplish this.)

5. Expected Cell Degradation

Referring to Figure 3-25 we see that for a proton of energy 50 to 100 Mev, the integrated flux, i.e., the dosage required for 25 percent degradation, is $10^{11}$ protons/cm$^2$. For the inner Van Allen belt, the time for 25 percent degradation $= 10^{11}/4 \times 10^4 = 2.5 \times 10^6$ sec = 1 month, where $4 \times 10^4$ is the intensity of protons/cm$^2$ - sec for E > 40 Mev.

Referring to Figure 3-26 we see that for E> 200 Kev the dosage required for 25 percent degradation of the p/n cell is $2 \times 10^{13}$ electrons/cm$^2$.

For the outer Van Allen belt, at the synchronous orbit altitude, we see from Van Allen radiation plots that the electron intensity is of the order of $10^6$ e/cm$^2$ - sec. The time required for a 25 percent degradation is therefore $2 \times 10^{13}/10^6 = 2 \times 10^7$ sec. = .63 year.

Using the n/p cell we get an improvement of 54 times, i.e., the time required for a 25 percent degradation is 0.63 x 54 = 34 years. It thus appears that it is not necessary to use any cell radiation protector for the effects of Van Allen radiation to cover a year's operation.

The effect of solar flares is a more difficult problem. Figure 3-28 shows the range of energetic electrons and protons in quartz. It is seen that the glass cover slide corresponding to 6-mil microsheet will shield out electrons of 190 kev energy and protons of 4.5 Mev. A 60-mil quartz filter will remove electrons of 0.9 Mev and protons of 17 Mev. Solar flares, however, have energies in the Bev range.

The effect of high energy protons is not clear. Assuming, however, that the proton energy effect is from the 1-100 Mev energy level, a bombardment of $10^6$ protons per cm$^2$ per sec can be expected.

For 25 percent degradation $10^{11}$ protons/cm$^2$ can be tolerated. Assuming the flare lasts for 3 days at $10^6$ protons/cm$^2$ - sec, then $10^6 \times 3600 \times 24 \times 3$ protons/flare period $= 2.60 \times 10^{11}$ protons/cm$^2$, or approximately 30 percent degradation due to solar flares for p/n cells, and 7.5 percent degradation for n/p cells.

A method of reducing the chance of mission failure due to solar flare radiation damage to the solar cell system would be to design approximately a 7.5 percent initial safety margin to allow for expected solar flare degradation.

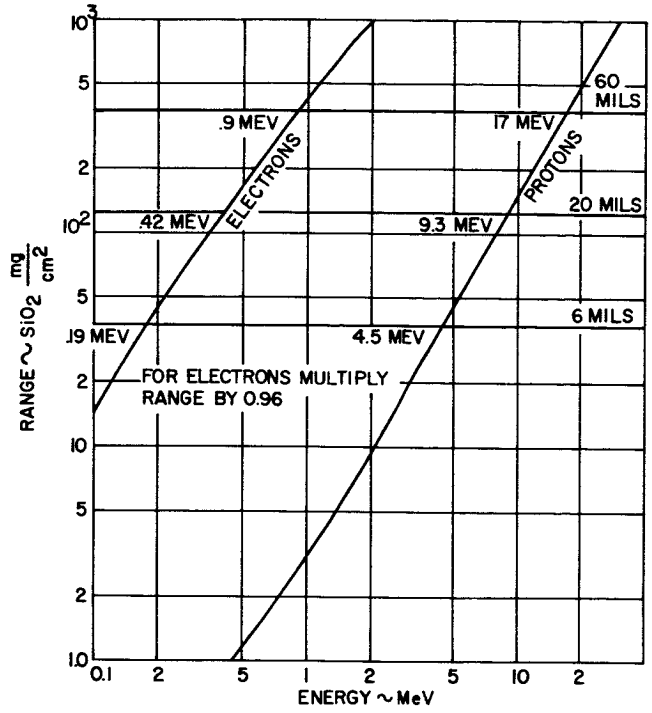


Figure 3-28. Range-Energy Curves for Electrons and Protons in Quartz

Several papers have been published on expected micrometeoroid fluxes in near-Earth space. The chance of penetrating a 6-mil cover slide of a solar cell panel is approximately once in 10 square feet per 1000 days. For a 40-square foot array the chance of a micrometeorite penetration is then 4(.365) = 1.46 per year. That is, there is a possibility of only 2 cells being damaged by micrometeorites.

In summary, it appears that the Van Allen radiation is not a problem at the synchronous orbit altitude. However, it would be preferable for protection against micrometeorite penetration and also for infrared filtering (heat effects) to use a 6-mil quartz cover over the silicon solar cells. If solar flares are anticipated, consideration should be given to increasing the solar cell area by approximately 7.5 percent.

## D. POWER SYSTEM DESIGN CONSIDERATIONS

The power supply configuration under consideration for the 3-axis stabilized SMS is shown in block diagram form in Figure 3-29. A series-parallel array of silicon solar cells mounted on a Sun-oriented panel is designed to develop a 28-volt potential at the output. Current from this array is used to charge a bank of secondary storage batteries through a battery charge regulator unit which will prevent current from passing from the battery back to the solar cell array.

The solar cell-battery combination drives the voltage regulator package, the output of which is the basic regulated voltage required by the various loads defined in Table 3-12. The battery charge regulator controls the rate at which the solar cells charge the batteries in order to prevent battery damage, and also

determines the point of switchover to battery power when the solar array output is insufficient, such as during acquisition and dark periods. Unusually high transient peak power requirements are supplied by operating both batteries and solar array simultaneously.

The one year minimum lifetime objective of the satellite rules out the use of primary batteries alone, above conventional fuel cells, and chemically-powered systems. The choice is therefore restricted to nuclear and solar sources. The maximum power requirement of less than 500 watts rules out nuclear systems in their present stage of development. Present nuclear systems do not become weight competitive until the power requirements exceed about 10 kilowatts.

TABLE 3-12

| Item | Acquisition (watt-hrs) | | | Normal Operation (watts) Avg | Peak |
|---|---|---|---|---|---|
| Attitude control and station keeping | 79 x 1 | = | 79 | 105.0 | 241.0 |
| Communications | 60 x 6 | = | 360 | 50.0 | 75.0 |
| Data handling | 31.1 x 6 | = | 186.6 | 33.1 | 33.1 |
| Power supply | 7 x 6 | = | 42 | 7.0 | 7.0 |
| Sensor equipment | 10 x 6 | = | 60 | 77.1 | 131.0 |
| Total | | | 727.6 | 272.2 | 488.2 |

The power supply concept shown in Figure 3-29 will use n-on-p silicon solar cells mounted on external paddles which are oriented to face the Sun. Nickel-cadmium batteries are used to supply power during the period of time when the vehicle is in the shadow of the Earth and to supplement the solar cells during periods of peak power requirements. A single-shot primary silver-zinc battery is included in the configuration to provide power during the Earth acquisition period when solar power is not available from the silicon solar cells. As an alternative design, the rechargeable secondary batteries have been over-designed to provide power to the vehicle during the acquisition period, as well as during normal operation, without recourse to any auxiliary primary battery. Over-design of the secondary battery, thereby eliminating the need for a primary battery, will increase the total weight and volume of the power system but will have the beneficial effect of requiring less percentage discharge on the battery cycle during normal load operations and thereby improving the inherent reliability of the power supply system. (Subsection F shows the variations in power supply configurations when either normal or limited operations are assumed during the occult periods.)

Assuming that the choice has been made to use solar cells and nickel-cadmium batteries as the prime power system for the SMS, it is then necessary to determine the average power required during sunlight time and dark time for the most occulted orbit. Consideration is given to added load requirements for converters and regulators, keeping in mind the desirability of providing separate converters for individual subsystems where independent failures can be isolated so as not to result in entire loss of the mission.

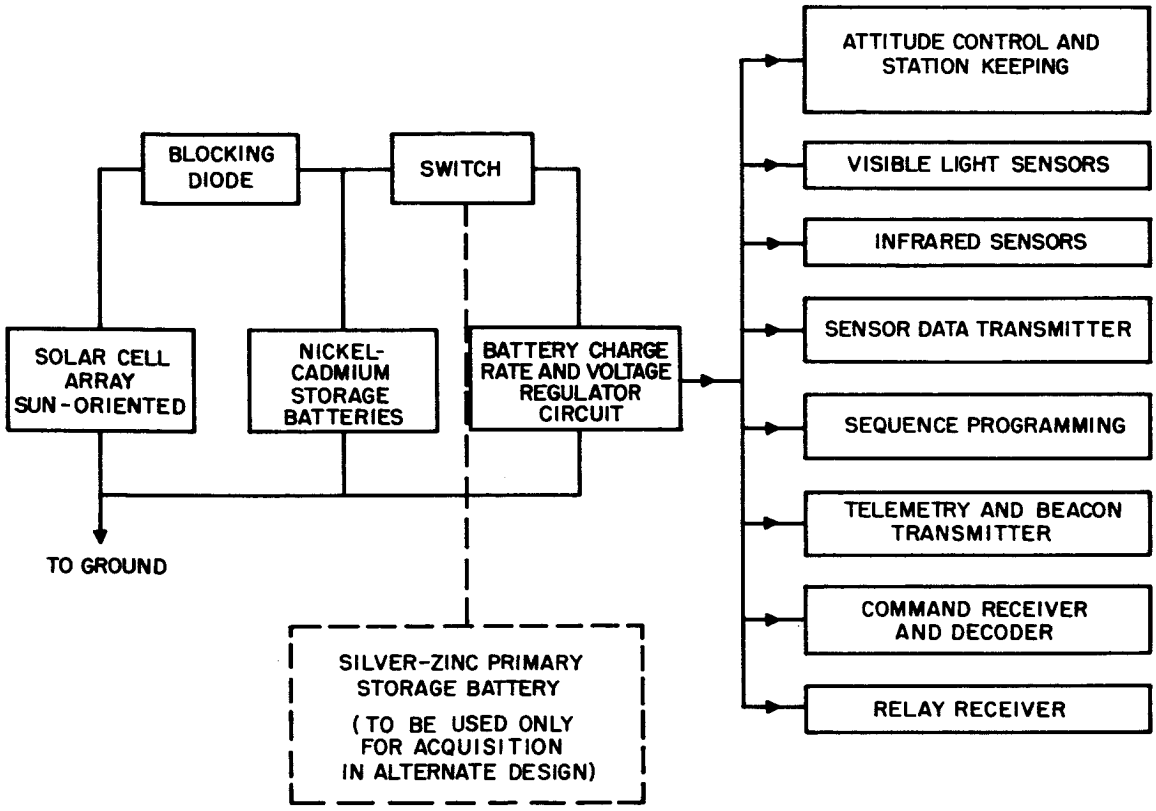


Figure 3-29. Power System Configuration

In the design of the solar array the following nine factors are considered.

(1) The match between system load line and the solar cell voltage vs. current characteristic, such that the operating point will be at or near the maximum power point.

(2) The effect and control of the solar-cell temperature.

(3) The orientation of the solar array. If the solar array is always pointing to the Sun, the problem is simplified since the output power during sunlight time will be constant. Further, if the vehicle is 3-axis stabilized, the horizon sensor will point the vehicle towards the Earth's center. The (single axis) solar array will always remain perpendicular to the orbital plane while the array will rotate about the pitch axis to face the Sun.

Assuming the Sun direction to be normal to the solar array at the equinoxes, the variation of the Sun direction at the solstices will be approximately ± 23.5° from the normal to the solar array. This results in 8.3 percent decrease in the Sun's illumination as a result of seasonal change.

(4) Series and parallel interconnection of solar cells for maximum reliability.

(5) Effects of radiation damage and the protection from same.

(6) Results of micrometeorite impact.

(7) Mounting and cell interconnection techniques.

(8) Control schemes for preventing battery discharge through the solar cells during dark periods.

(9) Panel structure and weights.

Factors affecting the design of the battery include:

(1) The maximum and minimum operating temperatures to be experienced.

(2) The maximum continuous charging rate which can occur.

(3) The maximum depth of discharge occurring during load cycle (prelaunch, acquisition or normal operation).

(4) Heat-transfer properties of the battery box and mounting provisions.

(5) Allowable weight for the power system.

During the equinox and solstice periods the SMS vehicle encounters a maximum shadow period of approximately 66 minutes in 24 hours. This occultation period occurs for a total of 82 days during the year. The battery will therefore experience a maximum of 82 cycles of this occult period in one year.

Referring to Figure 3-19 it can be seen that a discharge depth of over 80 percent of the battery capacity is theoretically possible under these conditions because a slow (constant current) charge rate over a period of almost 23 hours can be used with negligible possibility of damage to the cells. Since the power profile is such that there is a rapid occurrence of peak drains on the battery during normal operation, i.e., the sensing equipment is operational over consecutive half-hour cycles for extended periods of time, it will then be necessary to use a variable charge rate circuit rather than a slow constant current charge. This type of charging will charge the battery at a rapid rate immediately after an occult period and at a slower rate during normal operation. This will give the battery a rapid charge when it is in its lower state of charge, at which time the effects of rapid charge are not only "not harmful," but beneficial. The slower rate of charge takes place when the battery is almost up to its full charge state. In this condition, the heating effects of rapid charging could be detrimental to the battery.

## E. POWER AND ENERGY REQUIREMENTS OF THE SMS POWER SYSTEM

There are three sizes of satellites and primarily three types of vehicle configurations under consideration. The sizes are determined by Thor-Delta, Atlas-Agena, and Atlas-Centaur launch vehicle capabilities. For each vehicle, consideration is given to 3-axis stabilized, spin stabilized, and the gravity gradient configurations.

All systems will contain the following basic power consuming subsystems:

(1) Attitude control and station keeping equipment

(2) Sensor equipment

(3) Sensor data link transmitter

(4) Telemetry transmission subsystem

(5) Command receiver, decoder, control and timing units

(6) Power regulation, conversion and distribution

(7) Tracking aids (beacon)

(8) Communication relay for processed meteorological data

The estimated electrical power required for each of the subsystems of a medium capability satellite is listed in Table 3-12. It can be concluded from this table that the peak load is not likely to exceed 200 watts during acquisition and 500 watts during normal operation, nor is it likely to drop much below 100 watts during acquisition or 250 watts during normal operations.

The preferred technique of attitude control and stabilization consists of a torque generating system, horizon scanner, rate gyros, Sun-seeker, and a constant speed gyro wheel. The torque generating system will consist of a cold gas and reaction wheel system. Power requirements are different for the initial stabilization phase (acquisition) and for the long-term operational phase.

During the acquisition phase, approximately 6 hours, no power will be supplied by the solar cell array.

The sensors consist of a low-resolution vidicon camera system, a high-resolution image orthicon camera system, and an infrared scanner for heat budget measurements. One wide angle view with as many as 25 additional selected narrow angle images are taken during a 30-minute interval, each requiring 10 seconds for transmission back to Earth.

A summary of the power requirements of each subsystem for the medium weight 3-axis stabilized satellite are approximately as shown in Table 3-12. Allowances for the necessary inverter and converter efficiencies are included in these power requirements.

The loads in Table 3-12 do not include any factor for electrical system redundancy. Although it is safe to assume that the more critical subsystems will be duplicated for reliability reasons, the power supply design is based on the fact that, except for the command receiver, only one of each unit will be in operation at a time.

## F. POWER SYSTEM DESIGN ILLUSTRATION

This subsection presents a detailed parametric analysis for determining the power system configuration for the SMS vehicle. For purposes of illustration, the 3-axis stabilized medium capability satellite is chosen.

Table 3-13 gives a tabulation of the power requirements for the medium capability 3-axis stabilized satellite configuration.

In order to compute the solar array and battery requirements (without redundancy) the following parameters will be assumed:

(1) The power density of the solar array is 7.5 watts/ft$^2$.

(2) Weight of solar array (with mounting) is 1.5 lbs/ft$^2$.

(3) Maximum allowed depth of discharge of secondary battery (Ni-Cd) is 65 percent (during occult).

(4) Specific energy of Ni-Cd battery is 12 watt-hrs/lb.

(5) Specific energy of primary battery (Ag-Zn) is 40 watt-hrs/lb.

The design will consider two basic alternatives: 1) all normal satellite functions are carried on even during the period in which the satellite is in an eclipse of the Sun's energy, and 2) only the minimum "housekeeping" equipment such as telemetering, command, and heating units are in operation during the dark period (limited operation). Each of these two alternatives is considered in a design where a) both primary batteries (for acquisition) and secondary batteries (for normal operation) are employed, and the design b) where the secondary batteries are employed for both functions. In addition, each alternative case when in normal SMS operation will be considered under two types of load programs: one in which the sensor equipment is in random operation, i.e., the peak power drainage of the various sensing equipments could occur either individually or simultaneously during the 30-minute cycle; or secondly, when the sensor equipment is in a staggered operation, thus preventing a large peak power drainage from occurring at any one time.

Alternative (1a)

Normal operation during dark period with loads occurring randomly:

During acquisition, 727.6 watt-hrs are consumed.

During track, 272.2 watts (avg) and 487.1 watts (peak) are required of the power supply.

Using Ag-Zn primary batteries for the acquisition, 727.6/40 = 18.2 lbs.

The solar array supplies 7.5 watts/ft$^2$ at a weight of 1.5 lbs/ft$^2$. Hence the specific power of the solar array is 7.5/1.5 = 5 watts/lb.

The weight of the solar array (mounting included) required to supply 272.2 watts is 272.2/5 = 54.5 lbs, + 15 percent* = 63 lbs.

*An allowance of 15 percent is made for variations of angle between direction of solar radiation and the normal to the solar cell array.

TABLE 3-13
POWER REQUIREMENTS

| Item | Acquisition (watts) | Track Avg (watts) | Track Peak (watts) |
|---|---|---|---|
| Attitude Control & Station Keeping | | | |
| Cold gas system (vel injection corr) | 24 for 1 hr | 24 | 24 |
| Reaction wheels (2) | 0 | 9 | 18 |
| Constant speed wheel (1) | 0 | 18 | 36 |
| Horizon sensor (1) | 0 | 4 | 4 |
| Sun sensor | 0 | 0 | 0 |
| Rate gyros (3) | 42 for 1 hr | 24 | 84 |
| Electronic control assy (1) | 13 for 1 hr | 26 | 75 |
| Total | 79 | 105 | 241 |
| Communications | | | |
| Telemetry data transmitter (2) | 15 for 6 hrs | 15 | 15 |
| Sensor data transmitter (2) | 40 for 6 hrs | 30 | 55 |
| Relay receiver (2) | 3 for 6 hrs | 3 | 3 |
| Command receiver (2) | 2 for 6 hrs | 2 | 2 |
| Antenna system | 0 for 6 hrs | 0 | 0 |
| Total | 60.0 | 50.0 | 75.0 |

TABLE 3-13 (Cont'd)

| Item | Acquisition (watts) | Track Avg (watts) | Track Peak (watts) |
|---|---|---|---|
| 3. Data Handling | | | |
| Telemetry (1) | 17.6 for 6 hrs | 17.6 | 17.6 |
| Sensor (1) | 0 for 6 hrs | 2.0 | 2.0 |
| Command (1) | 11.5 for 6 hrs | 11.5 | 11.5 |
| Programming | 2.0 for 6 hrs | 2.0 | 2.0 |
| Total | 31.1 | 33.1 | 33.1 |
| 4. Power Supply | | | |
| Batteries - NiCd | 0 | 0 | 0 |
| Solar paddles | 0 | 0 | 0 |
| Charge regulator | 7.0 for 6 hrs | 7.0 | 7.0 |
| Total | 7.0 | 7.0 | 7.0 |
| 5. Sensor Equipment | | | |
| Low resolution, full Earth disc sys | 0 | 7.0 | 15 |
| High resolution, narrow field of view sys | 0 | 2.4 | 3 |
| Scanning mirror | 0 | 2.4 | 3 |
| High resolution TV camera | 0 | 47 | 50 |
| High resolution IR Earth heat budget | 10.0 for 6 hrs | 18.3 | 30 |
| Total | 10.0 | 77.1 | 131.0 |

The maximum dark period in the synchronous orbit is approximately 66 minutes. Considering the total dark period as 70 minutes for a conservative estimate, the secondary battery would be required to supply 272 x 70/60 = 320 watt-hrs.

Assuming that the depth of discharge of the batteries during the occult period is 65 percent, the secondary battery size = 320/.65 = 493 watt-hrs. Since Ni-Cd has a specific power of 12 watt-hrs/lb, the size of the secondary battery = 493/12 = 41 lbs. A Sun-oriented solar-paddle control system weights 3 lbs and a battery/solar-paddle charge regulator circuit for the power supply system weighs approximately 12 lbs. The total power system weight is, therefore, as follows:

| | |
|---|---|
| Primary batteries | 18.2 lbs |
| Secondary batteries | 41 lbs |
| Solar array | 63 lbs |
| Regulator-selector unit | 12 lbs |
| Solar-paddle drive | 3 lbs |
| Total = | 137.2 lbs |

The peak power which occurs for about 5 minutes each half-hour cycle will cause

$$\frac{1\ (487.1-272.2)}{6\ (493)} = .073 \text{ or } 7.3 \text{ percent depth of discharge}$$

Alternative (lb)

By increasing the size of the secondary battery supply in order to eliminate the necessity for primary batteries, one finds that 272 x 70/60 = 320 watt-hrs are required during track, and 727.6 watt-hrs are required during acquisition. Therefore, 727.6/12 = 61 lbs. Ni-Cd batteries are required. Hence, 320/727.6 = 44 percent of depth of discharge is required of the Ni-Cd batteries during the occult period. Under sunlight operations, the battery will be called upon to supply, for about 5 minutes of each half-hour cycle, a peak of 487.1 watts. Thus 1/6 (487.1-272)/726.6 = 0.049 or 4.9 percent depth of discharge is required of the battery during peak loads in each load cycle.

The total system weight is, therefore, as follows:

| | |
|---|---|
| Primary battery | 0 lbs |
| Secondary batteries | 61 |
| Solar array | 63 |
| Regulator-selector | 12 |
| Solar-paddle drive | 3 |
| Total | 139 lbs |

Thus, increasing the secondary battery results in only a total increase in power supply weight of about 1.3 percent but, more significantly, it increases the secondary battery reliability from an operation at 65 percent down to 44 percent depth of discharge during the maximum occult period. Furthermore, short reacquisition periods can be tolerated without risking a complete system failure.

Alternative (2a)

Limited operation during dark period, with loads occurring randomly:

An average of 272 watts are required during normal operation.

Solar array weight = 272/5 = 54.6 lbs, + 15 percent = 63 lbs and 727.6 watt-hrs are required during acquisition. Therefore 727.6/40 = 18.2 lbs is the weight of the required primary batteries.

Assuming that the secondary batteries will be designed for 10 percent depth of discharge to cover peak wattage requirements during normal sunlight operations, and a 65 percent depth of discharge to cover occult period power requirements, the secondary battery capacity is 1/6 (487.1-272)/ Secondary Battery Capacity = 10 percent. Therefore, secondary battery capacity = 358 watt-hrs; secondary battery weight = 358/12 = 30 lbs. (During darkness, the vehicle requires approximately 82 watt/hr to carry on command, telemetering, heat control, etc. As a result, during the maximum eclipse period of 70 minutes, the secondary battery will have to supply 82.0 x 70/60 = 96 watt-hrs. Assuming that a peak wattage period occurs just previous to the maximum eclipse period, the secondary battery would have to have a capacity of only 1/6(487.1-272)+96/.65 = 203 watt-hrs. Hence, this load will not be the controlling design factor in the secondary battery capacity.)

The total system weight is, therefore, as follows:

| | |
|---|---|
| Primary battery | 18.2 lbs |
| Secondary battery | 30 |
| Solar array | 63 |
| Regulator-selector | 12 |
| Solar-paddle drive | 3 |
| Total | 126.2 lbs |

Alternative (2b)

Without primary batteries the resulting system weight, as previously determined under Alternative (1b), is:

| | |
|---|---|
| Primary battery | 0 lbs |
| Secondary battery | 61 |
| Solar array | 63 |
| Regulator selector | 12 |
| Solar-paddle drive | 3 |
| Total | 139.0 lbs |

The reason the design with secondary batteries alone remains unchanged is a result of the fact that the power requirements for acquisition and (average) track are unchanged during limited operation as compared to normal operation. The only variation is in occult power requirements. But this does not affect the size of the secondary battery, since the acquisition power determines the secondary battery capacity.

There is therefore a difference of 12.8 lbs or 9.2 percent savings gained by utilizing both a primary battery and a secondary battery for the case in which the satellite is in limited operation.

Staggering Equipment Power Loads

From Table 3-13, it should be noticed that if the IR equipment operation is staggered with respect to the video equipment such that the IR sensors are not operating during the 5 minute operations period of the video sensors, it will enable the system to operate at reduced peak powers.

Therefore, instead of the peak being 15+3+3+50+60 = 131, it will become 15+3+3+50+10 = 81 watts. Hence, during the 5 minute operations period the total peak power of the system will be:

| | |
|---|---|
| Attitude control and station keeping | 241.0 watts |
| Communications | 75.0 |
| Data handling | 33.1 |
| Power supply | 7.0 |
| Sensor equipment | 81.0 |
| Total | 437.1 watts |

For Alternatives (1a) and (1b): The system design weights remain unchanged. However, the peak power will result in

$$\frac{1/6\ (437.1 - 272)}{493} = 5.6 \text{ percent}$$

a 5.6 percent depth of discharge when using primary and secondary batteries; and peak power will result in only

$$\frac{1/6\ (437.1 - 272)}{727.6} = 3.8 \text{ percent}$$

a 3.8 percent depth of discharge when using secondary batteries alone.

For Alternative (2a), the primary battery weight (as before) is 727.6/40 = 18.2 lbs. The secondary capacity is

$$\frac{1/6(437.1 - 272)}{\text{secondary battery capacity}} = 10 \text{ percent}$$

Thus secondary battery capacity is 275 watt-hrs and secondary battery weight is 275/12 = 22.9 lbs.

The resulting power system weight is:

| | |
|---|---|
| Primary batteries | 18.2 lbs |
| Secondary batteries | 22.9 |
| Solar array | 63 |
| Regulator-selector | 12 |
| Solar-paddle drive | 3 |
| Total | 119.1 lbs |

With secondary batteries alone, i.e., Alternative (2b), no weight reduction is realized by staggering the loads.

Summing up, the results obtained are shown in Table 3-14.

TABLE 3-14
3-AXIS MEDIUM CAPABILITY POWER SYSTEM (WEIGHT) CONFIGURATIONS

| | | Random Cycling System Wt (lbs) | | Staggered Cycling System Wt (lb |
|---|---|---|---|---|
| Alternative 1 (Normal operation during dark period) | (a) Prim. and Sec. Batt. | 137.2 | (a) | 137.2 |
| | (b) Sec. alone | 139.0 | (b) | 139.0 |
| Alternative 2 (Limited operation during dark period) | (a) Prim. and Sec. Batt. | 126.2 | (a) | 119.1 |
| | (b) Sec. alone | 139.0 | (b) | 139.0 |

Conclusions

When the full system operation is required during the occult period for purposes of increased reliability, it is preferable to use a secondary battery alone type design in spite of a slight weight disadvantage.

When the equipment is in limited operation during occult periods, i.e., Alternative 2, and the sensors are in random cycling, there is a 9.2 percent weight savings in using both primary and secondary batteries in the power design. If in addition the cycling is carried on in a staggered manner, there is a total saving in weight of 14.3 percent when using both primary and secondary batteries in preference to secondaries alone.

## G. BIBLIOGRAPHY


1. Power Supplies for Orbital and Space Vehicles - John H. Huth, Volume 1, Advances in Space Science, Academic Press, New York, 1959
2. Advanced Energy Conversion - Vol. I, Pergamon Press (Symposium of Thermoelectric Energy Conversion), 1961
3. Interplanetary Space Probe Auxiliary Power Systems - R. C. Hamilton, Jet Propulsion Laboratory, Pasadena, California, June 1959
4. Solar Concentration Cells - B. H. Clampitt and D. E. German, Boeing Airplane Co., April 1960
5. Space Power Systems, Vol. III and Vol. IV - Snyder, N. W. Academic Press, New York, 1961
6. Turboelectric Space Power Systems - V. R. Vovaik and T. A. Johnson, Thompson Ramo Woolridge Inc., January 1960
7. Space Vehicle Electrical Power Generation and Cooling Systems - S. Davidman, RAC 655-905, January 1961
8. The Battery Field - S. Padwo, Electrical Design News, January 1963
9. IRE Transactions on Military Electronics, January 1962
10. Hermetically Sealed Nickel-Cadmium Batteries for Aerospace Applications, AIEE paper No. CP61-426
11. Electrochemical Cells for Space Power, R.C. Shair, ARS Report No. 2165-61, October 1961
12. Space Vehicle Power Systems - E. B. Zwick, and R. L. Zimmerman, ARS Journal, Vol. 29, No. 8, August 1959
13. Available Power Systems for Space Vehicles - H. J. Howard and R. W. McJones, ARS Report No. 1032-59, 1959
14. Some Comments on the Transmission of Power by the Use of Microwave Beams - IRE Transactions on Antennas and Propagation, Vol 9, November 1961
15. Photochemical Regenerator Fuel Cell - W. R. Monyer, H. Silverman and M. Eisenberg, 15th Annual Power Sources Conference, Fort Monmouth, New Jersey
16. Nuclear Space Power Systems - H. M. Dieckamp, Atomics International, July 1962
17. Nuclear Auxiliary Power - Ralph Balent, IRE Transactions on Nuclear Science, Vol. NS-9, January 1962
18. SNAP Radioisotopic Power Systems - J. G. Morsi, IRE Transaction on Nuclear Science, Vol. NS-9, January 1962
19. Preliminary Engineering Analysis of Power Sources for Space Vehicles, Technical Memorandum RAD-TM-61-12, AF Ballistic Systems Division, USAF, Inglewood, California, August 1961

20. Space Radiation Effects - J. F. Willer, F. J. Campbell, J. W. Kallander, Electro-Technology, February 1962

21. Solar Cell Performance in the Artifical Radiation Belt - R. E. Fischell, ARS Space Power Systems Conference, September 1962

22. Design Criteria for Satellite Power Supplies Using Radiation Resistant Solar Cells - B. Ross, Hoffman Electronics Corp., El Monte, California, March 1963

23. N-on-P Solar Cells Gaining Wider Use - B. Miller, Aviation Week, March 4, 1963

# SECTION 4 - THERMAL CONTROL

## A. SUMMARY AND INTRODUCTION

### 1. Summary

Considerations, analyses, and solutions of the overall (and detailed) problem of thermal control of the Synchronous Meteorological Satellite (SMS) are presented in this section. The totality of energy sources and environmental conditions affecting the spacecraft in orbit are analyzed and evaluated.

Analytic and numerical solutions to the thermal interaction equations between the Sun and the Earth, and the satellite are given for various shapes of satellites. The umbra and penumbra characteristics are shown as a function of calendar time.

Generalized thermal-balance differential equations are presented for the three basic configurations, spin-stabilized, three-axis stabilized, and gravity-gradient stabilized. Satellite temperatures are shown as a function of time, surface characteristics, orientation, and internal power density.

Analyses are presented for thermal control by purely passive means, energy storage devices, shutter systems, forced convection loop (cold plate) systems, vapor, gas, and absorption cycle refrigerations, and thermoelectric cooling as applied to the SMS. Comparisons of weight, complexity, and integrability of the various thermal control systems are shown. Analyses and solutions to the problems of infrared sensor cooling and solar cell thermal protection are presented.

### 2. Introduction

The importance of spacecraft temperature control has been recognized in the early history of the space effort. Temperature control considerations played an eminent role in the design of the Vanguard and Explorer series and in all subsequent major space programs. A number of satellites and space vehicles have met with failure because of inadequate thermal control provisions. It is the purpose of this Section 4 to present the analyses and the solutions to the thermal control problems of the Synchronous Meteorological Satellite (SMS) system. The application of these analyses and solutions to the various SMS configurations are discussed in Sections 2 through 6 (Vol. 2) and in Section 5 (Vol. 6) of this report.

The basic temperature control problem associated with a satellite is to maintain equipment and payload temperatures at a safe level. This temperature control problem involves the following three basic areas of investigation:

(1) Recognition and analysis of all possible heat sources, sinks, and paths that affect the satellite throughout its lifetime in orbit, and discrimination between significant and negligible heat sources, sinks, and paths.

(2) Development, improvement, optimization, and integration of suitable surfaces, surface coatings, insulation, heat-storage devices, heat paths, and heat pumps necessary to maintain the desired temperature level.

(3) Experimental verification of the adequacy of the thermal design and the acceptability of the overall system concept.

Unlike the thermal environment within the atmosphere of a planet, the space environment has no temperature in the conventional sense. The high spatial kinetic temperatures (as high as $10^{10}$ degrees K within the Van Allen belts and $10^{6}$ degrees K within the solar environment at a distance of 1 astronomical unit) associated with high velocity particles have negligible effects on a satellite's thermal balance. This is because the peak mass flux in these regions is only between $10^{-19}$ to $10^{-15}$ gram per square centimeter-steradian-second. These high temperatures are thus only equivalent kinetic temperatures computed from particle velocities that describe the kinetic energy state of the particle.

The temperature control problem for the Synchronous Meteorological Satellite differs in a number of ways from that of a conventional, low altitude satellite. The thermal control of the SMS is importantly influenced by the fact that the satellite is in Earth shadow less than 1 percent (74.7 hours) of a year. The corresponding shadow times for conventional, low altitude satellites can be as high as 50 percent, depending on the hour and day of launch. In addition, the shadow periods of the SMS do not occur in symmetrical intervals: For almost 10 months of the year such a satellite is constantly exposed to sunlight. During March and September of each year, the satellite enters a daily shadow pattern with shadow periods ranging from zero to 65.95 minutes per day in the umbra and from zero to 24.1 minutes per day in the penumbra (see Figure 4-1). The

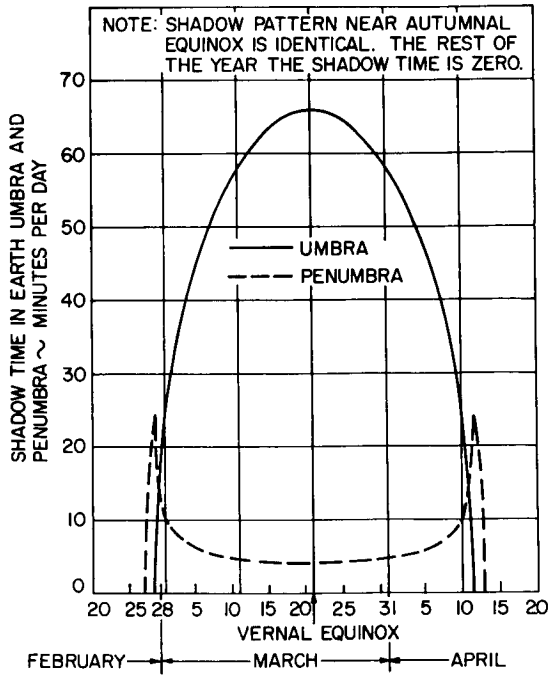


Figure 4-1. Umbra and Penumbra Patterns for a Synchronous Equatorial Satellite

umbra is the conical total shadow projected from a planet on the side opposite the Sun. The penumbra is the partial shadow between the umbra and the full-light region. In the penumbra, the light of the Sun is only partially cut off by the planet. The time the satellite is in the penumbra is only 13.35 percent of that of the umbra.

Another important consideration in the temperature control of the Synchronous Meteorological Satellite is the number of external heat sources that contribute significantly to the thermal environment of the satellite. In contrast to low orbit satellite external thermal sources, the only external thermal source of any significance in the case of the SMS is the Sun. As will be shown later, the terrestrial and reflected (albedo)* radiations at synchronous altitude (19,320 nautical miles) are 2.16 percent and 1.55 percent of their respective near-Earth values and only 0.323 percent and 0.62 percent of the solar flux, respectively.

The long orbital period of the SMS is another significant factor in the thermal analysis. Low altitude satellites have orbital periods in the order of 1.5 to 2 hours, thus making possible the utilization of thermal inertia to dampen out inherent orbital temperature fluctuations. With an orbital period that is 12 to 16 times as long (24 hours for the SMS), the additional degree of freedom of building thermal inertia into the satellite is practically nonexistent.

## B. FACTORS INFLUENCING THERMAL DESIGN

### 1. Introduction

The peak heat inputs to a space vehicle (or a ballistic missile) usually occur at the terminal points of its path, that is, the launch and re-entry points. These heat pulses are of short duration, compared with the total mission time, but are of such magnitude that special precautions are necessary to prevent overtemperatures and/or structural failure.

Theoretically, the trajectory of a satellite has no bound; that is, the flight path has only one terminal point, the launch site. The aerodynamic heating during the re-entry phase is generally orders of magnitude larger than the heating during the launch phase. Thus the terminal protection requirements are less stringent.

For this study, it is assumed that the carrier vehicle will have the necessary launch-phase thermal protection (insulation, heat sink, or ablative coating) to keep the satellite temperature within the required limits. It should be pointed out that recent tests have indicated that with temperatures encountered during the launch phase, the outgasing of shroud material contaminates exposed satellite surfaces. The elimination of this condition is imperative for successful passive temperature control.

---

* The term albedo is used here in referring to the returned energy rather than the ratio of this reflected energy to the solar energy.

The temperature of a satellite orbiting the Earth is a function of the following factors:

(1) The energy incident on the surface (external and internal)

(2) The nature of the skin surface

(3) The orientation of the skin relative to the incident energy

(4) The skin geometry

(5) The energy emitted by the vehicle surface

(6) The thermal capacity of the shell and equipment

2. Thermal Environment

The energy sources that influence the temperature of a satellite in orbit can be divided into two basic groups, external sources and internal sources. The external energy sources can be further subdivided into two main categories. One is the energy the satellite receives from remote sources; this includes cosmic, solar, terrestrial, albedo, lunar, and planetary radiation incident on the satellite. The other main category is the energy the satellite receives by contact with local surroundings. This includes the energy the satellite receives from aerodynamic heating and from meteoric impact.

a. Remote Energy Sources

1) Solar Radiation. The Sun is a slowly rotating body of hot and highly condensed gas surrounded by a layer of rarefied gas. The Sun emits electromagnetic (wave lengths ranging from 1 to 100,000 Angstroms) and corpuscular radiation in all directions. Most of the radiation is in the visible and infrared spectrum; the energy radiated in X-ray and ultraviolet bands is only an insignificant portion of the total solar energy.

In the vicinity of the Earth, the solar flux density, or the Earth's solar constant, is 442 Btu per hour-square foot (0.14 watt/cm$^2$). The Earth's solar constant is defined at the rate at which solar radiation impinges on a surface of unit area normal to the Sun's direction; the surface is outside the Earth's atmosphere at the Earth's mean distance from the Sun. A similar definition would hold for the solar constant for any planet. In the vicinity of the Earth, the solar constant varies from 97 percent to 103 percent of the mean value of 442 Btu per hour-square foot. Thus, a body at a point outside the Earth's atmosphere will absorb, if the absorptivity is unity, 442 Btu (± 3 percent) each hour for every square foot of surface area that is normal to the path of solar-energy propagation.

In the absence of an atmosphere, the solar radiation absorbed by a surface in space depends only on the zenith angle, $\phi$,* of the Sun, the absorptivity of the material with respect to solar radiation, and the exposed

* The zenith angle is the angle between a line connecting the centers of the Sun and the surface, and the normal to the surface area in question.

surface area. Thus, the solar energy, $Q_s$, received by a satellite surface is:

$$Q_s = \alpha_s SA \cos \phi \tag{4-1}$$

where $S$ = solar constant, 442 Btu/hr ft$^2$

$\alpha_s$ = the absorptivity of the material with respect to solar radiation

$A$ = the surface area in question

The orbit of the Earth around the Sun is an ellipse with an eccentricity of 0.0167. This means that when the Earth is farthest from the Sun (about July 1), the distance from Earth to Sun is 101.67 percent of the mean solar distance ($149.5985 \times 10^6 \pm 500$ kilometers, according to recent satellite data); when the Earth is nearest to the Sun (about January 1), the distance from Earth to Sun is 98.33 percent of the mean solar distance.

The Earth's axis of rotation is fixed (neglecting precession) in inertial space and is tilted 66.5 degrees to the ecliptic plane. This means that the plane of the Earth's equator is inclined 23.5 degrees to the orbit of the Earth; the South Pole is inclined towards the Sun in December, and the North Pole is inclined toward the Sun in June (see Figure 4-2). A satellite that maintains an orbit in the plane of the equator at a sufficiently high altitude will be exposed to direct solar radiation most of the year except during the two equinoxes (see Figure 4-2). The exact umbra and penumbra characteristics during an equinoctial passage are shown in Figure 4-1.

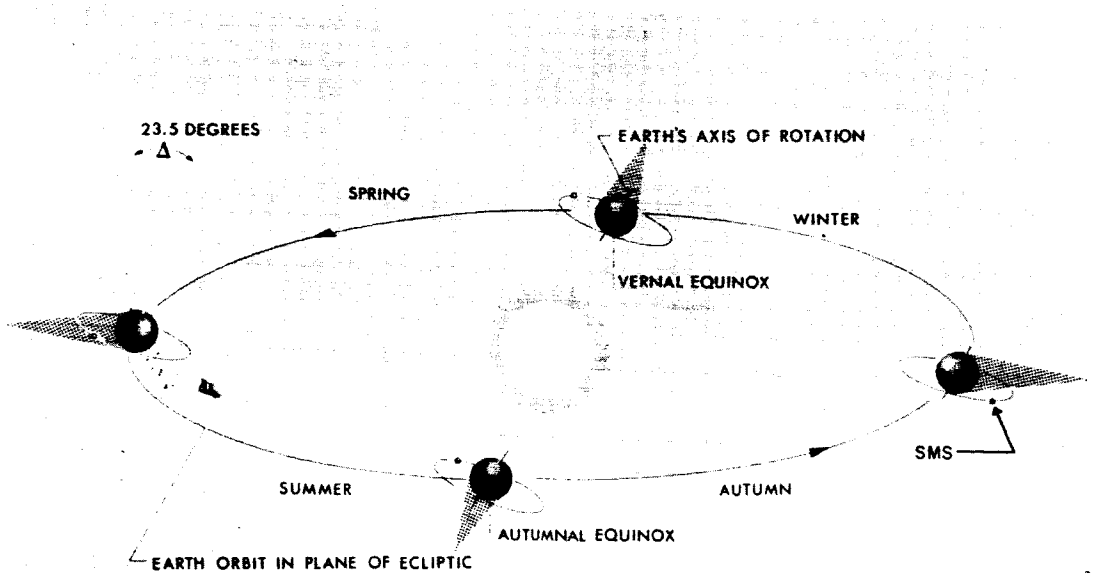


Figure 4-2. Effect of the Earth's Yearly Motion

The satellite thermal environment due to solar radiation will be different for the spin-stabilized configuration and for the three-axis stabilized configuration. For a cylindrically shaped satellite of diameter, D, and length, L, the received solar radiation is given by

$$Q_s = S\alpha_s \left(LD \operatorname{Sin} \phi + \frac{\pi D^2}{4} \operatorname{Cos} \phi\right) \tag{4-2}$$

where $\phi$ is the angle between the cylinder axis and the Sun-Earth vector. For the spin-stabilized configuration, $\phi$ is given by

$$\phi = \operatorname{Cos}^{-1}\left[\operatorname{Sin} \Delta \operatorname{Sin} (\omega_{E/S} t)\right] \tag{4-3}$$

where $\Delta$ = angle between the Earth axis of rotation and the normal to the ecliptic plane, degrees

$\omega_{E/S}$ = angular velocity of the Earth relative to the Sun

$t$ = time ($t = 0$ when Earth is at vernal equinox).

For the three-axis stabilized configuration $\phi$ is given by

$$\phi = \operatorname{Cos}^{-1}\left[\operatorname{Cos}\left(\omega_{E/S} t\right) \operatorname{Cos}\left(\omega_{S/E} t'\right) + \operatorname{Sin}\left(\omega_{E/S} t\right) \operatorname{Sin}\left(\omega_{S/E} t'\right) \operatorname{Cos} \Delta\right] \tag{4-4}$$

where $\omega_{S/E}$ = angular velocity of the satellite relative to the Earth

$t'$ = time ($t' = 0$ when cylinder axis is parallel to the Sun-vernal equinox vector).

The histories of the solar heat input to the spin-stabilized and the three-axis stabilized spacecraft configurations are shown in Figures 4-3 and 4-4, respectively, for the conditions specified on the figures.

2) Terrestrial (Infrared) Radiation. The temperature of the Earth is an equilibrium temperature that the Earth and its atmosphere maintain with the solar irradiation in order to keep the Earth's internal energy constant. The existence of such an equilibrium temperature is well established because there has been no significant change in the mean temperature of the Earth and its atmosphere in recorded history. To the equilibrium temperature, $T_E$, there corresponds an average black-body radiation flux that is given by $\sigma T_E^4$, where $\sigma$ is the Stefan-Boltzmann constant. The magnitude of this radiation flux at a given location on Earth depends on the local surface temperature and emission characteristics. As a result, terrestrial radiation will vary with topography, season, the time of day, and atmospheric conditions such as cloud coverage.

It is, however, possible to compute the average terrestrial radiation, neglecting the variations in local emission characteristics, on the basis of the thermal balance between the Sun and the Earth. Since the Earth is in thermal equilibrium, the energy that it radiates at a given instant must be equal to the energy it absorbs from the Sun. (It is assumed here that the Sun is the only significant energy source.) The total energy per unit time that the Earth absorbs from the Sun is given by

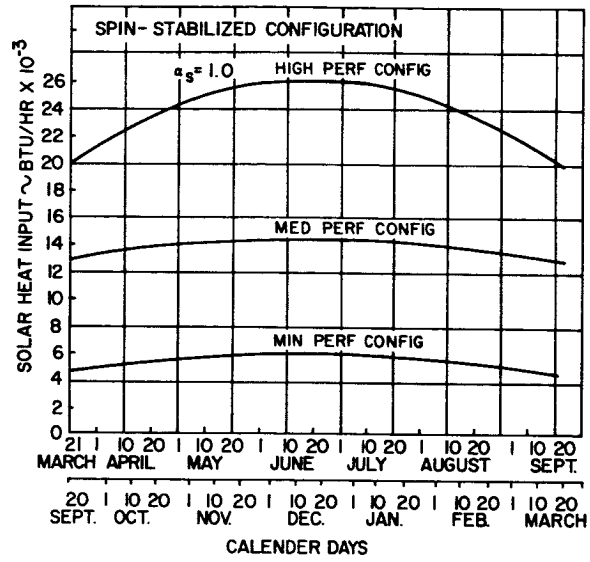


Figure 4-3. Variation of Solar Heat Input with Calendar Time Spin-Stabilized Configuration

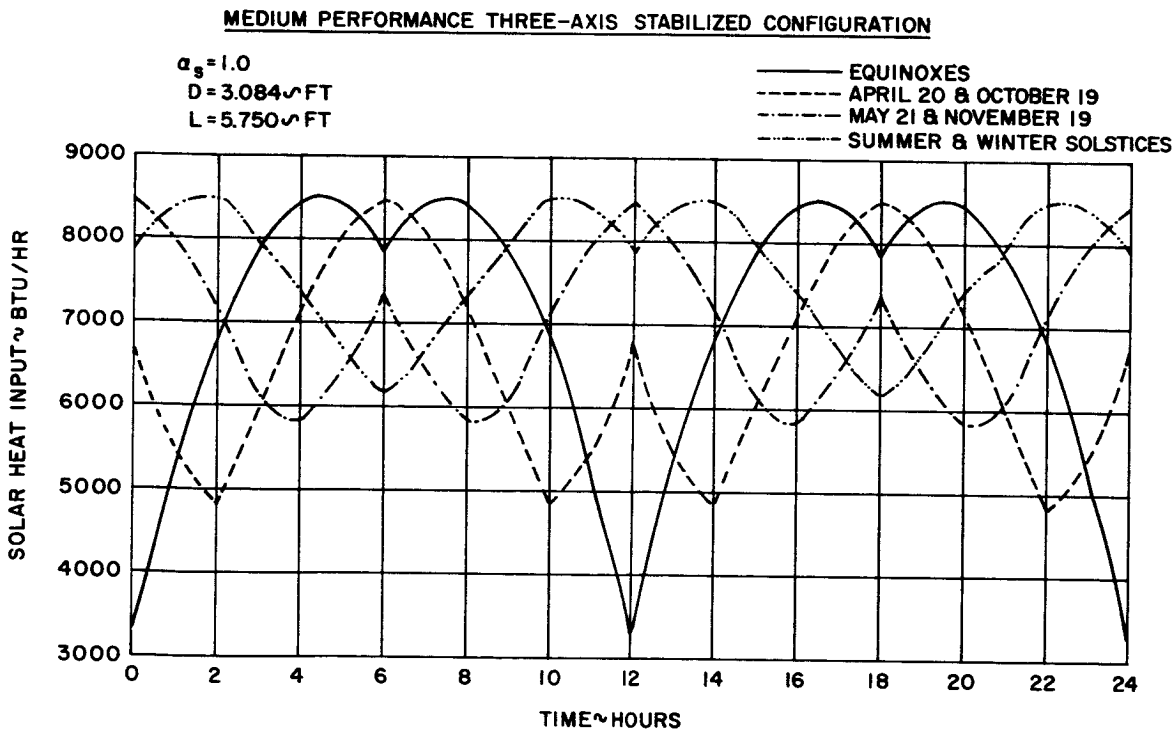


Figure 4-4. Variation of Solar Heat Input with Time of Day and Seasons

$$E = (1 - a_e)\, S\, \pi R_e^2 \tag{4-5}$$

where $E$ = energy that the Earth absorbs from Sun

$a_e$ = albedo of the Earth

$S$ = solar constant

$R_e$ = radius of the Earth

The Earth area effective in absorbing solar radiation is the projected area, $\pi R_e^2$, rather than the total surface area, $4\pi R_e^2$. The energy emitted per unit time from the Earth's entire surface is given by

$$\vec{E} = E_e (4\pi R_e^2) \tag{4-6}$$

where $\vec{E}$ = energy emitted by Earth

$E_e$ = total energy rate emitted by the Earth per unit Earth area

Equating E to $\vec{E}$ for equilibrium gives

$$E_e = \left(\frac{1 - a_e}{4}\right) S \tag{4-7}$$

The magnitude of the average terrestrial radiation is thus a function of the effective albedo of the Earth, $a_e$, and the solar constant, S. (See the next subsection for a discussion of the Earth's albedo.)

To determine the effect of terrestrial radiation on the heat balance of a satellite, it is important to establish the amount of this energy that will be intercepted by the satellite. Because terrestrial thermal radiation is not emitted in parallel rays, the amount of radiation intercepted by a satellite will depend on the satellite configuration and external shape. For a spherical satellite, the variation of terrestrial thermal emission with altitude is computed from

$$(Q_e)_{sp} = 2\left(\frac{1 - a_e}{4}\right) S \left(1 - \frac{\sqrt{2R_e h + h^2}}{R_e + h}\right) \tag{4-8}$$

where $(Q_e)_{sp}$ = terrestrial radiation received by spherical satellite, Btu per hour-square foot

$R_e$ = radius of the Earth, nautical miles

$h$ = altitude above the Earth, nautical miles

A plot of Eq. 4-8 is shown in Figure 4-5 with parameter $(Q_e)_{sp} / \left(\frac{1 - a_e}{4}\right) S$ as the ordinate. This plot will preserve the validity of the curve as more accurate values of the Earth albedo, $a_e$, and the solar constant, S, become available.

For a flat satellite surface, a more complicated expression can be derived. Figure 4-6 shows the variation of Earth thermal emission with altitude and surface attitude angle, $\gamma$, for a flat surface (Ref. 4-1).

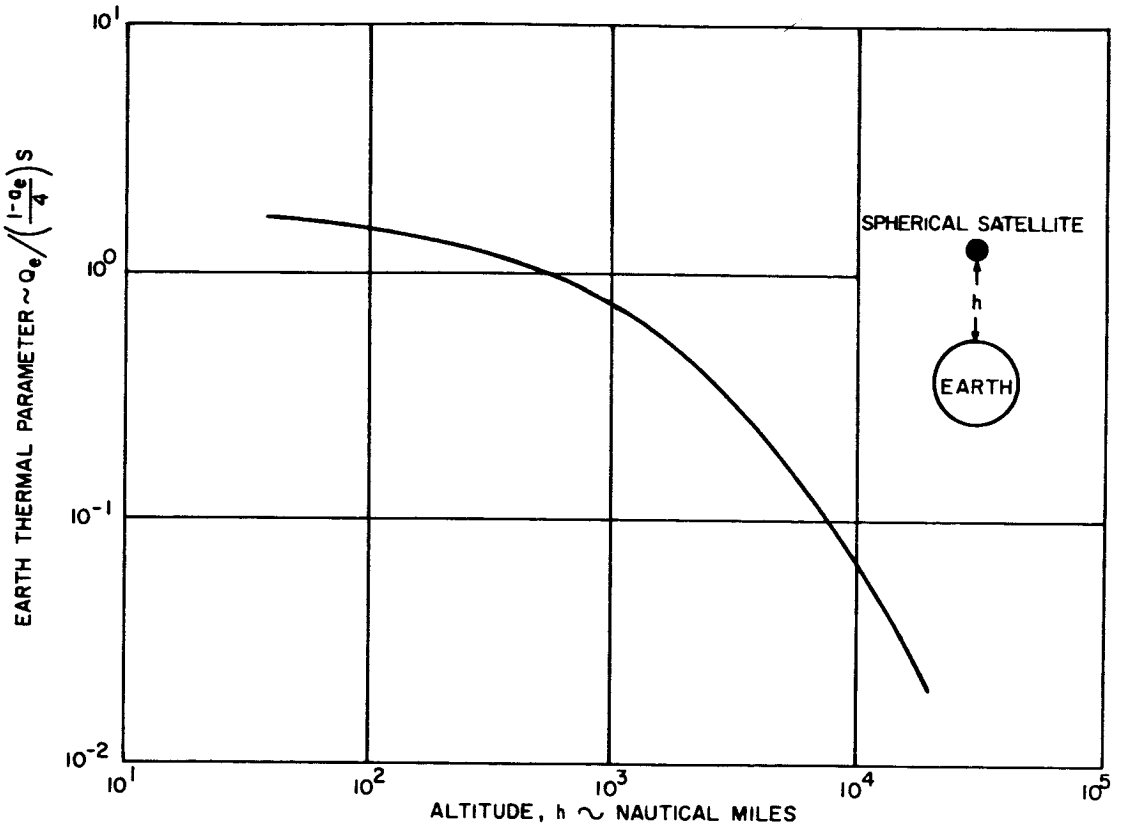


Figure 4-5. Parameter for Earth Thermal Emission Incident to a Spherical Satellite as a Function of Altitude

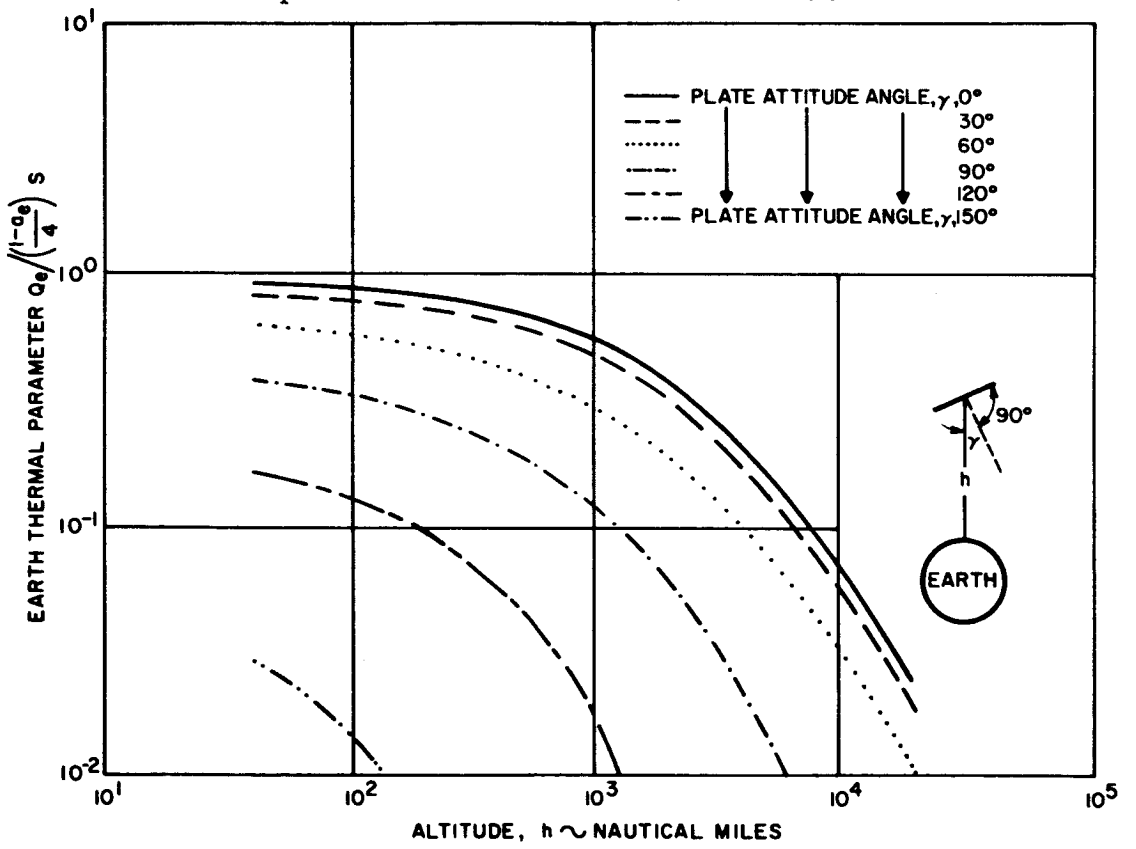


Figure 4-6. Parameter for Earth Thermal Emission Incident to a Flat Plate as a Function of Altitude and Plate Attitude Angle

With respect to heat emission to a satellite, the effective temperature of the Earth-atmosphere system is low enough to cause the bulk of the Earth-atmosphere thermal emission to be in the infrared band.

At the synchronous altitude, Eq. 4-8 gives a value of 1.43 Btu per hour-square foot for the terrestrial radiation received by any satellite. (At such high altitude, the satellite shape does not influence appreciably the amount of radiation received.) This is only 0.323 percent of the solar flux and can be neglected in the calculations.

3) Reflected Solar Radiation (Albedo). A fraction of the total solar radiation received by the Earth is returned to space by scattering and reflections in the Earth's atmosphere and by reflection from clouds and the Earth's surface. The amount of solar energy reflected is a function of the terrain, cloud coverage, optical thickness of the atmospheric gases, the Sun elevation angle, and the radiation wavelengths. The albedo* of a body is defined as the fraction of the solar radiation that is returned from the body to space.

The albedos of the Earth's surface, clouds, and atmosphere are computed separately in terms of the ultraviolet, visible, and infrared components. Of the total incident energy on the Earth, 2.3 percent is reflected by the Earth's surface, 23 percent is reflected by clouds, and 9 percent is reflected by the atmosphere. The albedos of the Earth-atmosphere system are 0.50, 0.39, and 0.28 in the ultraviolet, visible, and infrared wavelengths, respectively.

The effective albedo of the Earth ranges from 0.34 to 0.50; the value seems to depend mainly on the amount of the sky covered by clouds. The Earth's albedo can be computed from Eq. 4-9 (Ref. 4-2).

$$a_e = 0.17 + 0.53\ K \tag{4-9}$$

where K = the fraction of sky covered by clouds. In this report, the average albedo for the Earth is assumed to be 0.40.

In order to compute the amount of reflected solar radiation intercepted by a satellite, the Sun elevation angle, $\beta$, (the angle the Sun makes with the vehicle to Earth radius vector) has to be included in the analysis. This consideration complicates the problem over the case of terrestrial radiation, and a general, closed-form, analytical solution is not available except for special cases. For the case of $\beta = 0$ (for a spherical satellite), the variation of the reflected solar radiation from the Earth is computed from

---

* In some of the literature, the term albedo is also used in referring to the returned energy rather than the ratio of this reflected energy to the solar energy.

$$(Q_{rs})_{sp} = \frac{Sa_e}{2R_e(R_e+h)^2}\left\{\left[(R_e+h)^4 - R_e^4\right]\left[\frac{1}{h} - \frac{1}{\sqrt{2R_eh+h^2}}\right]\right.$$

$$\left. - 2(R_e+h)^2\left(\sqrt{2R_eh+h^2} - h\right) + \frac{(2R_eh+h^2)^{3/2} - h^3}{3}\right\} \qquad (4\text{-}10)$$

where $(Q_{rs})_{sp}$ = solar reflected radiation incident on spherical satellite, Btu per hour-square foot

Figure 4-7 is a plot of the Earth-reflected radiation parameter, $(Q_{rs})_{sp}/Sa_e$, as a function of altitude and Sun elevation angle, $\beta$. The calculations were based on numerical methods used in Ref. 4-1. A solution of Eq. 4-10 for the case of the SMS shows that the value for the reflected solar radiation from the Earth is 2.75 Btu per hour-square foot. Because Eq. 4-10 is for a Sun elevation angle of zero degrees, this is the maximum possible amount of reflected solar radiation that the satellite can receive in the synchronous orbit. As mentioned previously in subsection 2, the shape of the satellite at very high (synchronous) altitudes does not appreciably change the value of the radiation intercepted by it. The Earth's reflected solar radiation (2.75 Btu per hour-square foot) received by the synchronous satellite is 1.55 percent of the reflected solar radiation near Earth and is only 0.62 percent of the solar flux received by the satellite.

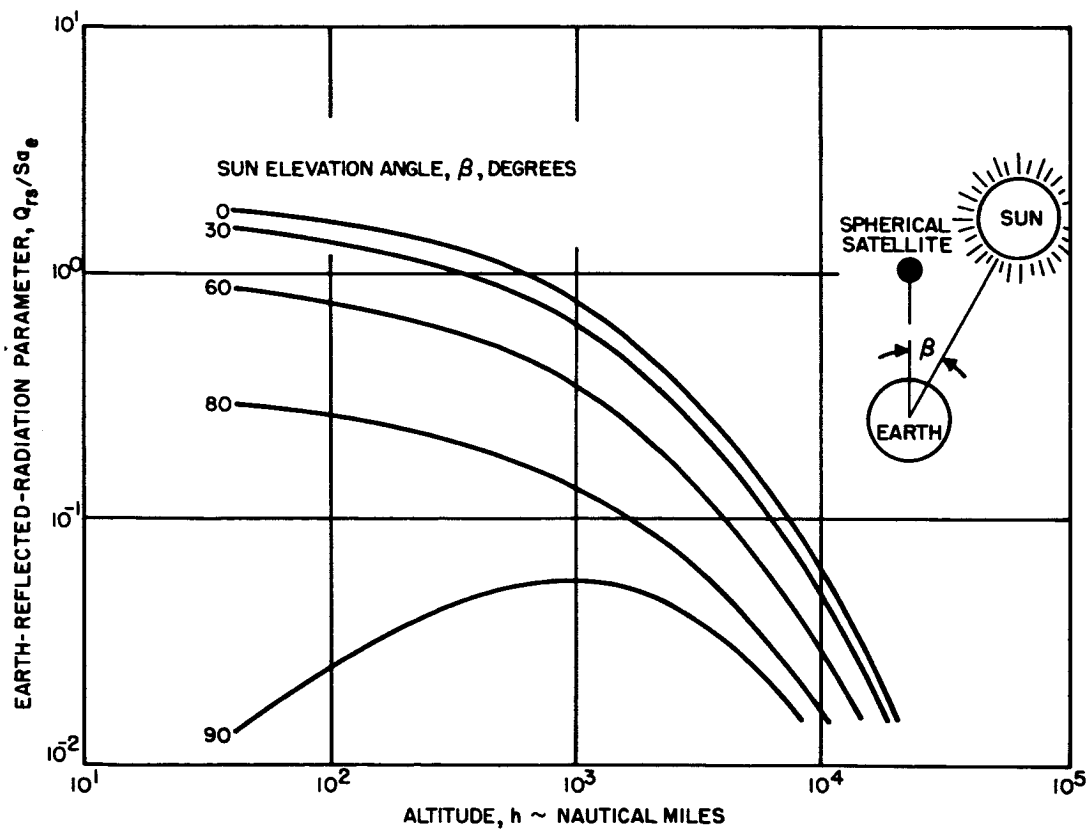


Figure 4-7. Parameter for Earth-Reflected Radiation Incident to a Spherical Satellite as a Function of Altitude and Sun Elevation Angle

4) Planetary Radiation. Present knowledge of the composition of planetary atmospheres is not sufficiently complete to perform detailed spectral analyses of their radiation. However, it is possible to estimate the average planetary temperatures and their average emission of radiation as was done in the case of terrestrial radiation. The total planetary radiation consists, as in the case of terrestrial radiation, of directly emitted radiation and reflected solar radiation. Equations 4-5 through 4-10, derived for terrestrial radiation, could actually be applied to any planet because no assumptions that hold only for the Earth were made in their derivation. Because these expressions are general, they can be applied to any planet by using the radius, solar constant, and albedo of that planet, and the altitude of the satellite above that planet.

Results of various investigations indicate that radiation effects of other planets on the Earth-Moon space are negligible. To verify this, the case for the closest planet, Venus, should be examined. The closest distance from Venus to Earth is approximately 21.3 million nautical miles. From Eq. 4-7 with proper values of S and the albedo for Venus (846.3 Btu per hour-square foot and 0.76, respectively), the thermal radiation emission of Venus was computed to be 50.78 Btu per hour-square foot. This is not significantly different from that of the Earth (66.36 Btu per hour-square foot). The mean radii of Earth and Venus are also approximately the same (3,441 and 3,307 nautical miles, respectively). Consequently, in comparing the effects of thermal radiation of Venus and Earth on a satellite, only the magnitudes of the satellite distance from Venus and Earth have to be compared. In the case of Earth, it was shown that thermal radiation for the 24-hour SMS satellite becomes negligible. This satellite would be at a distance from Venus of about $21 \times 10^6$ nautical miles, making the Venus thermal contribution practically nil.

5) Lunar Radiation. The effects of lunar thermal radiation (direct and reflected) on a conventional, low altitude satellite are usually neglected in the calculations of the thermal balance. The synchronous satellite, even though it is closer to the Moon than a low altitude satellite, is still at a minimum distance from the Moon of approximately 196,000 nautical miles. Use of Eq. 4-8 with values of the Moon's albedo (0.07) and radius (938 nautical miles) shows that the thermal radiation received by a synchronous satellite from the Moon is $3.14 \times 10^{-3}$ Btu per hour-square foot and can be neglected in the calculations.

6) Cosmic Radiation. The total cosmic-ray energy, averaged over the Earth's surface, is approximately $7 \times 10^{-10}$ of the solar energy received. The effect is negligible even if the total cosmic-ray energy was entirely absorbed by the satellite.

b. Contact Energy Sources

1) Micrometeoric Impact Energy. Any solid surface in space, such as the skin of a satellite, is subjected to the action of micrometeoric particles. The resultant effects can be classified either as punctures or as surface friction and erosion. The effects of surface puncture will not be discussed here. Two phenomena associated with micrometeor impact on satellites that are important with respect to thermal energy considerations are the impact energy transmitted

to the satellite and the surface erosion caused by the micrometeors. The latter would disturb the thermal balance on the vehicle by altering the surface characteristics. This effect is discussed later in subsection 3.c.

Generally micrometeoric velocities range from 40,000 to 100,000 feet per second. It can be calculated that the heat input caused by the impact energies is approximately $6.4 \times 10^{-7}$ Btu per hour-square foot, which is $1.43 \times 10^{-9}$ of solar radiation. It will not be considered in this analysis.

2) Aerodynamic Heating in Free Molecular Flow Regions. If the orbits of a satellite pass through the upper layers of the Earth's atmosphere, then the satellite will be subjected to significant aerodynamic heating. This type of heating is appreciable, for example, at an altitude of 400,000 feet above the Earth and at a velocity of 25,000 feet per second. In this case, the free molecular convective heat flux is about 1,100 Btu per hour-square foot. At altitudes above 500,000 feet, the heating rapidly decreases. At synchronous altitude the heating is virtually zero.

c. Internal Energy Sources

Internal energy sources that generate heat within the satellite include the electric and/or electronic equipment, propulsion elements, and power sources.

Internal heat generated within a satellite can be dissipated either by ejection of stored heat masses or by space radiators or by radiation from the shell exterior surface. The last method is presently used on most existing satellites.

The magnitude of the internal energy dissipated is exceedingly important in determining the equilibrium temperature of the synchronous satellite. Because the only significant external heat source affecting the satellite is the solar flux, the equilibrium temperature of any surface not facing the Sun will be determined solely by the magnitude of the internal energy dissipation. The critical nature of this source of energy in the synchronous satellite is thus evident.

3. Surface Characteristics

a. Thermal Properties

The thermal characteristics of the material that are important in the design of a satellite temperature-control system are: 1) Absorptivity, 2) Emissivity, 3) Transmissivity, 4) Reflectivity, 5) Thermal Conductivity, and 6) Specific Heat. The first four are determined by the condition and optical characteristics of the surface of the material.

The solar absorptivity, $\alpha_s$, and the infrared emissivity, $\epsilon$, are of primary importance. The ratio, $\alpha_s/\epsilon$, is also highly significant. For example, in the case where the only energy source to a flat satellite surface is solar, the heat balance equation (as shown later) is

$$\alpha_s S = \epsilon \sigma T_{av}^4 \tag{4-11}$$

where $T_{av}$ = the average satellite temperature, or

$$T_{av} = \left[\left(\frac{\alpha_s}{\epsilon}\right)\left(\frac{S}{\sigma}\right)\right]^{1/4} \tag{4-12}$$

It is thus seen that the average satellite temperature varies as the fourth root of the ratio $\alpha_s/\epsilon$. Therefore, by adjusting this ratio to the proper value, the desired temperature can be achieved. The spectrum of materials and coatings that have been tested for radiation characteristics is shown in Tables 4-1, 4-2 and 4-3.

b. Physical Properties

The physical parameters that affect the radiative behavior of materials, such as the angle of incidence, surface roughness, and the relationship of $\alpha_s$ and $\epsilon$ to the optical constants of the material, are being investigated. It has already been established that the radiative response of materials is determined completely by a very thin layer of the exposed surface. Reference 4-3 presented data on the variation of emissivity as a function of coating thickness while keeping the absorbtivity constant. A variation of emissivity from 0.03 to 0.4 was obtained by varying the thickness of SiO coating on a polished aluminum surface.

The effects of surface roughness and profile on radiative behavior can be correlated satisfactorily with the profile characteristic dimensions relative to the wavelength of the incident and emitted radiation. Although a surface with a profile of one micron appears rough to incident visible solar radiation, it appears smooth to infrared energy. Surface roughness can cause multiple reflectances and increased absorption.

c. Environmental Effects on Surface Characteristics

The stability and durability of materials in the space environment are essential for temperature control of satellites. Thin films, thin foils, and highly polished surfaces are particularly susceptible to sputtering, evaporation, and micrometeorite erosion and penetration.

Sputtering, which is the removal of atoms from the surface of a material by the impact of atomic or subatomic particles, becomes significant in the presence of solar winds. For example, the probability that an impacting solar-wind particle will remove one or several atoms from an aluminum surface is high. A 300-Å coating of aluminum would be destroyed in 1 month by a low-intensity solar wind. During a solar storm, it might be destroyed in a matter of hours.

Pitting and erosion by micrometeorite impact could also seriously alter the radiative characteristics of temperature-control surfaces. If the thin, oxide layer on a metal is lost and the metal is exposed, then the emissivity generally drops sharply and the temperature equilibrium changes. See Table 4-4 for the effect of micrometeoroids on various coatings (Ref. 4-4). The samples were bombarded with high-speed simulated micrometeorites.

TABLE 4-1

RADIATION CHARACTERISTICS OF MATERIALS

| Material | Tested by | Solar Absorptivity $\alpha_s$ | Infrared Emissivity $\epsilon$ | Comments |
|---|---|---|---|---|
| White Paint | STL | 0.22 | 0.75 - 0.85 | Zinc Sulphied - Silicon base - 4 coats req'd. Ultraviolet exposure raises $\alpha > 0.3$ |
| Black Paint | STL | 0.96 | 0.80 - 0.85 | Carbon black pigment - Silicon base |
| Aluminum Paint | STL | 0.20 - 0.24 | 0.20 - 0.24 | Leafing Aluminum in Silicon base. Values vary up to 0.3 (NRL) |
| Evaporated Gold | STL | 0.18 | 0.02 | Must be clean - use strippable coating prior to launch |
| Evaporated Aluminum | STL | 0.10 | 0.025 | Must be clean - use strippable coating prior to launch |
| Polished Aluminum | STL | 0.20 - 0.40 | 0.03 - 0.06 | |
| Polished Stainless Steel | STL | 0.30 - 0.50 | 0.10 - 0.20 | |
| Electroplated Gold | STL | 0.20 - 0.30 | 0.02 - 0.06 | Contamination problem |
| Aluminized Mylar | STL | 0.10 | 0.025 | |
| Evaporated Gold with SiO Coating | STL | 0.17 - 0.18 | 0.025 - 0.34 | $\epsilon$ a function of SiO pigment |
| Magnesium Oxide | | 0.14 | 0.90 | Plasma-sprayed |
| "Reflectal" | UCLA | 0.19 | 0.05 | Mechanical polish |
| "Reflectal" | UCLA | 0.15 | 0.75 | Mechanical polish, 15 min. anodize in 10% $H_2SO_4$ |
| "Reflectal" | UCLA | 0.15 | 0.05 | Mechanical polish, Jacquet electropolish 15 min., 40F, 24V |
| 1199 Al | UCLA | 0.15 | 0.74 | Mechanical polish, Brytal electropolish 15 min., anodize in 15% $H_2SO_4$ |
| AZ31BMg | LAD/NAA | 0.50 | 0.80 | Sandpaper treated, white HAE 65V, 40 min. |
| AZ31BMg | LAD/NAA | 0.70 | 0.60 | Sandpaper treated, 1/2 strength white HAE 85V, 4 min. |
| Fused Silica | | 0.10 | 0.80 | Developed by Corning Research Laboratory, Resistant to ultraviolet and particle radiation |

TABLE 4-2

RADIATION CHARACTERISTICS OF COATINGS ON SUBSTRATA

| Substrate | Coating | Thickness (inches) | Tested by | Solar Absorptivity $\alpha_s$ | Infrared Emissivity $\epsilon$ | $\alpha_s/\epsilon$ |
|---|---|---|---|---|---|---|
| 321 SS | PR-2 Enamel (Allied Chem.) | 0.003 | LAD/NAA | 0.20 | 0.90 | 0.22 |
| 321 SS | 3385 Melamine (Allied Chem.) | 0.010 | LAD/NAA | 0.17 | 0.94 | 0.17 |
| 1199 A1 | B-66 Acryloid | 0.002 | LAD/NAA | 0.24 | 0.85 | 0.28 |
| 1199 A1 Polished | B-72 Acryloid (Rohm & Hass) | 0.001 | LAD/NAA | 0.20 | 0.60 | 0.33 |
| 1199 Al Polished | B-82 Acryloid | 0.005 | LAD/NAA | 0.23 | 0.80 | 0.29 |
| 321 SS | B-66 Acryloid $TiO_2$ | 0.006 | LAD/NAA | 0.21 | 0.80 | 0.26 |
| 321 SS | B-82 Acryloid $TiO_2$ | 0.003 | LAD/NAA | 0.23 | 0.80 | 0.29 |
| 321 SS | B-72 Acryloid $TiO_2$ | 0.002 | LAD/NAA | 0.24 | 0.85 | 0.28 |

TABLE 4-3

RADIATION CHARACTERISTICS OF SOME ADDITIONAL MATERIALS

| Material | Surface Condition | Solar Absorptivity $\alpha_s$ | Infrared Emissivity $\epsilon$ | $\alpha_s/\epsilon$ |
|---|---|---|---|---|
| Aluminum | Polished and degreased | 0.387 | 0.027 | 14.35 |
| Gold plated on Stainless Steel | Polished | 0.301 | 0.028 | 10.77 |
| Gold over Titanium with Resin undercoat | Polished | 0.300 | 0.033 | 9.10 |
| Gold vacuum-deposited on Mil-A-148 slick, annealed Aluminum Foil | Polished | 0.282 | 0.034 | 8,29 |
| Aluminum Foil (dull side) | Crinkled and smoothed | 0.223 | 0.030 | 7.43 |
| Beryllium | Chemically and mechanically polished | 0.444 | 0.063 | 7.04 |
| Aluminum Foil | Cleaned with MEK and alcohol | 0.218 | 0.032 | 6.81 |
| Gold vacuum-deposited on Silicone Resin base | Polished | 0.344 | 0.051 | 6.75 |
| Aluminum Foil tape | As received | 0.238 | 0.043 | 5.54 |
| Aluminum Foil (shiny side) | Smooth | 0.192 | 0.036 | 5.33 |
| Inconel-X foil | Chemically polished | 0.624 | 0.143 | 4.36 |
| Aluminum | Mill finish | 0.218 | 0.051 | 4.28 |
| Molybdenum slug | Polished | 0.480 | 0.122 | 3.94 |
| Chrome-aluminized Mylar film | As received | 0.247 | 0.085 | 2.90 |
| Aquadag (4 coats) on Copper | Clean | 0.782 | 0.490 | 1.60 |
| Carbon-black-pigmented K silicate on Dow 17 on Magnesium | Clean | 0.908 | 0.780 | 1.16 |

TABLE 4-3 (Cont'd)

| | | | | |
|---|---|---|---|---|
| Rokide C (5 mils) on Rene' 41 | --- | 0.898 | 0.789 | 1.14 |
| Dull black micobond (four thick coats) on bare Magnesium | Clean | 0.936 | 0.844 | 1.11 |
| Aluminum Oxide (mil thickness) flame-sprayed on Aluminum | Clean | 0.422 | 0.765 | 0.55 |
| Silica (five coats) on Magnesium | Clean | 0.349 | 0.825 | 0.42 |
| Barium-titanate-pigmented silicone on Dow 17 on Magnesium | Clean | 0.341 | 0.836 | 0.41 |
| Zircon-pigmented K silicate on Dow 17 on Magnesium | Clean | 0.195 | 0.830 | 0.23 |
| Sodium silicate D and Wollastinite | Clean | 0.141 | 0.841 | 0.17 |

TABLE 4-4

MICROMETEORITE EFFECTS ON VARIOUS SURFACE COATINGS

| Material | As Coated | | | After Simulated Micrometeorite Impact | | |
|---|---|---|---|---|---|---|
| Inorganic ($Na_2SiO_2$-$TiO_2$) | $\alpha_s$ | $\epsilon$ | $\alpha_s/\epsilon$ | $\alpha_s$ | $\epsilon$ | $\alpha_s/\epsilon$ |
| Sample 1 | 0.24 | 0.93 | 0.26 | 0.27 | 0.93 | 0.29 |
| 2 | 0.24 | 0.93 | 0.26 | 0.28 | 0.92 | 0.30 |
| 3 | 0.23 | 0.92 | 0.25 | 0.27 | 0.90 | 0.29 |
| 4 | 0.24 | 0.93 | 0.25 | 0.27 | 0.91 | 0.29 |
| 5 | 0.23 | 0.93 | 0.25 | 0.24 | 0.90 | 0.26 |
| Organic (Krylon $TiO_2$) | | | | | | |
| Sample 1 | 0.23 | 0.83 | 0.28 | 0.29 | 0.82 | 0.35 |
| 2 | 0.23 | 0.80 | 0.29 | 0.28 | 0.81 | 0.34 |
| 3 | 0.22 | 0.79 | 0.28 | 0.27 | 0.82 | 0.33 |
| 4 | 0.21 | 0.79 | 0.27 | 0.29 | 0.84 | 0.34 |
| 5 | 0.23 | 0.77 | 0.30 | 0.26 | 0.83 | 0.31 |
| Anodize (1199 Al ) | | | | | | |
| Sample 1 | 0.27 | 0.83 | 0.33 | 0.20 | 0.038 | 6.97 |
| 2 | 0.30 | 0.48 | 0.40 | 0.17 | 0.024 | 7.16 |
| 3 | 0.22 | 0.77 | 0.29 | 0.26 | 0.039 | 6.72 |
| 4 | 0.20 | 0.73 | 0.28 | 0.33 | 0.056 | 5.82 |
| 5 | 0.20 | 0.74 | 0.27 | 0.24 | 0.099 | 2.45 |

The stability of plastic, rubber, and paint-type materials and coatings with respect to ultraviolet radiations in space has been the concern of recent investigations. The entire solar-energy spectrum is important in considering the radiation effects on materials in space, but it is believed that the ultraviolet portion of the spectrum (only about 8 percent of the total) will have the most deleterious effects on paints, plastics, and elastomers. Several inorganic paints that have a zirconium-oxide pigment have been proved to be relatively stable during a continuous 1-year exposure to the equivalent of solar radiation in space.

Many materials, although satisfactory in terrestrial applications, may be highly unsatisfactory in space due to discoloration caused by ultraviolet radiation. Absorption by the atmosphere of shorter wavelengths of solar radiation results in a much lower ultraviolet intensity at the Earth's surface than is encountered in space. In addition, oxidation and weather erosion tend to remove the degraded surface layers and mask the effects of ultraviolet in terrestrial applications.

The effect of ultraviolet degradation in vacuum on various white surfaces is shown in Figure 4-8 taken from Ref. 4-5. No significant change in emissivity was found for any of the three materials due to ultraviolet exposure. The results are shown in Table 4-5. These test results for exposure of 4,000 hours are applicable to the SMS mission since out of one year (8,760 hours) about half the time a given satellite surface "looks" away from the Sun. In using these data it is assumed that ultraviolet degradation is a function of the product of solar intensity and duration, that is, testing at double the solar intensity is equivalent to doubling the duration.

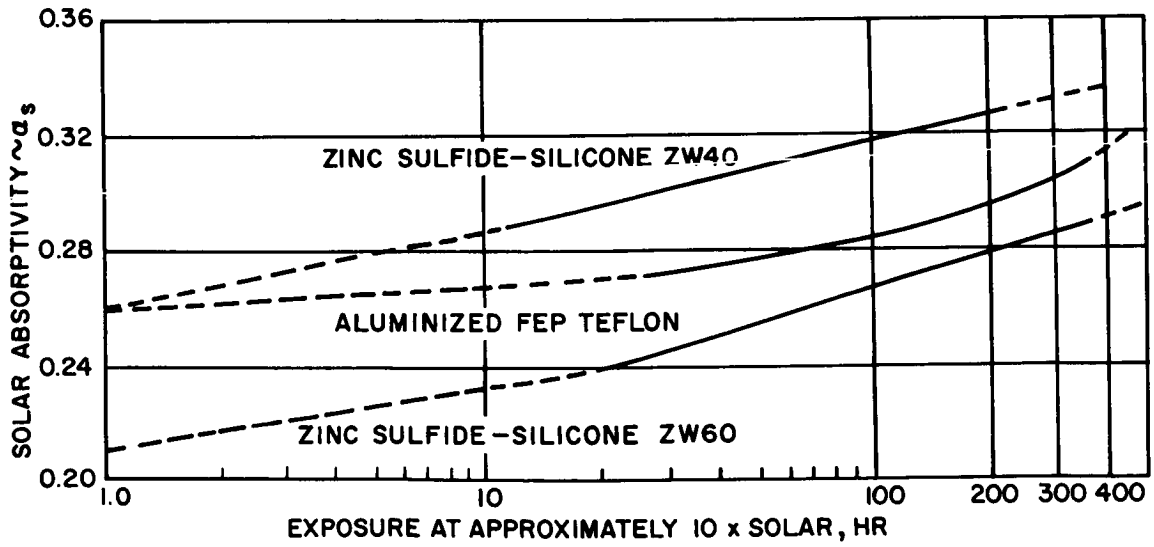


Figure 4-8. Ultraviolet Degradation of Thermal Control Paints in Vacuum

TABLE 4-5

EFFECT OF ULTRAVIOLET RADIATION

| Material | Initial Properties | | Properties after 4,000 hrs | |
|---|---|---|---|---|
| | $\alpha$ | $\epsilon$ | $\alpha$ | $\epsilon$ |
| Zinc sulfide-silicone ZW40 | 0.26 | 0.90 | 0.34 | 0.90 |
| Zinc sulfide-silicone ZW60 | 0.21 | 0.91 | 0.29 | 0.91 |
| Aluminized FEP teflon type A, 5 mil | 0.26 | 0.84 | 0.31 | 0.84 |

The evaporation and sublimation of materials caused by high vacuums in space will cause problems with temperature-control surface coatings. This phenomenon can be predicted theoretically with reasonable certainty.

4. Component Temperature Limits

Temperature control encompasses the necessary provisions for maintaining the satellite (or sections of the satellite) and components at proper operating levels. The temperatures can vary from the extremely low values encountered with infrared detector environments and cryogenic liquids to the usual military requirement of -65 to +165°F environment. For the SMS, the design goal is 25°C ±10°. The temperature of special equipment (such as used for inertial guidance) must be kept within narrower limits, usually between 40 and 90°F. Even more severe requirements are imposed by some types of reconnaissance equipment; temperature regulation within approximately 2°F and thermal gradient control within a fraction of a degree are required for some types. Although the trend in component development is in the direction of 500 to 1000°F as the upper operating temperatures, very few present-day components can operate in this region. Figure 4-9 shows typical temperature requirements for satellite and space vehicle components (Ref. 4-6). Figure 4-10 shows the failure rates of various electronic components as a function of ambient temperature (Ref. 4-7). The fact that the amount of heat that can be removed from a satellite is proportional to the fourth power of the radiator temperature makes it desirable to have the electronic equipment operate at as high a temperature as practical. There is still a great deal of uncertainty about the maximum temperature at which transistors, for example, will operate. First, there is a maximum theoretical value, the temperature of the junction. For germanium and silicon units this temperature is about 100°C and 300°C, respectively. In practice, however, there are other limitations, particularly with silicon. Solders used on a silicon base impose a limit of about 225°C. The ratio of the actual and the rated power dissipation is another practical limitation. The minimum transistor temperature is -65°C.

New materials are being developed for the manufacture of transistors for high temperature operation. Gallium arsenide permits a junction temperature of 400°C maximum. Silicon carbide transistors withstand 600°C operation but they

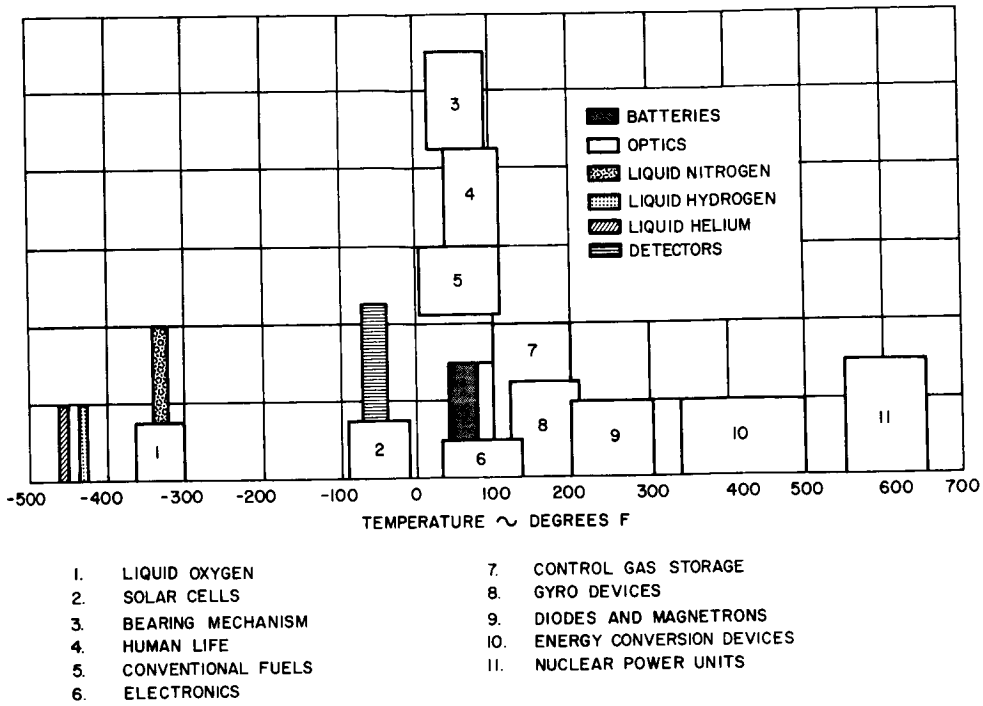


Figure 4-9. Approximate Component Temperature Limits

perform poorly at ordinary temperatures. Boron phosphide transistors will operate at 1800°F in an inert or reducing atmosphere, and at 1480°F in air. Transistors made of these materials are not yet on the market but gallium arsenide units may be available within about a year.

## C. PASSIVE TEMPERATURE CONTROL

### 1. Introduction

A passive temperature control system is one in which there are no moving parts and/or fluids effecting the control. In passive systems, temperature control is usually achieved by using surface coatings with an absorptivity-emissivity combination that will result in the permissible temperature range during all exposures of the spacecraft. Careful use of insulation, heat paths, radiation barriers, energy storage devices, and control of internal heat dissipation can often supplement the use of surface coatings to control the satellite temperature. In accordance with this definition, a thermal control system that incorporates a heater would still be passive even though the heater consumes power.

Considering the previously discussed parameters that influence the thermal design of the spacecraft, a thermal balance (in the form of a differential equation) between the energies entering, being stored in, and leaving the spacecraft can now be made. The result of such a balance would be the determination of the satellite temperature under given orbital conditions.

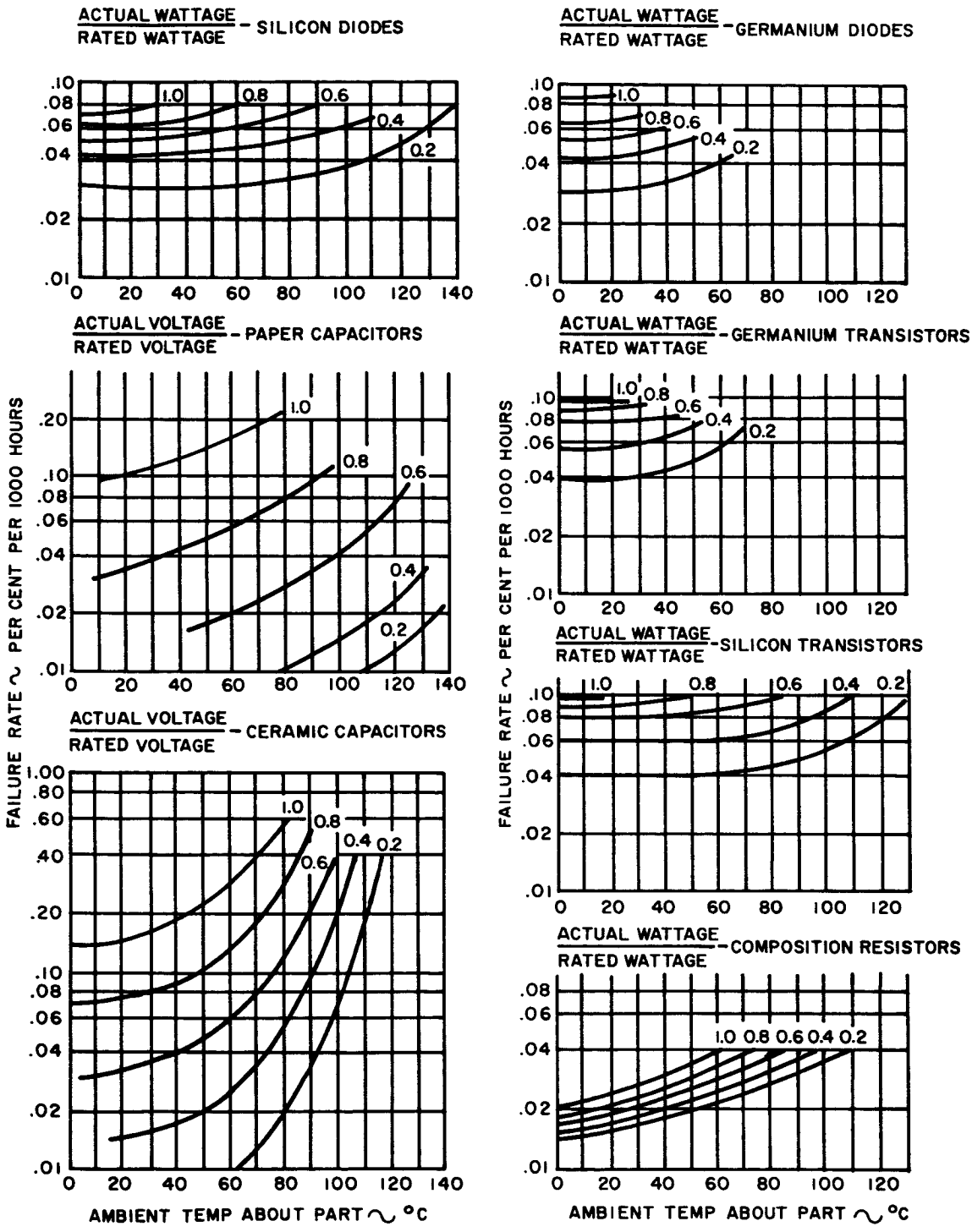


Figure 4-10. Failure Rates vs Ambient Temperature for Various Electronic Components

## 2. Thermal Analysis

Generally in thermo-analyses, the thermal state of the object to be analyzed is of significance. In some cases the geometric and thermal conditions can be such that they would tend to maintain the object in an isothermal state with respect to position. That is, at a given time the entire object would be at a constant (for practical purposes) temperature. The temperature may, however, change with time, in which case the condition would be transient or nonisothermal with respect to time. These cases are relatively easy to analyze. In other cases, due to complicated geometries and thermal environment, the object would be in a heterothermal state with respect to position. In addition to having a changing temperature within the object at a given time, the temperature at a given point may also undergo a change with time (heterothermal with respect to time). A satellite in this state is difficult to analyze rigorously.

In practice, satellites of sizeable payload capacities are heterothermal. This does not, however, preclude proper analysis since it is possible to thermally uncouple sections of such a satellite by proper design. The present trend in effective passive thermal control is to isolate components and equipment in separate compartments wherever possible. Such a scheme lends itself to more precise analysis, resulting in closer agreement between analysis and test.

### a. Heterothermal Satellite

A general differential equation for a satellite consisting of n heterothermal parts can be written. For the $j^{th}$ part, the equation is

$$\sum_{j,k=1}^{n} \left[ C_{jk} (T_k - T_j) + C'_{jk} (T_k - T_j) + r'_{jk} (T_k^4 - T_j^4) \right] + A_j \alpha_{sj} \cos \phi \, \xi S$$

$$+ A_j \alpha_{sj} Q_{rs} (h, \gamma, \beta) \xi_2 + A_j \epsilon_j Q_e (h, \gamma) + A_j (Q_i)_j - A_j \epsilon_j \sigma T_j^4$$

$$- W_j C''_j \frac{dT_j}{dt} = 0 \qquad (4\text{-}13)$$

where $j, k, = 1, 2, 3, \ldots$

$C_{jk}$ = conduction coefficient between points j and k (a function of the geometry and conductivity of the heat path between points j and k)

$T_j, T_k$ = temperature at points j and k

$C'_{jk}$ = total convection coefficient between points j and k (a function of the geometry and whether convection is forced or natural)

$r'_{jk}$ = radiation coefficient between points j and k (includes area, form factors and Stefan-Boltzmann constant)

$A_j$ = area of element j

$\phi$ = angle between the Sun-Earth vector and the normal to area of element j (given by Eqs. 4-3 and 4-4)

$\alpha_{sj}$ = absorbtivity of element j for solar radiation

S = solar constant

$\xi_1$ = step function ($\xi_1$ = 1 for sunlight; $\xi_1$ = 0 for the umbra; $0 < \xi_1 < 1$ for the penumbra)

$Q_{rs}(h,\gamma,\beta)$ = reflected solar radiation from Earth (obtained from Eq. 4-10 and Figure 4-7)

$\xi_2$ = step function ($\xi_2$ = 1 for orbit in hemisphere ±90° from Sun direction; $\xi_2$ = 0 for orbit in hemisphere opposite Sun direction)

$\epsilon_j$ = emissivity of element j with respect to infrared radiation

$Q_e(h,\gamma)$ = terrestrial thermal emission (obtained from Eq. 4-8 and Figures 4-5 and 4-6)

$(Q_i)_j$ = internal heat power density (electric, electronic, chemical, etc.)

$\sigma$ = Stefan-Boltzmann constant

$W_j$ = weight of element j

$C_j''$ = specific heat of element j

t = time

Equation 4-13 constitutes a system of n differential equations to be solved simultaneously. There are two conditions for which the system of equations has to be solved; the steady-state condition, and the transient condition. For the steady-state case, Eq. 4-13 can be reduced to a system of algebraic equations. For the transient case, solutions for Eq. 4-13 can be obtained, for a given physical satellite configuration, by numerical methods.

If the orbit of the SMS is analyzed, it is found that for the three-axis stabilized configuration, for example, one half of the spacecraft is in its own shadow for 12 hours out of 24 each day (disregarding the equinoxes). The other 12 hours it gets solar radiation as prescribed by

$$Q_s = S\,\alpha_s\,LD\sin\phi \qquad (4\text{-}14)$$

where $\phi$ is given by Eq. 4-4. This means that if isothermality with respect to position is not attained, the temperature of half the satellite surface will vary from a minimum during the 12-hour shade period to a maximum when this half is in sunlight. These temperature excursions will be periodic with a period of 24 hours.

To find out whether surface isothermality is attained with a three-axis stabilized configuration, a typical vehicle was analyzed. The analysis is presented later in subsection 2.c.2), "Effect of Spacecraft Spin on Thermal Design." Some of the results of the analysis are shown in Figure 4-11. It can

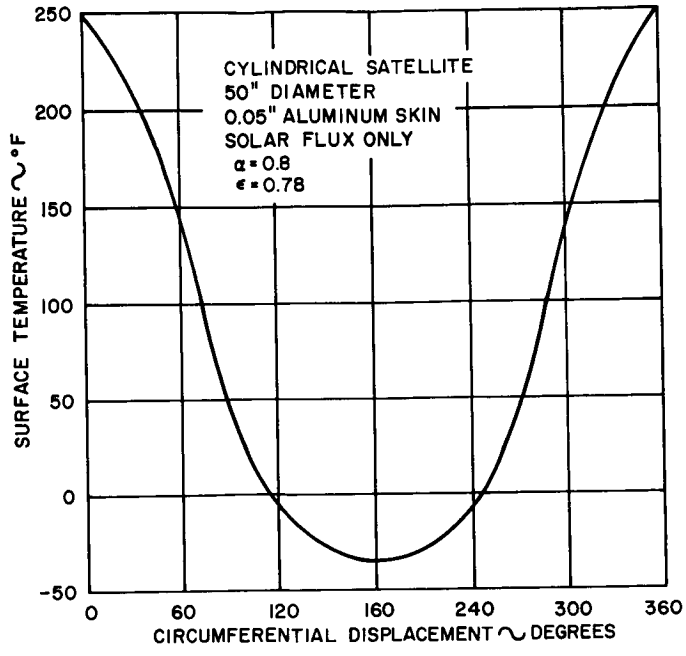


Figure 4-11. Surface Temperature Distribution on a Three-Axis Stabilized Satellite

be seen that the temperature along the satellite periphery is far from being isothermal with respect to position. Therefore, it follows that isothermality with respect to time is not attained either, and periodic surface temperature excursions will occur.

The effect of geometry, material properties, and surface characteristics on the isothermality of a cylindrically shaped satellite can be obtained from the relations below (Ref. 4-8). For a nonspinning satellite with the axis perpendicular to the Sun-Earth vector, the difference between the maximum and the minimum satellite skin temperature is given by

$$T_{max} - T_{min} = \frac{1}{4/\pi\left(\frac{\alpha_s S}{\pi \epsilon \sigma}\right)^{1/4} + \tau k/r^2 \alpha_s S} \tag{4-15}$$

where $\tau$ = skin thickness, ft

$k$ = thermal conductivity, Btu/hr ft°R

$r$ = satellite radius, ft

$\alpha_s$ = solar absorbtivity

S = solar constant, 442 Btu/hr $ft^2$

$\epsilon$ = surface emissivity

$\sigma$ = Stefan-Boltzmann constant, 0.173 Btu/hr $ft^2$ $°R^4$

The effects on satellite isothermality are presented in Figure 4-12. The parameter $\tau k$ (thickness multiplied by conductivity) and the radius were chosen as parameters. It may be observed that unless $\tau k$ is large the temperature fluctuations are considerable. A huge $\tau k$ means either a thick skin or a good conductor, or both. Since good conductors have high densities, a large $\tau k$ would result in a weight penalty. In addition, as shown by the figure, the effect of increasing the satellite radius is to increase the skin temperature fluctuations.

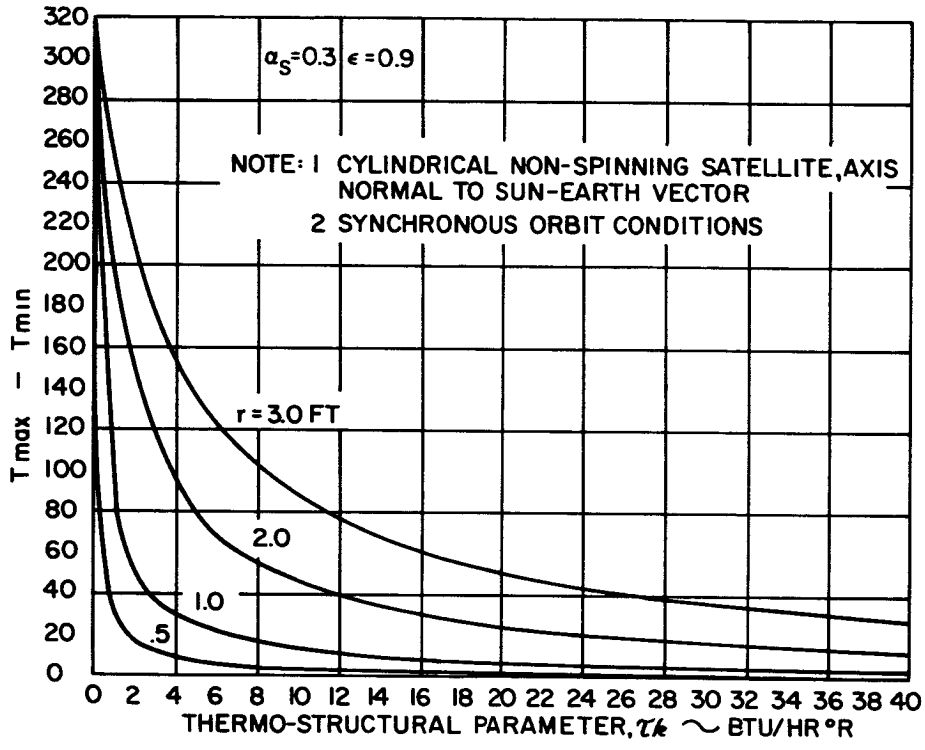


Figure 4-12. Effect of Thermo-Structural Parameters on Satellite Isothermality

b. SMS Thermal Design Approach

There are two schools of thought in passive temperature control design. Since the ultimate heat rejection is through the satellite skin, it is considered good design to place heat generating equipment as close to the outer skin as possible. This will eliminate the extra weight of conductive paths needed to transport the heat from the equipment to the skin. Such an approach, however, will subject the electronic equipment to the same variations in temperature as is the skin of the satellite.

Another design approach is to locate the equipment within the satellite interior, removed from the outer skin. This design tends to diminish the temperature excursions of the equipment due to the added thermal mass.

Here a weight penalty will have to be paid in providing sufficient heat paths from the satellite interior to the skin. Which of the two criteria should be followed in the SMS design will now be examined.

It is of great importance in satellite thermal design to determine the effects of skin temperature fluctuation on the behavior of the equipment temperature within the satellite. Such an analysis can be performed on the cylindrical satellite configuration shown in the sketch below.

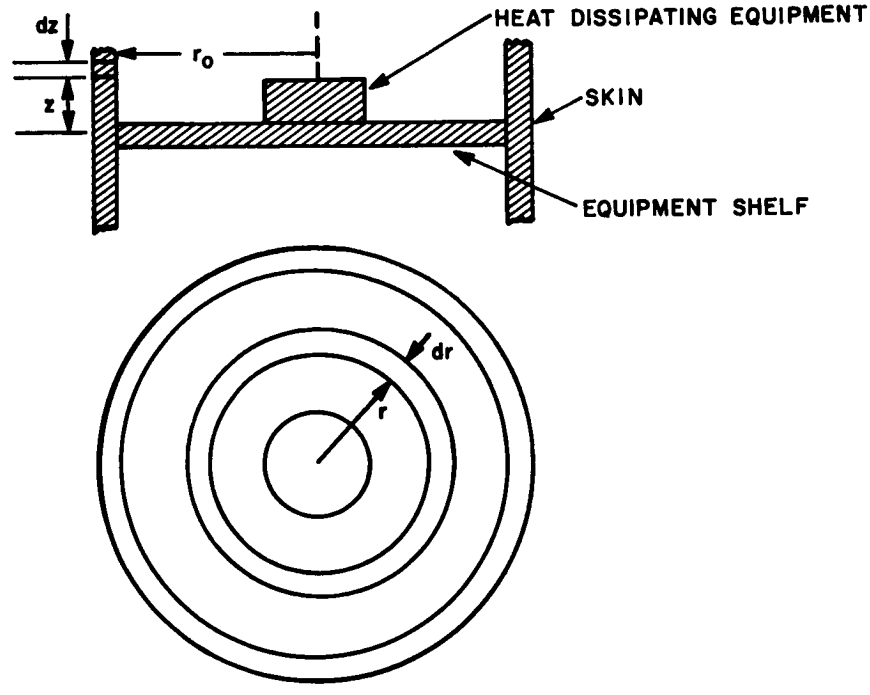


The heat dissipated from the component will flow radially outward through the shelf. If there is good contact between the shelf and the satellite skin, the heat will be conducted away from the shelf by the skin in the ±Z directions. It can be shown (Ref. 4-9) that for reasonable geometries the temperature gradient in the Z direction is small, and the skin temperature can be considered independently of Z.

For periodically varying skin temperatures (in the circumferential direction) the temperature at any point r is given by

$$T_r = T_{r_o} \frac{\mathrm{ber}\sqrt{\frac{\rho c_p \omega'}{k}}\, r + \bar{i}\ \mathrm{bei}\sqrt{\frac{\rho c_p \omega'}{k}}\, r}{\mathrm{ber}\sqrt{\frac{\rho c_p \omega'}{k}}\, r_o + \bar{i}\ \mathrm{bei}\sqrt{\frac{\rho c_p \omega'}{k}}\, r_o} \tag{4-16}$$

where $T_{r_o}$ = temperature at $r_o$ (skin temperature)

ber, bei = modified Bessel functions

$\rho$ = material density (shelf)

$c_p$ = material specific heat (shelf)

$\bar{i}$ = $\sqrt{-1}$

$\omega'$ = frequency

k = thermal conductivity

The ratio of the amplitude of the temperature variation at any point r to the amplitude of skin temperature variation is given by

$$\left|\frac{T_r}{T_{r_o}}\right| = \left(\frac{\mathrm{ber}^2\sqrt{\frac{\rho c_p \omega'}{k}}\, r + \mathrm{bei}^2\sqrt{\frac{\rho c_p \omega'}{k}}\, r}{\mathrm{ber}^2\sqrt{\frac{\rho c_p \omega'}{k}}\, r_o + \mathrm{bei}^2\sqrt{\frac{\rho c_p \omega'}{k}}\, r_o}\right)^{1/2} \tag{4-17}$$

Examination of this expression and the behavior of the (ber) and (bei) functions shows that as $r/r_o$ decreases, the amplitude ratio falls off, and the decrease with decreasing $r/r_o$ is more rapid for large $\omega$ (small period). Figure 4-13 shows the ratio of temperature amplitude as a function of frequency and radial distance from the axis. It can be concluded that for the SMS (frequency = 7.29 x $10^{-5}$ radians/sec), placing equipment in the satellite interior (removed from the skin) will not damp out the temperature excursions. The other approach, namely, to place the equipment along the satellite periphery, will therefore be followed. This approach has additional merits which are discussed in Volume 2 of this report.

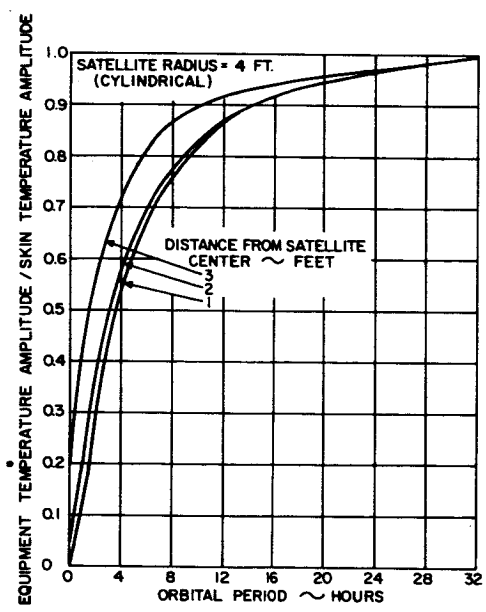


Figure 4-13. Effect of Equipment Position and Orbital Period on Temperature Amplitude Ratio

c. Isothermal Conditions

1) Steady State. By attaching heat generating equipment to the outer skin, it is possible to thermally decouple and compartmentize equipment. Over a given module the outer skin can thus be considered isothermal with respect to position, and Eq. 4-13 can (for a nearly flat surface at synchronous orbit conditions) be reduced to

$$\alpha_s \cos \phi S \xi_1 + 3.413\, Q_i - \epsilon \sigma T^4 - Wc_p \frac{dT}{dt} = 0 \tag{4-18}$$

For steady-state conditions Eq. 4-18 reduces to

$$T_s = \left[\frac{\alpha_s S \xi_1 \cos \phi + 3.413\, Q_i}{\sigma \epsilon}\right]^{1/4} \tag{4-19}$$

The angle $\phi$ is defined as the angle between the Sun-Earth vector and the normal to the surface in question. This angle, as given for the three-axis stabilized satellite, is

$$\cos \phi = \cos (\omega_{E/S} t) \sin \lambda \sin (\omega_{S/E} t') + \sin (\omega_{E/S} t) \left[ - \sin \Delta \cos \lambda + \cos \Delta \sin \lambda \cos (\omega_{S/E} t') \right] \tag{4-20}$$

where $\lambda$ is the angle between the normal to the area in question and the plus pitch axis. (See Volume 4, "Attitude and Station Control" for the accepted convention.) The other terms in Eq. 4-20 are defined in Eqs. 4-3 and 4-4.

2) Effect of Spacecraft Spin on Thermal Design. The problem considered is that of a cylindrical satellite rotating with uniform speed about its geometric axis and exposed to solar radiation. For the sake of analysis, the axis of the cylinder is assumed normal to the Earth-Sun vector. Synchronous orbit conditions are assumed under which only solar radiation is present. This problem is best analyzed by assuming the satellite stationary and the sun revolving around the satellite with a given speed. The situation can then be classified as a "moving heat source" problem which is treated in advanced texts on the subject.

The differntial equation for the temperature distribution around the cylindrical satellite surface is shown (Ref. 4-8) to be

$$\frac{d^2 T}{d\eta^2} + \frac{2\pi r}{\alpha'} \frac{dT}{d\eta} - \frac{4\pi^2 r^2 \sigma \epsilon}{\tau k} T^4 = \frac{4\pi^2 r^2 \alpha' S}{\tau k} \cos (2\pi\eta) \tag{4-21}$$

where $\eta$ = distance along the circumference

$\alpha'$ = thermal diffusivity of the skin material, $ft^2/hr$

$\tau$ = skin thickness, ft

$\cos (2\pi\eta)$ = rectified cosine function

This equation (linearized) was solved for SMS geometric and thermal conditions. The results are shown in Figure 4-14. It may be observed that even as low an

rpm as 0.5 will maintain the surface temperature within close limits (see Figure 4-11 for the case of zero rpm).

Computations were made on analog and digital computers to find the effect of internal power generation on the temperature amplitude. It was found that the internal power density only shifts the mean temperature up or down. There was no appreciable effect on the temperature excursion for a given rpm (see Figure 4-15).

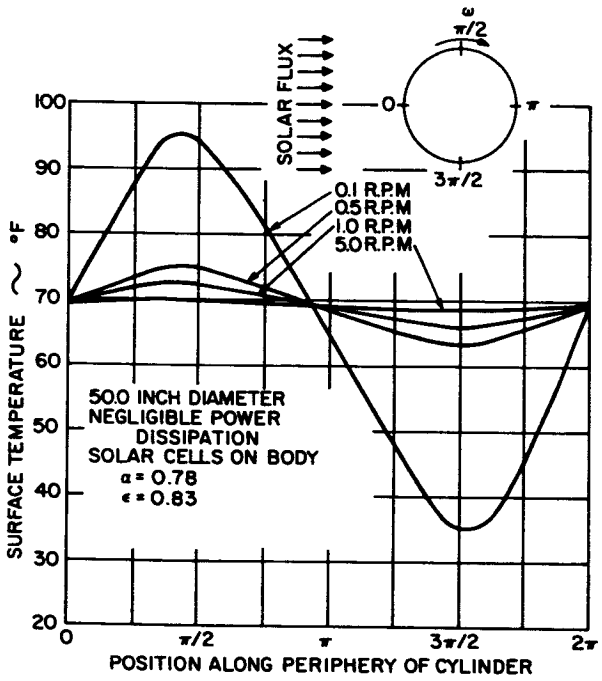


Figure 4-14. Temperature Distribution on a Spin-Stabilized Cylindrical Satellite

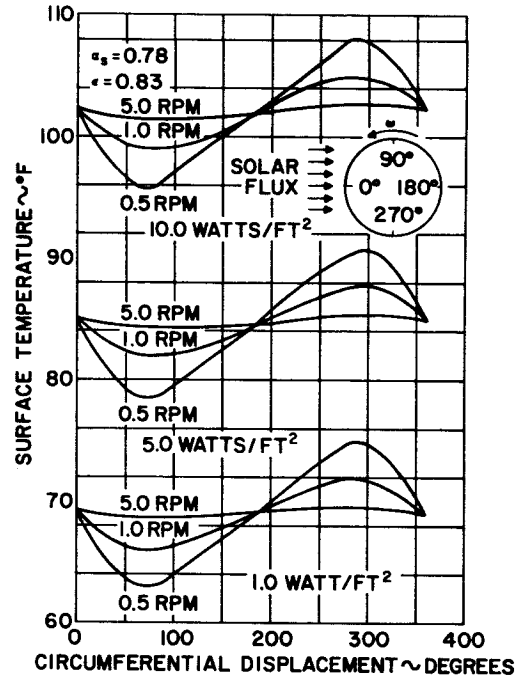


Figure 4-15. Effect of RPM & Power Density on a Spin-Stabilized, Solar-Cell-Covered Satellite

The desirability, from the standpoint of thermal control, of a spin-stabilized spacecraft is evident from Figures 4-14 and 4-15. In essence, the satellite is semiactively controlled by virtue of its being spin-stabilized. However, the rotation is imparted to the satellite for purposes of attitude control, so that from the point of view of thermal control the system is considered passive.

It should be noted from Figure 4-14 and 4-15 that the temperature oscillates about a mean. This mean temperature can be calculated from Eq. 4-18 for a spin-stabilized cylindrical satellite as

$$T_{mean} = \left[ \frac{\frac{\alpha_s S}{\pi} \sqrt{1 - \sin^2 \Delta \sin^2 (\omega_{E/S} t)} + 3.413\, Q_i}{\sigma \epsilon} \right]^{1/4} \qquad (4\text{-}22)$$

Results are shown in Figures 4-16 through 4-21. Each figure is plotted for a different power level as indicated. For any combination of $\alpha_s$, $\epsilon$, and power density, the mean temperature of a spin-stabilized satellite can be obtained from these graphs. To find out the temperature fluctuations about the mean for a given rpm, Figure 4-14 should be consulted.

3) Transient State. An important phase in the thermal study of the SMS was the analysis of the satellite as it is alternately subjected to sunlight and earth shadow during the equinoctial passes (Figure 4-1). The maximum time per day that the satellite is in the Earth's umbra is 65.95 minutes. For a cylindrical satellite, Eq. 4-18 can be written as

$$\frac{1}{\pi \epsilon \sigma}\left[\alpha_s S + \frac{3.413\, Q_i'}{2\, r\, L}\right] - T^4 - \frac{Wc_p}{2\pi r L \epsilon \sigma}\left(\frac{dT}{dt}\right) = 0 \qquad (4\text{-}23)$$

The solution to this differential equation is

$$\frac{1}{2G\left(\frac{H}{G}\right)^{3/4}}\left\{\frac{1}{2}\ln\left|\frac{T+\left(\frac{H}{G}\right)^{1/4}}{T-\left(\frac{H}{G}\right)^{1/4}}\right| + \text{arc Tan}\left[\frac{T}{(H/G)^{1/4}}\right]\right\} = t + k' \qquad (4\text{-}24)$$

where $G = \frac{2\pi r L \epsilon \sigma}{Wc_p}$, $H = \frac{2\, r\, L}{Wc_p}\left[\alpha_s S + \frac{3.413\, Q_i'}{2\, r\, L}\right]$

and $k'$ is the constant of integration . This constant is given by

$$k' = \frac{1}{2G\left(\frac{H}{G}\right)^{3/4}}\left\{\frac{1}{2}\ln\left|\frac{T_o+\left(\frac{H}{G}\right)^{1/4}}{T_o-\left(\frac{H}{G}\right)^{1/4}}\right| + \text{arc Tan}\left[\frac{T_o}{(H/G)^{1/4}}\right]\right\} \qquad (4\text{-}25)$$

where $T_o$ is the temperature before entering the shadow. Figures 4-22 through 4-25 show the temperature response curves as a function of internal power density for the satellite passing from sunlight to shadow and back to sunlight as the Earth passes either of the equinoctial points. Figure 4-22 is a generalized curve, while Figures 4-23, 4-24 and 4-25 are specific curves for the three basic configurations studied for the SMS. As observed from the figures, steady-state temperatures are not reached during the 65.95 minutes of occultation. This is the longest occultation period the entire satellite can ever have.

## 3. Thermal Control Schemes

There is a variety of possible thermal control schemes within the realm of passive systems. The exploration of every possible means of passive thermal control is essential for long life-time spacecraft of the SMS class. In spite of the great strides made in space exploration within the past decade, there is still a vast number of unknowns that can affect adversely the otherwise most superbly designed spacecraft. The probability of survival of a given thermal

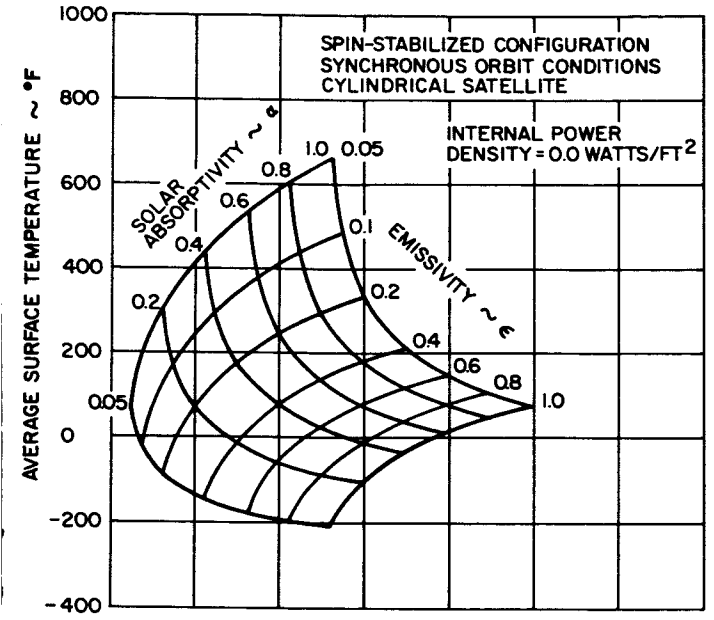


Figure 4-16. Effect of Surface Characteristics and Internal Power Density on Spacecraft Surface Temperature, 0.0 watts/ft$^2$, Spin-Stabilized Configuration

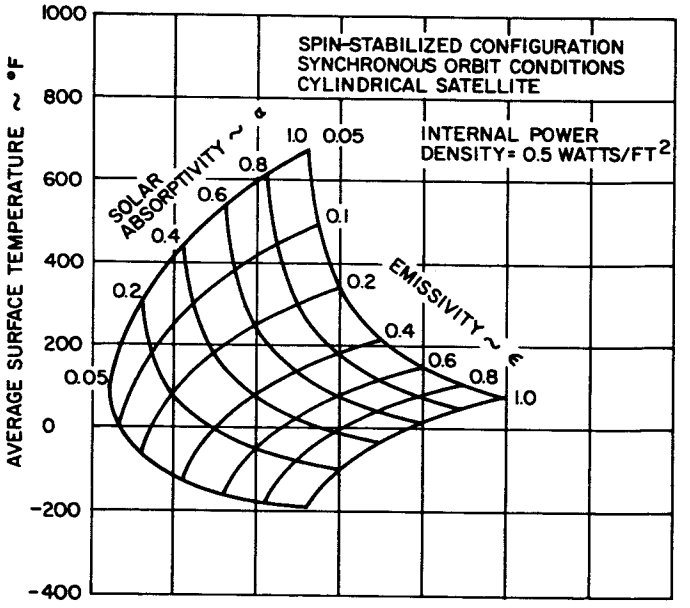


Figure 4-17. Effect of Surface Characteristics and Internal Power Density on Spacecraft Surface Temperature, 0.5 watts/ft$^2$, Spin-Stabilized Configuration

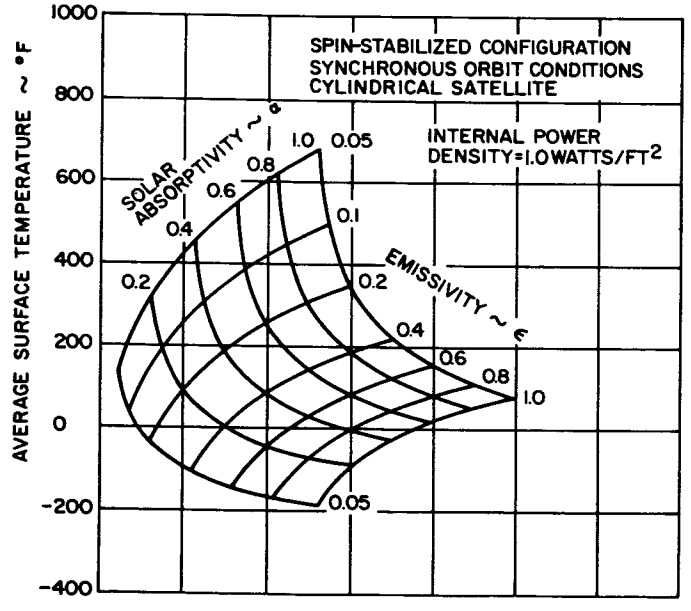


Figure 4-18. Effect of Surface Characteristics and Internal Power Density on Spacecraft Surface Temperature, 1.0 watts/ft$^2$, Spin-Stabilized Configuration

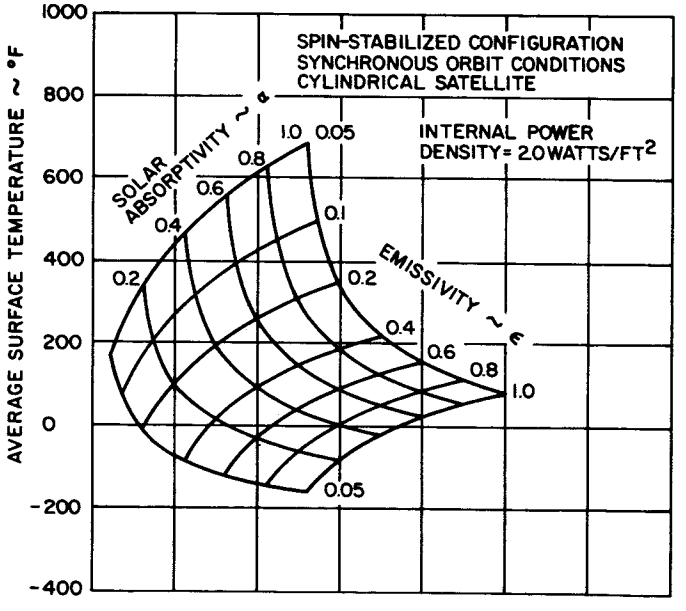


Figure 4-19. Effect of Surface Characteristics and Internal Power Density on Spacecraft Surface Temperature, 2.0 watts/ft$^2$, Spin-Stabilized Configuration

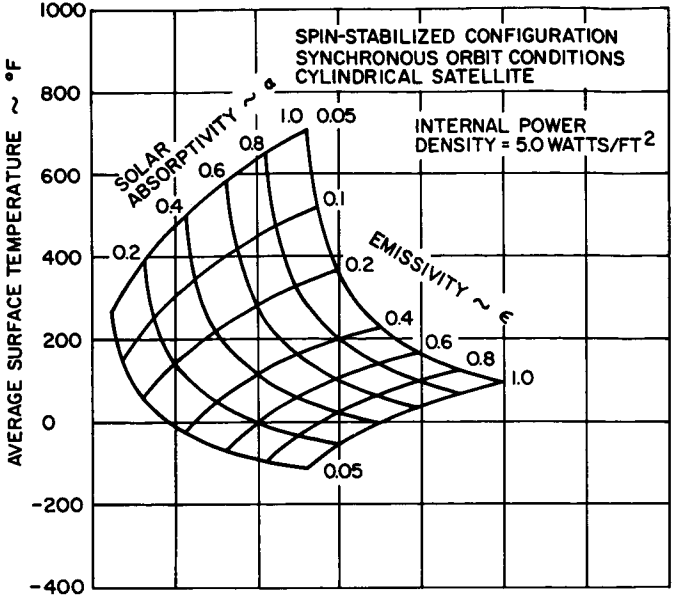


Figure 4-20. Effect of Surface Characteristics and Internal Power Density on Spacecraft Surface Temperature, 5.0 watts/ft$^2$, Spin-Stabilized Configuration

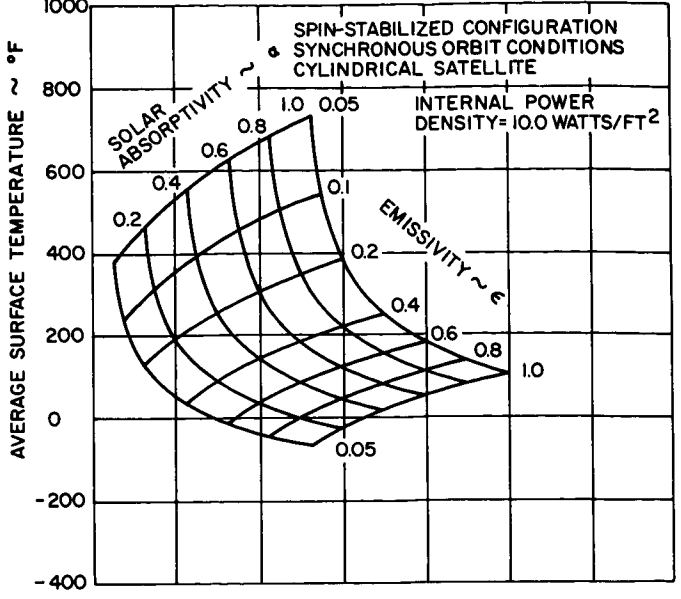


Figure 4-21. Effect of Surface Characteristics and Internal Power Density on Spacecraft Surface Temperature, 10.0 watts/ft$^2$, Spin-Stabilized Configuration

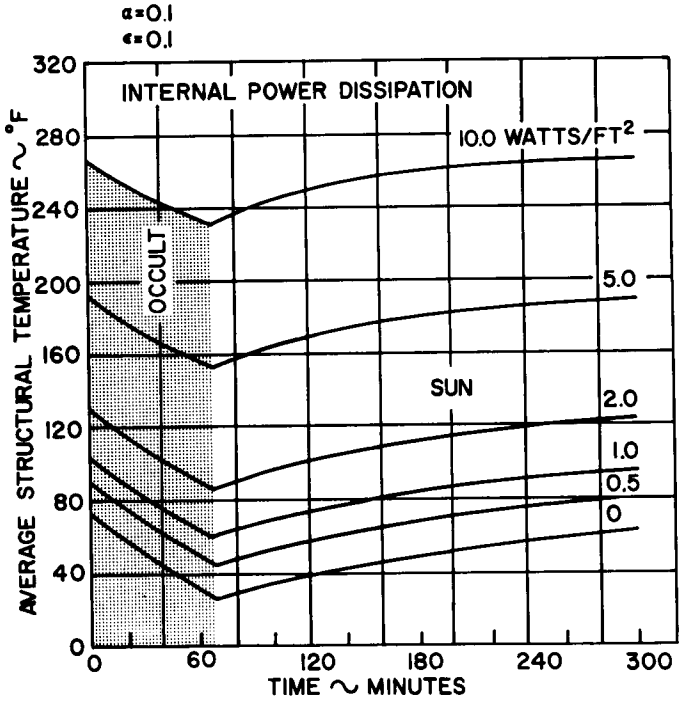


Figure 4-22. Temperature Response Characteristics During Equinoctial Passage, Cylindrical Satellite

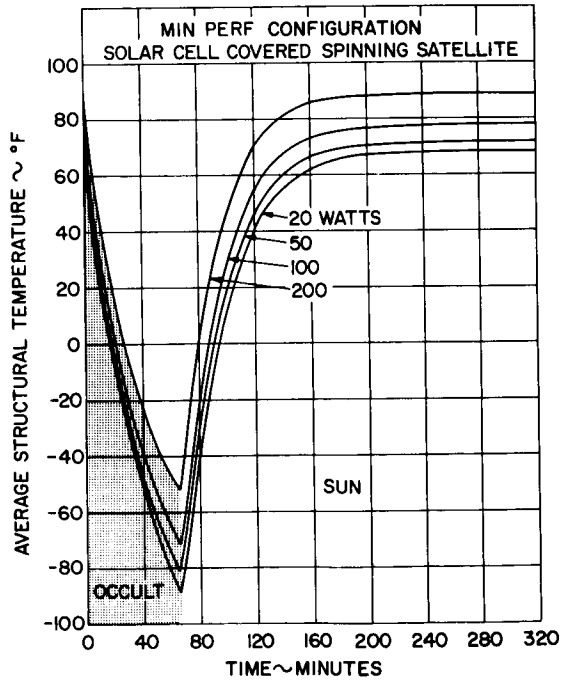


Figure 4-23. Temperature Response Characteristics During Equinoctial Passage, Minimum Performance Configuration

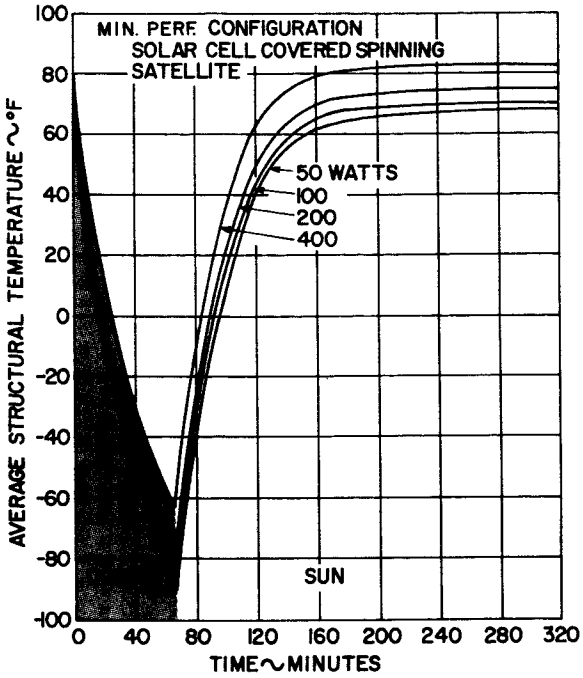


Figure 4-24. Temperature Response Characteristics During Equinoctial Passage, Medium Performance Configuration

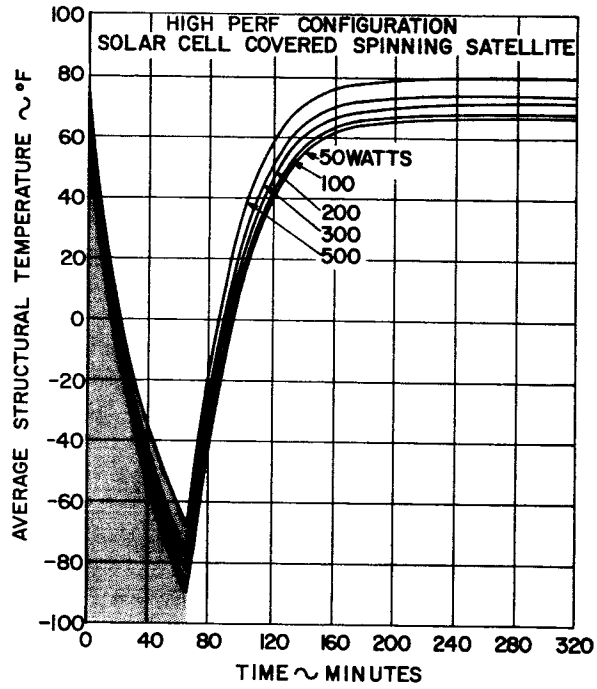


Figure 4-25. Temperature Response Characteristics During Equinoctial Passage, High Performance Configuration

control system will be greatly enhanced if its dependence upon power, moving parts, or moving fluids is eliminated or at least reduced. The thermal control schemes described below can be applied independently or in combination with any or some of the others. For the SMS configurations, most or all of these schemes will have to be employed.

a. Thermal Control by Surface Properties

The simplest form of passive temperature control is by means of selecting desirable surface properties for the exposed spacecraft surfaces. As previously shown, the spacecraft temperature is significantly influenced by $\alpha_s$ and $\epsilon$ of the outer surface. Using Eqs. 4-19 and 4-20, calculations were made to determine the maintainable temperature range on the SMS by passive control surfaces only. The results are shown in Figures 4-26 through 4-31. Each figure is plotted for a different level of internal power dissipation as indicated on the graph. It should be noted that each $\alpha_s = 0$ line represents the case when the surface receives no solar radiation. Each graph thus presents both ends of the temperature spectrum, i.e., the maximum and minimum possible temperature of the surface for the given power density and surface thermal characteristics. Table 4-6 summarizes the maintainable temperature ranges with this scheme for various internal power densities.

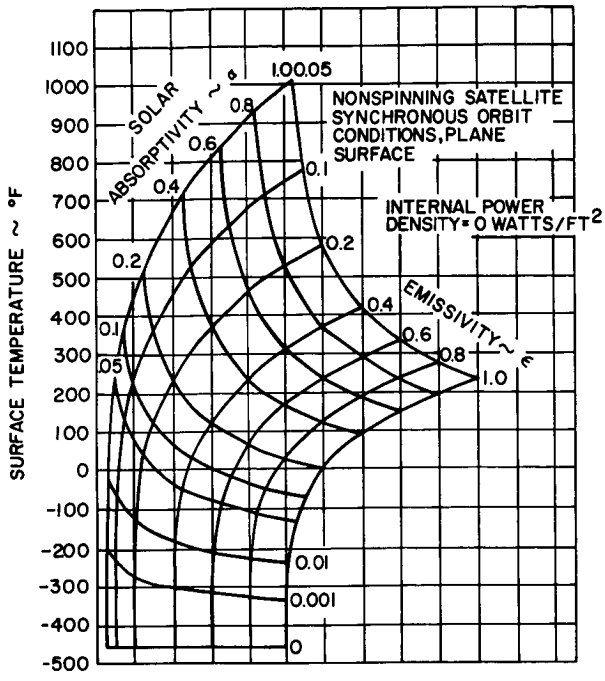


Figure 4-26. Effect of Surface Characteristics and Internal Power Density on Spacecraft Surface Temperature, 0 watts/ft$^2$, Non-Spinning Satellite

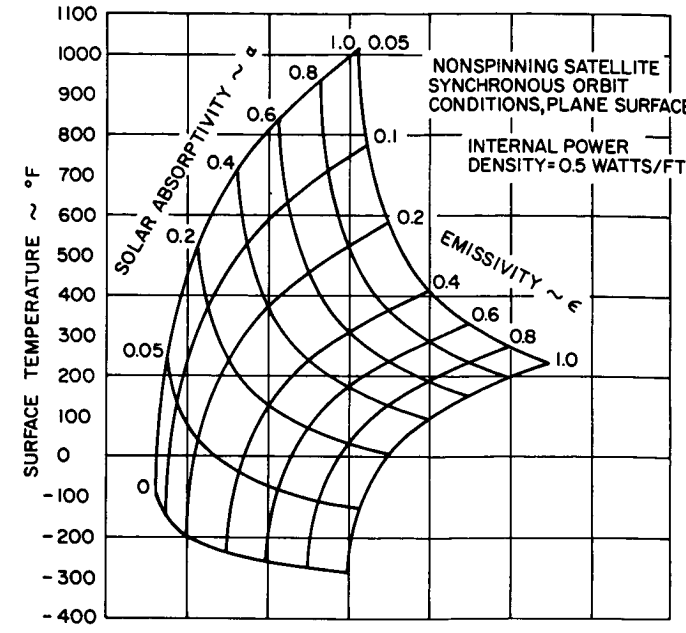


Figure 4-27. Effect of Surface Characteristics and Internal Power Density on Spacecraft Temperature, 0.5 watts/ft$^2$, Non-Spinning Satellite

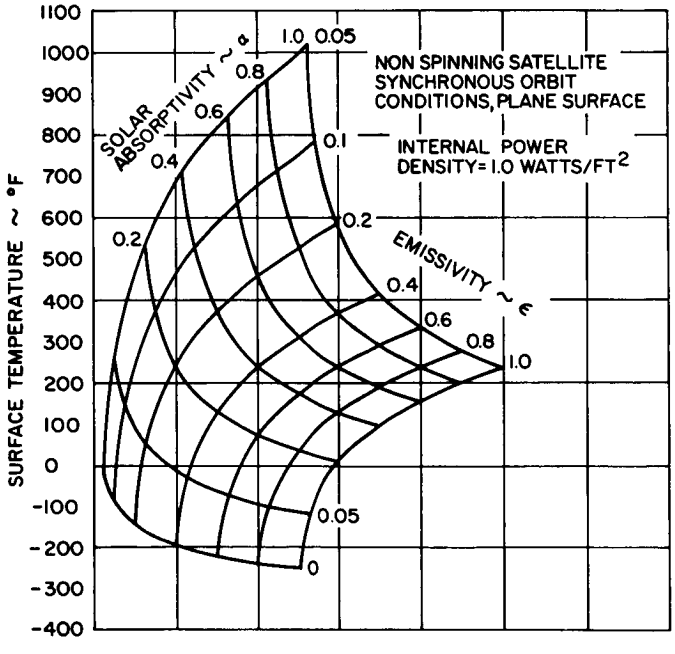


Figure 4-28. Effect of Surface Characteristics and Internal Power Density on Spacecraft Surface Temperature, 1.0 watts/ft$^2$, Non-Spinning Satellite

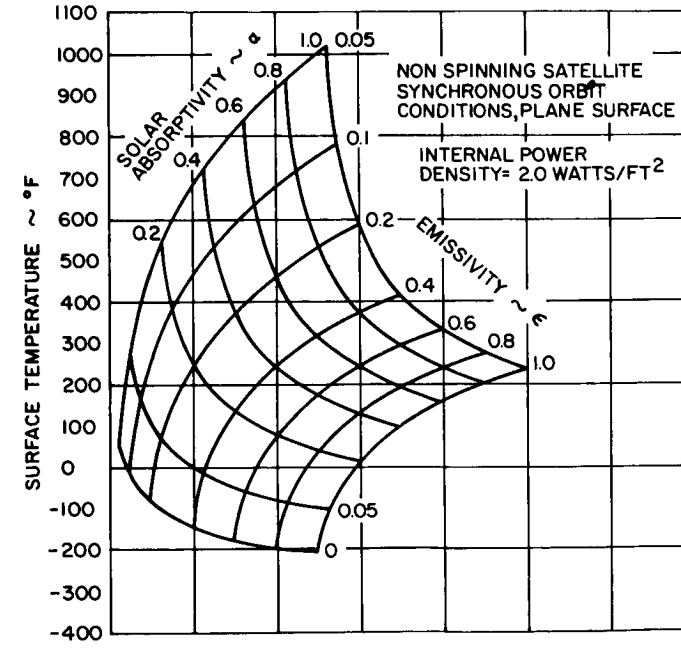


Figure 4-29. Effect of Surface Characteristics and Internal Power Density on Spacecraft Surface Temperature, 2.0 watts/ft$^2$, Non-Spinning Satellite

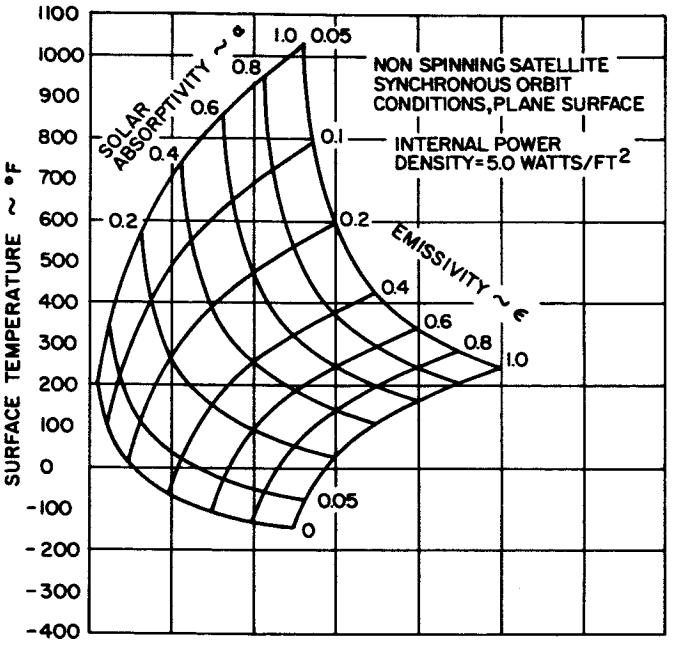


Figure 4-30. Effect of Surface Characteristics and Internal Power Density on Spacecraft Surface Temperature 5.0 watts/ft$^2$, Non-Spinning Satellite

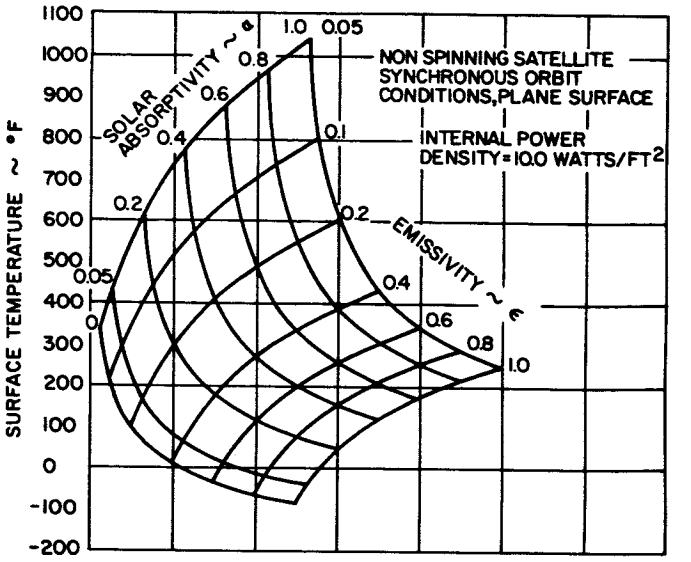


Figure 4-31. Effect of Surface Characteristics and Internal Power Density on Spacecraft Surface Temperature, 10.0 watts/ft$^2$, Non-Spinning Satellite

TABLE 4-6

TEMPERATURE RANGES WITH SURFACE PROPERTIES
THERMAL CONTROL

| Power Density, watts/ft$^2$ | 0 | 0.5 | 1.0 | 2.0 | 5.0 | 10.0 |
|---|---|---|---|---|---|---|
| $T_{max}$, °F | 130 | 140 | 150 | 168 | 115 | 110 |
| $T_{min}$, °F | -453 | -145 | - 85 | - 12 | 15 | 50 |
| $\Delta T$, °F | 583 | 285 | 235 | 180 | 100 | 60 |
| $\alpha_s$ | 0.05 | 0.05 | 0.05 | 0.05 | 0.05 | 0.05 |
| $\epsilon$ | 0.1 | 0.1 | 0.1 | 0.1 | 0.2 | 0.3 |

It may be observed from Figures 4-26 through 4-31 and Table 4-6 that the higher the internal power dissipation, the less the temperature excursions are. On the other hand, a high power density requires a high weight penalty in the form of adequate heat paths from the internal equipment to the outer skin.

The thermal properties of various thermal-control materials are given in Tables 4-1 through 4-3. The effects of micrometeorites and ultraviolet radiation or surface properties are shown in Tables 4-4 and 4-5, respectively. Subsection B.3 contains a discussion on surface characteristics of thermal control surfaces.

b. Shadow-Box Thermal Control

The shadow-box method of controlling temperature is particularly adaptable to the SMS three-axis stabilized configuration. The principle behind the shadow-box scheme is simple. Imagine a satellite shaped like a cube whose orbit is in the plane of the ecliptic. If two opposite surfaces of the cube are maintained parallel to this orbital plane, the two surfaces will never be exposed to solar radiation (see sketch below). If the satellite altitude is sufficiently high (above 20,000 miles), terrestrial and solar reflected radiations will be negligible, and the two surfaces will be exposed only to the internal power dissipation of the satellite. For a constant power dissipation, the temperature of the two surfaces will be constant throughout the entire satellite orbit (provided the two surfaces are insulated from the rest of the satellite).

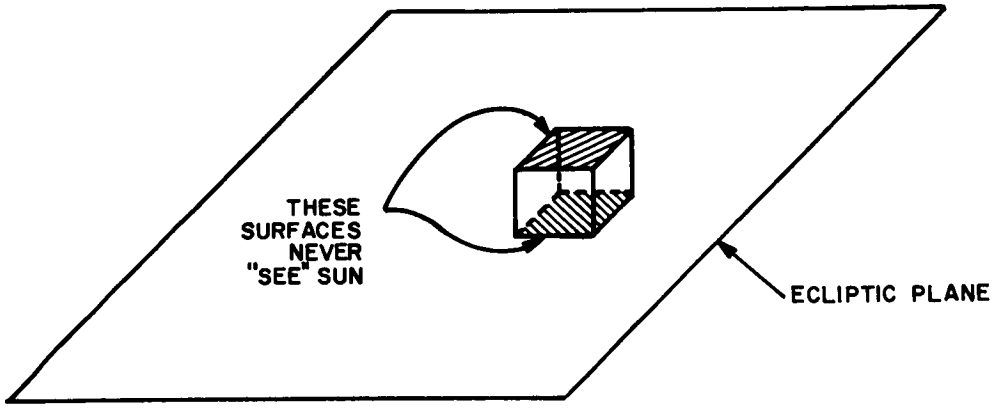


Suppose that the satellite orbit is inclined at an angle, $\Delta$, with the ecliptic plane. In order for the two surfaces not to be exposed to the Sun at any point in the orbit, a shadow box of height given by

$$h' = \ell \tan \Delta \tag{4-26}$$

will have to be constructed on the extremes of the surfaces as shown below.

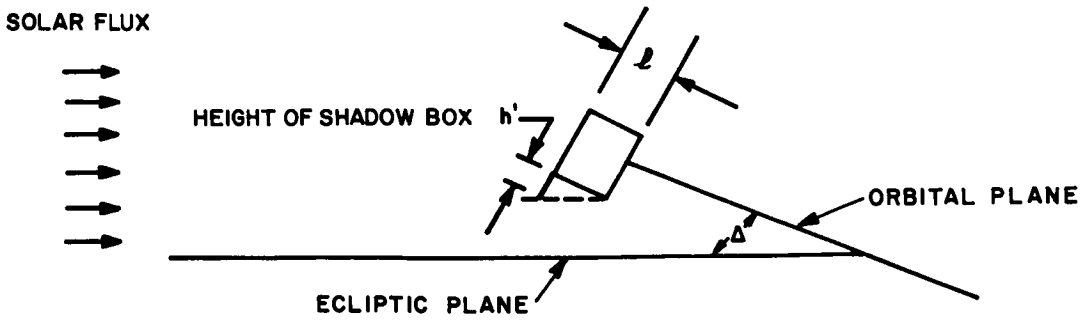

In order to reduce the height of the shadow-box, it may be compartmentized as shown below.

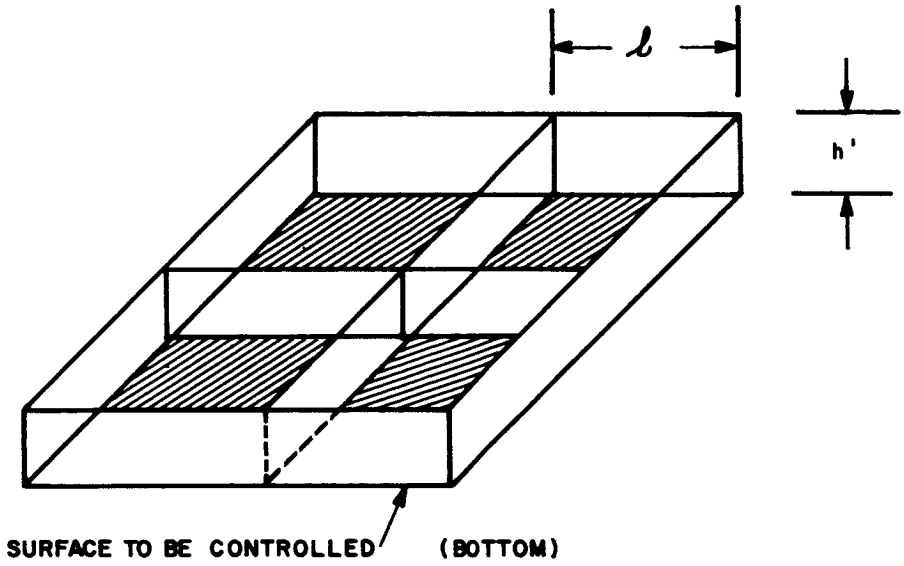


The height of the shadow box in this case is also given by Eq. 4-26, but now the length, $\ell$, is the dimension of the smallest compartment. An analysis on a shadow-box configuration results in the following two simultaneous equations

$$[\sigma\epsilon_1(4\epsilon_{bi}F_{(1-2)}+1)]T_1^4-(4F_{(1-b)}\epsilon_1\epsilon_{bi}\sigma)T_b^4-3.413\,Q_i=0 \qquad (4\text{-}27)$$

$$(2F_{(b-1)}\epsilon_1\epsilon_{bi}\sigma)T_1^4-[2\sigma(\epsilon_{bi}+\epsilon_{bo}+F_{(b-1)}\epsilon_1\epsilon_{bi})]T_b^4+\alpha_b S\cos\Delta=0 \qquad (4\text{-}28)$$

where subscript 1 refers to the surface to be protected
subscript b refers to the shadow box

$F$ = configuration factor (a function of height-to-length ratio of the box which can be found in any heat text book)

$\epsilon_{bi}$ = emissivity of box inside surface

$\epsilon_{bo}$ = emissivity of box outside surface

Table 4-7 shows two cases that were checked with the above equations. It can be observed that the temperature to be controlled changes a negligible amount as the satellite goes from sun exposure to shadow.

TABLE 4-7

SHADOW-BOX PERFORMANCE

| Surface Orientation | Exposed To Sun | In Shadow | Exposed To Sun | In Shadow |
|---|---|---|---|---|
| Power Density watts/ft$^2$ | 0.5 | 0.5 | 5.0 | 5.0 |
| $T_1$, °F | 10 | 8 | 372 | 372 |
| $T_b$, °F | -21 | -398 | -21 | -350 |

Inputs $\epsilon_1 = 0.05$, $\epsilon_{bi} = 0.05$, $\epsilon_{bo} = 0.9$, $\Delta = 28.5°$

$\alpha_b = 0.3$, $F_{(1-b)} = 0.15$, $F_{(b-1)} = 0.29$

The shadow-box principle looks attractive for application to the three-axis stabilized configuration. Since the satellite is stabilized about every axis, a flat surface normal to the pitch axis will "see" the Sun at a maximum glance angle of 23.5° plus the allowable tolerance. For an injection error of 5° the maximum glance angle would be 28.5°. A shadow box with a height given by Eq. 4-26 will maintain the surface temperature reasonably constant throughout the entire orbit. The temperature can be maintained constant even for long mission durations when surface property degradations take place as shown in the next paragraph.

Some of the advantages of the shadow box temperature control scheme are as follows:

(1) Not sensitive to ultraviolet degradation. - The temperature of a surface controlled by a shadow box is a function only of $\epsilon$ and not of $\alpha_s$. Vacuum tests with materials exposed to ultraviolet radiation have shown no degradation in $\epsilon$ (see Table 4-5). It therefore follows that surface degradation due to ultraviolet radiation will not affect surfaces controlled by a shadow box.

(2) Not affected by occult. - Since surfaces controlled by a shadow box are obstructed from sunlight, the satellite occult will not affect the controlled surfaces. It should be remembered that any shadow-box controlled surface and the module behind it will have to be thermally decoupled from the rest of the satellite.

(3) Reduced deterioration due to micrometeorites. - Since the compartmentized shadow box constitutes a network of "fences" on the surface to be controlled, the chances of micrometeorite erosion are considerably reduced.

c. Thermal Control by Heat Storage Materials

When the incident orbital fluxes on a spacecraft are wide ranging, and adequate thermal control by surface properties is not feasible, control by

heat-storage material can be an attractive scheme. Basically, this scheme of temperature control consists of a metallic core filled with a material capable of undergoing a phase change at a predetermined temperature. The core is sandwiched between the components to be controlled and the outside surface of the vehicle which serves as the space radiator. When a component is exposed to solar flux the heat-storage material core will absorb the excess heat and melt, keeping the temperature constant. During the shaded portion of the orbital period, the material would harden, giving off the heat it had absorbed, and still keep the component at the same temperature.

In order to evaluate the merits of thermal-storage temperature control, the following analysis is performed. For a cylindrical satellite, on the sunlit side, the following relation holds true.

$$[S' \alpha_s LD + 3.413 \frac{Q_i'}{2} - \frac{\pi DL}{2} \sigma \epsilon T_f^4 ] t - H_f W = 0 \tag{4-29}$$

where $S'$ = the integrated solar flux during the sunlit period, Btu/hr ft$^2$

$T_f$ = temperature of material fusion point, °R (about equal to the temperature to be maintained for equipment)

$W$ = weight of thermal-storage material, lb

$t$ = time of sunlit period, hours

$Q_i'$ = internal heat dissipation, watts

$H_f$ = heat of fusion of material, Btu/lb

On the dark side, the following relation can be written.

$$[3.413 \frac{Q_i'}{2} - \frac{\pi DL}{2} \sigma \epsilon T_f^4 ] t + H_f W = 0 \tag{4-30}$$

If an individual component has to be analyzed, the satellite skin can be considered locally flat (if the component is not large relative to the satellite). For this case, the above equations reduce to

$$W' = \frac{\alpha_s S' t}{2H_f} \tag{4-31}$$

$$\epsilon = \frac{3.413 Q_i + H_f W'/t}{\sigma T_f^4} \tag{4-32}$$

where $W'$ = pounds of material per square foot

$Q_i$ = internal power density, watts/ft$^2$

It should be observed from Eq. 4-31 that for a given material ($H_f$ fixed) and given orbital conditions ($S'$ and $t$ fixed), the amount of material needed is a function only of $\alpha_s$. For a known $\alpha_s$ the corresponding $\epsilon$ is found from Eq. 4-32.

The performance of various thermal-storage materials is shown in Figure 4-32. The "Transit Heet" materials are manufactured by Cryo-Therm, Inc., which specializes in the development of new and improved thermal-storage materials. According to Dr. Maria Telkes of Cryo-Therm, Inc., it is possible, with some additional development, to produce a material with a heat of fusion of near 150 Btu/lb.

d. Thermal Control by Heating Elements

Another approach to passive temperature control is the use of heating elements. In this method, the radiator surface properties $\alpha_s$ and $\epsilon$ are chosen to give the desired temperature under maximum solar insolation. On the dark side of the orbit, heating elements are turned on to keep the temperature above the allowable minimum.

This method of temperature control requires the design of extremely efficient heating elements in order to avoid excessive power consumption. Present effective heating elements are of the "electric blanket" type, either in mesh form or in spray-on form. The mesh heating elements are laminated between two thin layers of electrical insulation and wrapped around the components to be controlled. The weight of these surface type heating elements is between 0.07 to 0.33 lb/ft$^2$. Closely spaced fine wires in parallel, up to 50 per inch, carry the current. They are held in position by a woven cross wire which serves as an electrical tie between the strands. For a given watt density, multiple conductors distribute heat more uniformly than does a single large conductor and operate at lower conduction temperatures. In addition, the cross wires offer parallel paths if a wire is broken.

The amount of power required to maintain a given component at a required bulk temperature is a function of the component mass, specific heat, surface area, heat path resistance and the temperature difference that has to be overcome. For a component in a vacuum interacting only with the satellite skin, the amount of power needed is given by

$$Q_h = \frac{A\,(T_c - T_s)}{\sum_{i=1}^{n} \frac{x_i}{k_i} + \frac{T_c - T_s}{\sigma F_e F_c (T_c^4 - T_s^4)}} + \frac{W C''(T_c - T_{co})}{t} \qquad (4\text{-}33)$$

where
- $x_i$ = length of the $i^{th}$ conduction path, ft
- $k_i$ = conductivity of $i^{th}$ conduction path, Btu/hr ft °R
- $T_c$ = desired component bulk temperature, °R
- $T_s$ = satellite skin temperature, °R
- $T_{co}$ = initial component temperature, °R
- $F_e$ = emissivity factor
- $F_c$ = configuration factor
- $t$ = component warm-up time, hr
- $W$ = component weight, lb
- $C''$ = component specific heat, Btu/lb °R

Unless the detailed geometry and thermal properties of the components and their surroundings are known, the power requirements for systems employing heating elements are difficult to compute.

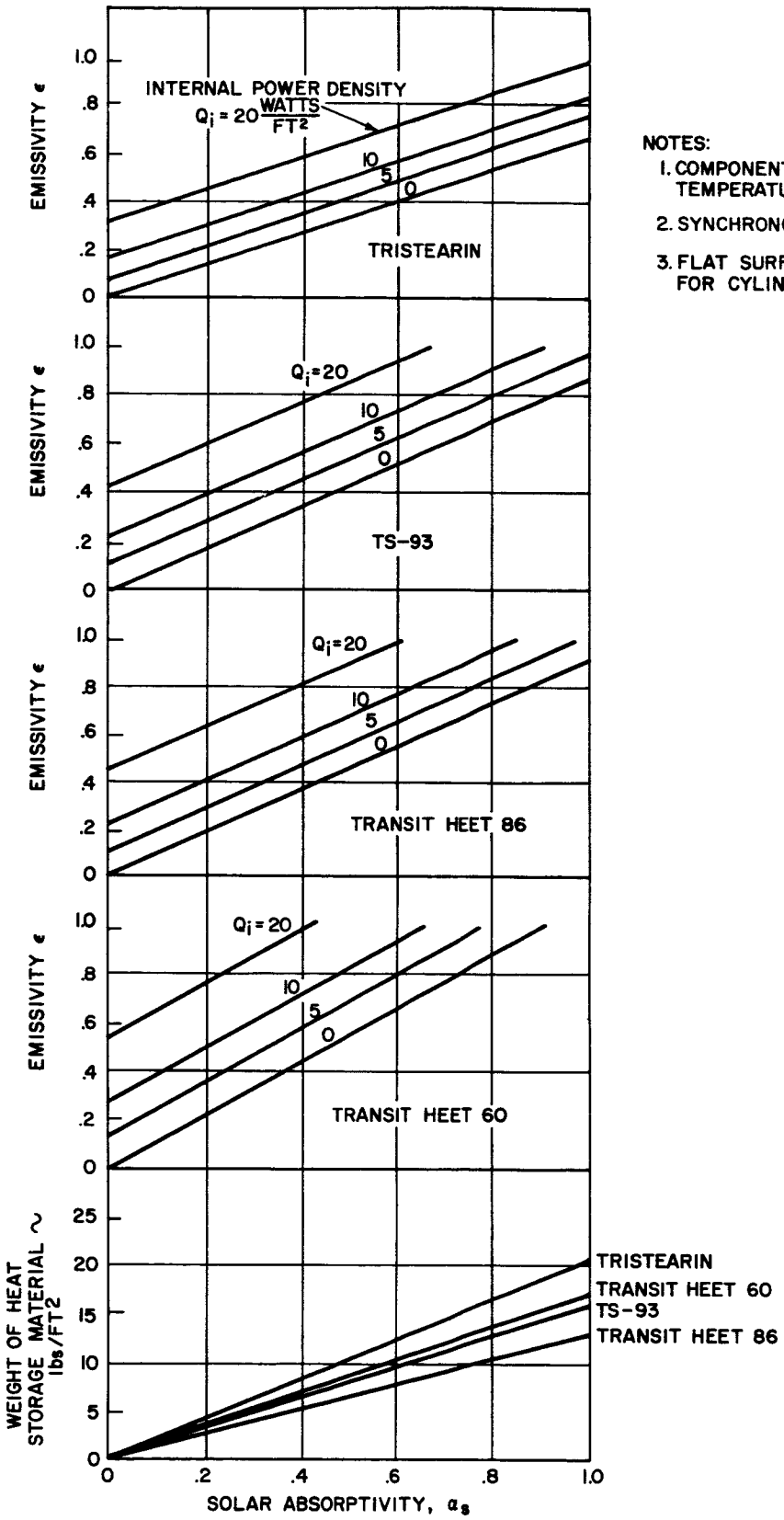


NOTES:

1. COMPONENT TEMPERATURE ≈ FUSION TEMPERATURE.
2. SYNCHRONOUS ORBIT CONDITIONS.
3. FLAT SURFACE. SEE VOL. 2, SECTION 2 FOR CYLINDRICAL SURFACE.

| MATERIAL | HEAT OF FUSION BTU/lb | FUSION TEMP °F | DENSITY lbs/FT2 |
|---|---|---|---|
| TRISTEARIN | 82.1 | 133 | — |
| TS-93 | 107 | 93 | — |
| TRANSIT HEET 86 | 130 | 86 | 100 |
| TRANSIT HEET 60 | 100 | 60 | 100 |

Figure 4-32. Performance of Thermal-Storage Temperature Control Systems

## D. SEMIACTIVE TEMPERATURE CONTROL

### 1. Introduction

There is a lack of general agreement on the definition of a semiactive temperature control system. Thus, for clarification as used in this report, a semiactive temperature control system is defined as one in which there are moving parts and/or fluids, but the system specifically excludes a heat pump. In a semiactive temperature control system, heat is rejected at or below the source temperature.

Where the spacecraft temperature limits are such that a passive temperature control is feasible, the temperature control system has the advantages of being simple, inexpensive, lightweight and, above all, reliable. In contrast, a semiactive temperature control system requires a temperature sensor, a controller, an actuator, and a movable vane or shutter to change the radiative properties of a thermal control surface. A system incorporating these components adds weight, complexity, cost, and unreliability to the spacecraft. Table 4-8 gives a partial list of spacecraft that have, or will have, semiactive thermal controls.

TABLE 4-8
SPACECRAFT EMPLOYING SEMIACTIVE THERMAL CONTROLS

| Spacecraft | Types of Control |
|---|---|
| ABLE | Bimetallic-actuated discs |
| TELSTAR | Gas-actuated radiation cover |
| RELAY | Gas-actuated circular discs |
| NIMBUS | Gas-actuated movable shutters |
| OGO | Bimetallic-actuated movable shutters |

### 2. Mechanically Variable Radiative Surface Properties

#### a. Movable Shutters

If a space radiator with a high-emissivity surface, which is desirable while exposed to sunlight, could have its surface radiative properties changed while in the shadow, then a large part of the temperature control problem would be solved. A temperature control device capable of performing this is shown in Figure 4-33. When the low-emissivity shutters are closed, the surface will emit little heat, and vice versa. By varying the degree of shutter opening, any value between the minimum and maximum emittance can be obtained.

The shutter movement can be preprogrammed, closed-loop controlled, or self-regulated by a bimetallic element that is controlled by the satellite temperature.

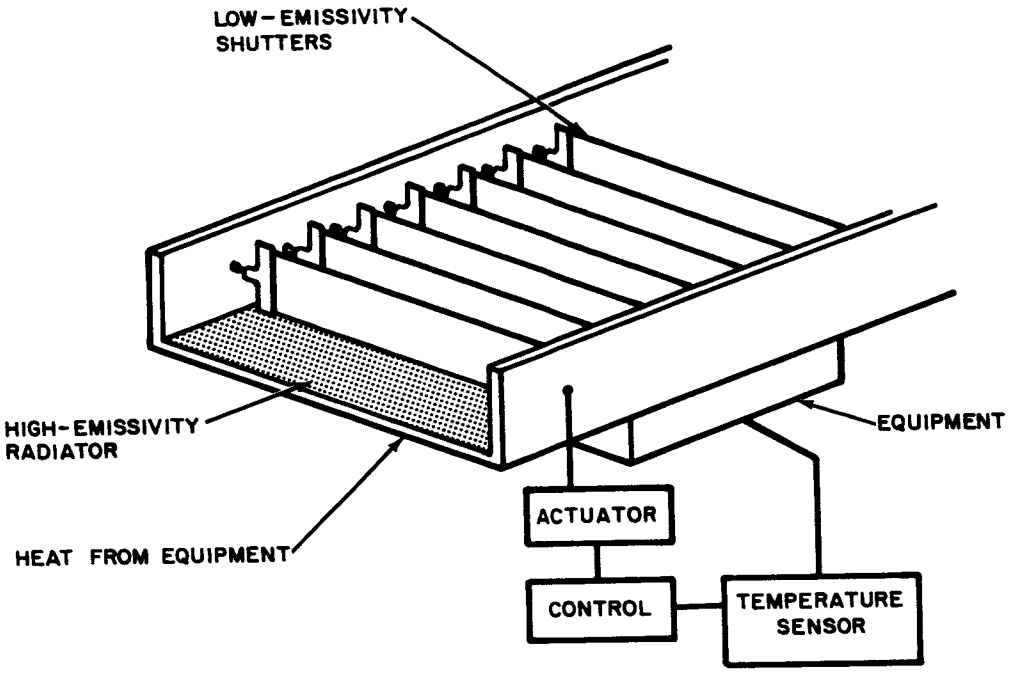


Figure 4-33. Closed-Loop, Movable Shutter System

The governing equations for a continuously responsive system are given below. The equations hold for the three-axis stabilized configuration having shutters at any point of the cylinder circumference with their hinge axes parallel to the cylinder axis.

$$\alpha_{sh} S \cos\mu + \sigma\left[F_c(\theta)\, F_e(\theta)\,(T_s^4 - T_{sh}^4) + F_c(180-\theta) F_e(180-\theta)(T_s^4 - T_{sh}^4) - \epsilon_{sh} T_{sh}^4\right] = 0 \tag{4-34}$$

$$\alpha_s S(1-\cos\theta)\cos\nu + 3.413\, Q_i - \sigma\left[F_c(\theta) F_e(\theta)(T_s^4 - T_{sh}^4) + F_c(180-\theta) F_e(180-\theta)(T_s^4 - T_{sh}^4) + \epsilon_s T_s^4 (1-\cos\theta)\right] = 0 \tag{4-35}$$

$$\cos\mu = \cos(\omega_{E/S} t)\sin(\lambda+\theta)\sin(\omega_{S/E} t') + \sin(\omega_{E/S} t)\left[-\sin\Delta\cos(\lambda+\theta) + \cos\Delta\sin(\lambda+\theta)\cos(\omega_{E/S} t)\right] = 0 \tag{4-36}$$

$$\cos\nu = \cos(\omega_{E/S} t)\sin\lambda\sin(\omega_{S/E} t') + \sin(\omega_{E/S} t)\left[-\sin\Delta\cos\lambda + \cos\Delta\sin\lambda(\omega_{E/S} t)\right] \tag{4-37}$$

where $\theta$ = shutter opening angle

$\mu$ = angle between shutter normal and Earth-Sun vector

$F_c(\theta)$ = configuration factor evaluated at $\theta$

$F_c(180-\theta)$ = configuration factor evaluated at $(180-\theta)$

$F_e(\theta)$ = emissivity factor evaluated at $\theta$

$F_e(180-\theta)$ = emissivity factor evaluated at $(180-\theta)$

$\nu$ = angle between the normal to the surface behind the shutter and the Earth-Sun vector

$\lambda$ = angle between the shutter hinge line and the pitch axis

sh = subscript refers to shutter

Note: See Eqs. 4-3 and 4-4 for the definitions of the other terms.

The power requirements for a movable shutter system are nominal. For a bimetallic-actuated system there is no power requred. The weight of the shutters and controls, exculsive of radiator, are in the range of 0.15 to 0.4 lb/ft$^2$. The operation of bearings and controls in vacuum is subject to uncertanity and to meteoritic impact damage.

b. Rotatable Vanes

Another temperature control device capable of varying the absorptivity or the emissivity of a radiating surface is the rotatable vane. This device, shown schematically in Figure 4-34, consists of a circular radiator with alternate sectors of high-emissivity and low-emissivity coatings and a rotatable vane. By rotating the vane to different positions, the effective emissivity of the radiator is changed. In addition to the vane-radiator assembly, the system consists of an actuator, controller, and a temperature sensor.

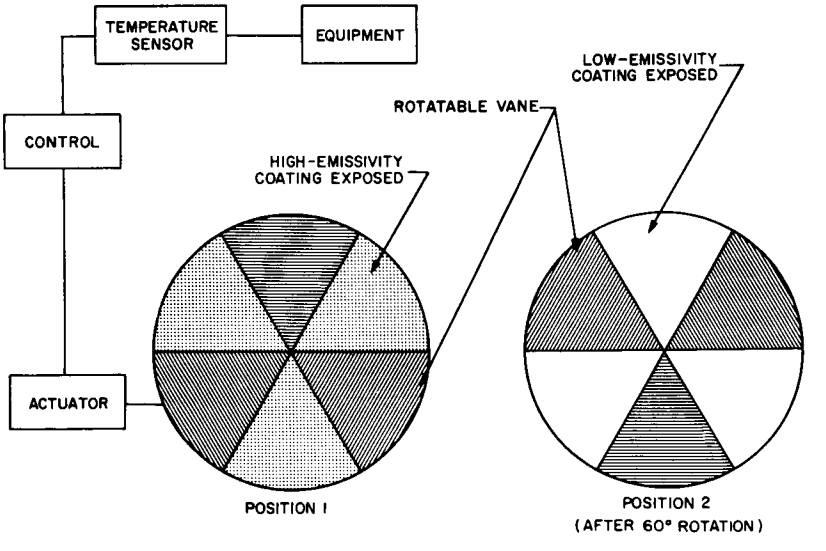


Figure 4-34. Closed-Loop Rotatable-Vane System

The effectiveness of this type of temperature control system is a function of the relative amount of total area in which surface radiation properties can be changed. In this respect the rotatable system is less effective than the movable shutter system because in the rotatable vane system the maximum area in which radiation properties can be changed is only 50 percent of the total. In the movable shutter system, however, all the radiator area can be subjected to radiation property changes.

### 3. Mechanically Variable Thermal Resistance

#### a. Variable Conductance Devices (Thermal Switch)

The use of a variable conductance device can be very effective in a semiactive temperature control system. If a given quantity of heat, $Q = C(T_e - T_s)$, generated in the interior of the satellite is transported to the satellite skin (radiator), then the product $C(T_e - T_s)$ has to stay constant. (C is the conductance, $T_e$ is the equipment temperature, and $T_s$ is the skin temperature.) For $T_e$ to be reasonably constant as $T_s$ fluctates because of sunlight and shadow exposure, C has to vary accordingly.

The thermal switch is a device by which the conductance in a thermal circuit can be varied. When two surfaces are held together under pressure, the effective contact area is a function of the contact material, the surface conditions, and the contact pressure. The variation of conductance with pressure for various materials is shown in Figure 4-35 (Ref. 4-10). A schematic of a typical thermal switch is shown in Figure 4-36.

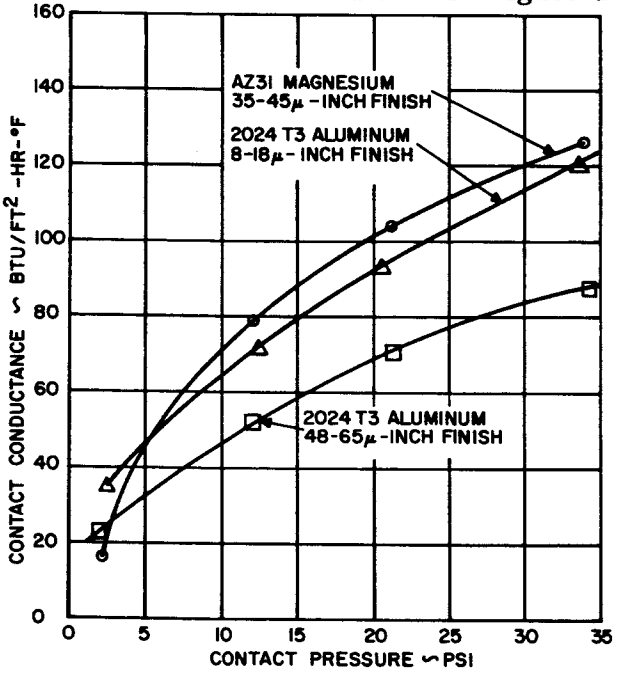


Figure 4-35. Thermal Contact Conductance For Aluminum and Magnesium Joints in Vacuum

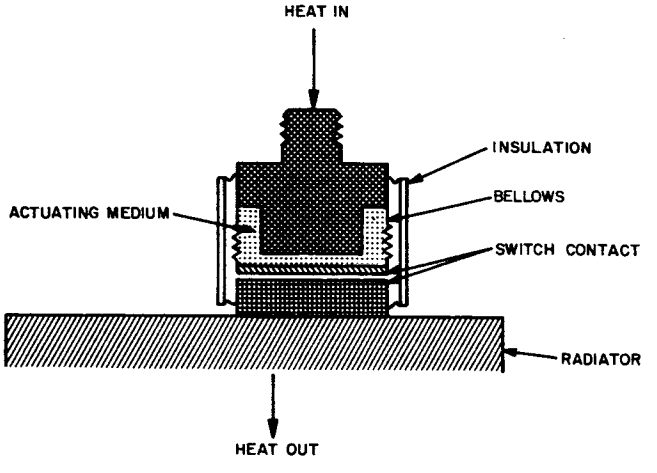


Figure 4-36. Thermal Switch for Control of Conductivity

The operation of a thermal switch involves the partial opening and closing of a thermal conductive circuit in response to a temperature change. A bellows filled with a temperature sensitive fluid would vary the contact pressure, thus varying the conductance.

b. Variable Contact Area Devices

In the previous discussion of variable conductance it was assumed that the gross contact area is not varied. However, the conductance is directly proportional to the contact area, and by varying the contact area a variation in circuit conductance can be obtained. A possible device for contact area variation is shown in Figure 4-37. In this method the contact-area variation is obtained by varying the shape of the highly conductive liquid-metal layer interposed between two conductors.

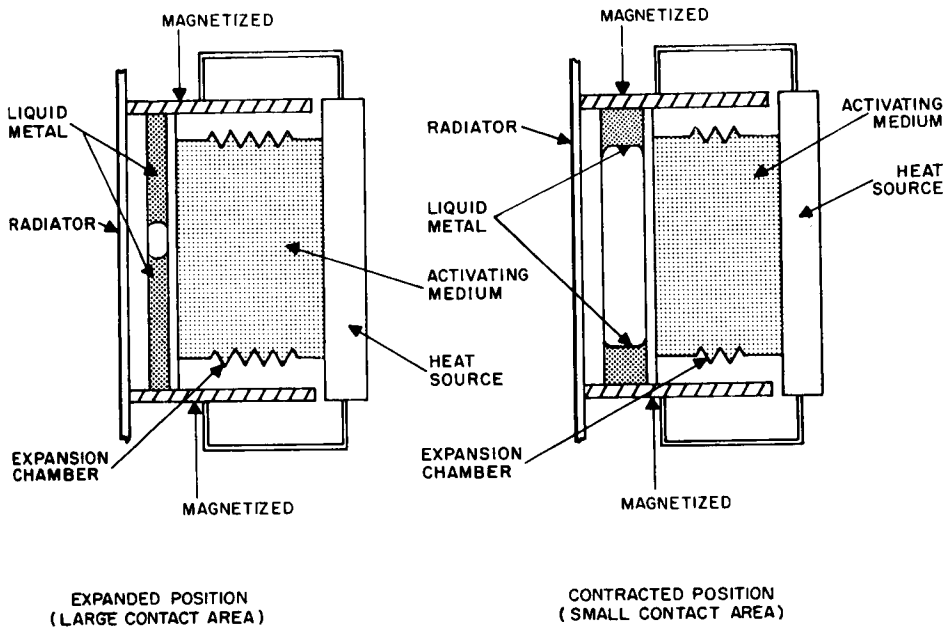


Figure 4-37. Device for Contact-Area Variation

This method of temperature control is based on the principle of fluid volume variation produced by a change in the temperature or phase of the fluid. The range of contact area variation that can be achieved with this method is from 100 percent to almost zero. No external power is required with this method, and the system tends to be self-controlled. The problem of zero g operation can be overcome by the use of permanent magnets or electromagnets.

4. Forced Convection Loop (Cold-Plate System)

a. System Operation

One way to control the operating temperature of electronic and similar equipment is through the use of cold plates. If the temperature to be controlled and the sink temperature are of the right relative magnitude, a light weight, reliable and compact system can be designed, based upon this principle. For this system to be applicable the maximum allowable equipment temperature must be higher than the available sink temperature.

A cold-plate system, generally, consists of the cold plates, a heat transport fluid, a pump, a radiator, and associated controls to maintain the required temperature tolerance. Figure 4-38 is a sketch of the basic components and the arrangement of a typical system. The transport fluid is circulated through the closed-loop system by a pump. The fluid absorbs the heat load as it passes through the cold plates. The heat load is transported to the radiator and dissipated to the receiving medium through an appropriately designed radiator.

Cold plates are, generally, constructed of two sheets of metal separated by a sheet of heat transfer material. Figure 4-39 presents this typical configuration. The assembly is permanently bonded together to form a rigid, lightweight unit with high thermal conductivity. The material used for construction can be aluminum, copper, steel or any material that is compatible with the transport fluid and the equipment to be cooled. Bonding is usually by dip brazing or furnace brazing, but gluing is sometimes used for low temperature applications.

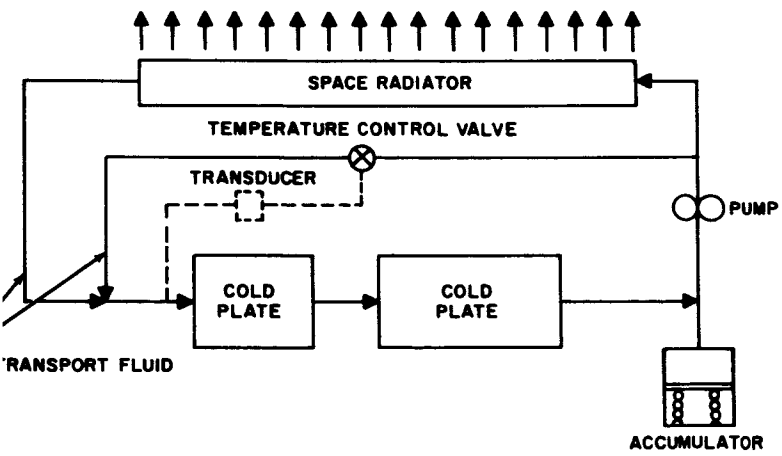


Figure 4-38. Cold Plate System Schematic

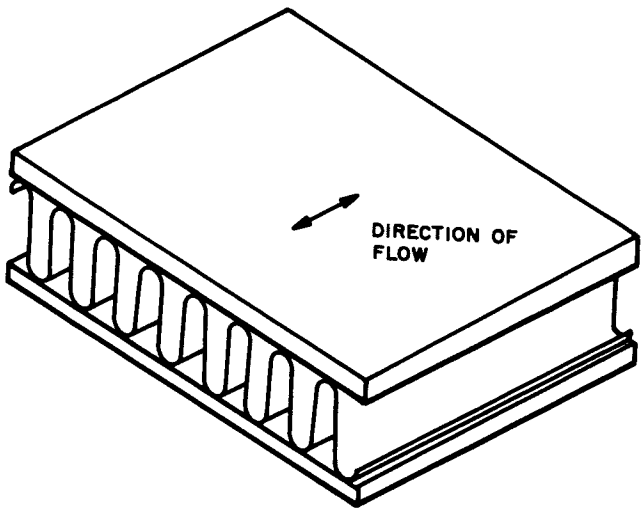


Figure 4-39. Typical Cold Plate Schematic

The components to be cooled are placed on the cold plates and heat is transferred from them to the cold plate by conduction. The critical part of this arrangement is the contact resistance between the component and the cold plate. This resistance is a function of the cleanliness of the mating surface, the pressure, the flatness, the finish and the area of contact. The resistance can be reduced by spreading grease, developed for this purpose, between the mating surfaces. The heat can be conducted down posts and into the cold plate. The posts are dip brazed to the surface of the cold plate to reduce the contact resistance. The cold plate can form part of the chassis and act as support for the enclosure.

The transport fluid can be a gas or a liquid. A liquid is preferable because its heat transfer characteristics are superior to a gas, the pumping power required is less, and the equipment can generally be constructed smaller and lighter. The liquid can be water, ethylene-glycol/water, FC-75, Coolanol 45 or any other suitable fluid.

If a fluid is used as the heat transport medium, any appropriate pump will suffice to circulate it. When an electric motor is used to drive the pump the "wet motor" design is usually preferable if the start-up temperature is not so low that fluid viscosity will be a problem. The "wet motor" design eliminates the need for a fluid seal between the pump and the motor by permitting the fluid to pass over the motor then into the pump. This design also provides a controlled environment for the motor.

The radiator can be any design that will transfer the required amount of heat from the transport fluid to the receiving medium. The receiving medium can be air, liquid or the space void. The radiator normally is of the compact, plate-fin design for the first two mediums and is a standard space radiator for the last medium.

Cold plates are inherently adaptable to space applications because their performance is not affected by zero gravity and they do not require an atmosphere to transfer the heat from the component to be cooled to the transport fluid.

b. Possible SMS Design

A detailed analysis must be performed upon a given design before it can safely be selected. This analysis is necessary to determine if the design is susceptible to such adverse affects as the following:

(1) Insufficient pressure drop of the transport fluid through the cold plate to ensure even distribution

(2) The formation of laminar flow over regions requiring turbulent flow for high heat transfer coefficients

(3) The percentage of channel and header volume to overall volume for obtaining the correct wet weight

(4) The effect upon the pressure drop and heat transfer characteristics caused by placing module mounting inserts in the fluid passage

Such problems as these are not evident when design curves alone are used to arrive at a configuration.

In order to arrive at an optimum cold-plate design, a detailed knowledge of equipment location and geometry, power distribution, and temperature limits of individual components is required. In applying the cold-plate method of temperature control to the SMS, the medium performance three-axis stabilized configuration was chosen as typical. The analysis is based on the characteristics of the F-3 aluminum fin manufactured by the Fairchild Stratos Corporation, Bay Shore, N. Y. The following design inputs were assumed:

Cold-plate heat load = 350 watts

Maximum allowable component base temperature = 77°F

Heat transport fluid = Ethylene-glycol/water

Heat transport fluid flow rate = 1 gpm

Total cold-plate area = 10 $ft^2$ (subdivided among the equipment shelves)

The total cold-plate area is generally determined by the minimum mounting area required by the equipment and not from heat transfer considerations. If the width of a cold-plate is too wide to obtain ample pressure drop for good fluid distribution, separators can be put in the plate so that the fluid is required to make several passes across the plate before the total area is covered. The heat flux is the average wattage absorbed per unit of area. If there are concentrated heat loads they must be analysed to determine the maximum component base temperature that can be tolerated.

The results of this analysis are listed as follows:

Temperature of fluid entering cold plate = 72°F

Temperature of fluid leaving cold plate = 75°F

Pressure drop across cold plate = 3.6 psi

Power input to circulating pump = 7 watts (based upon assumed circuit pressure drop = 7.5 psi)

Cold-plate dry weight = 8.85 pounds (weight can vary with required sheet thickness)

Estimated wet weight of system excluding space radiator = 12.5 pounds

Radiator allowable pressure drop = 3.0 psi

Radiator mean temperature = 74°F

Table 4-9 shows a summary of the cold-plate design.

TABLE 4-9. COLD-PLATE COOLING SYSTEM RESULTS

| | |
|---|---|
| System wet weight (excluding radiator), lb | 12.5 |
| Cold-plate dry weight, lb | 8.85 |
| Radiator area, $ft^2$ | 14.2 |
| Radiator dry weight, lb | 7.1 |
| Radiator wet weight, lb | 7.93 |
| Overall system weight, lb | 21 |
| Required power, watts | 7 |

## E. ACTIVE TEMPERATURE CONTROL

### 1. Introduction

If a heat pump is used to transfer all of the heat generated internally to the vehicle surface, the system is termed "active." In this system, heat is dissipated at a higher temperature than the source temperature. An active temperature control system is more complex and is usually heavier than semiactive or passive systems. However, some of the advantages of an active control system are:

(1) Some compensation may be made for surface properties changing due to space environment

(2) The control may be accomplished with narrower temperature limits

(3) Limited compensation may be made for time-dependent change in internal generations

(4) Anticipation control can be utilized

Some techniques that can be used in an active thermal control system are: 1) Vapor Cycle Refrigeration, 2) Gas Cycle Refrigeration, 3) Absorption Cycle Refrigeration, and 4) Thermoelectrical (Pelteir) Cooling. A brief description and evaluation of these devices will be presented in this subsection E.

### 2. Vapor Cycle Refrigeration

#### a. Description

The simple vapor cycle, shown schematically in Figure 4-40, is composed of a vapor compressor, condenser (radiator), expansion device and evaporator. The refrigerant exits the expansion valve as a mixture of saturated liquid and saturated vapor. In the evaporator, the liquid refrigerant changes at constant pressure into a vapor by absorbing heat from the region to be cooled. Depending on the characteristic of the device that meters refrigerant into the evaporator, the refrigerant may leave the evaporator as a saturated vapor, as a mixture of saturated liquid and vapor, or as a slightly superheated vapor. The refrigerant then enters the compressor where it is compressed isentropically to the condenser pressure. It then flows through the condenser at constant pressure and rejects the heat added during evaporation and compression to the ulti-

mate heat sink. Finally, the refrigerant leaving the condenser as a liquid flows through the throttling valve back to the evaporator to repeat the cycle.

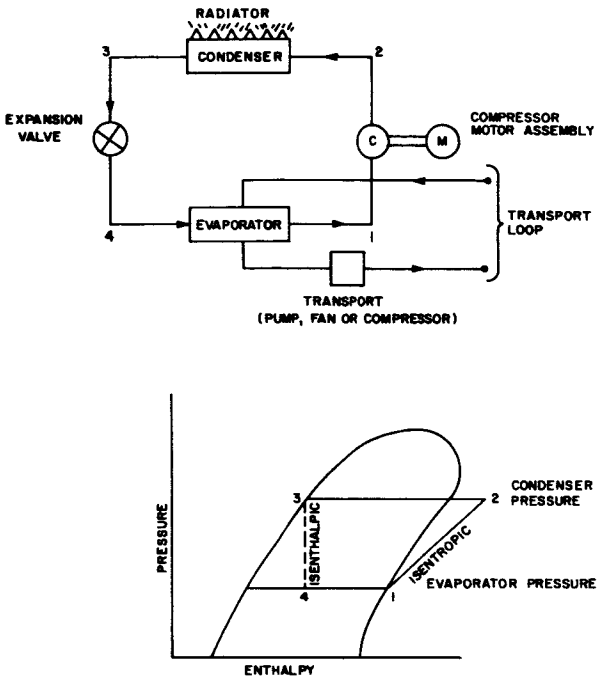


Figure 4-40. Vapor Cycle Refrigeration Schematic

b. Analysis (Ref. 4-11)

1) Refrigerants. Very few desirable refrigerants are available for vapor cycle systems operating with a high condenser temperature. Of available refrigerants, Freon 11, 21, 113, 114 and water appear applicable for continuous operations below 350°F. Freon 11, 21 and water were selected for this analysis because of the relatively high coefficients of performance obtainable with their use and they are preferable from a thermodynamic standpoint because slightly less work is required for a given cooling load, evaporator temperature and condenser temperature. New, high temperature refrigerants need to be developed because, even though relatively high performance can be obtained with presently available low temperature refrigerants, large radiators and power units are required.

2) Assumptions. A simple cycle system with isentropic compression was considered representative of the more complicated thermodynamic cycles. Although no allowances were made for the less efficient actual compression processes, no refinements of the cycle were considered either. Vapor cycles utilizing regenerative subcooling and interstage compressor cooling will approach very closely the simple cycle with isentropic compression. Therefore, the performance determined for the simple cycle was considered approximately valid for practical refined cycles. However, in considering the overall weight of a system, where individual components must be accounted for, a practical system must be considered.

A completely isolated radiator (condenser) was assumed. No heat was transferred to the radiator except that from the cooling system's fluid, and no heat was lost from the radiator except that radiated to space at absolute zero. The radiator was assumed to be shielded from the Sun's rays. The radiator will be the underside of the solar panels, insulated and coated to achieve the desired temperature. The emissivity of the radiator was assumed to be unity. The radiator areas need only to be divided by the actual emissivity of the radiator surface for more accurate values.

The temperature of the radiator surface was assumed equal to the heat rejection temperature of the cooling system's fluid. The actual temperature difference should be very small for condensing such fluids as the refrigerant used in vapor cycles. For liquids or gases, the temperature drop would be considerably larger and could not be ignored without introducing a significant error. For this reason, as well as for simplicity, condensing the fluid within the radiator is more desirable than using a coolant fluid to transport heat from the condenser to the radiator.

Based upon the latest state of the art information, radiator weight can be estimated by assuming .25 lb/ft$^2$ for a radiator that is integrated with the vehicle structure and from 1 to 2 lb/ft$^2$ for deployable radiators. A conservative weight of .5 lb/ft$^2$ (nondeployable) was assumed for this analysis.

3) Weight. In estimating the weight penalty of various active thermal control systems, the total weight is subdivided into three parts; namely, radiator weight, power unit weight and individual component weights.

a) Radiator Weight. The radiator weight required for the cooling system, based on a cooling capacity of one kilowatt, was determined by the equation for radiator area using 0.5 lb/ft$^2$ for a conversion factor.

$$A_{rad} = \frac{Q_R}{\sigma F_e F_c (T_{rad})^4} \tag{4-38}$$

where $Q_R$ = heat rejected in radiator, Btu/hr/kw

$A_{rad}$ = area of radiator, ft$^2$

$\sigma$ = Stefan-Boltzmann constant = $0.173 \times 10^{-8}$, Btu/hr-sq ft-°R$^{-4}$

$F_e$ = emissivity factor, assumed = 1.0

$F_c$ = geometric or configuration factor, assumed = 1.0

$T_{rad}$ = temperature of radiator in °R, assumed equal to the heat rejection temperature of cycle's fluid ($T_R$)

Based on a one kilowatt cooling capacity, the heat rejected in the radiator in Btu/hr/kw, is

$$Q_R = 3413 \frac{i_2 - i_3}{i_1 - i_4} \tag{4-39}$$

where $i$ = enthalpy of refrigerant, Btu/lb

1, 2.., = subscripts referring to static point (Figure 4-40)

The required compressor work, $Q_{wk}$, in hp/kw was determined from the equation

$$Q_{wk} = \frac{3413}{2545} \frac{i_2 - i_1}{i_1 - i_4} \tag{4-40}$$

The refrigerant weight flow in lb/hr/kw is

$$\dot{W} = \frac{3413}{i_1 - i_4} \tag{4-41}$$

Figures 4-41, 4-42 and 4-43 present the radiator weight and compressor work per kilowatt of cooling capacity as a function of radiator temperature for freon 11, 21 and water, respectively. Three cycles for each refrigerant were considered, the variable being the evaporator temperature. An evaporator temperature of 40°F is indicative of cooling a compartment to 75°F, an evaporator temperature of 80°F is indicative of cooling a compartment to 115°F, and an evaporator temperture of 120°F is indicative of cooling electronic equipment to about 150°F.

Figure 4-44 presents the compressor's pressure ratios required at the various radiator temperatures for the respective refrigerants. It should be noted that multistage compressors would be required to produce pressure ratios of this order.

Based upon the data presented, the minimum radiator weight for the cooling system exists when the radiator temperature is approximately 275°F for the freon cycles and approximately 300°F when water is used as the refrigerant. In some cases water shows a slight decrease in weight penalty over the freons. However, the compressor's required pressure ratio is high (Figure 4-44) and coupled with water's low molecular weight and high freezing temperature, makes the refrigerant undesirable for space application.

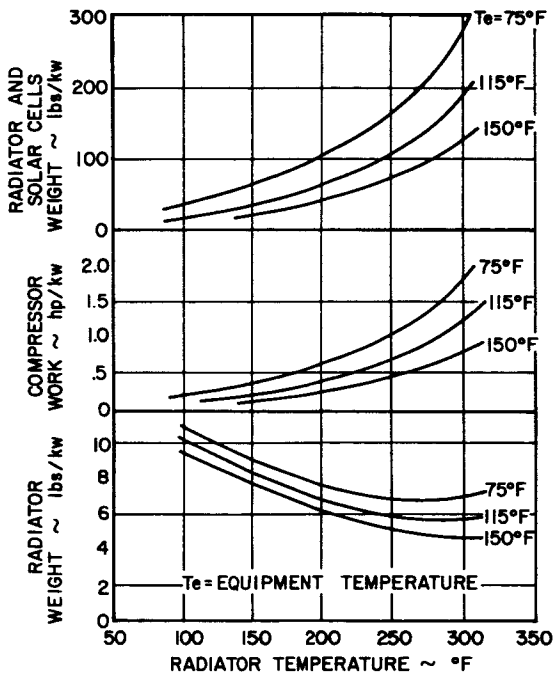


Figure 4-41. Vapor Cycle Performance, Freon-11

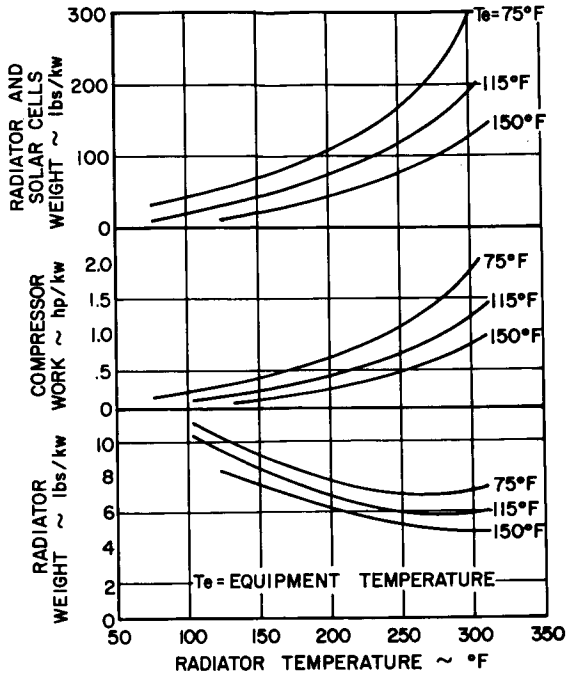


Figure 4-42. Vapor Cycle Performance, Freon-21

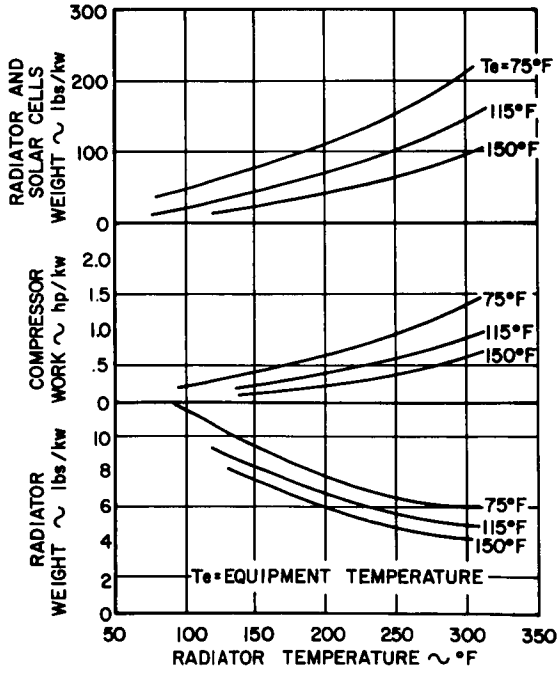


Figure 4-43. Vapor Cycle Performance, Water

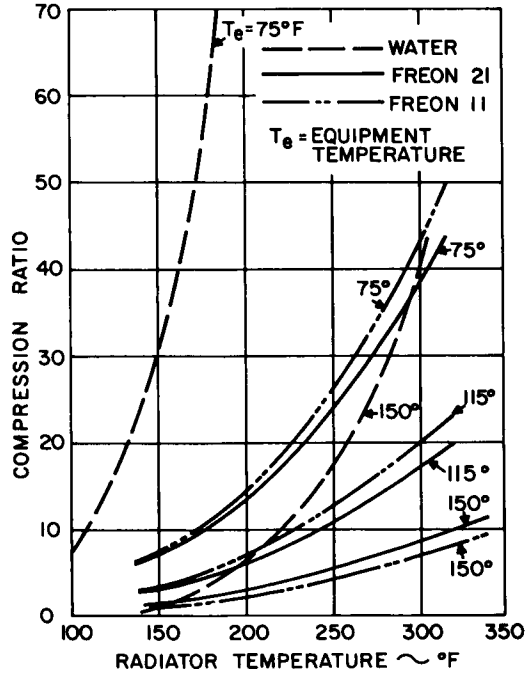


Figure 4-44. Vapor Cycle, Refrigeration Compression Ratio

b) Power Unit Weight. Special consideration must be given to the power unit required to drive the cooling system since this additional work from the power unit significantly increases the total weight of the overall system. At the present time the most efficient source of power in the SMS power range (50 to 500 watts) is the solar cell. It has been estimated that for every five watts of power, the solar cell array would weigh one pound.

The top curves of Figures 4-41, 4-42 and 4-43 give the combined weight of the radiator and solar cells required for one kilowatt of internal load. The most significant fact that can be seen from these curves is that the lower the cooling system's radiator temperature, the smaller the weight required for the radiator and solar cells. The optimum radiator temperature is that which is equal to the mean temperature within the evaporator. This condition is approximately equivalent to a semiactive cooling system. This indicates that the optimum active system reduces to a semiactive system. Thus a vapor cycle could be replaced by a fluid being pumped through the system with only the pumping power required sufficient to overcome ducting and heat exchanger pressure drop. See results of forced circulation (cold-plate system) analysis in subsection D-4.

c) Individual Component Weight. It has already been shown that a vapor cycle cooling system would not be applicable at this time due to the large weight penalty imposed by the use of solar cells for operating the cooling system. Therefore, a detailed analysis of component weights is not described here. This is also the case for an analysis on volume penalties.

3. Gas Cycle Refrigeration

a. Description

The gas cycle refrigeration system is composed of four major components: compressor, turbine, radiator and compartment heat exchanger (Figure 4-45). The pressure level of the gas contained within the vehicle or within a closed temperature control surface loop is raised by the compressor. The heat load and the heat of compression is rejected from the vehicle by a radiator. The high pressure circulating gas, after being cooled by the radiator, is then expanded across the turbine. During the expansion process the gas experiences a temperature drop to a level below the compressor inlet temperature. This low temperature gas is then used for cooling the vehicle load. After absorbing heat from the load, the gas returns to the compressor to repeat the cycle.

A makeup storage device is required to maintain the desired pressure level within the vehicle or within the gas circuit of the compartment closed temperature control system loop.

b. Analysis (Ref. 4-12)

1) Gases. For this analysis the two gases air and hydrogen were selected, representing low and high specific heat gases, respectively. They were treated as perfect gases (constant $c_p$), thereby introducing an error in the size of the radiator required. As the specific heat ($c_p$) at constant pressure

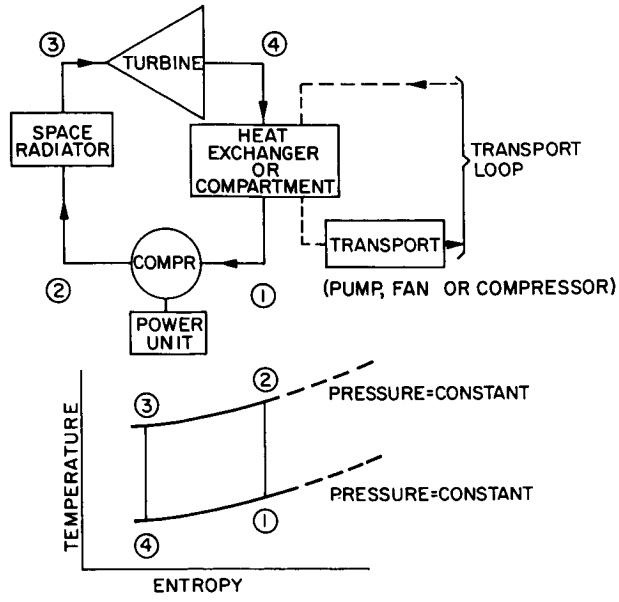


Figure 4-45. Gas Cycle Refrigeration Schematic

decreases, the temperature of the gas leaving the compressor decreases, thereby giving a lower radiator temperature. Since the ability of the radiator to radiate heat is directly proportional to the fourth power of the radiator temperature, a sizeable increase in the radiator area can be caused by a larger increase in $c_p$ and a larger decrease in $k'$, the ratio of specific heat at constant pressure to that at constant volume. This error is greater at higher temperature than at lower temperature. By treating air as a perfect gas and considering compressing it adiabatically from 50°F to 500°F, approximately a 3 percent smaller radiator is required than when compressing air adiabatically while considering its actual properties. Compressing air under the same conditions from 50 to 1000°F results in approximately a 10 percent smaller radiator than when considering the actual properties of air. About the same results are obtained for hydrogen.

2) Assumptions. A compression and a turbine efficiency of 85 percent were assumed. These efficiencies are representative of extremely well designed centrifugal machines operating over a low pressure ratio.

Adiabatic compression and expansion were assumed. Approximate adiabatic compression and expansion are obtained with centrifugal type machines because of the large gas flow through them. Small deviations from adiabatic processes in the compressor and turbine will tend to cancel one another, since heat will be lost from the compressor and gained by the turbine.

The assumptions made previously concerning the radiator under the vapor cycle refrigeration discussion applies for this analysis. However, it should be noted that the assumption of a zero temperature difference between the radiator's surface and the circulating gas in this analysis is not conservative. The actual reduction in radiator temperature caused by the gas-to-surface temperature drop will require a larger radiator than that indicated by this analysis. This increase in radiator size is apparent from the fact that the heat radiated is directly

and the temperature of the gas leaving the radiator and entering the turbine was

$$T_3 = \left(\frac{WK_e}{c_p}\right) + T_4 \tag{4-49}$$

The area required for the cooling system's radiator was found from Eq. 4-38 where $T_{rad} = T_M$.

Figure 4-46 presents the radiator weight per kilowatt of cooling as a function of radiator temperature for various turbine outlet-compressor inlet gas temperature rises. The curves are plotted for turbine outlet temperatures of 50 and 150°F.

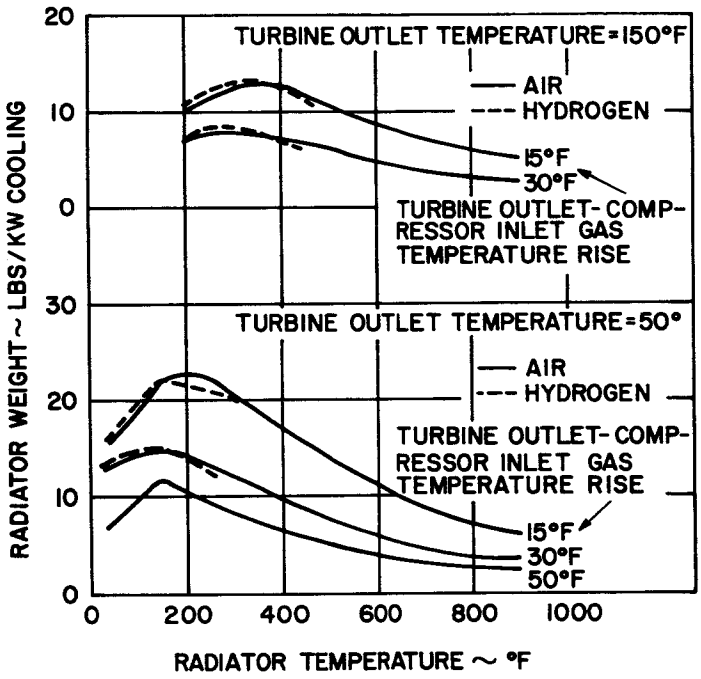


Figure 4-46. Gas Cycle Performance, Air and Hydrogen

The positive slope of the curve is a result of the heat absorbed from the compartment plus the heat of compression of the gas increasing rapidly while the increase in heat rejected from the radiator changes at a slower rate. The slopes become negative as the radiator heat rejection rate increases more rapidly.

proportional to the fourth power of the radiator temperature. For example, the temperature drop from gas to radiator surface at 800°F is about 60°F for air with a heat transfer coefficient of 25 Btu/hr/sq ft/°F. This 60°F temperature drop would require approximately a 17 percent larger radiator than one with zero temperature drop. For hydrogen, larger heat transfer coefficients are obtainable than for air, and at 800°F only a slightly larger radiator would be required (approximately 2 percent).

The heat rejection temperature of the radiator was assumed to be the arithmetic mean of the entering and leaving gas temperatures. This results in a negligibly smaller radiator than if the radiative mean temperature difference has been used.

The gas temperature entering and leaving the compartment heat exchanger was selected, for one case, to provide a compartment temperature of about 80°F and for the other case, a temperature of 180°F. The selected temperature difference between the mean compartment temperature and the mean gas temperature is compatible with the present state of the art of heat exchanger design.

3) Weights.

a) Radiator Weight. The work required for isentropic compression of a perfect gas was determined from

$$WK_c = \frac{1}{E'J}\left(\frac{k'}{k'-1}\right)\bar{R}T_1\left[\left(\frac{P_2}{P_1}\right)^{\frac{k'-1}{k'}} - 1\right] \tag{4-42}$$

where $WK_c$ = compressor work, Btu/lb gas

$E'$ = efficiency of compression, 0.85

$J$ = Joule's equivalent, 778 ft-lb/Btu

$k'$ = ratio of specific heat at constant pressure to specific heat at constant volume

$\bar{R}$ = gas constant, ft/°R

$T_1$ = temperature at compressor inlet, °R

$P_2$ = compressor outlet pressure, psi

$P_1$ = compressor inlet pressure, psi

The work generated by the gas in expanding from $P_3$ to $P_4$ is given by

$$WK_e = \frac{E'}{J}\left(\frac{k'}{k'-1}\right)\bar{R}T_4\left[\left(\frac{P_3}{P_4}\right)^{\frac{k'-1}{k'}} - 1\right] \tag{4-43}$$

where $WK_e$ = expansion work in Btu/lb gas

$E'$ = efficiency of expansion (0.85)

$P_3$ = turbine inlet pressure, psi

$P_4$ = turbine outlet pressure, psi

$T_4$ = temperature at turbine outlet, °R

The gas flow must be determined in order to calculate the work required for one kw cooling capacity.

$$\dot{W} = \frac{Q}{c_p \Delta T} \tag{4-44}$$

where $\dot{W}$ = gas flow per kw cooling, lb/hr

$Q$ = heat equivalent for 1 kw, 3413 Btu/hr

$c_p$ = specific heat of gas at constant pressure in Btu/lb°F

$\Delta T$ = temperature rise of gas through compartment heat exchanger, °F

The network input required of the power unit is

$$WK_{pu} = \frac{\dot{W}}{\bar{C}} \left(WK_c - WK_e\right) \tag{4-45}$$

where $WK_{pu}$ = work from power unit, hp/kw cooling capacity

$\dot{W}$ = gas flow, lb/hr

$\bar{C}$ = constant for conversion to hp, 2545 Btu/hp-hr

The heat to be rejected in the radiator per kw cooling was calculated from

$$Q_R = \dot{W} \left(WK_{pu}\right) + 3413 \tag{4-46}$$

where $Q_R$ = heat rejected per kw cooling, Btu/hr

The mean temperature of the radiator was found from

$$T_M = \frac{T_2 + T_3}{2} \tag{4-47}$$

where $T_M$ = mean radiator temperature, °R

$T_2$ = temperature of gas entering radiator, °R

$T_3$ = temperature of gas leaving the radiator, °R

The temperature of the gas leaving the compressor and entering the radiator was

$$T_2 = \left(\frac{WK_c}{c_p}\right) + T_1 \tag{4-48}$$

There is very little difference in radiator area required for air systems and hydrogen systems. Since the k's of hydrogen and air are approximately equal, the ratio of compressor work per pound of hydrogen to the work per pound of air varies as the ratio of their gas constants for the same pressure ratio. This ratio is 14.4. However, the ratio of the pounds of hydrogen to the pounds of air needed to provide a given cooling capacity varies as the inverse ratio of their specific heats. This ratio is 14.25. Therefore the total (not per pound) work of compression to be rejected for the two gases is approximately the same. In addition, as seen from Eq. 4-48, the compressor exit temperature (affecting the radiator temperature) for the two systems is also approximately the same (note again that the increase in specific compressor work for the hydrogen is canceled by the higher specific heat). This results in approximately the same radiator area and weight for the two systems.

Based on the curves of Figure 4-46, it appears that a high radiator temperature is desirable to reduce the size of a space vehicle radiator; however, as yet no consideration has been given to the power unit needed to supply shaft work to drive the cooling system.

b) Power Unit Weight. Figure 4-47 depicts the compressor work required to drive the gas refrigeration system. As in the case of a vapor cycle refrigeration system, solar cell power will be used to drive the compressor. Comparing the compressor work required to drive the compressor of the gas cycle with that for a vapor cycle, it can be seen that more work is required in a gas refrigeration cycle. The minimum radiator and solar cells weight is attained at a radiator temperature equal to the mean gas temperature within the compartment heat exchanger. Therefore, the previous discussion under Power Unit Weight for the vapor cycle system applies for the gas cycle also. When corrections are made for the assumptions discussed above for the gas refrigeration cycle, the overall weight becomes even more unattractive.

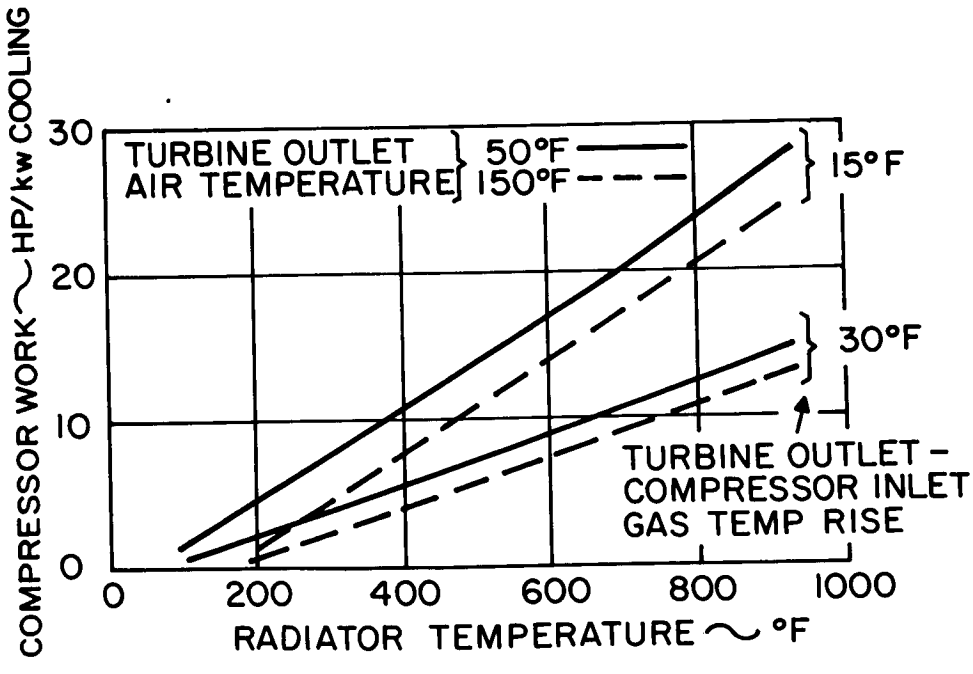


Figure 4-47. Gas Cycle Performance, Compressor Work

c) Individual Component Weight. The gas refrigeration cycle requires much larger and heavier equipment than a vapor refrigeration system of the same capacity, especially compressors and radiators.

4. Absorption Cycle Refrigeration

a. Description (Ref. 4-13)

The absorption refrigeration cycle is similar to the vapor cycle except that the compressor is replaced with a generator-absorbed assembly. Figure 4-48 shows a flow diagram of the basic system. The generator-absorber

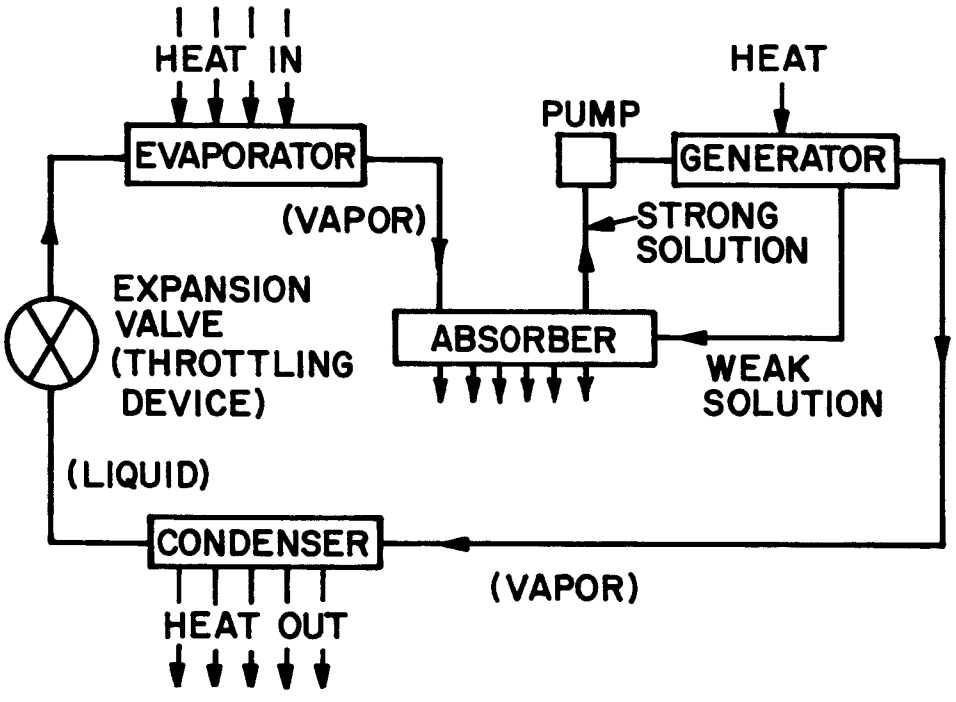


Figure 4-48. Absorption Cycle Refrigeration Schematic

assembly pumps refrigerant vapor from the evaporator pressure to the condenser pressure by first absorbing the vapor in a liquid, building up the pressure of the liquid to that of the condenser, and then liberating the vapor. As the refrigerant vapor enters into solution in the absorber, the temperature of the solution tends to rise. To resist this tendency, a cooling coil removes this heat of solution. The solution in the absorber is called a strong solution because it is rich in refrigerant. The pump draws the strong solution from the absorber, builds up the pressure, and forces the strong solution into the generator.

The addition of heat raises the temperature of the solution in the generator, driving off some of the refrigerant as a vapor at high pressure and temperature. As the refrigerant vapor leaves the solution in the generator, the solution becomes weak, i.e., has a low concentration of refrigerant. The weak solution flows back to the absorber through a restriction that maintains the pressure differential between the high and low sides of the system. From the generator, the refrigerant proceeds through the condenser, expansion valve, and evaporator, as it does in the vapor-compression system.

A feature of the absorption system is that very little mechanical work is required to operate the unit. Instead of the large quantity of mechanical energy demanded by the compressor in a vapor-compressor system, which made it undesirable for the particular space application under study, a negligible amount of energy is used by the pump. The principal cost of operation is in providing heat energy at the generator. The total heat and power requirement of an absorption system will be from 10 to 20 percent greater than for an equivalent compression system. The possibility of using solar power or waste heat for the greater part of the energy requirement of this system makes it worthy of study (Ref. 4-14).

b. Refrigerants

The traditional absorption system is the aqua-ammonia type which uses water as the absorber and amonia as the refrigerant. Up until a few years ago the aqua-ammonia system was virtually the only type used and it is still popular where low temperatures are required. In recent years absorption refrigeration units which use lithium bromide as the absorbent with water as the refrigerant have been employed. Since water is the refrigerant, the evaporator must be above 32°F, which limits the system to air conditioning or other high temperature refrigerating applications.

c. Disadvantages

The principal disadvantage to the absorption cycle refrigeration system for space application is that some difficulty could be expected under zero gravity conditions in the separation of the vapor and the circulating solvent. Until this problem is studied and solved, absorption refrigeration cycles cannot be used in a satellite. A possible solution to this problem, however, may be vapor-liquid separation by centrifugal means.

5. Thermoelectric (Peltier) Cooling

a. Description

A thermoelectric system, Figure 4-49, can be thought of as a single-phase heat pump, in which the transfer of energy is affected entirely on a microscopic scale, i.e., the only motion involved is that of the free electrons. The Peltier effect, which forms the basis of thermoelectric cooling, is due to the presence of a difference in potential at the junction of two dissimilar materials. When a current is made to flow in the direction of this potential difference, a cooling effect is present since heat is absorbed.

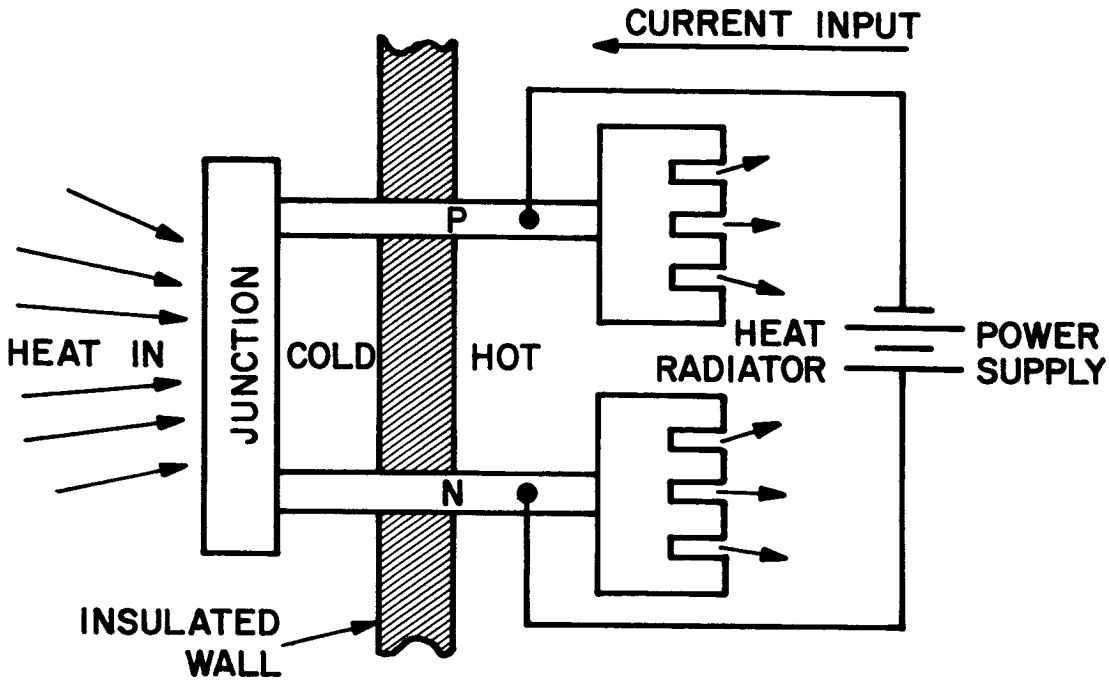


Figure 4-49. Thermoelectric (Peltier) Cooling System Schematic

b. Analysis (Ref. 4-15)

The Peltier heat absorbed at the junction of two dissimilar metals is given by

$$Q_p = \left(Y_a - Y_b\right)\left(T_{cold}\right)(I) \qquad (4\text{-}50)$$

where the Y's are the thermoelectric powers of the elements employed, T is the local temperature, and I is the current.

When a current is passed through a device such as shown in Figure 4-49, in addition to the Peltier effect, there exists a heat flow due to the Joule effect,

$$Q_j = I^2R : R = \text{resistance} \tag{4-51}$$

the conventional heat conduction,

$$Q_c = k\frac{A}{L}\left(T_{hot} - T_{cold}\right) \tag{4-52}$$

and the Thompson effect,

$$Q_T = -T\frac{dY}{dt}\left(T_{hot} - T_{cold}\right)(I) \tag{4-53}$$

which normally is sufficiently small to be ignored.

From the above considerations it can be shown that the net heat absorbed at the cold junction is given by

$$Q_{net} = Q_p - Q_j/2 - Q_c \pm Q_T = \left(Y_a - Y_b\right) I\left(T_{cold}\right) - I^2R/2$$

$$-\left(T_{hot} - T_{cold}\right)\left[\left(\frac{kA}{\ell}\right)_a + \left(\frac{kA}{\ell}\right)_b\right] \tag{4-54}$$

It is seen that in order to increase $Q_{net}$, materials with the following properties are needed: 1) high thermoelectric power, 2) high electrical conductivity and 3) low thermal conductivity. At present the materials known as semiconductors exhibit the most satisfactory combination of these properties.

The cold junction is usually a bridge made of material such as copper which possesses very good heat and electrical transfer properties, so that it is practically opaque to the p-n legs. A d-c current is passed in the n-p direction. The coefficient of performance of a refrigerator such as shown in Figure 4-49 is defined by

$$C.O.P. = \frac{Q_{net}}{P_e} \tag{4-55}$$

where $P_e$, the electrical power delivered, is given by

$$P_e = I\left[IR + \left(Y_a - Y_b\right)\left(T_h - T_c\right)\right] \tag{4-56}$$

In the above equation, the term IR corresponds to the voltage drop, V, across the cooler when the temperature difference between hot and cold junctions is zero: the second term in the bracket corresponds to the back emf induced in the cooler by the temperature difference. The ohmic resistance of the cooler, neglecting junction resistances, is given by

$$R = R_a + R_b = \frac{\rho'_a \ell_a}{s_a} + \frac{\rho'_b \ell_b}{s_b} \tag{4-57}$$

where $\rho'$ = electrical resistivity, ohm - cm
$\ell$ = length of thermoelement, cm
s = area of thermoelement, $cm^2$

If one assumes that both legs of the cooler have identical lengths, identical resistances, and identical values of conductive heat-transfer rates, the expression for the coefficient of performance can be shown to be

$$C.O.P. = \frac{(Y_a - Y_b) T_c I - I^2 R/2}{I^2 R + I(Y_a - Y_b)(T_h - T_c)} - \frac{(T_h - T_c)\left[(k_a \rho'_a)^{1/2} + (k_b \rho'_b)^{1/2}\right]^2 / R}{I^2 R + I(Y_a - Y_b)(T_h - T_c)} \tag{4-58}$$

Ioffe (Ref. 4-16) has shown that the above expression for the C.O.P. may be maximized with respect to current. The final expressions are repeated here in terms of the figure of merit, Z, of the semiconductor material, where Z is defined by

$$Z = \frac{(Y_a - Y_b)^2}{\left(\sqrt{k_a \rho'_a} + \sqrt{k_b \rho'_b}\right)^2} \tag{4-59}$$

The maximum coefficient of performance of this cooler, for the assumptions used, is given by

$$(C.O.P.)_{max} = \frac{T_c}{T_h - T_c} \; \frac{\sqrt{1 + Z(T_h + T_c)/2} - T_h/T_c}{\sqrt{1 + Z(T_h + T_c)/2} + 1} \tag{4-60}$$

Figure 4-50 shows a graphical representation of Eq. 4-60 for several values of the figure of merit, Z, and the temperature difference $(T_h - T_c)$ when $T_c$ is held at 273° K. It is evident from the plot that the maximum coefficient of performance increases with higher figures of merit and smaller temperature differences; this indicates that for large temperature drops, series arrangements of Peltier cells would be necessary.

Z values of approximately $3 \times 10^{-3}$/°K are obtainable at present. Leading materials manufacturers expect that an improvement to $5 \times 10^{-3}$/°K can be expected. The effect of this improvement on the C.O.P. and on the competitive position of thermoelectric cooling in general can be anticipated from Figure 4-50.

For larger temperature differences, staging becomes necessary. In this case the C.O.P. for an n-stage unit becomes

$$C.O.P. = e_{stage} = \frac{1}{\prod_{i=1}^{i=n} \left(1 + \frac{1}{e_i}\right) - 1} \tag{4-61}$$

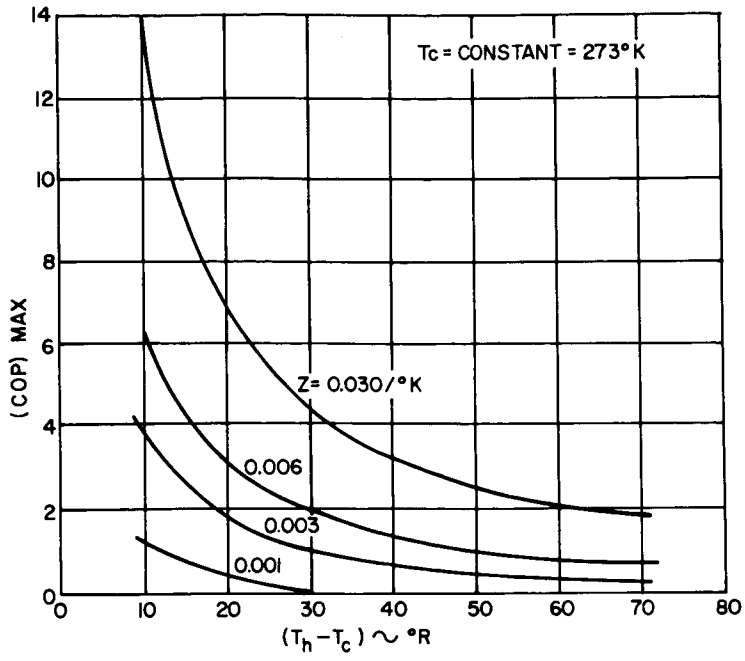


Figure 4-50. Dependence of Maximum Coefficient of Performance on the Temperature Difference and Z

where the symbol $\pi$ stands for "product" and e is the C.O.P. of the ith stage. For known values of T and Z, curves of the type shown in Figure 4-50 in conjunction with Eq. 4-61 allow the selection of the optimum number of stages.

c. Design

The following parameters must be known or specified before the design of the thermoelectric cooler can be made.

(1) $T_{cold} = T_c$, $T_{hot} = T_h$
(2) Refrigeration load, $Q_o$
(3) Voltage drop available, V
(4) Junction resistivity, $\bar{r}'$ (ohm - cm$^2$)
(5) Materials properties (y, $\rho$, k) a function of temperature
(6) Since the temperature dependence is almost linear, constant values taken at $(T_c + T_h)/2$ are sufficiently accurate

The following computations must be made.

(1) voltage drop across each element, $V_o$

$$V_o = \frac{(Y_a - Y_b)(T_h - T_c)\sqrt{1 + Z(T_h + T_c)/2}}{\sqrt{1 + Z(T_h + T_c)/2} - 1} \qquad (4\text{-}62)$$

(2) Power required, $P_r = \frac{Q_o}{C.O.P.}$

(3) Operating current, $I = \frac{P_r}{V}$

(4) Number of thermoelements required, $N = \frac{V}{V_o}$

(5) Overall element resistance, R

$$R = \frac{\left(Y_a - Y_b\right)\left(T_h - T_c\right)}{\left[\sqrt{1 + Z\left(T_h + T_c\right)/2} - 1\right] I_o} \qquad (4\text{-}63)$$

All these formulae are taken from Ioffe (Ref. 4-16) and are applicable to a design that has been optimized with respect to C.O.P.

Next comes the selection of the length of the thermoelement, $\ell$, which from the application standpoint is of the utmost importance.

It has been shown, Ref. 4-16, that for a given set of design requirements, the cross-sectional area of the thermoelements is linearly proportional to the element length, $\ell$. Theoretically, it suggests that the element of thermoelectric materials required for a given refrigeration load is proportional to $\ell^2$, which is a variable in the design. The possibility of designing a unit with elements 0.001-inch long suggests itself. The limit on the reduction of sizes is set by the fact that with materials currently available, 2.5 or more watts of heat must be dissipated from the hot junction for every watt of heat removed at the cold junctions. It is from this consideration that that the problem of heat removal from the hot junctions is of paramount engineering importance in any application since it ultimately controls the weight of the cooling unit.

d. System Disadvantages

(1) Present materials with a figure of merit of $3 \times 10^{-3}/°K$ do not compare well with conventional refrigeration cycles for larger cooling loads. This situation reverses at approximately $Z = 5 \times 10^{-3}$. This discussion has been included here since thermoelectric cooling may be applicable for spot cooling (such as infrared sensor cooling) within the space vehicle.

(2) The brittleness of such material as $Bi_2Te_3$ requires very special assembly methods to protect the elements from shock and stress. It is believed, however, that this problem will be solved.

(3) Semiconductors used in thermoelectric systems have the same susceptibility to damage from nuclear or cosmic radiation as transistors and therefore require shielding.

(4) Very little operating experience is available with thermoelectric systems.

e. Advantages

(1) With improved Z values, the thermoelectric system will offer an efficient, long life, maintenance-free system without moving parts and disturbing torques.

(2) The thermoelectric system is basically reversible and thus can be used to generate electricity. With clever design, an integrated power generation and cooling unit with obvious weight savings can be developed.

## F. INFRARED COOLING

### 1. Introduction

The operating temperatures of present day infrared dectectors range from 1.2°K (impurity activated indium antimonide) to 399°K for the lead salts. The proper temperature for a given dectector is determined by noting the temperature dependence of the optical and photoelectric properties, and choosing that temperature which provides the best results for the system of interest. The important characteristics that depend upon temperature are detectivity, time constant, spectral response, and resistance. The detector element, which requires cooling, is usually mounted in a vacuum flask, called a dewar, into which a cooling head may be placed. The flask is double-walled, with the detector mounted on the inner wall and an infrared-transmitting window incorporated in the outer wall. In situations where it is impractical to place the cooling head close to the detector, a highly conductive material (e.g., a ruby rod) is used as the heat transmitting medium between the detector and the cooling head.

Several methods are available for cooling an infrared detector to the required temperature and maintaining that temperature during the desired operating time. The cooling devices derived from these methods are of the following four major types:

(1) direct-contact coolers

(2) Joule-Thompson cryostats

(3) expansion engines

(4) thermoelectric coolers

A brief discussion of each of these types will follow.

### 2. Direct-Contact Coolers

The simplest technique for cooling infrared detectors is one in which the detector is in direct thermal contact with a supply of liquid coolant (e.g., nitrogen). Often the direct-contact cooler consists merely of an unpressurized supply of liquid in the detector dewar, but the systems vary in complexity up to types requiring pressure regulators, insulated supply lines, heating elements, pressurized cooling heads, and pressurized tanks. The physical operation of the system is as follows (see Figure 4-51): The supply valve opens, allowing liquid to flow from the supply tank into the pressurized chamber. As soon as a predetermined level is reached, the supply valve closes and the heater is turned on. The heater is controlled by a pressure sensor which is set to maintain a flow of liquid into the cooling head at a rate sufficient to replenish the liquid that boils off. Gas formed from the heat exchange with the apparatus flows through the return line and out the vent port. Any excess liquid flows back to the supply tank through the return line. As soon as the liquid level in the pressurized chamber falls below a certain level, the level sensor shuts off the heater and opens the supply valve, admitting more liquid from the supply tank. The process then repeats itself until the supply tank is empty.

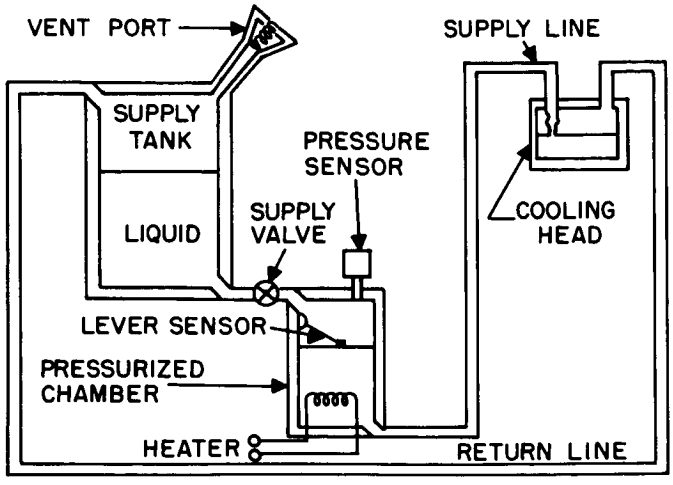


Figure 4-51. Basic Direct-Contact Cooling System Schematic

It is evident that the above system may be simplified without seriously limiting its performance as a cooling device. The pressurized tank, supply valve, and return line may be removed and the heater placed in the supply tank. The main problem encountered is the waste of liquid by overflow from the cooling head.

3. Joule-Thompson Cryostats

One of the more common methods for cooling infrared detectors employs a device known as a cryostat in which a high-pressure gas is caused to flow through a tube and expand to low pressure through an orifice at the end of the tube. Cooling accompanies the expansion due to the phenomenon known as the Joule-Thompson effect. The efficiency of the device is increased by allowing heat exchange between the cooled outgoing gas and the warm incoming gas.

The cryostat, as the Joule-Thompson cooler is usually called, is made from a length of finned tubing coiled around a mandrel, and having an orifice at the exit of the tube (Figure 4-52). A high-pressure gas enters the tube at a temperature below its maximum inversion temperature (maximum temperature on an isenthalpic curve). It passes through the tube and expands at the orifice, cooling by virtue of the Joule-Thompson effect. The gas, thus cooled, passes back over the finned tubing, cooling the incoming gas. The process is carried on continuously until liquid begins to emanate from the orifice. The temperature of the cooled gas is then constant, since the liquid-gas combination is a saturation state of the gas. This temperature is the boiling point of the gas at the exit pressure.

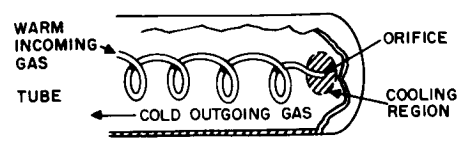


Figure 4-52. Joule-Thompson Cooler Schematic

The finned tubing must have a very small inside diameter in order to give a large ratio of surface area to volume and thus to provide efficient heat exchange. This narrow passageway is subject to clogging, since the extremely low temperature of the tubing causes any impurities in the gas to freeze on the surface. For this reason it is important that extremely high-purity gas be used in the cryostat and that the cryostat itself be kept free from contamination while it is not in use.

Closed-loop cryostats have been made which recycle the gas in order to provide continuous operation for long periods of time. To accomplish a continuously operating cycle of this type, the expanded gas must be pressurized by a noncontaminating compressor. Such a compressor may be built with a non-lubricated piston. Table 4-10 lists the performance of various existing infrared cooling systems based on the Joule-Thompson effect.

4. Expansion Engines

When a gas is allowed to expand and do work without exchanging heat with its surroundings, its internal energy is decreased by the amount of the work, and hence its temperature drops. A minaturized device designed specifically for the purpose of cooling small regions to extremely low temperature (utilizing a gas operating within a closed loop) consists of a very short piston, a compressor, and a thermal regenerator with a pair of intake and exhaust valves.

The cycle through which the engine goes is essentially the Sterling cycle, and may be described as follows (see Figure 4-53):

(1) The intake valve opens. The piston is at bottom dead center as high-pressure gas enters, pressurizing the regenerator and the connecting tubing.

(2) The piston completes its stroke. Upon completion of the piston stroke, the exhaust valve opens and the gas expands to a low pressure. As the cooled gas passes through the regenerator, it removes heat from the fins, causing a temperature drop in the regenerator.

(3) The piston returns to bottom dead center. The remainder of the cooled, expanded gas is forced through the regenerator and out the exhaust valve. As the gas repeatedly undergoes the cycle, the regenerator is progressively cooled until the work done by the gas exactly equals the heat flow into the system, at which point temperature equilibrium is reached.

A limiting factor in expansion engine devices is the material from which the regenerator is fabricated. The heat capacities of most solids fall off considerably at low temperatures, and consequently the ability of the solid to remove heat from the gas stream diminishes with decreased temperature. Materials such as aluminum, zinc, brass, and bronze have no significant heat capacity below 35°K, whereas lead is able to store fair amounts of heat down to approximately 14°K. See Figure 4-54 for the obtainable temperatures for different heat

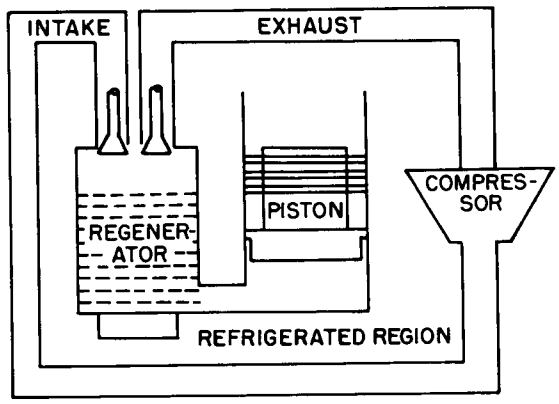


Figure 4-53. Gifford-McHamon Expansion Engine Schematic

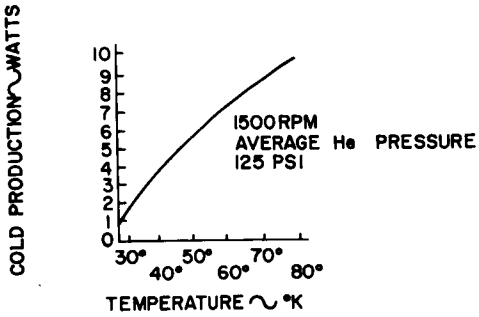


Figure 4-54. Performance of Expansion Engine, Infrared Cooler (Cryogenerator)

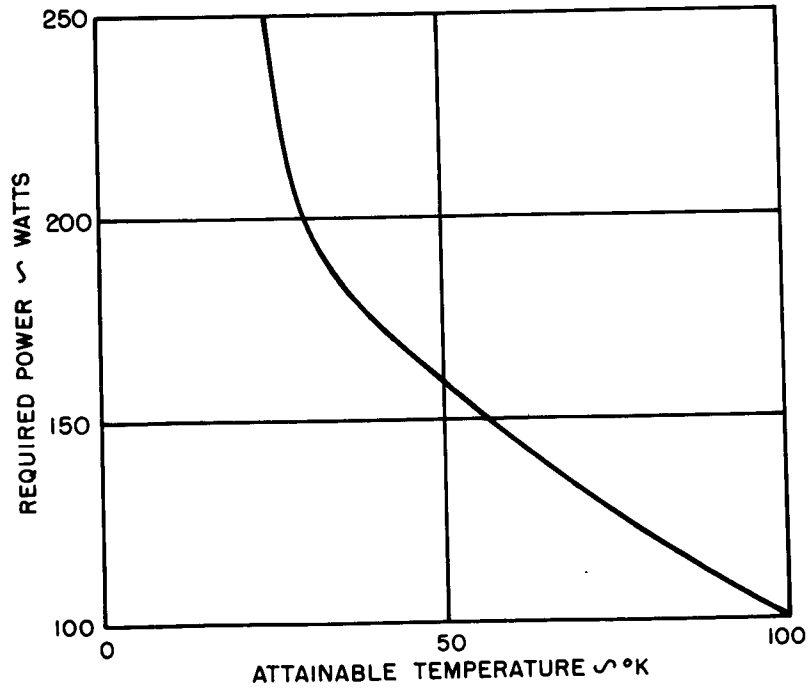


Figure 4-55. Power Requirements vs Attainable Temperature for Expansion Engine IR Cooler (Cryogenerator)

loads with expansion engines. Figure 4-55 shows the power requirements versus attainable temperature for an expansion engine infrared cooler. Table 4-10 lists the performance of existing infrared coolers based on the expansion engine principle.

5. Thermoelectric Coolers

Thermoelectric cooling devices have been discussed in detail under active thermal control systems in subsection E. Figure 4-56 shows a typical single-stage thermoelectric infrared cooling performance curve. Better performance is obtained by increasing the number of cooling stages.

Table 4-10 lists specific models of complete systems that have been proposed or are in production to satisfy the requirements of infrared cooling (Ref 4-17).

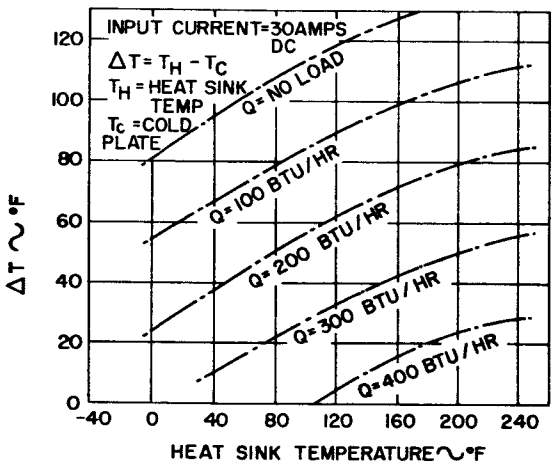


Figure 4-56. Performance of a Single Stage Thermoelectric Infrared Cooler (Ohio Semiconductors, TU-6 Unit)

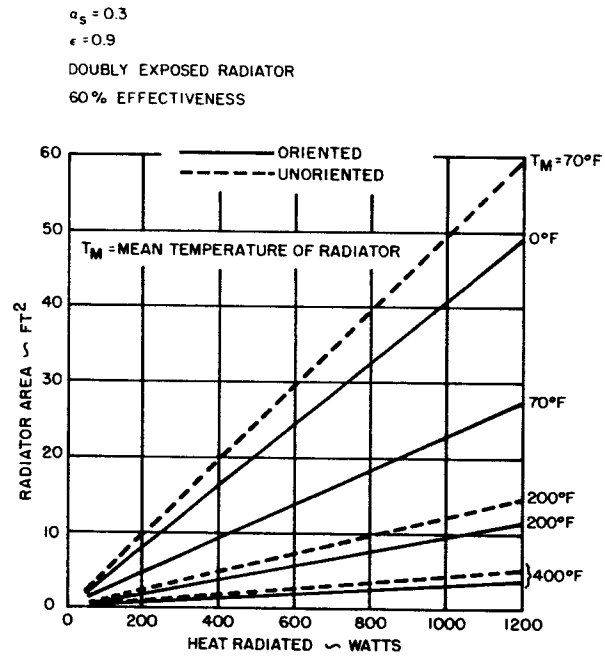


Figure 4-57. Infrared Cooling System, Required Radiator Areas

Figure 4-57 illustrates the estimated radiator area required to radiate the additional heat load added to the infrared system by the power supply.

The cryogenerator expansion engine (see Table 4-10) will have a life expectancy of 2000 hours (1965). There is little likelihood that the unit could operate for more than 4000 hours without attention. The contemplated SMS application (Infrared Earth heat budget measurements) calls for a duty cycle amounting to approximately 600 hours. With regard then to operating life, this unit may be applicable for the SMS mission.

## G. SOLAR CELLS

### 1. Introduction

Many solar cell power sources have been designed, constructed, and made operational in spacecraft applications. Since solar cells will probably be the power source for an operational SMS, thermal considerations of solar cells will be discussed here. The effect of temperature on the voltage-current characteristics of a typical p-n silicon cell is shown in Figure 4-58. The importance of keeping moderate cell temperatures is evident from the figure (Ref 4-18).

### 2. Analysis

The heat input to a solar paddle is the summation of absorbed direct solar energy, reflected solar radiation, terrestrial radiation, thermal radiation from nearby spacecraft surfaces, internal equipment heat dissipation, and conduction from other portions of the spacecraft. The energy output is the summation of thermal radiation to space and nearby surfaces, conduction to other portions of the vehicle, and the portion of the absorbed energy that is converted to electricity.

A mathematical equation that will enable the determination of cell equilibrium temperatures for synchronous orbit conditions can be expressed as

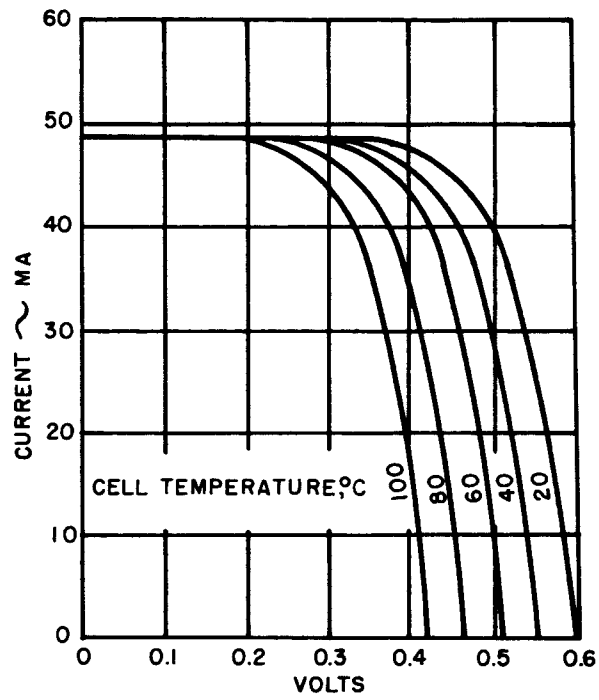


Figure 4-58. Temperature Degradation of a Typical Solar Cell

$$Q_i' + A_a S \alpha_s (1-E')\cos\phi + (F_c F_e)_{s-p} \sigma A_a (T_s^{\,4} - T_c'^{\,4}) + C(T_c' - T_p) = A_e \sigma \epsilon T_c'^{\,4} \quad (4\text{-}64)$$

where $Q_i'$ = internal equipment heat dissipation

$\phi$ = angle between Earth-Sun vector and normal to area in question

$A_a$ = projected absorbing area

$A_e$ = emitting area

| | | |
|---|---|---|
| $E'$ | = | solar cell efficiency |
| $T_s$ | = | average satellite skin temperature |
| $T_c'$ | = | solar cell temperature |
| $(F_c F_e)_{s-p}$ | = | product of configuration and emissivity factors between the satellite and the solar cell paddle |
| $C$ | = | conduction factor between satellite and paddle |

In most cases the solar cell paddle temperature is not different enough from the average satellite temperature to effect satellite-paddle heat exchange. Even for cases where the paddle and satellite temperatures differ, the configuration and conduction factors involved are usually small and the satellite-paddle heat exchange can be neglected. Equation 4-64 then reduces to

$$T_c' = \left[\frac{S(1-E')\sqrt{1-\sin^2\Delta\,\sin^2(\omega_{E/S}t)}\left(\frac{A_a}{A_e}\right)\left(\frac{\alpha_s}{\epsilon}\right)+\frac{Q_i}{\epsilon}}{\sigma}\right]^{\frac{1}{4}} \tag{4-65}$$

for the spin-stabilized satellite and to

$$T_c' = \left[\frac{-S(1-E')\sqrt{1-\left[\cos(\omega_{E/S}t)\cos(\omega_{S/E}t')+\sin(\omega_{E/S}t)\sin(\omega_{S/E}t')\cos\Delta\right]^2}}{\sigma}\right]^{1/4} \times \left[\frac{\left(\frac{A_a}{A_e}\right)\left(\frac{\alpha_s}{\epsilon}\right)+\frac{Q_i}{\epsilon}}{\sigma}\right]^{1/4} \tag{4-66}$$

for the gravity-gradient stabilized satellite. In the above equations the cells are assumed to be on the satellite body. Equation 4-66 gives the average (with respect to cell position) temperature of the cells. The individual cell temperature distribution is shown in Figure 4-61.

For the three-axis stabilized configuration where the cells are mounted on paddles, the temperature of the cells is given by

$$T_c' = \left[\frac{S(1-E')\cos\phi}{\sigma}\left(\frac{A_a}{A_e}\right)\left(\frac{\alpha_s}{\epsilon}\right)\right]^{\frac{1}{4}} \tag{4-67}$$

where $\phi$ is given by

$$\phi = \mathrm{Cos}^{-1}\left[\frac{\cos\Delta}{\sqrt{1-\sin^2\Delta\cos^2\omega_{E/S}t'}}\right]$$

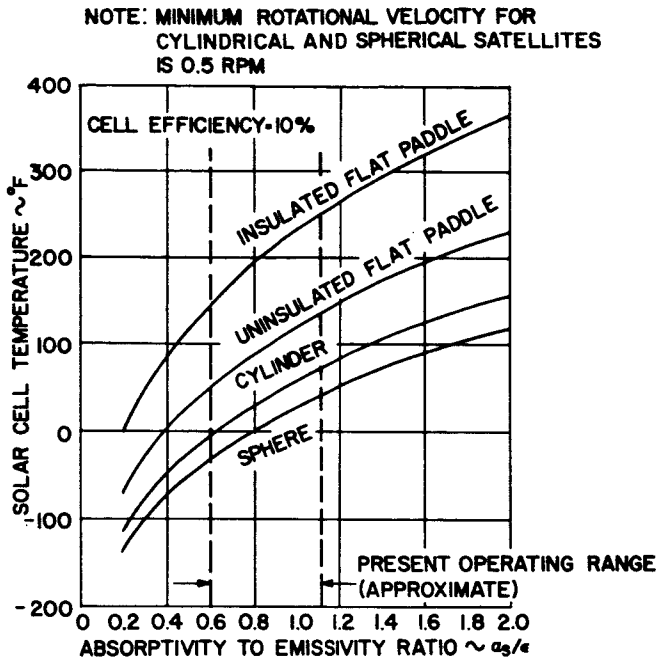


Figure 4-59. Effect of Solar Cell Mounting Geometry on Cell Temperature

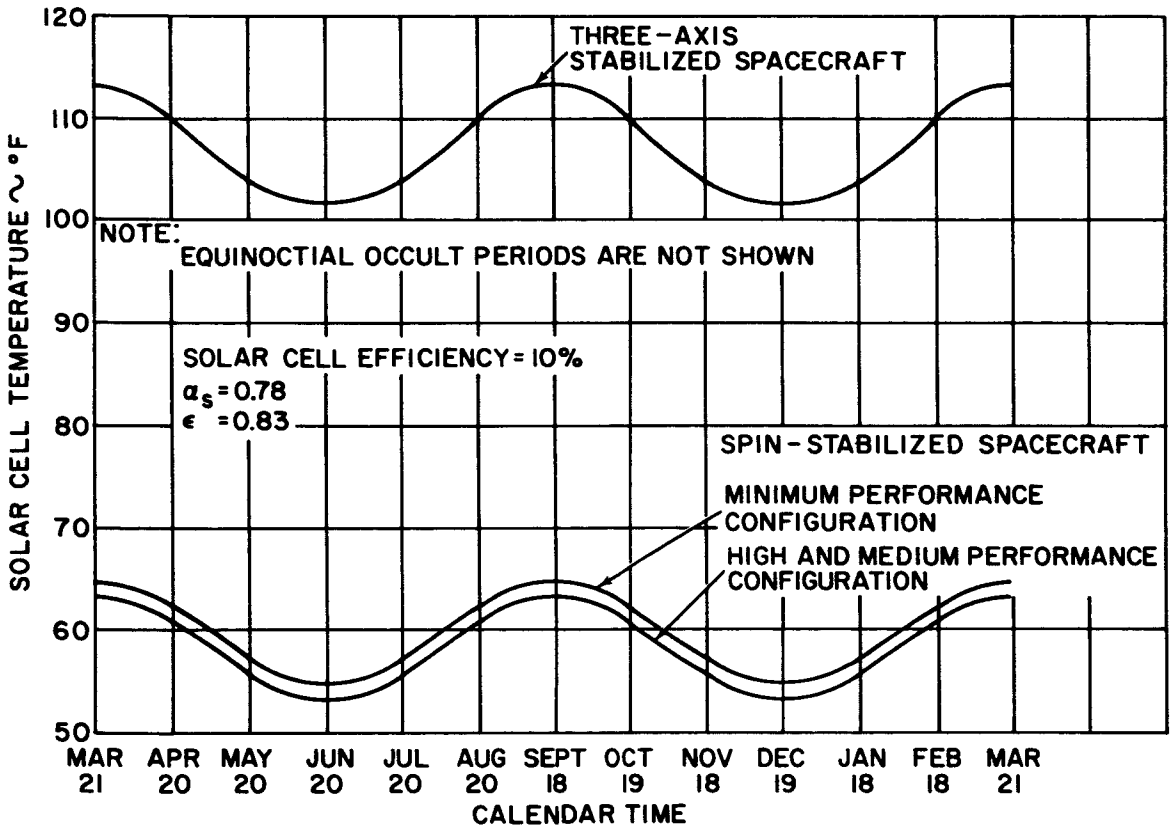


Figure 4-60. Solar Cell Temperature Histories for the Various Configurations

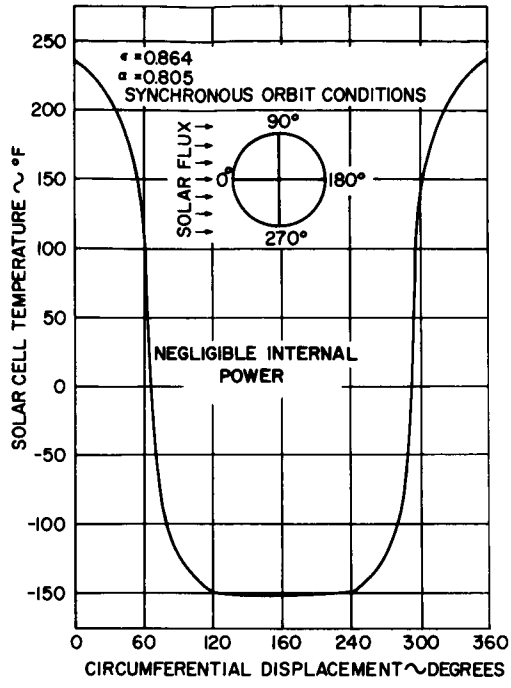


Figure 4-61. Solar Cell Temperature Distribution on a Gravity Gradient Cylindrical Satellite

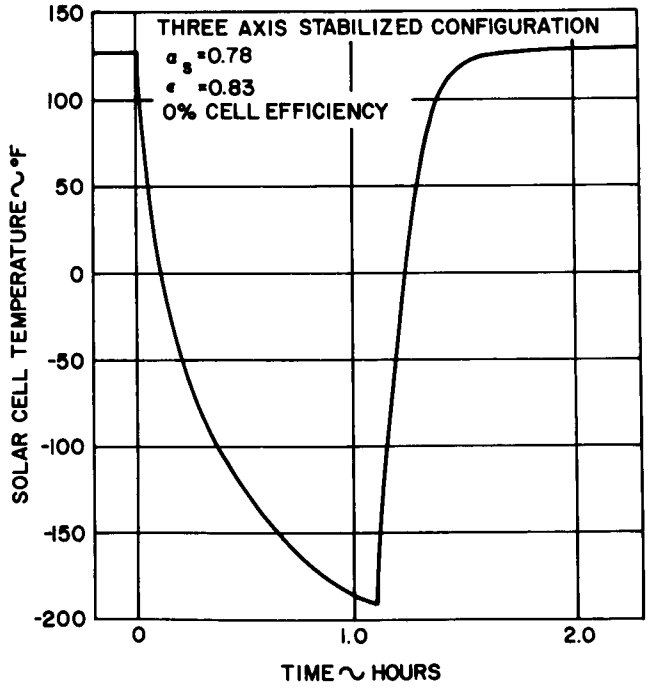


Figure 4-62. Solar Cell Temperature History During the the Equinoctial Occultations

3. Results

From the standpoint of solar cell temperatures there are definite advantages as to the type of cell mounting structure. From Eqs 4-65, 4-66 and 4-67, it may be observed that the cell temperature is a function of the absorption to emission area ratio, $A_a/A_e$. For a sphere, cylinder, uninsulated flat plate, and an insulated flat plate these ratios are 0.25, 0.32.0.5, and 1.0, respectively. The solar cell temperatures for various mounting geometries as a function of the absorbtivity to emissivity ratio are shown in Figure 4-59. The solar cell temperature histories for the spin-stabilized, 3-axis stabilized and gravity-gradient stabilized configurations are shown in Figures 4-60 and 4-61. The cell temperature distribution for the gravity-gradient stabilized configuration is for the case where the cells would be mounted on the satellite body. The exact temperature distribution would be different for a different time of year and different time of day than shown in Figure 4-61. But basically the circumferential temperature distribution shown in the figure is typical. The cell temperature history during the equinoctial occulation periods is shown in Figure 4-62.

## H. LIST OF SYMBOLS

| | | |
|---|---|---|
| $A$ | = | surface area, $ft^2$ |
| $A_a$ | = | projected absorbing area, $ft^2$ |
| $A_e$ | = | emitting area, $ft^2$ |
| $C$ | = | conductive coefficient, Btu/hr-°R |
| $C'$ | = | convection coefficient, Btu/hr-°R |
| $C''$ | = | specific heat of solid, Btu/lb-°R |
| $\overline{C}$ | = | conversion constant for hp = 2545 Btu/hp-hr |
| C. O. P. | = | coefficient of performance, dimensionless |
| $D$ | = | diameter, ft |
| $E$ | = | energy that the Earth absorbs from Sun, Btu/hr |
| $\overline{E}$ | = | energy emitted by Earth, Btu/hr |
| $E'$ | = | efficiency, dimensionless |
| $E_e$ | = | total energy rate emitted by the Earth per unit Earth area, Btu/hr-$ft^2$ |
| $F = F_c$ | = | configuration factor, $F_c$ ( $\measuredangle$ ) configuration factor evaluated at the angle, dimensionless |
| $F_e$ | = | emissivity factor, $F_e$ ( $\measuredangle$ ) emissivity factor evaluated at the angle, dimensionless |
| $G$ | = | defined by Eq 4-24 |
| $H$ | = | defined by Eq 4-24 |
| $H_f$ | = | heat of fusion of material, Btu/lb |
| $I$ | = | current, amperes |
| $J$ | = | Joule's equivalent, 778 ft-lb/Btu |
| $K$ | = | the fraction of sky covered by clouds, dimensionless |
| $L$ | = | satellite length, ft |
| $N$ | = | number of thermal elements |
| $P_e$ | = | electrical power, watts |
| $P_r$ | = | power required, watts |
| $P_1$ | = | compressor inlet pressure, psia |
| $P_2$ | = | compressor outlet pressure, psia |
| $P_3$ | = | turbine inlet pressure, psia |
| $P_4$ | = | turbine outlet pressure, psia |
| $Q$ | = | heat equivalent for 1 kw = 3413 Btu/hr |
| $Q_T$ | = | Thompson's heat effect, watts |

| | | |
|---|---|---|
| $Q_h$ | = | heater required power, watts |
| $Q_i$ | = | internal heat dissipation, watts/ft$^2$ |
| $Q_i'$ | = | internal heat dissipation, watts |
| $Q_j$ | = | Joule's heat effect, watts |
| $Q_o$ | = | refrigeration load, watts |
| $Q_p$ | = | Peltier's heat, watts |
| $Q_R$ | = | heat rejected in condenser (radiator), Btu/hr/kw |
| $Q_s$ | = | solar energy, Btu/hr |
| $(Q_e)_{sp}$ | = | terrestrial radiation received by spherical satellite, Btu/hr-ft$^2$ |
| $(Q_{rs})_{sp}$ | = | solar reflected radiation incident on spherical satellite, Btu/hr-ft$^2$ |
| $Q_{wk}$ | = | compressor work, hp/kw |
| $\overline{R}$ | = | gas constant, ft/°R |
| $R$ | = | resistance, ohms |
| $R_e$ | = | radius of Earth, nautical miles |
| $S$ | = | solar constant, 442 Btu/hr-ft$^2$ |
| $S'$ | = | integrated solar flux, Btu/hr-ft$^2$ |
| $T$ | = | temperature, °R |
| $T_{av}$ | = | average satellite temperature, °R |
| $T_c'$ | = | solar cell temperature, °R |
| $T_{co}$ | = | initial component temperature, °R |
| $T_{cold}$ | = | temperature of cold junction, °R |
| $T_e$ | = | equipment temperature, °R |
| $T_f$ | = | temperature of material fusion point, °R |
| $T_{hot}$ | = | temperature of hot junction, °R |
| $T_i$ | = | desired component bulk temperature, °R |
| $T_M$ | = | mean temperature, °R |
| $T_o$ | = | temperature before entering the shadow, °R |
| $T_R$ | = | rejection temperature of cycle's fluid, °R |
| $T_{rad}$ | = | radiator temperature, °R |
| $T_{ro}$ | = | temperature at $r_o$ (skin temperature), °R |
| $T_s$ | = | satellite skin temperature, °R |
| $T_1$ | = | temperature at compressor inlet, °R |
| $T_2$ | = | temperature of gas entering radiator, °R |

| | | |
|---|---|---|
| $T_3$ | = | temperature of gas leaving radiator, °R |
| $V$ | = | voltage drop, volts |
| $V_o$ | = | voltage across element, volts |
| $W$ | = | weight, pounds |
| $W'$ | = | pounds of material per $ft^2$ |
| $\dot{W}$ | = | refrigerant weight flow, lbs/hr/kw |
| $WK_c$ | = | compressor work, Btu/lb gas |
| $WK_e$ | = | expansion work, Btu/lb |
| $WK_{pu}$ | = | power unit work, hp/kw |
| $Y$ | = | thermoelectric power, volts/°C |
| $Z$ | = | figure of merit, $°C^{-1}$ |
| $a_e$ | = | albedo, dimensionless |
| ber, bei | = | modified bessel functions |
| $c_p$ | = | specific heat, Btu/lb-°F |
| $e$ | = | C.O.P., Coefficient of Performance |
| $h$ | = | altitude, nautical miles |
| $\bar{i}$ | = | $\sqrt{-1}$ |
| $i$ | = | enthalpy, Btu/lb |
| $k$ | = | thermal conductivity, Btu-ft/hr $ft^2$- °R, watts/cm°C |
| $k'$ | = | ratio of specific heats, dimensionless: also used as constant of integration |
| $\ell$ | = | length of shadow box, ft |
| $\ell$ | = | length of thermoelement, cm |
| p-n | = | positive - negative |
| $r$ | = | satellite radius, feet |
| $r'$ | = | radiation coefficient, Btu/hr-$°R^4$ |
| $\bar{r}'$ | = | junction resistivity, ohms-$cm^2$ |
| $s$ | = | area of thermoelement, $cm^2$ |
| sh | = | subscript refers to shutter |
| $t$ | = | component warm up time or time in sunlight, hr |
| $t$ | = | time ($t$=0 when Earth is at vernal equinox), days |
| $t'$ | = | time ($t'$=0 when cylinder axis is parallel to Sun-vernal equinox vector, hr |
| $w$ | = | component weight, lb |
| $x_i$ | = | length of $i^{th}$ conduction path, ft |
| $\alpha'$ | = | thermal diffusivity of the skin material, $ft^2$/hr |

| | | |
|---|---|---|
| $\alpha_s$ | = | absorptivity with respect to solar radiation, dimensionless |
| $\beta$ | = | angle the Sun makes with the vehicle radius vector, degrees |
| $\gamma$ | = | surface altitude angle, degrees |
| $\Delta$ | = | ∢ between Earth axes of rotation and the normal to ecliptic plane, degrees |
| $\epsilon$ | = | infrared emissivity, dimensionless |
| $\eta$ | = | distance a long circumference, radians |
| $\theta$ | = | shutter opening angle, degrees |
| $\lambda$ | = | angle between normal to the area in question and plus pitch axis (also displacement between shutter hinge line and pitch axis), degrees |
| $\mu$ | = | angle between shutter normal and Earth-Sun vector, degrees |
| $\nu$ | = | angle between the normal to the surface behind the shutter and the Earth-Sun vector, degrees |
| $\xi$ | = | step function, dimensionless |
| $\rho$ | = | density, $lbs/ft^3$ |
| $\rho'$ | = | electrical resistivity = 1/ohm-cm |
| $\sigma$ | = | Stefan-Boltzmann constant = 0.173 $Btu/hr\text{-}ft^2\text{-}°R^4$ |
| $\tau$ | = | thickness, ft |
| $\phi$ | = | angle between the cylinder axis and the Sun-Earth axis, degrees |
| $\omega'$ | = | frequency, radians/hr |
| $\omega_{S/E}$ | = | angular velocity of the satellite relative to the Earth, degrees/hr |
| $\omega_{E/S}$ | = | angular velocity of the Earth relative to the Sun, degrees/day |
| $\cos(2\pi\eta)$ | = | rectified cosine function, dimensionless |

## I. REFERENCES


4-1 Stevenson, J., and Grafton, J., "Radiation Heat Transfer Analysis for Space Vehicles,"ASD Technical Report 61-119, Part 1, December 1961

4-2 Krieth, F., Radiation Heat Transfer and Thermal Control of Spacecraft Oklahoma State University, April 1960

4-3 Hass, G., Drummeter, L., and Schach, M., "Temperature Stabilization of Highly Reflecting Spherical Satellites," J. Opt. Soc. Am., September 1959

4-4 Grafton, J., and Nordwall, H., "Radiation Heat Transfer Analysis for Space Vehicles," ASD Technical Report 61-119 Part II, April 1962

4-5 Carroll, W., "Development of Stable Temperature Control Surfaces for Spacecraft," CIT/JPL TR 32-340, November 1962

4-6 Gaumer, R., and McKelber, L., "Thermal Radiative Control Surfaces for Spacecraft," Lockheed Missiles and Space Division Technical Report LMSD-704014, March 1961

4-7 Aeronautical Systems Division, Air Force Systems Command, "Environmental Control System Selection for Manned Space Vehicles," ASD Technical Report 61-240, May 1962

4-8 Charnes, A., and Raynor, S., "Solar Heating of a Rotating Cylindrical Space Vehicle," ARS J.,May 1960

4-9 Jenness, J., "Temperature in a Cylindrical Satellite," Astron Acta, Vol. VI, Facsimile 5, 1960

4-10 Fried, E., "Thermal Joint Conductance in a Vacuum" ASME 63-AHGT-18, December 5, 1962

4-11 Moseley, T.D., "Vapor Cycle Cooling Systems for Space Vehicles," WADD T.N. 60-161, July 1960

4-12 Moseley, T.D., "Gas Cycle Cooling Systems for Space Vehicles," WADD T.N. 60-66, June 1960

4-13 Stoecker W.F., Refrigeration and Air Conditioning, McGraw-Hill Book Co. Inc., New York, 1958

4-14 Glasser, S.P. and Stelzriede, M.E.,"Integration and Optimization of Space Vehicle Environmental Control System," ASD Technical Report 61-176, December 1961

4-15 Republic Aviation Corporation, Technical Proposal "Space Vehicle Thermal and Atmospheric Control," (WADD PR 92069), April 1960.

4-16 Ioffe, A.F., Semiconductors, "Thermoelements and Thermoelectric Cooling," Infosearch Limited, London.

4-17 Wolfe, W., and Limperis, T., Infrared Information and Analysis State-of-the-Art Report, "Infrared Quantum Devices," Novexas P-2329, (2389-50-T), University of Michigan, July 1961

4-18 Evans, W.H., Mann, A.E., and Wright, Jr., W.V. "Solar Panel Design Considerations," American Rocket Society Paper 1296-60, September 1960.